Proiect cofinanţat din Fondul Social European prin Programul Operaţional Sectorial Dezvoltarea Resurselor Umane 2007-2013
Investeşte în oameni!
Proiect InnoRESEARCH - POSDRU/159/1.5/S/ 132395
Burse doctorale şi postdoctorale în sprijinul inovarii şi competitivităţii în cercetare

UNIVERSITATEA **POLITEHNICA** DIN BUCUREŞTI

Facultatea de INGINERIE ELECTRICĂ

Departamentul de ELECTROTEHNICĂ

Nr. Decizie Senat 238 din 30.09.2015

Teză de Doctorat
PhD Thesis

Denumirea tezei în engleză

Multiphysics Modelling of Radio Frequency Micro-Electro-Mechanical-Systems

Denumirea tezei în română

Modelarea Multifizică a Întrerupătoarelor Micro-Electro-Mecanice de Radio Frecvenţe

Autor: Ing. Aurel-Sorin LUP
Conducător de doctorat: Prof. dr. ing. Daniel IOAN

COMISIA DE DOCTORAT

Preşedinte	Prof. dr. ing. Sorin Dan GRIGORESCU	de la	UPB
Conducător de doctorat	Prof. dr. ing. Daniel IOAN	de la	UPB
Referent	Prof. dr. ing. Gabriela CIUPRINA	de la	UPB
Referent	Prof. dr. ing. Călin MUNTEANU	de la	UTCN
Referent	Dr. Alexandru MULLER, CSI	de la	IMT

BUCUREŞTI
2016

Abstract

Tema acestei teze de doctorat se referă la modelarea şi simularea atăt computaţională cât şi multifizică a dispozitivelor Micro-Electro-Mecanice (MEMS) de Radio Frecvenţă (RF). Scopul modelării este de a extrage un model compact, de ordin redus, care să poata fi simulat cu un efort de calcul cât mai mic, aceasta fiind o cerinţă foarte importantă a proiectanţilor de sisteme micro-electronice. Domeniul din care face parte cercetarea este cunoscut sub numele de Electronic Design Automation (EDA), obiectivul tezei fiind acela de a dezvolta noi metodologii şi tehnologii eficiente EDA, dedicate dispozitivelor MEMS de RF. Metodologia de cercetare aplicată în teză este bazată pe tehnici analitice, numerice şi experimentale.

Teza de doctorat este structurată în 7 capitole, primul fiind unul introductiv şi ultimul unul concluziv. Anexele şi lista bibliografică încheie teza. În Introducere se prezintă contextul tezei, importanţa şi actualitatea domeniului studiat, generalităţi despre MEMS-uri, obiectivul şi metodologia cercetării, precum şi structura lucrării. Primul capitol al lucrării descrie stadiul actual al cercetărilor din domeniul tezei de doctorat, cel al modelării dispozitivelor MEMS de radio-frecvenţă.

Capitolul al doilea este dedicat identificării principiilor teoretice ale modelării multifizice a dispozitivelor MEMS de RF. Se prezintă metodologia de modelare multifizică şi se discută conceptele teoretice care stau la baza modelării multifizice, în diferite discipline de interes pentru dispozitivele MEMS, cum sunt: Electrostatica, Electrodinamica, Mecanica structurală şi Mecanica fluidelor. În capitolul trei se prezintă studiul unui model conceptual unidimensional al unui comutator MEMS, simplificat la maxim, ca să admită o rezolvare analitică. În al patrulea capitol al lucrării se abordează problema modelării multifizice a întrerupătoarelor MEMS şi a validării modelelor extrase pe baza soluţionării lor numerice.

Capitolul cinci este dedicat studierii modelelor reduse ale comutatoarelor MEMS de RF. Acestea sunt de tipul celor prezentate în capitolul 3, dar parametrii nu sunt determinaţi pe cale analitică aproximativă, ci sunt extraşi pe baza rezultatelor numerice prezentate în capitolul 4. În capitolul şase se prezintă: concluziile generale ale lucrării, contribuţiile ei originale, subiectele deschise, ce trebuie abordate ulterior şi lista lucrărilor publicate pe perioada elaborării tezei.

Principalele contribuţii originale aduse prin teza de doctorat sunt următoarele: Analiza critică a stadiului actual al cercetărilor în domeniul modelării dispozitivelor de comutate RF MEMS. Analiza parametrică a celui mai simplu model analitic 1D al comutatoarelor RF MEMS. Dezvoltarea şi simularea cu FEM în COMSOL a modelelor numerice 2D şi 3D pentru dispozitive RF MEMS. A fost dezvoltat un algoritm eficient de extragere a unui model compact pentru comportarea statică şi dinamică a comutatoarelor RF MEMS, care a fost sintetizat în Spice. A fost dezvoltat un algoritm eficient de extragere a parametrilor modelului compact de tip TL-RLC-TL pentru comutatoarele RF MEMS. A fost dezvoltat un model parametric compact hibrid, pentru comutatoarele RF-MEMS, care conţine atât componenta de radiofrecvenţă cât şi componenta electro-mecanică multifizică.

"To my mum, with love"

Acknowledgments

I would like to thank Prof.dr.ing. *Daniel Ioan*, in his capacity as scientific adviser and supervisor of the development and completion of this thesis, for his patience and encouragement that he showed me, for his professionalism and attention with which he guided the research in these years.

Also I would like to thank Prof.dr.ing. *Gabriela Ciuprina*, with whom I had the pleasure to work along these years, a special person, who was always there when I needed guidance giving me a lot of support and the feeling to trust in myself.

I am grateful for the support I got from the team of the research project that inspired the topic of this thesis: the team from IMT – lead by dr.ing. Alexandra Ştefănescu, dr.ing. Dan Vasilache, dr.fiz. Alexandru Mulller and by professors of UPB that shared with me valuable knowledge on structural mechanics Prof.dr.ing Ştefan Sorohan and fluid dynamics Prof.dr.ing Dragoş Isvoranu. I am very thankful to Prof.dr.ing Valentin Ioniţă and Prof.dr.ing Mihai Iordache who were part of my scientific research advisory committee. And at last but not at least to Prof.dr.ing Călin Munteanu and Assoc.prof.dr.ing Adina Răcăşan the firs persons who guided me in the world of scientific research.

I am in dabbed to my colleagues: *Ruxi*, who had the patience to help me proofing this thesis, *Mihai P.* always willing to talk and discus any topic. To *Laura, Bogdan, Simona, Dan, Iulian, Mihai R.* for their support as members of the Numerical Modeling Laboratory (LMN) from PUB, that host me for the last three and a half years.

And last but not least to my family for their unconditional love.

The work has been funded by one grant and two research projects as follows: the Sectoral Operational Programme Human Resources Development 2007-2013 of the Ministry of European Funds through the Financial Agreement POSDRU/159/1.5/S/132395; the Romanian PN-II-PT-PCCA-2011-3 joint applied research project "Advanced Tools and Methodologies for the Multiphysics Modelling and Simulation of RF MEMS Switches" (ToMeMS, mems.lmn.pub.ro); the TD COST Action TD1307 European Model Reduction Network (EU-MORNET, http://www.eu-mor.net/). The research benefited from the logistics support and computing facilities offered by the Numerical Modelling Lab (http://www.lmn.pub.ro/), Electrical Engineering Department, Politehnica University of Bucharest, Romania. The experimental data were obtained in the frame of the ToMeMS project, as a result with the joint collaboration with the National Institute for Research and Development in Microtechnologies (IMT) - Bucharest, Romania (`www.imt.ro`).

Table of Contents

List of Figures

List of Tables

Introduction

1. Context: MEMS Technology and Devices

Current technological progress can be largely attributed to advances in the micro- and nano-electronics field, their applications having an important impact on the human society. It is generally accepted that the invention of the transistor was a technological step forward of great importance, but not so the actual operation of the transistor itself as the possibility of its integration at microscopic level in solid-state circuits. This inexpensive and fast process determined its tremendous success which is considered the start of the information revolution.

These new micro-electronic systems, now known as Integrated Circuits (IC) and later as Very Large Scale Integrated (VLSI) Circuits have shown a significant increase in performance, functionality and reliability, at low production costs in very large series. The success of micro-electronics have extended the researchers prospect to other areas of physics. Miniaturization principles and micro-fabrication technology with movable parts patented by the integrated circuits was subsequently applied to obtain mechanical devices with movable parts, thus micro-electro-mechanical systems (MEMS) being created.

Integrated circuits have demonstrated their applicability in all technical fields and not only. However after decades of progress, the microchip industry is in crisis, mainly because of their excessive power dissipation at their highest running frequency. Gradually, integrated circuit manufacturers have realized that a reasonable energy efficiency can not be obtained only by reducing the dimensions of a transistor. This energy performance issue is more obvious at digital devices and integrated circuits that contain switches and/or breakers. The problem is generated because the transistors strictly speaking, are imperfect switches (even in open state there is a leakage current).

Therefore to manufacture a competitive switch for high frequency signals, a more efficient technology, in terms of energy, had to be searched and the viable solution was the use of MEMS technology. Despite the fact that MEMS devices are not yet as fast as transistors, they compensate through energy efficiency and better performance at high frequency. One of their important advantages is they can be produced by technological processes similar the manufacture of transistors, without a substantial change on the production line [1].

The research conducted in micro-electronics during the last decades have shown that it is possible and feasible significantly improvements of the next generation of radio fre-

quency devices components by using micro-electro-mechanical systems (RF-MEMS) [2]. The use of RF-MEMS components has yielded some remarkable properties of circuits in which they have been integrated, such as phase switches [3, 4], filters [5, 6], reconfigurable antenna [7, 8] etc. They have been successfully replaced devices such as PIN diodes, filters, field effect switches (FET), demonstrating substantial improvements in performance of the renewed systems.

It is expected that the RF-MEMS devices are an essential part of the new generation of smart RF systems, such as wireless sensors or other operating systems in telecommunications working in the frequency range of 1-100 GHz [9, 10, 11]. Such systems (eg. phased arrays, reconfigurable diaphragms, switching networks, etc.) are characterized by a low cost, compact design, high performance, flexibility and configurability. In short, the integration of RF-MEMS devices is a key technology to dramatically improve miniaturization, low-power, low-cost and system performance for wireless systems. They are essential elements of next-generation intelligent systems being characterized by models with effective costs, compact, high performance, flexibility and configurability.

Micro-**E**lectro-**M**echanical **S**ystems are very small mechanical devices built on semiconductor chips having the size less than one millimeter and therefore measured in micrometers. They have appeared in research labs in the 1950's and began to materialize as commercial products in the mid 1970's. They have been widely used in sensors applications to measure pressure, temperature, and vibration, chemical switches, gas based chromatography, light reflectors, accelerometers for airbags, vehicle controls, pacemakers and games. MEMS technology is also used to make ink jet printing heads, read/write micro-actuators heads, optical switches that reflect the light beams to corresponding output ports [12].

The growing demand for micro-fabricates having a superior energy performance, determined the reorientation of manufacturers to integrated circuits and hence the scientific community to the technology of micro-electro-mechanical systems, whose benefits, particularly in radio frequencies were highlighted in the last decade. Originally developed for military applications, this revolutionary new technology demonstrated excellent performance in radio frequency devices and beyond.

Moore's law, that is the observation that the number of transistors in a dense integrated circuit doubles approximately every two years, has powered mainstream microelectronics for the past decades, driving ICs down to 45nm and below, and promising lower costs for chip makers. This extreme scaling works well for memories and microprocessors in the digital world, but not for interfacing with the actual physical world, which is analog. Many applications such as radio frequency (RF) devices, power management subsystems, passive components, biochips, sensors, actuators play an equally important role in todays semiconductor products. Integrating analog functions into CMOS-based specialty technologies enables cost-optimized and value-added system solutions. These diversified technologies are known as "More than Moore". The term "More-than-Moore" was invented by Europe in the early 2000s to stress the fact that the value of a packaged system does not rely only on the performance of the CMOS technology for the digital information processing, but also on diversified technologies which does not necessarily perform better through a dimensional scaling (Fig.1) [13].

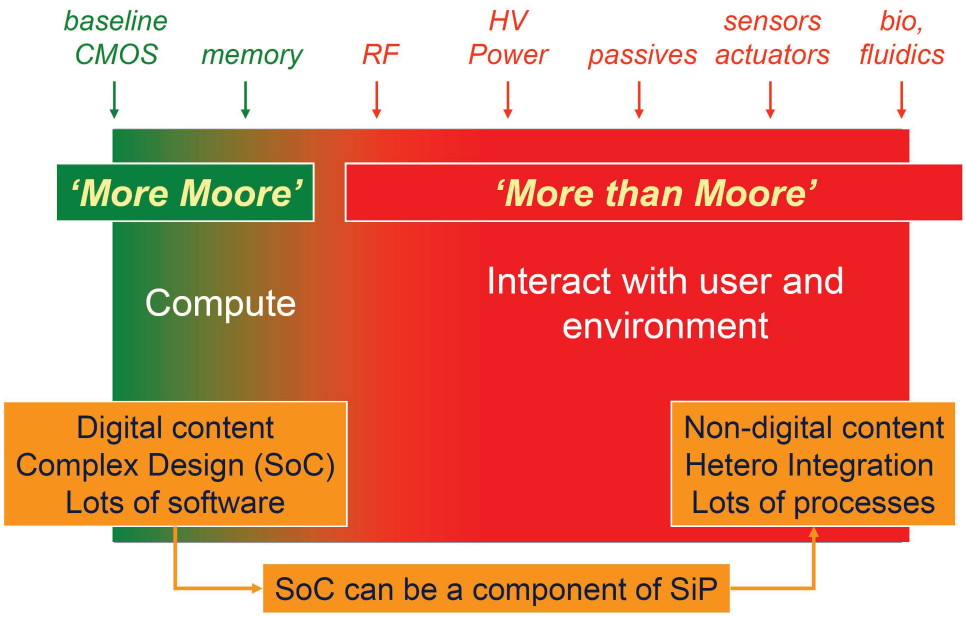

Figure 1: More than Moore scope and functionality [14].

"More-than Moore" technologies cover a wide range of fields. For example, MEMS applications include sensors, actuators and ink jet printers. RF CMOS applications include Bluetooth, GPS and Wi-Fi. CMOS image sensors are found in most digital cameras. High voltage drivers are used to power LED lights. "More-than Moore" technology, do not constitute an alternative or even a competitor to the digital trend as described by Moores Law. In fact, it is the heterogeneous integration of digital and non-digital functionalities into compact systems that will be the key driver for a wide variety of application fields, such as communication, automotive, environmental control, healthcare, security and entertainment. Whereas "More Moore" may be viewed as the brain of an intelligent compact system, "More-than Moore" refers to its capabilities to interact with the outside world and the users (Fig.2) [15].

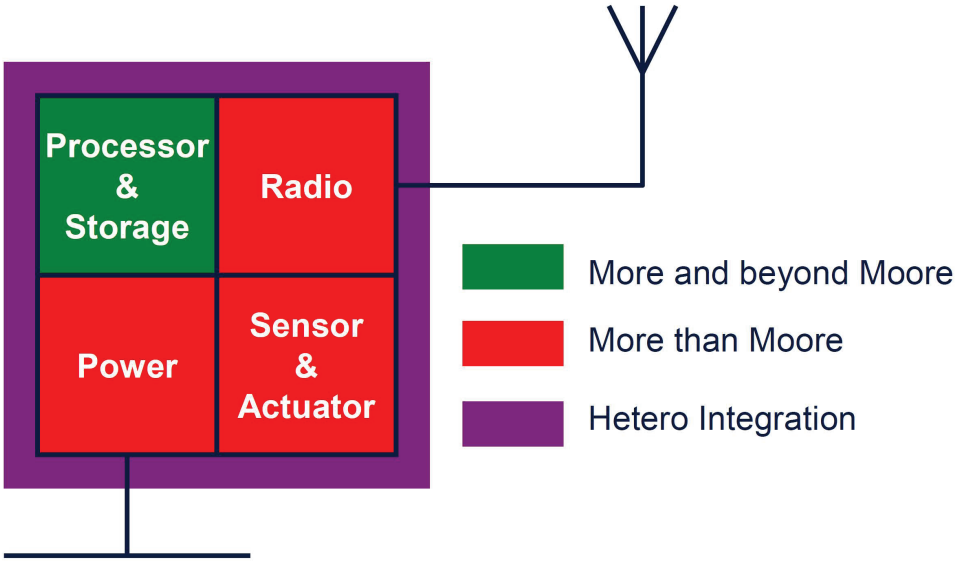

Figure 2: Intelligent systems incorporate "More Moore" and "More than Moore" [14].

The first MEMS pressure sensors were introduced in the 1970's for automotive appli-

cations. Pressure sensors are considered to be the first MEMS devices commercialized with successes. Since their introduction they have been deployed in various different automotive applications, such as manifold air pressure measurement and safety applications. Being typically used in safety applications, high-performance and reliability are required. In medical applications sensitivity and reliability are also highly required. In addition, biocompatibility and low power consumption are necessary features especially in implantable applications. MEMS pressure sensors have been on the market for approximately 40 years now and are considered to have reached a mature stage of development. Fig.3 presents the economic domains were MEMS sensors are used and the level of the demand [16].

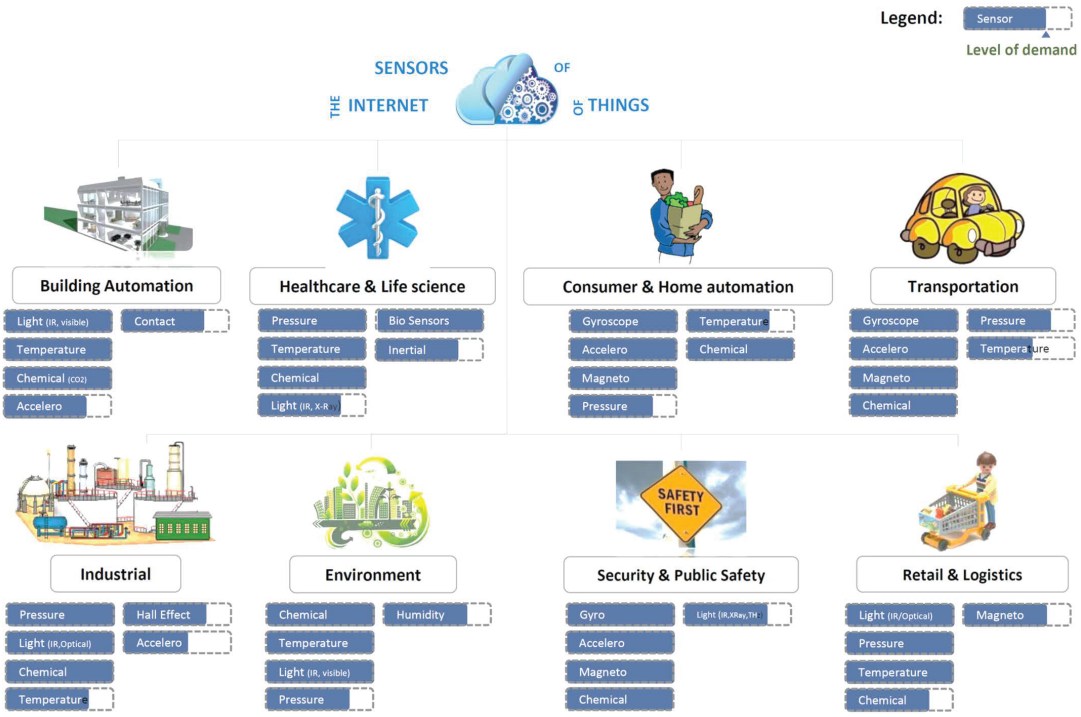

Figure 3: MEMS sensors economic domain and level of demand [17].

The first inkjet printheads were developed in the early 1980's by Hewlett Packard and were among the first MEMS devices. They are by far the most commercially successful MEMS-based microfluidic devices. Recently the first commercial inkjet printhead device for printed electronics applications, facilitating the production of electronics the cost being at a fraction from ones build with conventional technologies. Other potential future applications for inkjet printheads include three dimensional printing, conductive traces for LCD and plasma displays and biomedical applications, such as bioprinting for artificially constructing living tissue.

Accelerometers were the first inertial sensors that had been build using MEMS technology. Developed in the 1970's were first commercialized in the early 1990's. Since then they have been widely employed in various automotive applications such as airbag crash sensors, rollover detection and electronic stability control, among other functions. In the late 2000's accelerometers were applied in consumer electronics applications as well. During the last decades MEMS accelerometers have seen significant development. Their size has been even further reduced, their performance and functionality has improved and

their price has dropped considerably.

Another inertial sensor that was build using MEMS technology was the gyroscopes. They are fabricated from quartz or silicon and they typically employ vibrating mechanical elements instead of spinning masses used in conventional gyroscopes. The first MEMS gyroscopes were used in luxury cars during the late 1990's. Since then they have been widely employed in different automotive applications such as electronic stability control, rollover prevention and navigation. During the last couple of years, MEMS gyroscopes have entered the consumer electronics market. The adoption was significantly slower than with MEMS accelerometers due to the high price of the devices. Today they are used in various consumer electronics devices such as cell phones, video game controllers and cameras. MEMS gyroscopes can be expected to face high growth in both low-end and high-end applications especially once the technological issues have been resolved.

The first optical MEMS devices were introduced on the market in the late 1990's. Since then they have been used in various different applications ranging from optical communication to image displays and other optical systems. In optical communication MEMS devices are used to direct and modulate light in fiber optic systems. They are used, as variable optical attenuators, tunable filters and wavelength division multiplexing systems. The advantage of optical MEMS devices is that they enable all optical communication. Instead of having to convert optical signals to electrical signals and vice versa, optical MEMS devices require no O/E conversion. This enables lower cost, immunity from electromagnetic interference, increased density and wavelength independence. Another large application area for optical MEMS devices is image display systems, such as direct view displays and projection displays. This devices can also be used in a wide variety of other applications such as spectrometers, optical imaging systems, and infrared (IR) detectors.

The first MEMS microphone devices was first introduced in the early 2000's. The first devices were analog-output microphones intended for cell phones. Not long after, in 2006, came digital-output microphones, which were quickly deployed in laptops. To this day consumer electronics remain the largest market for MEMS microphones. The devices are employed in various portable applications, such as cell phones, laptops, tablets, headsets and cameras. MEMS microphones are also used in automotive and medical applications, such as hands frees, voice recognition and hearing aids. In medical applications they are used for in vivo- diagnostics in endoscopic devices.

RF-MEMS have been under extensive research for the last three decades, the devices have been relatively slow to move out of the laboratories and into commercial products. The first commercial RF MEMS devices were introduced on the market in turn of the millennium and yet today they have not reached a massive market adoption. So far RF MEMS devices have been used for research purposes in test equipment and instrumentation. The devices have also been deployed in mobile and wireless communication as well as military and aerospace applications. The fastest growing application area for RF MEMS devices is expected to be mobile communication, were the devices can offer reduction of signal interruptions and dropped calls, faster data transmission rates and improved design and power efficiency. Surface and bulk acoustic wave resonators are currently the most mature RF MEMS components and they represent the major part of RF MEMS. They are used for frequency selection in filters and duplexers in RF front-ends in replacement

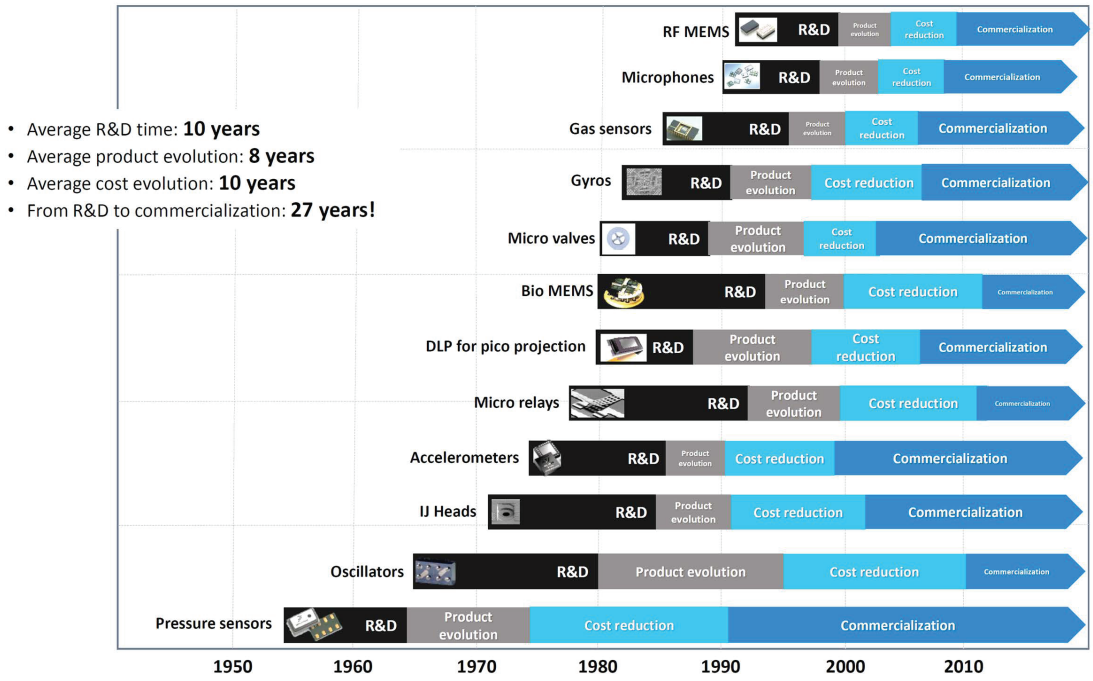

Figure 4: Time duration from R&D to comercialization [17].

of conventional technologies, which are too bulky for modern portable devices.

Thin-film bulk acoustic resonators have been recently deployed due to higher frequency capability. Extensive research works have also been carried out to develop MEMS oscillators to replace conventional quartz oscillators used in frequency reference and timing applications. The devices offer several advantages compared to conventional quartz oscillators including smaller size, better shock resistance, smaller form factor and better suitability for mass production. Capacitive and ohmic switches have long attracted much attention among RF MEMS products. The excellent performance of MEMS switches has demonstrated great potential for replacing conventional switches in numerous applications, including T/R switches, phase shifters, switchable filters and tunable antennas. Despite the high level of interest to RF MEMS switches, the commercialization of the devices has been rather slow. This is due to challenges regarding packaging, cost, reliability, self-heating and high actuation voltages. In 2011 RF-MEMS were first integrated and commercialized. The device is an impedance tuner containing various components such as variable capacitors and inductors. So far the device has been applied in smartphones for antenna tuning purposes and in wearable technologies. A time scale from R&D to commercialization for different applications that contain MEMS devices is presented in Fig.4.

Other aplications for MEMS devices are: magnetometers - sensors that measures strength or direction of magnetic fields; miniaturized MEMS-based power generators and micro fuel cells; BioMEMS like Microfluidics devices, Medical sensors used to measure a wide variety of physiological properties such as temperature, pressure, pH and the concentration of biological compounds; Atomic clocks used for frequency reference in timing applications, being the most accurate and stable devices available; Micro-coolers as thermoelectric coolers and cryogenic micro-coolers; Micro speakers are miniaturized electro-acoustic transducers that convert electrical signals into sound [18].

2. Generalities on RF-MEMS Devices

RF-MEMS switches are essentially miniature devices that use mechanical movement to create a short circuit or an open circuit of the RF signal in the transmission lines. They have an important development in recent years because of the huge potential for trade and defense. During the period 1985 to 2000, in which there were enormous progress in the field of GaAs HEMT (high electron mobility transistor) devices and the silicon base ones, research in the field of CMOS (complementary metal-oxide semiconductor) transistors switching devices did not show similar progress. In 1980, the maximum operating frequency of a CMOS silicon transistor was around 500 MHz, and now it is around 100 GHz. Also in 1980, the maximum operating frequency of GaAs HEMT devices was around 10-20 GHz, and now it goes up to 800 GHz. However, the maximum operating frequency GaAs or InP p-i-n diodes has improved from 500 GHz in 1985 to only 2000 GHz in 2001. There was a clear need for new technology to extend the maximum operating frequency of the switching devices to 40 GHz needed for applications with low losses and this could be achieved only through radio frequency micro-switches.

MEMS switches can be classified according to how the mechanical actuation is achieved, direction of motion, electrical configuration and type of contact. The forces that mechanical actuate RF-MEMS switches can be thermal, piezoelectric, electrostatic or magnetostatic. The most common actuation is the electrostatic one, based on electrostatic forces of attraction nature between two electrodes of different polarities, offering the advantage of low power consumption, owing to the fact that these types of switches requires electrical power only in time of commutation, not in a steady state of equilibrium.

Another great advantage of these types of switches follows from compatibility with the manufacturing of integrated circuits and the ability to integrate typical MEMS devices with other micro-fabricate circuits, transistors, amplifiers or diodes [3]. But the high driven voltages, in the range of 30 to 80 volts is in turn a disadvantage, especially in applications such as mobile telecommunications equipment, where power sources are limited to voltages of 3 to 8 volts.

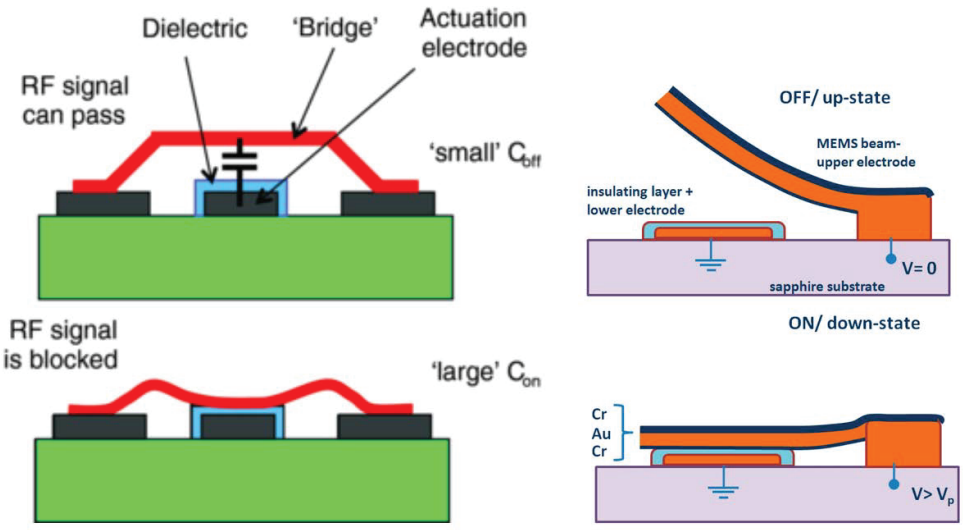

Figure 5: Capacitive MEMS switch, bridge type (left)[19] and cantilever type (right)[20].

From the construction point of view, the mechanical movement may be vertical (perpendicular to the substrate) or horizontal (parallel to the substrate). Most RF-MEMS switches made in the last 10 years have a vertical movement due to the a higher performance at high frequencies [10].

Fundamentally, there are two constructive solutions for RF MEMS switches, bridge type and cantilever type (Fig.5). Electrically there are also two principles: with ohmic (resistive or galvanic) contact and with capacitive contact, being connected series or shunt in the circuit. In the case of the resistive switches, metal-to-metal contact is achieved between the two electrodes, creating a short circuit, a connection characterized by a very low contact resistance. For capacitive contact switches, the metal membrane is moved by electrostatic forces, until making contact with a isolating layer covering the other electrode, creating a high capacitance that direct the RF signal. RF-MEMS capacitive switches used in variable bandpass filters have a typical shunt construction [21].

3. Objective, Research Methodology and the Layout of the Thesis

This PhD thesis has as main objective the multiphysics modelling of radio frequency micro-electro-mechanical devices, that takes in consideration all the phenomena that occur when these devices operate, such as electrostatic, structural mechanics, fluid flow and RF. The modelling is followed by the extraction of reduced order models that will allow fast and accurate simulations of electro-mechanical and RF behavior of RF-MEMS switches under several excitations.

The scientific and technical actuality of the RF-MEMS and the need for accurate and effective models required by the designers of advanced micro and nano-electronic systems, justify the importance of the research topics addressed by this PhD thesis.

The research for the PhD thesis was conducted following the **ACES** (Analytical, Computational, Experimental Solutions) methodology [22]. According to this methodology the problems are approached in three steps. First, the solution is obtain from a simplified formulation that uses an analytical approach. Second the problem is solved by using a numerical techniques. In the end the verification of the numerical solution is done by comparison with the experimental data. An adapted form of the ACES methodology is showed in Fig.6.

The thesis is structured in 7 chapters. The first being an introductory one, and the last a conclusive one. A short description follows.

The *Introduction* provides justification of the micro-electro-mechanical systems study, showing the importance and actuality of the research, areas of application, general presentation of RF-MEMS switches and in the end are presented the objecitves, methodology and structure of the thesis.

Chapter one, refers to the *state of the art in modelling MEMS devices*. It presents and comments the literature dedicated to modelling RF-MEMS devices

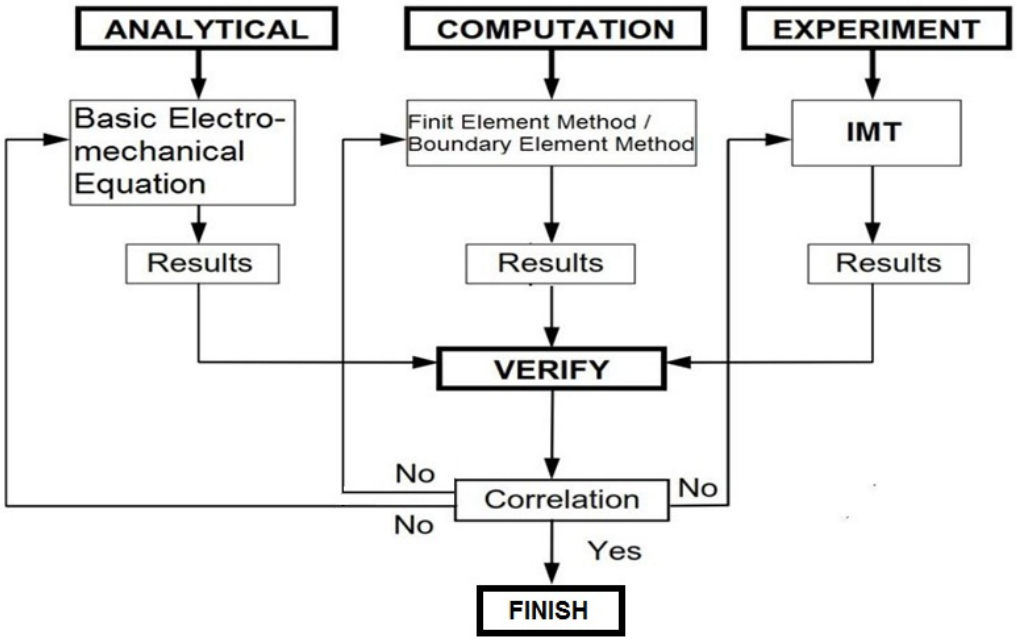

Figure 6: Analytical, Computational, Experimental Solutions (**ACES**) methodology [22]

Chapter two, *Theoretical Background of the Multiphysics Modelling*, presents the general concepts, methods, techniques and technologies that are used to characterize micro-electro-mechanical systems, focusing on multiphysics modelling. There are identified the most advanced modelling techniques and the software packages used in RF-MEMS simulation, as well as the main numerical methods used in computational modelling.

Chapter three, is a detailed study case of the *one dimensional model of MEMS switches*. It explains the analytical solution of the simplest test problem that we can imagine for RF-MEMS switches. Even if the example is extremely simple based on 1D geometrical model, it is fundamental for understanding of the concepts and the physical phenomena as well as this study case practical aspects of interest. The analysis of this study case go through the five steps of modelling, starting from a general dynamic problem and ending with a particularized static one. In this analysis, the most important physical aspects and quantities are highlighted and discussed.

Chapter four, entitle *Multiphysics Modelling of MEMS Switches*, refers to multiphysics and radio frequency modelling of two test cases. First the multiphysics problem formulation is given and then the 2D and 3D numerical models are conceived. The obtained models are analyzed in static, dynamic and full wave electromagnetic regimes. The multiphysics analysis is build up from a simple static 2D model, where electrostatic field is coupled with the structural-mechanical field. Next a dynamic 3D model is analyzed, where the effect of the air flow on the movement of the membrane is considered by solving a strong coupled three field problem. Studies of the influence of geometric parameters are also included in this chapter. Finally the numerical RF model is validated by comparison of simulation results with the results of experimental measurements.

Chapter five, refers to *Reduced Models for RF MEMS Switches*, it proposes effective methods for extraction the compact-lumped model of RF-MEMS device, considering multiphysics phenomena, as have been simulated numerically in the previous chapter. A

mixed circuit macro-model is created, that describes the entire behavior of the switch, that include both RF and multiphysics - movement phenomena. The extraction methods are validated by comparison of the simulation results of the macro-model with the result of numerical simulation of the field problems.

In the last chapter, the general conclusions are drafted together with the original contributions included in this thesis and the list of the articles published by the author in the various national and international conferences and journals. Also a list of future research directions is presented here. The Appendices and References list end the thesis.

Chapter 1

State of the Art in RF-MEMS Modelling

This chapter is dedicated to the state of the art in MEMS devices modelling. The most important articles and books written to describe the research achievements in this domain, as well as an overview of the main modelling tools are depicted.

By querying the Internet databases on information about MEMS devices, Google returns over 12,800,000 results. When polling "RF MEMS switches", Google Scholar returns more than 42,700 results and IEEE Explore returns over 1772 results, which shows that there is a very vast amount of information available. Fig.1.1 shows the evolution of the number of articles per year from 2000 to the present.

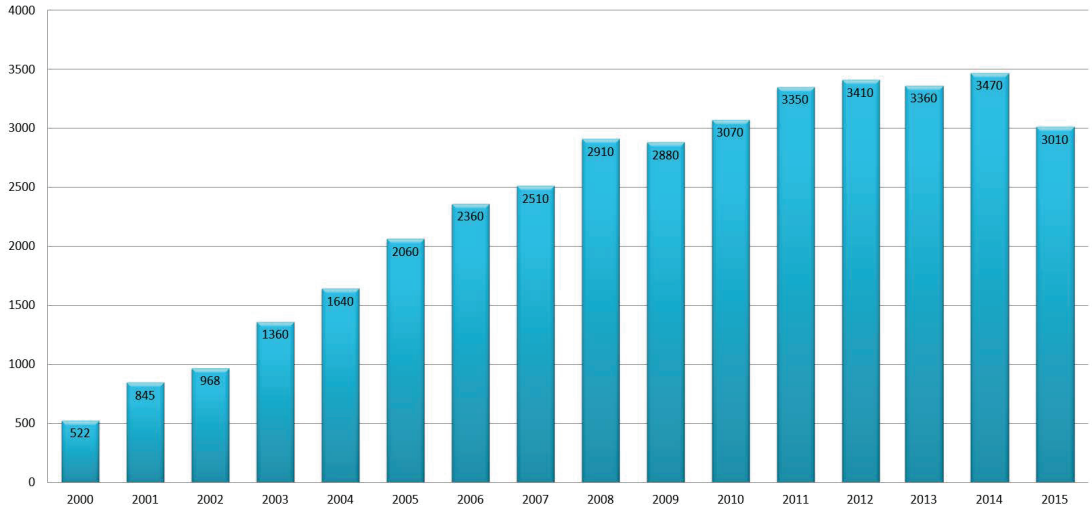

Figure 1.1: Evolution of the number of papers published per year having as a subject RF-MEMS according to `https://scholar.google.ro`.

In these circumstances, the identification and interpretation of the most relevant information is not an easy task. Thus, the data considered important for this thesis will be classified in the following categories [23]:

- Articles and communications about RF-MEMS:
  - with general aspects (introductory, overview, applicative aspects),

  - about modelling and simulations,
  - extraction of Reduced Order Models,
  - about optimization,
  - about experimental characterization;
- PhD thesis and dissertations about RF-MEMS;
- Books about MEMS and RF-MEMS;
- Software for RF-MEMS Modelling.

1.1 Articles and Communications

1.1.1 General Aspects

This category include articles and reviews describing general aspects about the characterization, structure, design, manufacturing and applications of RF-MEMS devices.

The authors of [24] Meng and coauthors present one of the first mathematical model developed to analyze the mechanical behavior of a membrane in both bridge and console construction. In [25] the revolutionary introduction of MEMS in radio frequency integrated circuits, in the context of the 90's is presented. Reference[26] exemplifies the use of MEMS switches for applications in the area of telecommunications systems such as filter and oscillators which are more advantageous than usual varactor diodes due to the high quality factor and lower losses. Yao in [1] presents a great diversity with many pictures of RF-MEMS components: switches, relays, variable capacitors, coils embedded resonators and mechanical filters. Their main applications in radio frequency circuits are also presented.

The most quoted article in the IEEE explore database dedicated to MEMS is the one by Rebeiz and Muldavin [27], which describes recent advances in RF micro-electromechanical switches and the circuits they are integrated. The authors describe different types of device component construction. The article presents the operating characteristics, highlighting the advantages that are brought by replacing the solid-state devices with RF MEMS devices for high frequency circuits operating up to 120 GHz.

In [3] Rebeiz presents and analyzes the Brownian effect of acoustic acceleration and power-supply noise from a switching circuit containing MEMS switches, specifically for a capacitive MEMS switch connected in parallel and for a resistive MEMS switch (metal to metal contact) connected in series with the TLs. The same author, presents in [9] the latest achievements and highlights the potential applications of RF-MEMS components. As main limitations the reduced reliability and high cost of hermetic packaging are identified. Finally several circuits with RF-MEMS devices that are used in telecommunications, UHF, up to 94 GHz are presented.

Reference [28] by Milosavljevic is a summary of the RF-MEMS switches, indicating their advantages compared to static switching devices. Modelling results are presented for

a switch with a transversal connection to CPW. Reference [29] by Lucyszyn passes through all stages of micro-electro-mechanical technology, from design process, technical aspects of micro-manufacturing and examples of applications. In [30] Bouchaud highlights the technical challenges that must be overcome, list several applications, in order to expand the use of RF-MEMS in communications and wireless circuits. The article [31] presents the perspectives of RF-MEMS technology development, as they were identified by the European project ARRRO (Applied Research Roadmap for Micro- and Nano- Systems).

In the overview paper [2] Lahiri discusses the limitations and research scenarios for the year 2009. In [32] Henry et al. do a comparative study upon switches based on MEMS devices and those based on transistors, the comparison is made in energy terms. The conclusion is that MEMS switches are superior and recommended for wireless applications and biomedical implants. Reference [33] is a presentation of the Raytheon results, made at the IEEE-MTT conference. The author also shows some information about the production process, factors that influence the lifespan, packaging and commercial applications. In [34] Puchades discuses the design of a radio receiver based on MEMS switches, the fabrication process and the main challenges of this new technology.

Reference [35] by Jau describes the S-parameter performance of on-board RF-MEMS switches from DC to 4 GHz. It also explores the hot-switching reliability of MEMS switches using different types of input signals. Finally, it evaluates a possibility for improving the reliability of MEMS switches using an external circuit. Rebeiz and coauthors, present in [36] the design and characterization of a compact high-power RF micro-electro-mechanical system single-pole single-throw (SPST) and single-pole four-throw (SP4T) metal-contact switches. The SPST design results in a contact force of 1.9-2.8 mN at 80-90 V distributed over eight contacts and using four independent quadrants for actuation. Reference [37] by Dhal and Demde describes the latest emerging technology of the RF-MEMS and the utility of the RF MEMS switch.

The article [38] by Goldsmith presents a variable capacitor obtained by combing 14 bridge type MEMS devices with the actuation voltages from 30 to 55 V. The device operates at a maximum frequency of 40 GHz and represents a performant alternative to the electronic varactors. In [39] Mohamed et al. propose a design for a RF-MEMS tunable capacitor constructed on standard IC technology of 5 μm. The high quality factor of the device permitted the realization of a voltage controlled oscillator having the frequency from 60 to 950 MHz. Reference [40] by Borwick presents an adjustable MEMS capacitor that can be integrated in a UHF filter working on a frequency range from 225 to 400 MHz. The obtained rate of adjustment is from 1 to 8.4 and the quality factor Q exceeds 100. Nguyen in [41] presents an original design for comb type tunable capacitor using RF-MEMS switches with an angular vertical movement, with a quality factor of 270.

The pair of papers [42] and [43] by Entesari and coauthors present tunable filters build with RF-MEMS devices. Reference [7] by Huff presents how MEMS switches are integrated in micro-strip reconfigurable antennas. Liu in [44] summarize the achievements in RF-MEMS domain and them use in RF tunable circuits. In [45] Chen presents band-pass filters designed with tunable transmission line resonators. The paper [8] by Campo talks about reconfigurable antennas with RF-MEMS devices that operate at 24 GHz. In [46] Carrier et al. refers to micro-cells reflectors controlled by RF-MEMS switches.

The used method allows a fast and accurate analysis of the performance of these cells, relatively independent of the number of switches and their state. Reference [47] by Shim presents a new performant tunable band-pass filter build with 12 tunable electrostatic actuated MEMS capacitors that operates in the frequency range from 0.1 to 1 GHz. The performances of this IC is higher compared to printed circuits described in the literature.

1.1.2 Modelling and Simulations

This category refers to the papers describing aspect of multiphysics modelling (using original techniques and several commercial software packages) or describing the entire modelling process (ES, MEC, CFD, RF, EM) and its results, as well as papers which describe new design strategies based on EDA tools and packages.

In [48] Hung et al. describe FEM simulation of dynamic problems and extraction of reduced-order models of the analyzed micro-structures. As a case study, a pressure sensor built with MEMS technology of bridge type was used. References [49] and [50] by prof. White's team refer particularly to the modeling of the ES field. The authors identify three major challenges: the need for the development of fast algorithms for calculating superficial forces produced by the electrostatic field or external fluid interaction, a more efficient coupling of the different equations describing the operation of the device and the fact that designers expect dynamic models, enabling very fast simulation of the device. They are desired models that have few degrees of freedom, well related to the design parameters, such as geometric dimensions and material constants. Because this requirement is not fulfilled by 3D simulation where the complex geometry can generate (tens of) thousands of degrees of freedom, it is imperative an order reduction step that correlate the degrees of freedom of the system generated by meshing with those of a nonlinear compact macro-model. In [51] the author talk about an efficient algorithm for analyzing an adaptive 3D micro-electro-mechanical systems (MEMS). The algorithm does not use matrices, and requires the adoption of Newton multilevel techniques for solving coupled electro-mechanical equation. A 2D model was analyzed for a cantilever type MEMS device.

References [52] and [53] by Muldavin and Rebeiz are two important articles, the first one being dedicated to the EM modeling of a RF-MEMS device and the second one referring to the extraction of a equivalent R-L-C model, which was validated by comparison with measurements. In [54] Pacheco refers to the design of a capacitive shunt type RF-MEMS switch, having the pull-in voltage as low as possible. It aims to increase the mobile armature's area and its elastic suspension by a meandric system with several (from 1-5) switchbacks.

Reference [55] by Qian et al. is dedicated to the EM modelling at high frequency of a bridge type MEMS switch. The S parameters are computed by using ANSOFT-HFSS for a simple geometry, the lumped parameters are extracted and the validation was made by comparison with measurements. In [56] by the same author continues the previous study proposing here a more efficient EM model for an RF-MEMS device, the R-L-C parameters are also extracted and their validation was made by comparison with measurements.

In [57] Muldavin and Rebeiz present the model of the switching mechanism for a MEMS device. The analysis is based on electro-mechanics analysis, which takes into account the variation of damping force versus position (in time). The model calculates the switching current based on the capacity and the time behavior of the voltage. The model predicts the time dependency of the switching current and the dissipated energy during the switching process. In [58] Mercier et al. presents a new parametric model for a simple MEMS capacitive switch with electrostatic actuation, extracted from analysis of the nonlinear movement of the bridge and the capacitance variation. The extracted model can also be used for the EM analysis.

Reference [59] by Pierantoni describes the investigation and comparison of simulation results with three different modelling techiques for complex planar circuits. The first method is Transmission Line Matrix (TLM) second method is a combination of TLM method and Integral Equation method (IE) and the last method is based on Generalized Transverse Resonance Diffraction (GTRD). Electromagnetic analysis was performed by using different electromagnetic solvers, both in time and in frequency domain. To test the proposed methods, the authors modeled different structures including MEMS devices and compared the measurements results with computed S parameters. In [60] by Dubuc a comparison between different modelling methods is depicted, aiming to obtain a high accuracy prediction of the MEMS devices behavior.

Zhang in his work [61] refers to electro-mechanical model for RF-MEMS switches of the bridge type, for which he develops analytical models, dimensionless structures with 1D, respectively 2D geometry. The paper [62] presents a transient modelling technique for the movement of a MEMS components. The author of [63] proposes a more general and more accurate expression of the elastic constant for a better mechanical and electrical modelling of a MEMS switch.

Lee in [64] and Kawano in [65] present a FDTD analysis of a MEMS switch. In [66] Sudipto et al. present the dynamic analysis of a MEMS switch. The nonlinear coupling of the phenomena (electrical and mechanical) being made by an algorithm based on a complete diagram of Lagrange type, which makes re-meshing of the domain before each ES analysis no longer necessary. The article refers to an earlier program (MEMCAD [67]) where an integrated formulation for ES problems and finite element method for mechanical problems is used.

In the article [68] Schlegel applies MOR to reduce the simulation time, and Lee in [69] adopts the finite element modelling to extract a linear model by using artificial neural networks for RF-MEMS. In reference [70] Simion presents the electromagnetic modeling and simulation by IE3D Zeland, of a RF-MEMS switch using exact geometry. The procedure uses the equivalent circuit of a RF-MEMS switch, which was extracted from S parameters obtained from electromagnetic analysis.

The article [71] by Czaplewski and coauthors study the time dependency of the actuation voltage aiming a smooth contact in the case of a resistive type MEMS switch. Peyroul in [72] tries to give an idea of several critical modeling aspects: RF, contact and residual stress using three simulation with different software. Reference [73] by Yuan presents the simulation of a Spice circuit model to analyze the charging of the dielectric in a MEMES

devices, and [74] by Yuan using a RF-MEMS device it studies the electromagnetic wave radiation emitted during the commutation time.

In [44] Liu analysis a resistive cantilever type RF-MEMS switch, DelTin in [75] presents a new method to extract reduced electro-mechanical models, reference [76] by Peyrou presents the modelling process of a MEMS devices using COMSOL and MATLAB and Pasquale in [77] studies the damage caused by fatigue of oscillating micro-structures. In [78] Peyrou studies the influence of the contact and its roughness upon the electric parameters of the armatures. To capture the 3D structure of the contact surface, an optical profilometer (VEECO) and an atomic force microscope (AFM) were used.

In the paper [79] Sumant propose a FEM-ANSYA based method to analyze coupled ES-MEC problems for RF-MEMS switches. In [80] Halder propose a modelling method using a Spice circuit, validating the results against experimental data. In reference [81] Llamas propose different modelling strategies using lumped and distributed parameters, that take in consideration mechanical and technological proprieties. The article [82]by Achkar, presents a study on the parameters that influence the pull-in voltage of a MEMS switch.

The authors of [83] Halder et al. present an extended version of [80] where they create models for electro-thermic and thermo-mechanic switches. Iannacci and coauthors in [84] discuss various aspects of circuit simulation and RF-MEMS devices, presenting a fast simulation tool based on a lumped parameters library for MEMS component that was previously developed by the author. Components such as the right bar, flexible or rigid suspended plates, were described in VERILOG and simulation in Cadence. Combining these elements allows a rapid simulation for a complex device in SPECTRE. In [85] Niessner presents a macro-model for a resistive RF-MEMS switch in a standard integrated circuits design tool. The article [86] by Chaterjee et al. studies the squeeze film phenomena and its effects, developing a semi-analytical model for the movement of the bridge.

The authors of [87] and [88] by Jain and coauthors develop a theoretical modelling procedure of the charging of the dielectric and they analyze a resistive MEMS switch. In [89] Do presents the dynamic results of a cantilever type switch using Euler-Bernouli method that incorporates squeeze film phenomena. Kurth in [90] presents a frequency study for several resistive RF-MEMS switches, analyzing some that have the bridge placed longitudinal with the signal lines for the frequency range from 0 to 40 GHz and some that have the bridge placed transversal with the signal lines for the range of frequencies up to 80 GHz.

1.1.3 Extraction of Reduced Order Models

This paper [91] by Bazaz presents a critical review of the strategies for parameter dependency preservation in reduced order models, which have been proposed over the years, and attempts to contextualize the problem from a proper physical and numerical perspective. The open problems in the area are also identified, along with a discussion on some potential application areas.

The the authors of [92] Salimbahrami at el. propose two methods for solving the problem of order reduction for large-scale linear time invariant systems. First, the approach presented by Su in [93] is generalized and the number of matching moments is increased. Second, a new approach via first-order models is presented, resulting an even higher number of matching moments. Both solutions preserve the specific structure of the second-order type model. In [94] Beattie examines the Krylov-based model reduction of second order systems where proportional damping is used to model the energy dissipation. The detailed analysis of the distribution of system poles, and then, through a connection with potential theory, is given. To obtain an optimal single shift strategy used in rational Krylov model reduction the structure of these poles is exploited. Finally the authors show that one can build up approximating subspaces satisfying all required conditions much more cheaply as direct sums of standard rational Krylov subspaces within the smaller component subspaces towards the general case that requires usage of a second-order Krylov subspace structure. Numerical examples are provided to illustrate and support the analysis.

In [95] Vasilyev et al. propose a method for generating reduced models for a class of nonlinear dynamical systems, based on truncated balanced realization (TBR) algorithm and a recently developed trajectory piecewise-linear (TPWL) model order reduction approach. They also present a scheme which uses both Krylov-based and TBR-based projections. Computational results, obtained for examples of nonlinear circuits and a micro-electro-mechanical system (MEMS), indicate that the proposed reduction scheme generates nonlinear macro-models with superior accuracy as compared to reduction algorithms based solely on Krylov subspace projections, while maintaining a relatively low model extraction cost.

Reference [96] by Rewienski and coauthors present an approach to the nonlinear model reduction using the nonlinear system with a piecewise-linear system and then reducing each of the pieces with a Krylov projection. Instead of approximating the individual components as piecewise-linear and then composing hundreds of components to make a system with exponentially many different linear regions, the authors generate a small set of linearizations about the state trajectory which is the response to a “training input”. The computational results and performance data are presented for two study cases: a nonlinear circuit and a MEMS device with a fixed-fixed beam. These examples demonstrate that the macro-models obtained with the proposed reduction algorithm are significantly more accurate than models obtained with linear or the quadratic reduction techniques. Finally, they shown that the proposed technique is computationally inexpensive, and that the models can be constructed 'on-the-fly', to accelerate simulation of the system response. In [97] the same authors continue the previous work adding a procedure for a posteriori estimation of the simulation error, which may be used to determine the accuracy of the extracted trajectory piecewise-linear reduced-order models.

The goal of the paper [98] by Rudnyi is to review the use of modern mathematical methods to reduce a system's dimension from an engineering perspective. It is shown that in many cases important for practice, the order of ODEs can be reduced by several orders of magnitude almost without sacrificing precision. In [99] the same authors described a software tool to perform moment-matching model reduction via the Arnoldi algorithm

directly to ANSYS finite element models. The application of the tool is discussed, referring to a structural mechanical problem with a second order linear differential equation. The authors of [100] Han, Rudnyi and Korvink focus their paper on the application of model order reduction techniques to optimal design to reduce the transient analysis time for an optimization process. In order to achieve this, they created an open-source software *mor4ansys* that performs model order reductions using Arnoldi algorithm directly to ANSYS finite element models. The study case chosen to demonstrate the advantages of this approach was a micro accelerometer. The harmonic and transient results of a reduced-order model of the accelerometer yield very good agreement with that from the original high-dimensional ANSYS model. The use of reduced-order models within the optimization iterations produces almost the same results as those without model order reduction, and speeds up the total computation by at least an order of magnitude.

Reference [101] by Kohler present a model order reduction algorithm for linear time-invariant descriptor systems of arbitrary derivative order that incorporates sensitivity analysis for network parameters in respect to design parameters. It is based on implicit moment matching via rational Krylov subspace methods with adaptive choice of expansion points and number of moments based on an error indicator. Additionally, it is demonstrated how parametric reduced order models can be obtained at nearly no extra costs, such that parameter studies are extremely accelerated. The finite element model of a yaw rate sensor MEMS device has been chosen as a numerical example, but our method is also applicable to systems arising in modelling and simulation of electromagnetics, electrical circuits, machine tools, heat conduction and other phenomena. In [102] Santorelli addresses and proposes solutions to practical issues concerning model order reduction when applied to finite element equations. Mesh generation, condition number and size of matrices are typical issues that are encountered. MEMS examples are studied to highlight these issues and to prove the effectiveness of such a model in reducing the system size significantly, while performing with high accuracy over a large range of parameter values. This paper [103] by Parent et al. reports a novel model-order reduction (MOR) approach for creating fast-running, nonlinear, multiphysics models in Verilog-A. This new approach differs from previous work by creating the reduced order model (ROM) directly from an accurate, nonlinear, multiphysics representation. The mechanical and electrical nonlinearities of the MEMS structure are persevered to capture effects such as quadrature, amplitude-dependent frequency shifting and electrostatic softening. The reduction algorithm has been implemented in the commercial MEMS/IC co-design tool MEMS+. The approach's effectiveness is validated for a state-of-the-art, three-axis, capacitive gyroscope from Murata Electronics by comparing simulations of the created Verilog-A model with experimental data.

1.1.4 Optimization

The pair of papers [104] and [105] by Kolchuzhin et al. present reduced order models of MEMS devices considering coupled phenomena, performing finite element simulation, and computing not only system matrices but also computing higher order partial derivatives with respect to the design parameters, by using automatic differential procedure. The output quantities for other values of design parameters are then calculated by using Taylor

series expansions near the initial design. Model order reduction of nonlinear coupled electrostatic-mechanical system is extracted knowing that the state of mechanical system can be described by as a weighted combination of its eigenmodes. The algorithm was implemented in MATLAB and the mesh is generated in ANSYS. The procedure is more effective than the one based on "data sampling + fitting" because automatic differentiation is less expensive than additional simulations based on FEM (used in the paper to validate the accuracy of the extracted parametric models). The extracted parametric reduced models may be used in an efficient manner for the device optimization.

In [106] Suhas refers to the mechanical modelling and optimization of a MEMS structure from the pull-in voltage point of view. Reference [107] by Allen present how in RF analysis the dynamic response of the system is optimized for an electrostatic actuated MEMS device, to obtain a robust design solution with low influence of the technological, material and geometric variations. The paper [108] by Kolchuzhin presents the challenges in parametric modelling, opportunities and difficulties applying the mode superposition method for a coupled ES-MEC analysis for a MEMS device. In [109] Shalaby presents the optimization of a cantilever type RF-MEMS switch, with direct contact aiming a minimum actuation voltage and a maximum RF power. The parameters used in the study where the width of the console section and curvature size. In [110] Pasha refers to a bridge type RF-MEMS, aiming to optimize its actuation mechanism.

The work presented in [111] by Kolchuzhin continues his previous studies including a multilevel parametric methodology based on EM. In [112] Angira and coauthors present the modelling, analysis and simulation of a resistive MEMS switch, using optimizations techniques to decreasing its pull-in voltage. Reference [113] by Ding propose an intelligent circuit for the control of the switch's actuation voltage. The control is based on a fine tuning of the amplitude of the actuation voltage, according to the difference between the measured and desired capacity. Smart control is achieved by alternating actuation voltage sign, in the case that the necessary amplitude to maintain the desired capacity changes significantly. The article [114] by Philippine uses the "Topology Optimization" method to optimize a capacitive switch. The methods requires a FEM solving procedure to calculate the sensitivities and based of them, the objective function. A multi-objective problem with restrictions which refers to the mechanical parameters is formulated and solved.

1.1.5 Experimental Characterization

The papers mentioned below summarize some of the new methods for measurement and characterization of MEMS and RF-MEMS devices.

The paper [115] by Girbau presents a new method of measurement for the dynamic and energetic characteristics of a RF-MEMS device. The method extracts from the RF characteristics the demodulated quadrature component that contains information about the mechanical characteristics and the switching time. In [116] Lee presents a new method of monitoring the charging of the dielectric, method that can predict the life duration of the device. The method relays on the identification of the resonant frequency of the mobile armature, and from the variation of this frequency it can detect the uniformity of the electric field.

In [117] Ruan proposes new tests to determine the fatigue acceleration of a bridge type capacitive RF-MEMS switch, it describs the equipment and necessary tools to monitor the aging effects of the device. The paper [118] by Kosla describes a new method for the monitoring of the reliability and the degradation of a MEMS device by measurements of the switching time. Reference [119] by Makasheva describes methods through which structural and charging characteristics can be determine. In [120] Palit propose a new experimental characterization of the charging of the dielectric by measuring the C-V characteristic at high speed variations of the input signal. The article [121] by Koutsoureli and coauthors makes a critique study upon the methods of monitoring the charging of the dielectric for capacitive MEMS switches. They conclude that Kelvin Probe force microscopy (KPFM) and atomic force microscopy (AFM) are complementary methods and for a good characterization of the charge of the dielectric both methods must be used. In this paper [122] Kosla et al. present an automatic reliability detection/prediction system for manufacturing ohmic MEMS switches based on dynamic time measurements. The developed method allows device monitoring and highlights the influence of both restoring and surface forces evolution on switch reliability.

1.2 PhD Thesis and Dissertations

The dissertation thesis [123] by Bradley N. Bond at MIT refers to the development of techniques for generating parameterized reduced order models (PROMs) of nonlinear dynamical systems such as MEMS devices. The study presented combines elements from a non-parameterized trajectory piecewise linear method for nonlinear systems with a moment matching parameterized technique for linear systems. Using a MEMS switch and two nonlinear analog circuits, the developed algorithms were tested. Examples contain distributed strong non-linearities and possess dependence on several geometric parameters.

The doctoral thesis of [124] by G.K. Fedder from Berkeley University of California, is dedicated to simulation of MEMS systems. It demonstrates how relatively complex electro-mechanical systems can be modeled as a system with lumped parameters and then simulated with Spice or MATLAB. Reference [125] by J. Phillip is a doctoral thesis at MIT devoted to finding quick solutions for integral equations that describe electric potential in complicated 3D geometries. The procedure can be applied to compute electrostatic field of MEMS devices. The author develops a new highly effective method for solving these problems, based on meshing of the integral equations. The preconditioning proposed algorithm, based on FFT is as efficient as the multiple multipole technique (MMP), but it can be applied to a wider range of IE kernels. Based on this algorithm a new version of FastCap was developed, for numerical computation of capacitances of complicated 3D shapes. Reference [126] by D. Ramaswamy is a doctoral thesis also at MIT dedicated to MEMS devices simulation tools. The thesis presents effective techniques to solve problems that arise in complicated electromechanical MEMS technology, including those developed in [125]. The rigid-flexible systems problems lead to thousands of degrees of freedom. The proposed formulation shows his advantage after being embedded in a coupled domain simulation. It describes the procedure for obtaining reduced order models

without significant loss of the accuracy.

The MIT doctoral thesis [127] by X. Wang is dedicated quick fluidic MEMS simulation. Reference [128] by D. Perouli is a doctoral thesis at University Michigan USA, dedicated to RF-MEMS devices for multifunction integrated circuits and antennas. Reference [129] by I.V. Avdeev is a doctoral thesis presented at the University Pittsburgh US dedicated to a new formulation for finite element modeling MEMS systems operated electrostatically. The doctoral thesis [130] by Q. Jing, (led by Gary Fedder) is dedicated to modeling and simulation for new designs of suspended MEMS systems. The author develops a procedure for modeling MEMS devices with lumped parameters described in Verilog-A language, which is actually a standard hardware description language (HDL). Reference [131] by C. Pinto Coelho is a doctoral thesis carried out at MIT, under the guidance of Professor Jacob White, devoted to efficient tools for the design and simulation of micro-electromechanical systems and micro-fluidic. Reference [132] by F. Solazzi is a PhD thesis presented at the University of Trento in Italy, on the topic of finding new design solutions for RF-MEMS switches with high reliability for space applications.

An interesting thesis by S. Hannot [133] at Delft University, having the primary goal to present a framework for the numerical solution of electro-mechanical problems based on physical level modeling. The developed framework presents a logical ordering of the available methods for electro-mechanical modeling. The thesis is an extensive one, composed from 4 parts that contain 13 chapters. The first 3 parts concentrate on the electro-mechanical modelling, quasi-static simulation, dynamic simulation and model reduction methods for electro mechanically actuated systems. These are combined in the last part that include also the final conclusions and recommendations.

Part one depicts the electro-mechanical modelling. The basic equations of electro-statics are introduced. An analytical solution can be very useful in the early stages of modelling MEMS devices and to be able to evaluate the numerical modeling techniques. The description of the equations of electro-mechanical coupling are formulated. Here, the author also discuss the well formulating of the problem, the discretization of the equations in 2D and 3D and their solutions including the precautions that should be taken when electrostatic forces are computed.

The second part is dedicated to the quasi-static aspect of electrostatic MEMS, describing the pull-in phenomenon and the load-displacement curve. The author also gives a definition for the pull-in voltage in quasi-static regime as the maximum voltage for which the system is still stable. Numerical algorithm to find these curves are developed and evaluated in chapter 5. In chapter 6 a numerical approach to obtain the design sensitivity of this pull-in voltage is presented, which is used to perform a stochastic analysis to estimate the uncertainty of the pull-in voltage in chapter 7. Stochastic FEM was applied on the pull-in problem for the propagation of thickness and elasticity randomness. This part treats both the uncertainty as well as the reliability of the device. Two scenarios were applied: when the device is small, giving statistically uniform properties and when the device is big, giving statistical properties that are random fields. For each scenario two cases were inspected: when the device is designed to operate below pull-in, hence it fails if the pull-in voltage is too low and when the device is designed to switch, thus it fails if the pull-in is too high.

The third part treats the dynamic simulation. In chapter 8 undamped modelling is depicted: transient as well as eigenfrequency modelling. Also the dynamic version of the pull-in voltage is defined in this chapter. In the ninth chapter the stochastic properties of dynamic pull-in are derived. In chapter 10 a plate model of a micro switch is used to discuss the modeling of dynamics including damping. A FEM model of the Reynolds equation is derived and used to describe squeeze film damping due to gas interaction. The stochastic properties of the damped frequencies are investigated a chapter later. The last chapter of this part is filled with the goal of developing reduced order dynamic models from the very big damped electromechanical models.

The last part of the thesis combines the work done in the previous parts presenting the main goal of the thesis to develop an integrated framework of electromechanical modelling strategies. This was presented in the form of a schematic representation of the relation between the methods derived and discussed in this thesis, presenting a logical order of the available methods for electro-mechanical modelling. The final conclusions end the thesis.

A thesis dedicated to parametric modelling and simulation of MEMS devices using finite element methods and order reduction technologies is [134] authored by V. Kolchuzhin at Chemnitz University of Technology. The general objective of this thesis is to investigate in detail capabilities and limitations of the High Order Derivatives Method (HODM) as a novel approaches for the parametric MEMS simulation. The thesis is subdivided into seven chapters. After an introduction and a short survey of MEMS design and methods developed over the past decade, a brief description of finite element method is given with particular attention to MEMS application. The ROM design framework which implements system simulation of MEMS is summarized.

Computational approaches and challenges in reduced order modelling based on mode superposition method of the coupled electrostatic-structural domains, including nonlinear effects, fluid-structure interactions and packaging effects are presented. The mathematical basis of HODM for parametrization of the overall analysis procedures is described in chapter 3 and implemented using finite element analysis in chapter 4. In Chapter 5 the developed method is assessed on a number of examples in the static, modal, frequency response domains on the basis of the structural, electrostatic and coupled field analysis. The demonstration of the viability of HOD methods for MEMS macro-models generation using a single FE run for ROM data extraction is presented in chapter 6, the automation of the method allows the acceleration of the the generation of macro-models.

The thesis [135] by C.D. Diţă at PUB, is dedicated to the electromagnetic modelling of integrated micro-systems. The thesis is composed of 6 chapters. The first chapter explains the importance of the research in micro-electro-mechanical systems. It describe the main domain of applications and gives a some general notions about modelling and designing these devices. In the second chapter a state of the art is depicted regarding the methods, techniques and technologies used in modelling micro-electro-mechanical systems and in the third chapter the the modelling main steps are described. The thesis presents a method to extract a compact distributed/lumped (TL-RLC-TL) models for RF behavior of MEMS switches.

The main limitations of electromagnetic modelling of integrated micro-systems are

related to computing resources, memory and time needed to obtain the field solution. This thesis investigates different methods to reduce the computational effort, using various approaches and techniques, aiming to obtain, in a small period of time, accurate models to help the designers of integrated circuits. This goal can be achieved using different approaches. In the fourth chapter, strategies and techniques to reduce the complexity of a system before reducing the order of the model is presents. The method used here treats independently the disjoint parts of the problem, solves them and then reassembles the system to get the complete model. The method is effective for the devices that have a homogeneous computing domain in which for the analysis is not necessary to considered all the effects of the field. Simplifying assumptions can lead to a considerable reduction of the computational effort. On the other hand, compared with the problem without partitioning identifying boundary conditions that describe the coupling between sub-domains requires finding interface connector, which basically introduces additional computational effort. This is often balanced by the fast generation of the sub-domains system. For those the analysis takes place in particular regimes of the field (such as EQS, MQS, ES) facilitated by a smart choosing of the connectors. Using FIT to discretize Maxwell equations with EMCE boundary conditions generates an indefinite, non-symmetric and complex matrix, that is very hard to be solved with standard direct or iterative methods. In this case a preconditioning method is imperative.

In chapter 5, the main methods and techniques for a fast and correct extraction of the effective models for micro-mechanical systems are depicted. This chapter also includes specific techniques to reduce the computational effort and methods to reduce the model's order. The advantages of using multiprocessor architectures are discussed. Chapter 6 presents a multitude of study cases of test and real problem validating the results of the research. The main conclusion is that using FIT implies using a direct method to solve the equations system. The direct methods can only be used to solve relatively small problems, under a million of DoFs. To solve a complex problem like the electromagnetic modelling of a micro-electro-mechanical systems a domain-partitioning approach must be used.

1.3 Books about MEMS and RF-MEMS

Due to very high interest in this area, given by the large number of articles published per year, in recent years, books on general aspects of characterization of MEMS and RF-MEMS devices and their applications have been published. There are some of the most complete that have a high quality of information.

The book written by *Rebeiz et al.* [21] is one of the most complete and important books in the field. Although published in 2003, it can be used as a reliable source because it is exhaustive and explains thoroughly how the construction and operation of RF-MEMS devices is made, and describes the existing applications at the time, demonstrating the advantages of these solutions compared with PIN diodes and FET switches. The author describes the main actuation for mechanical and electrostatic capacitive MEMS switches. As the author mentions the book is meant to be "deep". However, the book focus is on

the design of MEMS devices, and not on modelling research. It is a reference book for MEMS device users. After a introductory review, following chapters refer to: mechanics modelling(static analysis), dynamic analysis, electrical modelling, switches made in the world, manufacturing and packaging, reliability, design. Some applications: phase shifters, oscillators, tunable inductors, reconfigurable circuit, noise and future trends are included in the book. The book is consistent, with nearly 500 pages, but its level is not high, even if it has the content information extremely helpful and well presented.

The book written by *Esposito et al.* [136] is a monography, devoted to mathematical modelling of RF-MEMS containing the analysis of partial differential equations that describe the electrostatic operated RF-MEMS devices. In the first chapter, with introductory character, the used equations in modelling these devices are presented. The following chapters focus on actuation voltage problem and assumption of nonlinear elliptic singularities, familiarizing the reader with PDE equations theory, measure theory and functional analysis. The last two chapters focus on dynamic models based on partial differential equations of parabolic type, with linear singularities. *Liu* throughout its book [10], presents simple constructive solutions for the RF micro-switches, classified in terms of movement toward the silicon substrate vertically and horizontally, describing different possible ways of actuation, namely electrostatic, electro-thermal, magnetic. In addition, in one of the chapters, an analytical approach is intended to approximate the elastic constant of the membrane for both bridge and cantilever construction type, based on the fixed-fixed beam and one side fixed beam equations. Parametric formulas are proposed that may include the residual stress from inside the bridge.

Another book is the one by *Lee* [11]. In the introductory chapter the fundamental concepts related to structural and electrostatic models of a bridge and cantilever beams are presented. Chapter 3 describes the resistance of materials needed in the analysis of ordinary micro-switches. This chapter is very useful to understand the behavior of membranes in various applications. In Chapter 4 various constructive solutions are presented. Theoretical aspects related the residual stresses are helpful for understanding the mechanical aspects involved in micro-electro-mechanical switches. Chapter 5 deals with the dynamic response of discrete systems and, in particular defines the quality factor Q. Here the author talks about effective parameters such as the effective mass, damping and stiffness equivalent in mechanical systems. Chapter 6 deals with fundamental aspects of fluid mechanics, modeling squeeze film (gas) phenomena starting with partial differential equations. Chapter 9 is dedicated to electrostatic and magnetic micro-switches.

1.4 Dedicated Software for Modelling MEMS Devices

COMSOL Multiphysics® Modeling Software [137] is a modelling environment for multiphysics problems using finite element method. It has a user interface that allows the description of the geometry of the problem, materials data and field sources, performs the discretization of the computational domain, equations and boundary conditions, solving them, and finally in the post processing step, it allows graphical or numerical viewing of the solution and derived quantities.

The program can solve problems in the area of: electrostatics, electromagnetism, mechanics, fluid flow, heat transfer, chemistry and coupled problems. For MEMS related problems to facilitate the coupling of the phenomena a dedicated MEMS module is provided (`http://www.comsol.com/products/mems/`).

The user has many options for describing the problem and many ways of solving them. A particular advantage of the software is that it enables the coupling with MATLAB from or where can be imported or exported data, results but also equations resulting from the domain discretization. In MEMS module, steady state, transient, modal, parametric, quasi-stationary and frequency analyzes can be perform.

ANSYS Simulation Software [138] is also a modeling environment for multiphysics problems using finite element. The functions provided by this program are similar and in some cases even stronger (for each particular area) than those of competitor software COMSOL Multiphysics®. However the first program that allowed multiphysics coupling was COMSOL.

The application Diagram available in [139] suggestively describes the advanced way in which ANSYS can be used in designing MEMS devices. From here you can see the imported files are .GDS type and that analysis is not only finite element (FEM) but also with boundary elements (BEM) and the process is concluded with reduction order step. The presentation [140] describes a case study where the capabilities of the modeling environment are presented.

CoventorWare is a dedicated environment for modelling micro-electro-mechanical systems using FEM. CoventorWare environment consists of multiple modules, which together provide a complete design software:

- *MEMS+* is the design, simulation and product development part. A friendly interface of the software stands out, adding easy using of the design tools. At first glance it gives the impression of containing a extensive library of parametrized elements from which you can quickly get the item just by changing parameter, it also contains a materials library.
- *ANALYZER* is the part dedicated to the solving of the problem, using tools for meshing the computational domain and the equations based on finite element method applied the model created by *MEMS+* for solving problems of electrostatics, mechanical, thermal, electromagnetic and coupled problems. After simulation, the results can be visualized by using the post processing options. You can also create reduced order models using the results from the finite element method analysis, models that are circuit like in the Spice created using *ARCHITECT3D*. The software allows the extraction of the 2D layout elements. It contains automatic meshing routines with 6 possibilities to obtain the optimal mesh.
- *MICROFLUIDICS* provides multi-dimensional numerical simulations (2-D, 3-D, axisymmetric) of two-phase flow: drops and bubbles, transport and impact. The module uses volume of fluid method (VOF) to model the two-phase flow. The module offers tools for application design and development based on drop generation technology, including solving problems like Drop-on-Demand, continuous jet,

multi-phase flow, steady state fluids and suspended particles in a laminar flow.

- *SEMulator3D* module is ideal for the modelling of semiconductors and also for manufacturing of MEMS devices, noticing errors of the process and optimize the process. Environment gives the possibility to create an animation of the entire manufacturing process.

CoventorWare environment appears to be a complex modelling and simulation software, offering complete solutions in the analysis of micro-electro-mechanical systems, based on the finite element method for solving problems of electrostatics, mechanical, thermal, electromagnetic and coupled problems specific to MEMS devices.

Apart of the three commercial softwares presented which in my opinion are the most complex, dedicated to coupled multiphysics problems there are other commercial and open-source software available dedicated to modelling and simulation of MEMS devices. In [141] some criteria were defined, whose implementation in professional software packages are consider necessary for the analysis, modelling and simulation of multiphysics problems. According to the defined criteria some of the commercial and open-source software are characterized. The intention is to offer certain guidelines for those interested to tackle the field of multiphysics modelling and simulation.

1.5 Conclusions

In this chapter the current state of research in the area of micro-electro-mechanical systems modelling was presented. The chapter is a critical review of the simulation and modeling techniques currently used for designing MEMS devices. Precisely multitude of techniques presented proves that there is no perfect approach. Each has its limitations, whether accuracy is unsatisfactory, either the computing effort for modeling and simulation is too high. Due to the vast information in the MEMS modeling domain the data considered important for this thesis was classified in the 4 categories: articles and communications, PhD thesis and dissertations, books and software, making a study of the publications and prior research from the recent years.

From the multitude of documentation presented, the following references are the most relevant and they influenced in a direct manner the current thesis: [21, 10, 11, 133, 135, 102, 103, 96, 84, 55, 56, 57, 2, 1, 49, 81], because it presents aspects that have been take on and improved in this thesis.

Chapter 2

Theoretical Background of the Multiphysics Modelling

Modelling a device or a real system is a fundamental action of science and engineering, which consists in developing a series of abstract scientific and mathematical images and representations of the modeled object, or digital type-numeric representation of that object [142]. This chapter is dedicated to the multiphysics modelling procedure and formulation of the multiphysics problems that will be analyzed in the following chapters. It is not an original contribution, but a continuation of the results presented in literature, in most parts being a reproduction in ideas from [143, 144] and [145]. Its goal is to identify the theoretical framework of the research developed in thesis, to formulate the kinds of problems to be solved and the types of methods and approaches to be used to solve them.

2.1 Multiphysics Modelling

The representation of an object can be done by several models, more or less accurate. Usually, precise models are more complicated and their extraction and simulation have a higher cost. Choosing the most appropriate model depends on the context and it reflects a compromise between the optimum accuracy and simplicity which are contradictory requirements. A parametric model describes the entire class of real, similar objects. The number of geometric parameter and/or material constants which allows the identification of the instance-object in the class defines the complexity of the parametric model.

Multiphysics modelling is a procedure successfully developed in LMN - the laboratory where the thesis research was developed, which comprises the following main steps to be taken in sequence:

- *Conceptual modelling.* At this stage simplifying assumptions and neglected aspects are decided, from physical and geometric perspective.
- *Mathematical modelling.* This step includes the mathematical description of the model as a well-formulated problem.
- *The approximate analytic modelling.* It is a step that determines the simplified

relationship between the input and output characteristic quantities of the modeled device, in the analytical form, by solving an approximation of the model's equations.

- *Numerical and computational modelling.* It aims to create a dedicated algorithm able to solve the model's equations based on the dsicrete reformulation of the problem, which ultimately determines how the response of the modeled object varies with respects to its excitations.
- *Verification and validation of the model.* In this stage the numerical algorithm is implemented on a computing system. A series of simulations are carried out and their results are virified by subtitution in problem's equations or by comparison with results of numerical simulations based on other solving methods. The model is validated by comparison with the results of experimental measurements.
- *Reduced Order Modelling (ROM).* At this stage, using either discretized - numerical form of the equations or simulation results, simplified parametric models (pROM) are extracted, with an order much lower than that of the system of equations generated by meshing. It is desirable that these parametric models to be as compact as possible and to have an acceptable accuracy, preserving the esssential aspects of the model's behavior.
- *Optimization.* At this stage the compact parametric models are used to identify that device from the parametric modeled class that has the best technical and/or economic characteristics. It is a fundamental engineering activity related to optimal (re)design of components and systems.

Multiphysics modelling of MEMS devices is an important issue, both theoretically and practically. This is because the modelling and simulation of these devices should take in consideration several physical coupled phenomena. The nowadays technology of integrated circuits production as any other productions is unthinkable without a prior modelling, simulation and optimization of the new designed devices.

The design of these micro-electro-mechanical devices that operate at radio frequencies requires effective procedures for modelling and software capable of simulating coupled multiphysics models involving mechanical, electrical, thermodynamic or fluid flow phenomena. Therefor, in the thesis the following *field models* will be considered:

- *Electrostatic (ES) Model* of electric field aiming to calculate the forces acting on the mobile membrane, for its different forms. By using the elastic-mechanical model coupled to ES, the minimum ES actuation voltage/switching of the device will be determined.
- *Mechanical-Structural (MEC) Model*, from which the equilibrium position of the membrane for different actuation voltages and time evolution of its shape under the action of electrostatic forces may be determined. This model will be coupled with the electrostatic model.
- *Aerodynamic (FD) Model*, in which, besides the previous model, the air damping during the membrane movement will be considered.
- *Radio frequency (RF) Model of the EM field*, in which the frequency dependence of

the S parameters is computed and a reduced order, compact circuit model will be extract for the two stable positions of the membrane (closed - DOWN and open - UP).

The advanced physical models may take into account other effects, such as the thermal aspects, the contact between the mobile electrode and the fixed one or residual mechanical stresses in the material of the membrane. The research in the field of RF-MEMS is manly directed to development at a cost as low as possible of effective models with high accuracy with a reduced complexity. Simulation and optimization of these models using computing machines, leads to the development of designs for MEMS devices with the best performance for a specific application.

Even the most aspects of the modelling activity are automated within engineering software environments as COMSOL or ANSYS, a deep understanding of the theoretical ideas and concepts used in software implementation is essential for a readable and efficient modeling activity.

2.1.1 Conceptual Modelling

This is the first stage of modelling, which aims to describe the simplified geometry and physical phenomena. It starts with geometric modelling, describing the structure of modeled object, followed by physical modelling, in which the operating principle is identified and analyzed.

In the *geometric modelling*, the first step is to identify the structure of the modeled object. It is imaginary decomposed into its component parts, identifying their materials, approximating them with simple geometric shapes and relevant characteristic dimensions. Then, the structure of the assembled object is identified, i.e. how the parts are linked and which are the surfaces, edges or points of contact.

The geometry of every object is numerically or symbolically described by using an appropriate reference coordinate systems. Most often, these are of Cartesian type, but other coordinate systems may be used, coordinate of which the most frequently used are the cylindrical and spherical systems. The points are indicated in 3D by the coordinate triplets, curves and surfaces by equations (more exactly the parameters of these equations). The domains having nonzero volume are described usually by their borders. The goal is to describe the complete geometrical structure to a computer, by a so called "*geometrical computational model*".

At this stage of modeling, besides the concrete way through which the description the geometry is made, the most important aspect is the idealization of the real forms. Rough surfaces shall be treated with some perfectly smooth surfaces, the parts of the ideal geometry will be described by a few parameters and several geometric details, which are not essential for the model (as much or assembly details), are removed.

But the most important idealization occurs when we assume that characteristic quantities (data and unknowns) are not dependent on one or several coordinates. Accordingly, this are the following *categories of geometric models* [144]:

- *1D* - model where local quantities depend only on one spatial coordinate, usually a Cartesian system;
- *1.5D* - local model having quantities that depend only on the radius r of a cylindrical coordinate system. Mathematically, it is a one-dimensional model, but physically it is a two-dimensional model. It is a plan-parallel model (along the Oz axis) but also an axisymmetric one (Oz is the axis of symmetry);
- *2D* - model where local quantities depend only on two spatial coordinates, usually the Cartesian system, so this model is called also plane-parallel;
- *2.5D* - local quantities depend only on the spatial coordinates z, r of a cylindrical system, where the model is called axisymmetric (because the quantities does not depend on θ, the model has Oz the axis of symmetry). Mathematically, it is a two-dimensional model, but physically it is three-dimensional;
- *3D* - model having local quantities depend on all three spatial coordinates.

The *computational domain* is the most important aspect of geometric modelling. Most often, the geometric model is limited to a mathematical domain with a finite volume, bounded by a tangible surface (e.g. the casing of the modeled object) or a fictitious one. Many methods of modelling physical fields require that the domain in which they are defined, be a bounded one. Cropping real domain to a computational one that is bordered, is an idealization that must be made in a explicit way. At the end of the modelling, all idealizations should be inventoried in a list of simplifying assumptions, because each of them is likely to generate modelling errors. This list will be of great utility when the causes due to which the model departs from reality will be studied. The list of simplifying assumptions will be used when the possibility to refine the model will be examined, in order to obtain another more precise one.

Physical modelling is performed starting from a qualitative (natural language) description of the functioning of the modeled device. On this occasion, the key physical quantities that describe the state and subject-matter interactions and the causal relationships between them will be identified, thus recognizing physical phenomena underlying its operation.

Once physical phenomena are identified, fundamentals physical laws or relationships they describe are gathered. For multiphysics coupled phenomena local and instant quantities best describe fully the state of the computational domain, represented mathematically by scalar, vector or tensor fields, described by functions versus space and time. In terms of physical fields they are electrical, magnetic, deformations, pressures, speeds, temperatures or other fields. Fundamental equations satisfied by these fields are usually partial differential equations, specific to the domain of physics to which they belong: electromagnetism, continuum mechanics, thermodynamics, etc. They are general, conservation or constitutive (material description equations). Particular attention should be paid to the relationships that describe the coupling between different domain (transfer relationships or connections) and those of energetic nature.

A significant step in physical modelling is the analysis of how local quantities varies in space and time. The first determines the spatial dimensional (1D-3D), while the way in

which it is assumed to variate over time determines the operating mode (also of the field) and the type of later simulations. Most often the following regimes are considered:

- *Static/Steady-state*, where quantities do not depend on time (or the effects of this dependencies are neglected);
- *Harmonic*, quantities have a sinusoidal variation versus time, with the same frequency f (that regime may be encountered only in linear systems);
- *Periodical*, the quantities having a periodic non-sinusoidal variation in time, with the same period T;
- *Transient* variation, were quantities do not have a specified time variation in the interval of interest (*0,* t_{max}).
- *Modal* analysis, which seeks the eigenmodes of oscillation, which can occur in some structures after canceling excitations.

In each of these regimes, physical fields have different equations. These equations contain beside the solution fields, material constants and what is most important, field sources, described by local or global quantities. In many cases they are physical quantities of domain with which the field is coupled.

It appears that in some cases, various sub-domains may encounter different regimes of the field. They should be identified with particular attention because they can be a valuable resource for reducing the complexity of the extracted model.

The description of the phenomena can be done using different forms of the fundamental equations, for example: integral, global or variational forms, according to the requirements of the most effective method used for solving the problem. The main goal is to identify all physical aspects (such as local state, field sources or material behavior) related to the further mathematical formulation of the problems, when physical quantities became mathematical objects and the relationships became mathematical equations.

In many cases the fields sources are not only internal, so there are not only described by local physical quantities, defined in the computational domain (spatial in Cartesian product with the time interval), but they can be external for the computational spatial domain or prior to the analyzed transient regime. These external sources are described by using boundary conditions and initial conditions respectively. At this stage of modelling all sources which influence the solution of the problem should be identified, namely the variation in time and space of modeled physical fields.

The main objective of the physical modelling stage is to identify the *physical regime* of each field, the sources of these fields and highlighting the coupling relations, i.e. the transition from a qualitative, phenomenological understanding towards a quantitative one. This step should be concluded by listing the adopted simplifying assumptions. Each assumption (neglected phenomena or effect) should be justified and if possible, the quantitative effect of its adoption should be estimated.

Nowadays problems do not involve only physical processes covered by a single traditional discipline. Complex systems encountered in all advanced applications involves

many distinct physical processes. Because they are interdependent, the key term to describe the new multiphysics paradigm is "the coupling" between several problems, which up to now were approached independently.

Coupling models of different events at different scales and governed by of different physical laws is an enormously challenging area for future research. The coupled computer simulation is not quite new, it is based on the traditional "divide-and-conquer" paradigm. However, coupling individual simulation may introduce limitations in stability or accuracy. Moreover the data conversion required for coupling may generate a surprising overload cost. Thus "one plus one" may be more expensive than "two"', making process less more scalable than expected [145].

Non-biased analysis of coupling may reveals new opportunities for leveraging successful approaches and software across physically disparate disciplines and identifying the gap of understanding which limits the advances. Multiphysics coupling is often approached bottom-up as assembling of individual components, single physics being described by diagonal blocks and coupling as additional off diagonal data in the matrix of the equations system to be solved. This paradigm has its limits, and is recommended examining coupling strength before decoupling [145].

The usage of the term "*multiphysics*" has been often used liberally during the past years by various researchers. However, it has been used in more than one undeclared contexts not always allowing the occasional consumers of the term to be able to isolate the meaning intended by the originators of the term. Some of the frequently attributed meanings of the term have been those of: "*multi-field*" to denote the simultaneous excitation and response of the system by multiple physical fields; "*multi-domain*" to denote the interaction among continuum representations of systems with drastically different properties (e.g. Fluid-structure interaction, moving solidification boundary problems e.t.c.) through sharable boundaries; "*multi-scale*" to denote the consistent bridging of various behavioral models of the system at hand, at various length scales as required by a multitude of scopes ranging from manufacturing process perspective to macro-behavioral utilization. In addition, any combination of these three semantic possibilities generates four more meanings of the term "multiphysics" including the one that reflects the co-existence of all three of them [146].

This suggests the definition of a *conceptual attribute space* (Fig.2.1) spanned by the three basis attributes namely, "*multi-field*", "*multi-domain*" and "*multi-scale*". All other cases for the potential meaning of the term "*multi-field*" are embedded implicitly in this space and can be thought of as linear combinations of the three base-cases. In addition, the "*multi-field*" and "*multi-domain*" bases are endowed with a measure defined in terms of two discrete increments for "one" and "many". The "*multi-scale*" base is similarly endowed by a measure defined in terms of the discrete increments in the term set "nano", "micro", "macro" roughly corresponding to applying these as prefixes to the term "meter" when used as a length unit [146].

Any discrete volume in this discrete space as shown in Fig.2.1, is defined by a triplet of coordinates originating from each one of these attribute axes, and represents a region encompassing certain classes of physical problems. This signifies that these problems can

be modeled in a multiphysics sense as defined by their corresponding coordinates [146].

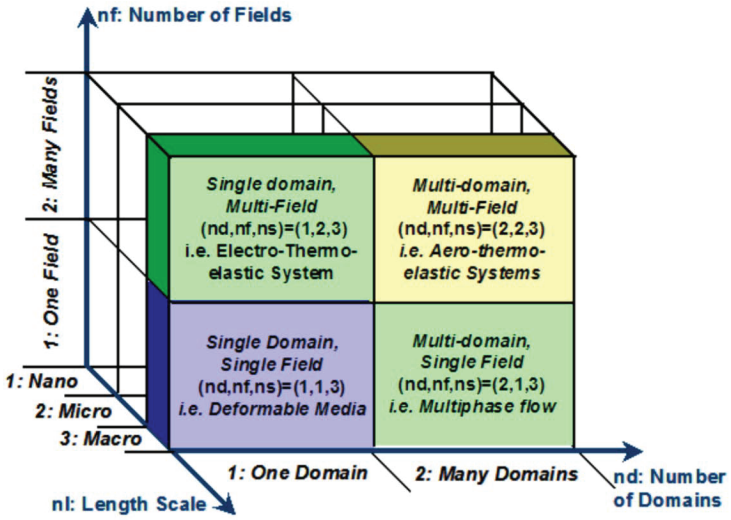

Figure 2.1: Multiphysics attribute space [146].

A *coupled problem* is one in which physically or computationally heterogeneous components interact dynamically. The interaction is multi-way in the sense that the solution has to be obtained by a simultaneous analysis of the coupled equations which model the problem. It is obvious that the "coupling" is the key word in the multiphysics approach.

A coupled multi-field problem is one in which the individual field equations are depend on the other field variables governing the problem which requires the simultaneous treatment of multiple dependent fields in a model. Every coupled problem is *per se* a coupled multi-field problem.

A coupled multi-physics problem is a coupled problem which handles simultaneously multiple physical models or phenomena. That is, if different discretization techniques are used for individual sub-problems on different (possibly coinciding) spatial domains or individual field variables represent distinctly different but mutually interacting physical phenomena. A coupled multi-field problem is not *per se* a coupled multi-physics problem.

Coupled problems are, in contrast, characterized by the immanent interaction of essentially different physical phenomena within the same spatial domain (e.g. electrical and mechanical interaction). In fact, the coupling is inherent in the governing balance relations specified by some constitutive laws describing the different physical phenomena. In the case of two problems, they can be unidirectional or bidirectional coupled (Fig.2.2), while in the multiple problems we have multiple (acyclic) unidirectional couplings and bidirectional (cyclic) couplings(Fig.2.3). These couplings are described by an oriented graph, called the coupling diagram. An appropriate example for cyclic couplings is the multiple connected Electro-Magnetic Circuit Element (MEMCE) presented in Fig.2.4, solved by Domain Decomposition.

The coupling strength is commonly classified from *weak* or *loose* to *strong* or *tight* depending on the degree of subsystem interaction [148, 149]. A coupling is regarded as strong if the solution depends significantly on the accuracy of the coupling term calculation. In this connection, the course of interaction yields an additional indicator, where

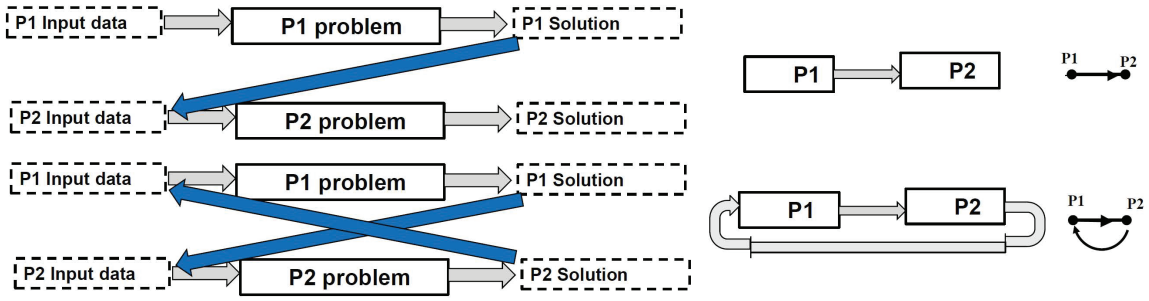

Figure 2.2: Unidirectional and Bidirectional coupling in the case of two problems [145].

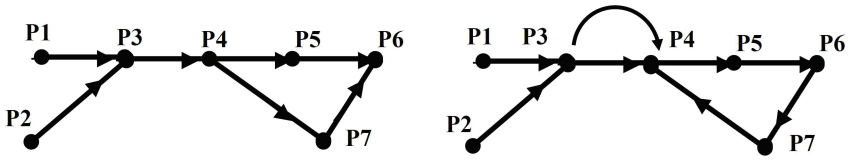

Figure 2.3: Unidirectional and Bidirectional coupling in the case of multiple problems [145].

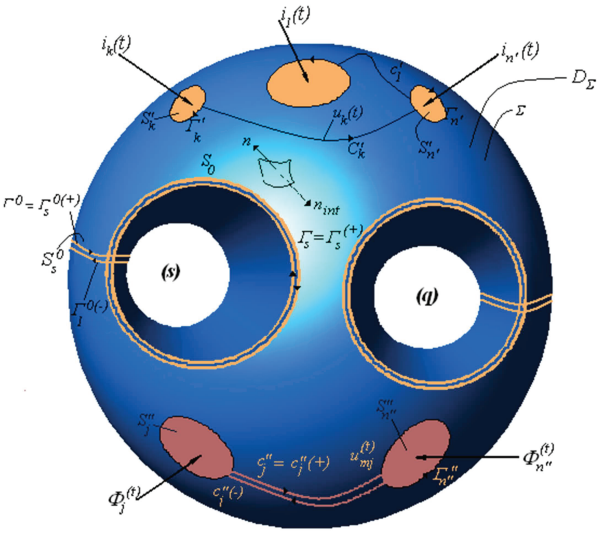

Figure 2.4: The multiple connected Electro-Magnetic Circuit Element (MEMCE) [147]

one-way coupling is considered as weak, for instance, between a thermal field and a structure, and two-way or multi-way coupling is considered as strong, such as in general FSI problems, because the overall state, in contrast to the former, has to be simultaneously updated over interacting subsystems. From a computational perspective, this biases the choice of a convenient combined method by which the individual time-discretized subsystems are algorithmically coupled. For instance, explicitly using some staggering scheme in the weak case and implicitly applying a direct monolithic or an iterative partitioned approach in the strong case[148].

However, to distinguish between weak and strong coupling, even on a numerical basis, is a very subjective classification which depends on the type of coupled problem as well as the physical properties and inter-dependencies controlled by the involved constitutive parameters. Especially, if non-linearities come into play, such that material parameters non-linearly depend on the primal field variables, the strength of coupling may change during the solution of the problem[150].

However some authors as [145] makes difference between: *Strong* (S) versus *Weak* (W) coupling of physical models: intrinsic interaction between natural processes. The off-diagonal blocks in Jacobian matrix which describes the coupling are full and/or large and *Tight* (T) versus *Loose* (L) coupling of numerical models: which describe how the state variables of several computer/algorithmic constituent (sub)models are synchronized in concurrent simulations. In tight coupling, they are as synchronized as soon as possible, across different models at all times. As consequence, any of four combination (ST, RL, WT, WL) may be encountered.

2.1.2 Mathematical Modelling

This step aims to formulate the problem solely in mathematical terms and verify if the problem is well formulated. Usually a direct problem is encounter, which in its original form would require the solving of a system of partial differential equations with appropriate boundary conditions. For a simple checking of the correct formulation conditions implies reformulation of the original problem in an equivalent one from one or several points of view. Typically, this involves passing from the strong form of the differential equations to their weak form (also called the variational form). This involves, mathematically, a profound transformation of the problem, especially because the solution is no longer a classic function. It is substituted by a generalized function. Consequently, classic mathematical analysis is no longer sufficient and aspects of modern mathematics are needed e.g. functional analysis applied to the partial derivative equations, and therefore to the spaces of functions such as the Lebesgue square-integrable, generalized derivative, Sobolev and/or distribution. The problem reformulation from strong to weak form has a series of advantages, from mathematical point of view, facilitating the proof of several theorems and the developing of several numerical approaches. It is illustrated in details in [142, 151].

A fundamental aspect of mathematical modelling is to set up the *functional framework*. Without it, a proper formulation of the problem to be solved can not be described

in mathematical terms. The list of the main categories of input data of the problem, describing "*what is given*" includes:

- **Data referring to the computational spatial domain** describing in mathematical terms its shape and dimensions, without any ambiguity. Independent parameters should be identified at the beginning. Others parameters will be expressed in terms of these independent parameters so that scaling can be done easily for any model. For this, computational geometry tools are typically used (paramount in Computer Aided Design - CAD/CAE and solid modelling), [152, 153, 154];
- **Data describing the behavior materials** in any point of the computational domain. Linear materials are described by real numbers (material constant if they are anisotropic) or real tensors (if they are anisotropic). Consequently, in this case they are scalar or tonsorial fields, defined over the computational domain. Their number and of course their physical meaning (e.g. permeability, permittivity, conductance, etc.) depend on the field regime. The nonlinear materials are described by their characteristic functions (e.g. magnetization characteristic) or by more complex models as in the hysteresis case. It appears that in most practical problems, the computational domain is composed from a finite number of homogeneous subdomains, so to characterize the behavior of materials from the entire domain a finite set of real numbers is sufficient;
- **Internal field sources**, for any point of the computational domain. Consequently they are scalar, vectorial or tonsorial fields, defined over the computational domain. Sometimes they are included in the material characteristics;
- **Boundary conditions**, data which describes the effect of the field's external sources. They have to describe any existent field source but to not over-determinate the solution. They need to be known in any point on the boundary, for any point of time and for the entire time range of the simulation (for some particular problems they may be global quantities);
- **Initial conditions**, for transient simulations, they describe the initial state of the system generated by its evolution in the time period precedent to the modelling interval.

The unknowns are the field components, local physical quantities are represented mathematically data using function defined over the entire computational domain (spatial and temporal). These data describes "*what is required*" in problem analysis. The problem is completely formulated by adding to the previous described input and output data, *the relationships (equations) satisfied by the solution*, together with the appropriate boundary and initial conditions.

Several *fundamental equations* are used to describe the different physical fields [145]. For electromagnetic field these relationships are Maxwell's equations [155], stress/strain fields of elastic bodies are described by the equations of motion and deformation [156], the fluid fields are described using Navier-Stokes equations [157] and temperature fields are described by Fourier equation [158]. They will briefly detailed later. As we may see they are PDE and under simplified assumptions, in the case of discrete circuits (networks) with

lumped parameters, they became ODE. To highlight the non-electromagnetic effects of electromagnetic field and therefore the coupling between several disciplines, other relations or formulas should be added that describe thermal effects or mechanical fields, such as Joule, Lorentz, Ampere, the Maxwell stress, generalized forces expressions, etc. These relationships define the derived quantities of the problem (computed quantities using the main unknowns, which are scalar or vectorial components of the field or potential). Multiphysics field equations do not remain in their general form, but they are customized according to geometrical degeneration (0D - as in the circuits approximation, 1D - threads, medium fibers beams, 2D - plates, etc.) or field regimes. As it was mentioned before, often, this relationships are reformulated in equivalent forms, which are more convenient for solving, such as integral, variational or weak forms (which are actually a integral consequence of differential equations).

The fields analysis problem described above is the issue covered in the case of *simulation*. As to the *modelling*, another more complicated problem have to be formulated, which has to identify and describe how the output signals (system responses) depend on the input signals (system excitation = field sources) for a known initial state. We find, therefore, that modeled device equations must be restored to the equations of an input-output system, so as to describe in mathematical terms the causal relationship that occurs between excitation and response signals. For this the system's inputs and outputs must be identified, that are often global quantities, defined on the boundary of the computational domain. The input intervene in the description of the boundary conditions. The mathematical expressions have to describe in a precise manner the physical reality, characteristic phenomena and their relationships.

In many situations, the computational domain is decomposed into disjoint sub-domains, each being defined as an input-output subsystem. The system corresponding to a sub-domain can be further decomposed into subsystems corresponding to partial separation of the different physical aspects: electrical, mechanical, thermal, etc. All these subsystems are coupled together through interfaces (common boundaries of the sub-domains), or common physical quantities that describe multiphysics coupling. These can be parameters of materials (which depend on the field from another physically domain, for example electrical conductivity depends on temperature), field's internal sources (for example, power dissipation, the free term of the heat equation depends on the current density, through Joule relation) or boundary conditions (for example, the surface temperature of the solid depends on the temperature and velocity of the fluid outside the body). It follows therefore a interconnection of the subsystems defined separately by decomposition in domains (spatial or physical) to finally get the global model. Decomposition in sub-domains can be successfully exploited to generate performant modelling and simulation procedures, for example some suited for multiprocessor computers. It has also the advantage that encapsulates each sub-domain modelling, which enable a more simple development, hierarchical, independent, for each sub-domain and therefore more flexible computer objects (algorithms and data structures).

The decomposition in physical or geometric domains, highlights another aspect, namely the *type of coupling between fields*. If an area influences an other but not vice versa, we say we have a one-way coupling, otherwise the coupling is bidirectional. If equations in a

domain must be solved simultaneously (direct or iterative) with those of other domain, we say we have a strong coupling otherwise, even when equations at a time can be solved separately, we say we have a weak coupling. The coupling between several (sub)components of the multiphysics problems is described by a *coupling diagram*. It essence it is an oriented graph having (sub)problems as nodes, their edges describing interdependences. Basically there are there *types of coupled* (sub)systems [145]:

(a) systems within a shared spatial domain;

(b) systems coupled by means of their interfaces;

(c) at least one coupled (sub)systems is a network.

Let consider for simplicity only two fields, and their fundamental problems of field analysis: Problem P1

- Spatial domain D1,
- Material parameters M1,
- Internal field causes C1,
- Boundary conditions B1,
- Initial conditions I1;

and Problem P2

- Spatial domain D2,
- Material parameters M2,
- Internal field causes C2,
- Boundary conditions B2,
- Initial conditions I2.

A system P2 is coupled (controlled) if it has the input data of its fundamental problem of field analysis dependent by the output results of other (control) problem P1 (Fig.2.3). So the couplings may be realized by:

- Domain shape and size (P1 may change the domain of P2);
- Material parameters (of P2 are influenced by P1 solution), it is of type a);
- Internal field sources (P1 domain is includes strict or not in the domain of P2, and the solution of P1 describes the sources of field in P2), type a);
- External field sources, boundary conditions (the coupled problems share a part of their boundaries, there is an unidirectional or bidirectional influence between the b.c. of P1 and P2), including type c) couplings, e.g. ECE;
- Initial conditions (solution of P1 influence the initial values of P2), it is of type a).

We can imagine 5 uni- and 10 bi-directional *simplest couplings*. Each table entry may be influenced by the solution of the other problem. In the real systems they may

be combined. Solutions of two problems are S1(D1,M1,C1,B1,I1); S2(D2,M2,C2,B2,I2). They are coupled if there is at least one nontrivial interdependence:

- S1(D1(S2),M1(S2),C1(S2),B1(S2),I1(S2));
- S2(D2(S1),M2 (S1),C2 (S1),B2(S1),I2 (S1)).

These interdepnedences should be identified and described just form the beginning of the formulation of the coupled problem. It is an essential step in the multiphysics problem formulation.

The *correct formulation* of the problem to be analyzed involves following three conditions [159]:

- **The existence of a solution** – for any excitation of a class of functions, the problem must have a solution;
- **The uniqueness of the solution** – the analyzed problem must have a single solution;
- **Well-conditioning of the problem** – the solution depends continuously on the problem data, small deviations of data do not generate excessive deviation of the solution (to solve the problem, the error will not increase excessively)

According to [160], this called a well-posed problem (in the Hadamard sense). This three conditions should be satisfied by any elementary problem related to a field, but also by the coupled problem, as well as by the problem resulted after the numerical discretization.

An analysis problem involves the solving of a set of equations that can be written generically as an implicit relationship often under the symbolic form $F(x) = y$, where $x \in X$ is the solution, $y \in Y$ is the known data (the right term of the equation) and the mapping $F : X \to Y$ is the equation to be solved. A well-formulated problem should guarantee that for every y in Y there is x in the solution space X that verifies the equation, and that x is unique. It appears that these are the very conditions that the mapper F may be reversed (i.e. it is bijective). Consequently, F must be surjective and injective. *Injectivity* condition is given by the theorem of uniqueness of the solution, and the *surjectivity* is given by the theorem of existence.

In addition, a third condition must be fulfilled, the *continuity of the inverse* F^{-1} of F, which links data to solution [161]. Consequently, the two spaces X and Y must not be only *algebraic* but also *topological* (to be able to talk about continuity, time, distance, convergence, etc.). The convergence is important because many existence theorems are demonstrated constructive (e.g. by using the fixed-point theorem) and they underpin iterative type numerical algorithms, were a series of numerical solutions is built, approximation that converges to the exact solution. That is why, the well formulated conditions can not be submitted without the exact specification (mathematical) of the space where the solution will be searched and the space where the data are placed. These are definition spaces, having therefore a space vector structure (possibly affine) but have also a topological structure (usually Banach or Hilbert spaces because they are complete and therefore any Cauchy sequences are convergent).

If F is a *linear operator*, things are simplified because the uniqueness is ensured (equation has unique solution for any $x \in X$), if the homogeneous equation $F(x) = 0$ has only the trivial solution $x = 0$, i.e. if the kernel of F operator is reduced to zero. In the particular case of the finite dimensional F is represented by a matrix $\mathbf{F}$, which should have null kernel. This implies there are no null eigenvalues. In order to exist a solution, the free term should belong to the image of matrix $\mathbf{F}$ (if $\mathbf{F}$ is square matrix the uniqueness condition for the solution of the linear system of equations is equivalent to the existence one).

To characterize quantitatively how well a problem is formulated in the Hadamard's sense, its *number of conditioning* denoted by $\kappa(\mathbf{F})$ is used. This expresses how big can be the relative errors of the solution, reported to errors of data [162]. In the case of linear finite dimensional matrix $\mathbf{F}$ conditioning number is $\kappa(\mathbf{F}) = \|\mathbf{F}\| \cdot \left\|\mathbf{F}^{-1}\right\|$, equal for symmetric and positive definite matrices with the ratio between the maximum and the minimum eigenvalues of the matrix $\mathbf{F}$. When the amplification factor is large, the problem is badly conditioned and it is more difficult to solve using either direct or iterative methods, the larger is his conditioning number, the weaker is the convergence to solution, which at the limit may diverge.

For well formulated problems, the continuity condition actually is expressed in mathematical terms as a stronger condition: there exist a real constant L, so that $\left\|F^{-1}(\mathbf{u}) - F^{-1}(\mathbf{v})\right\|_X \leq L \|\mathbf{u}\text{-}\mathbf{v}\|_Y$ for any $\mathbf{u},\mathbf{v} \in Y$, called *Lipschitz's condition*. In the linear case, the Lipschitz constant L is proportional to the number of conditioning of the problem $\kappa(F) = L \|x\| / \|y\|$. With this condition, with reasonable values imposed to the conditioning number of the problem, that is dependent on the accuracy which is considered acceptable , the problem is well formulated.

In conclusion, it appears that there can not be mathematically correct formulation of the problem unless are identified the spaces Y and X, where the solution is search and where the problem data can be found. In mathematical modelling this fundamental operation is called *establish the functional framework* of the problem. They are very close related to the weak formulation of the problem. Even if the things simplifies, and in practice some steps of the mathematical modelling are bypass, the uniqueness theorem can not be waived. The boundary conditions must be checked so that they ensure the uniqueness of the solution. As can be seen from the weak formulation, boundary conditions may be essential or natural [142], but both are equally important. Neglecting this step can cause serious modelling errors.

2.1.3 The Approximate Analytic Modelling

Once the problem has been well formulated, the next step is to solve it; but in the case of real applications this is not a very simple task, mainly due to the geometric complexity of the modeled devices. Therefore it is advisable to define at first a simpler version of the problem, which can be solved by analytic methods. To achieve this objective, additional simplifying assumptions are considered, which are usually quite far from being satisfied in reality. But even if this approach is a coarse approximation of the reality, the presence of analytical solutions is of great help to validate the numerical solution and to understand

how the solution depends on several input data. Most often analytical solutions are obtained by using a highly simplified geometric modeling. The simplest case is obviously 1D, but analytical approximations for 2D may be relevant as well.

In terms of time variations, the first thing to try is to find a *steady-state solution*, that is useful also for the dynamic study, of transient regime, to identify the permanent initial and final state. If a harmonic solution is needed, the most effective solution is determined by *complex representation*. Also in operational form, obtained by *Laplace transform*, the transient analysis is carried out in frequency domain. Obviously, these techniques can be applied only if the system is linear. If the system is nonlinear, then the only solution is to apply *linearization*, operating with only minor variations around a stationary solution. Perturbation methods are often used for finding an approximate solution to a problem [163].

The solving of the equations describing a simplified model analytical solution, can be carried out either by hand or calculations, using either *MAPLE* or equivalent package from *MATLAB* symbolic or *MATHEMATICA*. *SciLab* has a strong support for symbolic calculations on polynomials and rational functions. The 2D stationary fields equations are in the most cases elliptic type equations with (generalized) Laplace operator, as it happen also in dynamic regimens after operational or complex representation. They have Dirichlet [164] and Neumann [165] type boundary conditions and in 1D they are Sturm-Liouville [166] type equations with bilocal boundary conditions.

A method to find analytical solutions to these kinds of equations is to approximate the spatial derivatives by *finite difference method*. Thus a discrete system with a relatively small number of degrees of freedom is obtained, which approximates the analytical solution. Finally a system with lumped parameters it is built, unlike the original system described by distributed parameters [167].

Another approach is to determine the analytical solutions with distributed parameters system by integrating differential equations with bilocal boundary conditions, in 1D case, or by the separation of variables method or complex representation in 2D case [168, 169]. Such techniques are applied, for example, when some electromagnetic problem is solved by *transmission lines method*. After obtaining analytic solution by manual or symbolic means, a graphical representation of the result is usefull as well as the sensitivities analysis, by deriving (manual or symbolic) the obtained expression.

Analytical solutions are ideal for building *equivalent electric circuit models* with lumped parameters, which can then be analytical or numerical analyzed, e.g. by *Spice*. For graphics, but even for numerical simulations of the model with lumped parameters, the most efficient way is to use *MATLAB* (possibly with *Simulink*). An alternative would be a description of the model in a hardware description language such as *VHDL* or *VERILOG*, which can be simulated in *SPECTRE* from *CANDENCE* [170].

The circuit models which are build based on the analytic approximations are called *compact models* and they are intensively used in the design procedures, being preferred by the designers due to their simplicity and flexibility.

2.1.4 Numerical Modelling

In the case of complicated geometric structures and configurations more accurate solutions may be obtained by numerical approaches, based on using computers to evaluate an approximate solution. Several approaches are available, of which the most important being described in this section.

Various numerical techniques are applied today to model transient wave fields in acoustics, electromagnetic, and elastodynamics, as well as coupled effects there of: for instance, the Finite-Difference (FD), Finite-Element (FE), Finite-Volume (FV), Finite-Difference Time-Domain (FDTD), Finite-Integration(FI), and Finite-Volume Time-Domain (FVTD) Methods, as well as the Micro-cell Time-Domain (MCTD) Method, which is an extension of the cell method as well as Boundary Element Method (BEM), Integral equations (IE), Method of Moments (MoM), etc.

2.1.4.1 Finite Element Method (FEM)

In FEM an unstructured mesh consisting of simple shapes such as triangles, quadrilateral, tetrahedra, hexagon, etc. is used to mesh the computational domain. The weak form of the field equations is discretized and a system of ODE (Ordinary Differential Equations) is generated by projection on the finite dimension space of base (trial and/or test) functions. It is a system of real algebraic equation in the steady-state case (it is complex in the case of harmonic problems). These systems are solved by numerical (directe or iterative) methods in order to build the numerical solution. Usually, their solutions (DoF - Degree of Freedoms) are the unknowns related to the mesh elements (e.g. mesh nodes or edges). The FEM solving procedures is detailed for several regimes of EM, MEC or FD fields in reference books such as [171, 142, 172]. To illustrate the presentation, let consider the static case.

The finite element (FE) analysis of any field problem involves the following steps [173, 174]:

- discretization of the spatial domain of the problem in a finite number of elementary sub-domains of simple shapes;
- choosing the type of variation of numerical solution in a typical element;
- assembly the contribution of each matrix element and right hand side term of the system, by using the week form of the equations;
- solving the linear algebraic equations system.

In FEM, in the most cases, the weak variational form, of Galerkin type is used. The strong problem F(v)=y, usually an elliptic (e.g. Poisson) PDE reformulated so [142]: find $v \in X$ so that $a(v,u) = f(u),\ \forall u \in X$, where X is a Hilbert space where the solution v is searched. $a(v,u)$ is a bi-linear function, "of energy", and $f(u)$ is a linear functional that represents the field sources. The advantages of this approach are that the f functional represents also the natural boundary conditions, while the forced boundary conditions are set by the X space definition.

Lets consider, for example, the simple case of the Poisson type equation:

$$-\mathrm{div}(\varepsilon \mathrm{grad} V) = \rho \tag{2.1}$$

satisfied by the scalar electrostatic potential V in the computational domain Ω, with boundary conditions of Dirichlet type $V = f_D(P)$ for $P \in S_D$ part of the Ω boundary and Neumann type $\mathrm{d}V/\mathrm{d}n = f_N(P)$ for $P \in S_N = \Omega - S_D$. In this case H is the space of all square integrable function L^2 on Ω with the generalized derivative of square integrable on Ω and that satisfy the Dirichlet type boundary condition $V = f_D(P)$ and

$$a(U,V) = \int_\Omega \varepsilon \mathrm{grad} U \mathrm{grad} V \mathrm{d}v; \quad f(U) = \int_\Omega \rho U \mathrm{d}v + \int_{S_D} f_N \mathrm{d}A \tag{2.2}$$

After meshing, the approximate, numerical solution of the problem is search in a finite dimensional space, denoted X_h, and if $X_h \subset X$ then the discretization is conform, reducing the problem to be solved at:

$$\text{Find } v_h \in X, \text{ so that } a(v_h, u_h) = f(u_h), \forall u_h \in X_h \tag{2.3}$$

that is a linear algebraic equations system. The h parameter is used to describe the norm of the mesh. If $h \to 0$, then the numerical solution converges to the real solution.

Galerkin method is based on the possibility of going from continuous to discrete by choosing test (v) and trial (φ) functions. The finite dimensional spatial elements X_h are expressed by linear combinations of base functions also called shape or interpolation functions (test functions = trial functions) $\varphi_1, \varphi_2, \ldots, \varphi_N$,:

$$u_h = \sum_{i=1}^{2} u_i^h \cdot \varphi_i, \tag{2.4}$$

where u_i represent the DoFs of the problem (FEM unknowns). In the simplest case (of the first order - nodal elements), the base functions are polynomials of first degree and DoFs are the values of the numerical solution in the nodes (triangle vertices).

Replacing u_h in (2.3) yields:

$$\mathbf{A} \cdot \mathbf{u} = \mathbf{f} \tag{2.5}$$

where $u = [u_i^h] \in \mathbb{R}^N$, the system matrix $\mathbf{A} = [a(\varphi, \varphi_i)] \in \mathbb{R}^{N \times N}$ is the so called rigidity matrix, and the right hand side vector $\mathbf{f} = [f(\varphi_j)] \in \mathbb{R}^N$ is the sources vector. N is the number of DoFs equal to the number of internal mesh nodes plus the number of nodes on the S_N - with natural boundary conditions.

For the sake of simplicity, let consider the 2D case, with $d = 2$. When choosing a triangle as a reference for the finite elements method, a fundamental assumption is that material properties be uniform for every finite element $K \in \tau_h$. The triangle has a great advantage is a simplex figure, and it is a shape that can follow easily the contour of the border of the computational domain Ω. Using bijective, continuous and differentiable transformation $\phi_k : \hat{K} \to K$, the reference element $\hat{K}$ is transformed in a physic element (Fig.2.5), linking the reference element coordinates $\hat{x}$ and the ones of the physic element

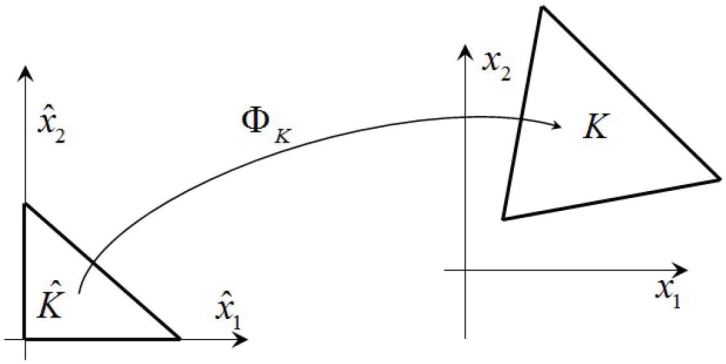

Figure 2.5: K Element [142].

$x = \phi_K(\hat{x})$. In the simplest case, the physic and reference elements having similar shapes, ϕ may be an affine transformation:

$$\phi_K(\hat{x}) = B_K\hat{x} + b_K \tag{2.6}$$

where $B_K \in \mathbb{R}^{d\times d}$ and $b_K \in \mathbb{R}^d$. Consequently, in this case , the physic element is obtained from reference element by translation, rotation and/or scaling,which allows its mapping on any triangle of the mesh.

Assembling the system matrix is the central part of FEM. This is done in a loop that goes through each element of triangulation τ_h, its contribution being added to the stiffness matrix ($\mathbf{A}$) and the right hand terms vector ($\mathbf{f}$), yielding:

$$\mathbf{A} = \sum_{K\to\tau_h} (\mathbf{C}^K)^T \mathbf{A}^K \mathbf{C}^K, \tag{2.7}$$

$$\mathbf{f} = \sum_{K\to\tau_h} (\mathbf{C}^K)^T \mathbf{f}^K, \tag{2.8}$$

where $\mathbf{C}$ is a topological matrix that describes the relationships between the local and global DoFs. The base functions chosen in FEM have null values for the current element $K \in \tau_h$ and the one adjacent to this, resulting that $\mathbf{A}$ and $\mathbf{C}$ are sparse matrices.

2.1.4.2 Finite Difference Method (FDM)

FDM or its variations, such as finite volume method (FVM) or finite integral technique (FIT), uses a regular topology network, lattice (tensor product of 1D networks) to discretize the computational domain. In the case of FDM, the differential form of field equations is discretized by finite difference method. Whereas in the FIT case, there are discretized the global form or the field equations. These methods are detailed in the reference books such as [175, 176].

As in the previous FEM case, we will illustrate the application of the numerical method only in a very simple study case. The method is quite simple to define and implement, especially in rectangular computational domains with uniform grids (Fig.2.6). In these cases, the resulting matrices are well structured and sparse. Discretization of the ordinary or partial differential operators is achieved by polynomial function approximation that

can be easily derived. Using Newton polynomial interpolation method for the nodes of the mesh, the derivative's value in one of the nodes it is estimated. The expression of finite difference which is a linear combination of function values in nodes is used as an approximation to the exact value of the derivative of the function. Depending on how the derivative is estimate with regard to the interpolation nodes, it can be distinguish: progressive, regressive and centered differences. Using Taylor series expansion, it can be proven that the accuracy of the first two formulas (progressive, regressive differences) is of $O(h)$ order and the centered difference is of $O(h^2)$.

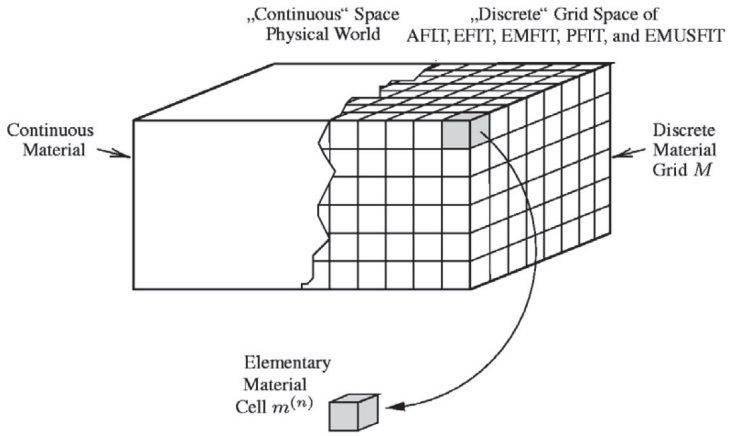

Figure 2.6: A discretization of the material in elementary material cells $m^{(n)}$, defining the material grid M [177].

Taking for example the Poisson equation with Dirichlet boundary conditions, and the 2D Laplace operator:

$$\Delta = \frac{\partial^2}{\partial x_1^2} + \frac{\partial^2}{\partial x_2^2}, \tag{2.9}$$

for a discretization step h_1 for x_1 and h_2 for x_2 it can be approximated using centered differences as

$$\begin{aligned} \Delta u(x) = &\frac{u(x_1 + h_1, x_2) - 2u(x_1, x_2) + u(x_1 - h_1, x_2)}{h_1^2} + \\ &+ \frac{u(x_1, x_2 + h_2) - 2u(x_1, x_2) + u(x_1, x_2 - h_2)}{h_2^2}. \end{aligned} \tag{2.10}$$

If the computational domain is a rectangle with the sides l_1, l_2, both intervals are discretized using $n_1 + 2$ and $n_2 + 2$ points, then:

$$h_1 = \frac{l_1}{n_1 + 1} \text{ and } h_2 = \frac{l_2}{n_2 + 1}. \tag{2.11}$$

Consequently applying (2.10) in all internal grid-nodes is obtained a system of sparse linear equations. Its solution give the numerical solution of the Laplace equation with Dirichlet boundary conditions.

2.1.4.3 Boundary Element Method (BEM)

Also known as the method of moments (MoM) or the method of the integral equations (MIE), BEM uses a mesh only on the boundary of the domains or on the interfaces

between homogeneous subdomains. Usually this mesh is non-structured. In this method, the integral form of the field equations is discretized. Reference books in which this method is detailed are [178, 179, 180, 70].

If the computational domain has, for example, two dimensions, square shape, with each side meshed in n segments, then the "volume" methods such as finite differences (FDM) and finite element (FEM) have the number of unknowns of order n^2, and because the equations system of matrix is sparse, it has from $5n^2$ to $9n^2$ nonzero elements, whereas in case of BEM, only the values of the solution on the four sides of the square is considered, so the system has only $4n$ unknown (Fig.2.7). Given that n is very large, since BEM system matrix is full, with $16n^2$ nonzero elements, the difference between BEM and FEM or finite differences methods, regarding the size of the system, greatly increases. So this disadvantage considerably limits the use of boundary elements method in terms of computing resources having the limitations imposed by the memory of the computing system. However, since the system matrix shows properties that allow effective use of preconditioning followed by the application of fast iterative solving methods, BEM can provide excellent performance [49, 50].

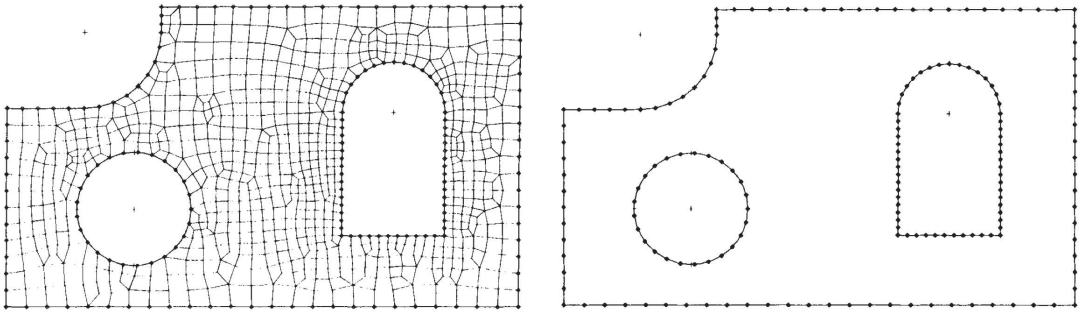

Figure 2.7: Left - Domain (FEM) and Right- boundary (BEM) discretization [179].

Taking for example an electrostatic problem, the Poisson equation $-\Delta u = f$, satisfied by the electric potential in a homogenous dielectric, has in the case of an inhomogeneous domain the general form:

$$-\nabla \cdot (\varepsilon \nabla V) = \rho, \tag{2.12}$$

where $V : \Omega \to \mathbb{R}$ is the scalar electric potential.

Considering charge point (or filiform rectilinear in case of a plan-parallel problem), unitary, placed in an arbitrary position r', within the computational domain, equation (2.12) point r' will be:

$$-\nabla \cdot (\varepsilon(r')\nabla V(r')) = \rho(r'). \tag{2.13}$$

The solution of this problem is the Green function associated to the domain, that satisfies:

$$-\nabla \cdot (\varepsilon(r')\nabla G(r, r')) = \gamma(r' - r), \tag{2.14}$$

where $\gamma()$ is the Dirac delta function. The solution of the problem (2.12) with null boundary conditions is obtain by superposition of the elementary solutions, considering the point charge in different positions within the computational domain. When the domain is homogenous ($\varepsilon(r') = \varepsilon =$ constant) the solution is

$$-\nabla \cdot (\nabla G(r, r')) = \frac{\gamma(r' - r)}{\varepsilon}, \tag{2.15}$$

If we consider:

$$\begin{aligned}\nabla \cdot (G(r,r')\varepsilon(r')\nabla V(r')) &= \varepsilon(r')\nabla V(r')\nabla G(r,r') + G(r,r')\nabla \cdot [\varepsilon(r')\nabla V(r')],\\ \nabla \cdot (V(r')\varepsilon(r')\nabla G(r,r')) &= \varepsilon(r')\nabla V(r')\nabla G(r,r') + V(r')\nabla \cdot [\varepsilon(r')\nabla G(r,r')],\end{aligned} \tag{2.16}$$

operating a subtraction and integrating on Ω, considering (2.12), (2.14), the Dirac function filtration propriety and Gauss-Ostrogradsky expression it follows that:

$$\begin{aligned}V(r) = &\int_{\Omega} G(r,r')\rho(r')\mathrm{d}v_{r'} + \oint_{\partial\omega} G(r,r')\varepsilon(r')\frac{\partial V}{\partial n_{r'}}\mathrm{d}A_{r'} -\\ &- \oint_{\partial\omega} V(r')\varepsilon(r')\nabla G(r,r')\cdot \mathbf{n}_{r'}\mathrm{d}A_{r'}.\end{aligned} \tag{2.17}$$

also know as the *expression of the three electric potentials*[142].

If the problem has no inner field sources with Dirichlet boundary conditions then the first integral vanishes. Moreover, bringing the point in an arbitrary position on the boundary, an integral equation is obtained, linking the potential value of various points on the boundary with the values of the potential's normal derivative assessed also on the computational domain boundary. Thus obtaining the surface integral equation (Boundary Integral Equation - BIE) of electrostatics, a particular case of the relationship (2.17):

$$V(r) = \oint_{\partial\omega} G(r,r')\varepsilon(r')\frac{\partial V}{\partial n_{r'}}\mathrm{d}A_{r'} - \oint_{\partial\omega} V(r')\varepsilon(r')\nabla G(r,r')\cdot \mathbf{n}_{r'}\mathrm{d}A_{r'}, \tag{2.18}$$

where the Green function constitute the kernel of the integral equation.

In 2D the Green function has the expression of the logarithmic potential, while in 3D the Green function has the expression:

$$G(r,r') = 1/4\pi\varepsilon_0 \left\|r - r'\right\|^2 \tag{2.19}$$

and by discretization of (2.18) along the boundary of the computational domain, and considering r placed successively in all boundary nodes (were V is known, due to the Dirichlet boundary condition) is obtained a linear system of equations having as unknowns the normal derivative of potential $\mathrm{d}V/\mathrm{d}n$ in the nodes placed on boundary. Consequently, the discrete form of (2.18) allow the estimation of the solution V in any internal point r form Ω.

An essential characteristic of each numerical method is the set of DoFs, and its size. Once the numerical model is implemented as a computer code (program/object = data structure + algorithm) it became a computational model. In order to obtain a reliable software product, the most advanced Software Engineering principles and technologies have to be applied in its development. Many free and commercial software products of different complexities are nowadays available and dedicated to solve several PDEs, to compute several physical fields or to solve multiphysics problems, helping researchers, engineers and designers to solve their CAD/CAE problems and to design new and better products.

2.1.5 Verification and Validation of the Models

Verification ensures that the solution was built according to the requirements of mathematical formulation of the problem while validating in turn ensures that the formulation is correct, in line with reality. In short, the first step is to verify that the solution satisfies the equations, that it is not erroneous, and the second, if equations are not erroneous. To check the field solution of a problem, the problem is solved for particular excitation (field source) and determine to what extent the solution satisfies its field equations and boundary conditions. To do this, the field-solution is replaced in equations and the numerical residue of the equation and/or of the boundary condition are computed.

In mass production it can usual happen that the products are not completely identical, each product having a small deviations of material constants, or geometry. These are the reasons why, in the current engineering deviations which can go up to quite high values are acceptable, not only over 1% but even up to 5% or even 10%. Obviously there are special applications, for example the production of the measurement devices, were the requirements are strict and these deviation are not acceptable. This happens in all cases where devices are directly connected with the safety risks to people or material assets, as in the aerospace, aeronautical or nuclear industries. Otherwise, the development and use of models with high accuracy is not economically justified. But even so, they must be checked because there is always the risk of unacceptable errors. These are the reasons for which in the designing process an appropriate accuracy is required for the models of real devices.

A first verification refers to the solution of the system of equations obtained by discretization of the fields equation. The residue of these equations is a first measure of the error with which the problem is solved. Another simple approach is to consider a particular field, chosen arbitrarily, and to determine from the equations what sources produce that field. Afterward, the direct problem considering that sources is solved and check whether its solution is close to the original one.

A very useful way to verify the solution is to check consequences of the equations, such as power/energy balances or to check other quantities, for particular variation of the input. The advantage is that checking of the total power balance is synthetic, with a global character, referring to the behavior of the solution throughout the entire domain, and in the case of energy, during the entire time interval as well.

Checking models represented as input/output systems means determining the output signals for a particular variations of the input. Most often, they assume particular or even degenerate forms, such as: constant, sinusoidal, exponential, more or less smooth particular imposed, step function, etc. It is important in that case to determine the response analytically or otherwise (e.g. symbolic). The order reduction should be checked separately, when possible. Validation of reduced input-output models means the comparison between simulation results of numerical (field) models and reduced (circuit) models.

The first problem that arises in the quantitative assessment refers to the fact that after verifying results a deviation vector is obtained, and it is desired to have a single numerical criteria that expresses synthetically the deviation, i.e. to measure the distance between

what should be obtain and what actually has been obtained. From a mathematical perspective, this dilemma comes down to choosing the vector norm with which the deviation is synthetically express. The relative error is the residue norm divided to the norm of the right side term. The situation is similar in the case of perfect nonlinear systems, but also in other equations, including ordinary differential or partial differential equations, only the equation operator changes. The most common vector norms used in practice are the Euclidean norm (root of the sum of squares of components) and Chebyshev norm (maximum module of components). The first describes the average square deviation and the second describes the maximum deviation.

The residue equation in discrete form or in continuous form, is not always the most relevant quantity to characterize the quality of the solution. This is the reason why is preferred that the verification procedures estimates the solution deviation with regard to the residue.

Closely related to this aspect of verification is therefore the value of the conditioning number of the problem. If we can even calculate its approximate value, then we can say to what extent the residue norm is relevant to verify the solution. But for this an analysis should be done of the variability of the solution, i.e. is to analyze the effect of data variations on the variation of the problem solution. A first approach is the variability analysis for determining the sensitivities of the solution or of derived quantities with respect to the characteristic parameters of the problem, which may be geometrical or material. Mathematical analysis is reduced to determining the values of the partial derivatives of output quantities to the parameters that describe the situation. Others refer to parametric analysis, such as higher order sensitivity statistical analysis or identifying the worst case (including some correlations that exist between inputs). Ideally, the problem is solved not only to determine the solution in the nominal case but also its statistical parameters (e.g, average and standard deviation) when data parameters are statistical known.

The variability analysis can be done by theoretical or empirical methods. The results of theoretical analysis can be implemented in the form of effective procedures for computing sensitivities, the underlying variability analysis. Empirical analysis of the variability of field problem solving is done by numerical experiments with different input data. Input data can be generated randomly, as in the Monte Carlo method and other stochastic methods, or carefully chosen, as it is done in the case of design techniques experiments. Otherwise, by using brute force method to verify the numerical solution and extract the parameter variation model a high number of numerical experiments are needed, that is prohibitive.

We find that all aspects of verification concerns the relationship between the numerical solution and the equation or mathematical formulation problem of that equation that has been solved. Discussions carries in the mathematical, functional framework of the problem or a similar problem that is a discrete approximation.

Another procedure to be performed after checking the model is validation. This will ensure that the built model is useful in design activities. The robust method of checking a model is the comparison with reality. This time we design a set of tests consisting of

a range of scenarios, the excitation of both the real device and its model is made with similar input signals applied in similar circumstances. Experimental validation of the model takes place only if the answer of the model has an acceptable deviation with regard to the real objects response.

Arrangements made to experimental validate numerical models should be made with great care to select relevant features. They have to be agreed with the modelling team and described in detail (both experimental and post-processing arrangement applied to the measurements results) to remove any aspect which could lead to inconsistencies.

In literature, RF-MEMS devices operated electrostatic are characterized experimentally as follows:

- Steady-state regime, by C-V actuation characteristic with hysteresis;
- Radio frequency, through S parameters dependency on frequency;
- Transient regime, by measuring the time variation mode of the capacity during switching transient regime in both directions. In some cases directly measure the time variation of the membrane position.

The first validation to be performed is based on a comparison between the results of model simulations and analytical-approximative model, which are not expected to be identical. Especially for complicated problems, the results can be quite different quantitatively, however it is expected a qualitative similarity and deviations must have a plausible explanation.

Verification and validation of numerical models is conceptually similar to validate the software components. As in the case of computer programs and models, testing is a crucial stage in their development. It is the procedure which seeks to identify errors. The set of tests must meet the following conditions:

- Have a proper complexity, preferably progressive;
- To be strong, to have great chances to discover errors, if any;
- To be relevant and easy to measure (to give clear indication if there is an error and where it is possible to enable quick troubleshooting);
- Be convincing and credible for a potential user.

2.1.6 Extraction of Reduced Order Models

Due to the pressing need for efficient numerical techniques for simulations of extremely large-scale dynamical systems arising from circuit simulation, structural dynamics, and micro-electro-mechanical systems, in recent years, an interest in developing new models order reduction techniques increased. The main idea is to find an approximate model of the studied devices having fewer DoFs than the original model, based on numerical methods to solve PDEs which describe these devices. The Model Order Reduction (MOR) should be a procedure which preserve the main characteristics of the model, assuring not only the accuracy of the model but also its essential properties, such as passivity, stability,

causality or reciprocity. A great deal of attention has been devoted to *SVD*-based and *Krylov* subspace-based techniques for reduced-order modeling of large-scale dynamical systems [181].

These approaches are usually applied in the State Space forms of the time domain analysis, which is a a system of first order of ODE. However second order systems arise naturally not only in the dynamic analysis of the mechanical structures but also in many other many areas of engineering ([182, 183, 184]) with the following form[185]:

$$\begin{cases} M\ddot{q}(t) + D\dot{q}(t) + Sq(t) = F^{in}u(t); \\ \\ \qquad\qquad y(t) = F^{out}q(t). \end{cases} \tag{2.20}$$

Assuming that $u(t) \in \mathbb{R}^m, y(t) \in \mathbb{R}^p, q(t) \in \mathbb{R}^N, F^{in} \in \mathbb{R}^{N\times m}, F^{\text{out}} \in \mathbb{R}^{p\times N}$ and $M, D, S \in \mathbb{R}^{N\times N}$ with M invertible. In case of a mechanical system the matrices M, D and S represent, respectively, the *mass* (or inertia), *damping* and *stiffness* matrices, $u(t)$ corresponds to the vector of external forces, F^{in} is the input distribution matrix, $y(\cdot)$ is the vector of output signals, F^{out} is the output measurement matrix, and *q(t)* to the vector of internal generalized coordinates.

For the system (2.20), the transfer matrix is:

$$R(s)\doteq F^{\text{out}}P(s)^{-1}F^{\text{in}}, \tag{2.21}$$

where $P(s) = Ms^2+Ds+S$ is the characteristic polynomial matrix. The zeros of $\det(P(s))$ are also known as the characteristic frequencies of the system and play an important role in model reduction, e.g., the system is stable if these zeros lie in the left half plane.

In many cases, the original system is too large to allow the efficient solution of various control or simulation tasks. In order to address this problem, techniques that produce a reduced system of size $N \ll n$ that possesses the essential properties of the full order model have been developed. Such a reduced model can then be used effectively, e.g., in real-time, for controlling or simulating the phenomena described by the original system. Therefore the reduced model [185] is:

$$\begin{cases} \hat{M}\ddot{\hat{q}}(t) + \hat{D}\dot{\hat{q}}(t) + \hat{S}\hat{q}(t) = \hat{F}^{\text{in}}u(t); \\ \\ \qquad\qquad \hat{y}(t) = \hat{F}^{\text{out}}q(t). \end{cases} \tag{2.22}$$

where $\hat{q}(t) \in \mathbb{R}^n, \hat{M}, \hat{D}, \hat{S} \in \mathbb{R}^{n\times n}, \hat{F}^{\text{in}} \in \mathbb{R}^{n\times m}, \hat{F}^{\text{out}} \in \mathbb{R}^{p\times n}$ such that its transfer function is "close" to the original transfer function.

In contrast with second order systems, first order systems can be represented as follows:

$$\begin{cases} \dot{x}(t) = Ax(t) + Bu(t) \\ \\ \qquad y(t) = Cx(t) \end{cases} \tag{2.23}$$

where

- $x(t) \in \mathbb{R}^N$ is the state vector,

- $u(t) \in \mathbb{R}^m$ is the input vector,
- m is the number of inputs,
- $C \in \mathbb{R}^{p \times N}$ is the output matrix,
- $B \in \mathbb{R}^{N \times m}$ is the input matrix,
- $y(t) \in \mathbb{R}^p$ is the output vector,
- N is the order of the system,
- p is the number of outputs,
- $A \in \mathbb{R}^{N \times N}$ is the state matrix,,

The transfer function associated with the system 2.23 that links the inputs to the outputs in the Laplace domain is:

$$R(s) \doteq C(sI_N - A)^{-1}B, \tag{2.24}$$

Rewriting the system from (2.20) as:

$$\begin{cases} \dot{x}(t) = \begin{bmatrix} 0 & I_N \\ -S_M & -D_M \end{bmatrix} x(t) + \begin{bmatrix} 0 \\ F_M^{\text{in}} \end{bmatrix} u(t) \\ \\ y(t) = [F_M^{out} 0]\, x(t) \end{cases} \tag{2.25}$$

where the state *x(t)* is $q(t)^T \dot{q}(t)^T]$, and where we have chosen a coordinate system in which the mass matrix M is the identity (for simplicity, the mass matrix M is assumed to be invertible, and one can write for example: $S_M = M^{-1}S, D_M = M^{-1}D, F_M^{\text{in}} = M^{-1}F^{\text{in}}, F_M^{\text{out}} = F^{\text{out}}$), system (2.23) can be recovered.

Rewriting (2.21) as:

$$R(s) \doteq C(sI_{2N} - A)^{-1}B, \tag{2.26}$$

were

$$A \doteq \begin{bmatrix} 0 & I_N \\ -S_M & -D_M \end{bmatrix},\ B \doteq \begin{bmatrix} 0 \\ F_M^{in} \end{bmatrix} u(t),\ C \doteq \begin{bmatrix} F_M^{out} & 0 \end{bmatrix}. \tag{2.27}$$

The dimension of the state $q(t)$ of the original second order system (2.20) is equal to N, the order of its corresponding linearized state space realization (2.27) (also called the Mc Millan degree of $R(s)$ if the (C;A;B) is minimal) is equal to $2N$.

A reduced model for the second order system (2.20) could be produced by applying standard linear model reduction techniques to (C;A;B) in (2.27) to yield a small linear system $(\hat{C}; \hat{A}; \hat{B})$. Unfortunately, there is no guarantee that the matrices defining the reduced system $(\hat{C}; \hat{A}; \hat{B})$ have the nonzero structure necessary to preserve the second order form of the original system. Such a guarantee requires the development of second order structure preserving model reduction techniques.

Most popular model reduction techniques for linear systems can be placed in one of two categories [186]: *SVD*-based and *Krylov* subspace-based techniques. Perhaps the most popular model reduction technique for linear systems is the Balanced Truncation method. This *SVD*-based technique has many advantages: the stability of the original

system is preserved and there exists an a priori global bound on the error between the original and the reduced system. The main drawback is that the technique cannot be applied to large-scale systems of order N, i.e., those systems where $O(N^3)$ computations is an unacceptably large cost. On the other hand, *Krylov* subspace-based techniques that are based on imposing moment matching conditions between the original and the reduced transfer function, such as rational/tangential interpolation methods, can be applied to large-scale systems but do not provide global error bounds and depend significantly on the choice of certain parameters. A brief description of these methods applied to the second order systems is given in [185]. Other reduction methods are presented in [123, 187, 134], in addition to [92, 93, 94, 95, 96, 97, 98, 99, 100, 101, 102, 103, 104, 105, 106, 107, 108, 109, 110, 111, 112, 113] presented in 1.1.3.

Because models of RF-MEMS we developed are strongly nonlinear, the order reduction procedure developed in this thesis is based on multiphysics considerations, aiming to a smallest of second order reduced model with N=1.

2.2 Theoretical Concepts

In the general operation of MEMS devices, occur several physical phenomena that must be studied. The actuation of the device is done by applying an actuation voltage, that forms an electrostatic force, for which an electrostatic problem must be formulated and solved. For the deformation and movement of the mobile membrane a structural-mechanical problem must be formulated and solved. If the device is not not packaged in vacuum, the movement suffers air damping. For this a fluid-flow problem must be formulated and solved. As was mentioned above, the electromagnetic analysis is essential for the operation of RF-MEMS devices. Because all these phenomena influence each other, a series if interaction must be identified and described. In this section, the fundamental equations which describe these fields, phenomena and interactions are briefly presented.

2.2.1 Electrostatics

In this section is formulated in a correct physical (conceptual) and mathematical manner the fundamental problem of the electrostatic field and are presented the methods to compute the mechanical effects of the electrostatic fields, an important component in the extraction of the multiphysics models of MEMS devices.

The **fundamental problem of the electrostatic regime** consists in determining the electric field starting from its sources; so the know data is represented by the following quantities and characteristics [144, 188, 189, 190, 155, 191]:

- the shape and size of the computing domain D;
- the dielectric parameter (it must be known in every point of the computing domain, in the linear medium it is described by the permittivity ε, which is a positive defined value, symmetric scalar or tensor);

- the internal field sources (they must be known in every point of the computing domain, being described by the electric charge density ρ and the permanent polarization vector $\mathbf{P}_p$);
- the external field sources described by the boundary conditions (of Dirichlet or Neumann type, as they are described below).

The electrostatic regime is based on the following assumptions:

- the bodies do not move: $v = 0$;
- all quantities are constant in time: $\frac{\mathrm{d}}{\mathrm{dt}} = 0$;
- there are no energy transformations occurring, the currents are null $p = 0 \Rightarrow \mathbf{J} = \mathbf{0}$;
- there is no interest in the magnetic field distribution, so it may assumed that $\mathbf{B} = \mathbf{0}$ and $\mathbf{H} = \mathbf{0}$.

The fundamental equations of the electrostatic regime are:

- The electric flux law

$$\begin{cases} \Psi_\Sigma = q_{D_\Sigma} \quad \int\limits_\Sigma \mathbf{D} \cdot \mathrm{d}\mathbf{A} = \int\limits_{D_\Sigma} \rho \mathrm{d}v, \\ \mathrm{div}\mathbf{D} = \rho, \\ \mathbf{n}_{12} \cdot (\mathbf{D}_2 - \mathbf{D}_1) = \rho_s \Longleftrightarrow \mathrm{div}_s \mathbf{D} = \rho_s. \end{cases} \tag{2.28}$$

- The law of electromagnetic induction (Faraday law) becomes the theorem of static electric potential

$$\begin{cases} u_\Gamma = -\frac{\mathrm{d}\varphi_{S_\Gamma}}{\mathrm{d}t} = 0 \Longleftrightarrow \int\limits_\Sigma \mathbf{E} \cdot \mathrm{d}\mathbf{r} = 0, \\ \mathrm{rot}\mathbf{E} = \mathbf{0} \Rightarrow \mathbf{E} = -\mathrm{grad}\, V, \\ \mathbf{n}_{12} \times (\mathbf{E}_2 - \mathbf{E}_1) = 0 \Longleftrightarrow \mathbf{E}_{t1} = \mathbf{E}_{t2}. \end{cases} \tag{2.29}$$

- The constitutive relationship, that links $\mathbf{D}$ and $\mathbf{E}$

$$\begin{cases} \mathbf{D} = f(\mathbf{E}) \Longrightarrow \mathbf{D} = \varepsilon_0 \mathbf{E} + \mathbf{P}, \\ \mathbf{P} = \mathbf{P}_t(\mathbf{E}) + \mathbf{P}_p \Rightarrow \mathbf{D} = \overline{\overline{\varepsilon}}(\mathbf{E}) + \mathbf{P}_p. \end{cases} \tag{2.30}$$

- The conduction law, the condition for electrostatic equilibrium in conductors

$$\begin{cases} \mathbf{J} = \overline{\overline{\sigma}}(\mathbf{E} + \mathbf{E_i}) = 0 \Rightarrow \overline{\overline{\sigma}}(\mathbf{E} + \mathbf{E_i}) = \mathbf{0} \Rightarrow \mathbf{E} = -\mathbf{E_i} \\ \mathbf{E_i} = \mathbf{0} \Longrightarrow \rho = 0; \mathbf{D} = \mathbf{0}; \mathbf{E} = \mathbf{0}. \end{cases} \tag{2.31}$$

The electric field sources in this regime are shown in Figure 2.8, where ρ is the electric charge, $\mathbf{P}_p$ is the permanent polarization, $\mathbf{E}_i$ is the intrinsic electric field strength and ε is the material constant.

The 2^{nd} order equation of electrostatics is the partial differential equation satisfied by the potential V. One starts from the system of 1^{st} order equations in their local form (2.32):

$$\begin{cases} \mathrm{div}\mathbf{D} = \rho \Rightarrow \mathrm{div}(-\varepsilon \mathrm{grad} V + \mathbf{P}_p) = \rho, \\ \mathrm{rot}\mathbf{E} = \mathbf{0} \Rightarrow \mathbf{E} = -\mathrm{grad}\ V \Rightarrow \\ \mathbf{D} = \overline{\overline{\varepsilon}}(\mathbf{E}) + \mathbf{P}_p \end{cases} \tag{2.32}$$

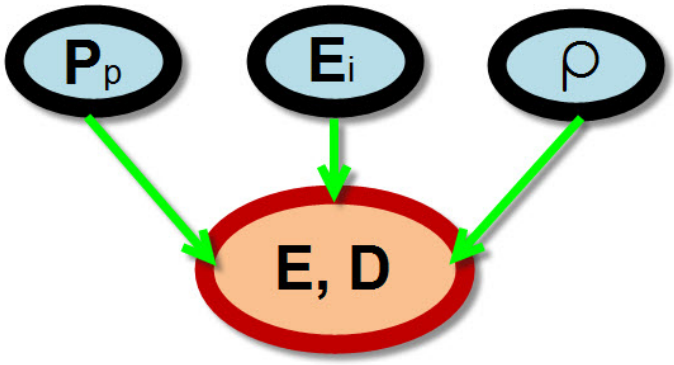

Figure 2.8: The electric field sources.

The 2^{nd} order equation has the form (2.33), which is a Poisson generalized elliptic equation:

$$\begin{aligned} &-\operatorname{div}(\bar{\bar{\varepsilon}}\operatorname{grad}V) = \rho_t, \\ &\rho_t = \rho + \rho_p;\ \rho_p = -\operatorname{div}\mathbf{P}_p. \end{aligned} \tag{2.33}$$

By writing the equation (2.33) for a homogeneous isotropic material ε we obtain (2.34) which is a Poisson equation and if in (2.34) $\rho_t = 0$, we get (2.35), which is a Laplace equation:

$$\Delta V = -\frac{\rho_t}{\varepsilon}, \tag{2.34}$$

$$\Delta V = 0. \tag{2.35}$$

At interfaces between materials with different electric properties, the electric potential satisfies:

$$\left\{ \begin{array}{l} \mathbf{E_{t1}} = \mathbf{E_{t2}} \\ \mathbf{n}_{12} \cdot (\mathbf{D}_2 - \mathbf{D}_1) = \rho_s \end{array} \right. \Rightarrow \left\{ \begin{array}{l} V_1 = V_2 \\ \varepsilon_1 \frac{\mathrm{d}V_1}{\mathrm{d}n_{12}} - \varepsilon_2 \frac{\mathrm{d}V_2}{\mathrm{d}n_{12}} = \rho_s \end{array} \right. \tag{2.36}$$

The electrostatic energy theorem. The energy of the electric field can be determined either by integrating the energy density, meaning in linear media the semi-product of the electric field strength and the electric flux density over the whole domain occupied by the electric field, either by integrating the half-product of the charge density and the electric potential. It can be noted that one must add to the last integral not only conductors charges, multiplied by their potentials, but also the boundary contribution, which can be considered as being composed of several superficially charged conductors.

In the case of dielectrics with affine characteristic, the co-energy/energy density is:

$$\begin{aligned}
&\mathbf{D} = \mathbf{f}(\mathbf{E}) = \overline{\overline{\varepsilon}}\mathbf{E} + \mathbf{P}_p \Rightarrow w_e^* = \int_0^E \mathbf{D}' \ \cdot \mathrm{d}\mathbf{E}' = \int_0^E \mathbf{f}(\mathbf{E}') \ \cdot \mathrm{d}\mathbf{E}' = \\
&= \int_0^E (\overline{\overline{\varepsilon}}\mathbf{E} + \mathbf{P}_p) \ \cdot \mathrm{d}\mathbf{E} = \frac{\mathbf{E} \cdot \overline{\overline{\varepsilon}}\mathbf{E}}{2} + \mathbf{P}_p \cdot \mathbf{E} = \frac{\mathbf{D} \cdot \mathbf{E}}{2} + \frac{\mathbf{P}_p \cdot \mathbf{E}}{2} \\
&w_e = \mathbf{D} \cdot \mathbf{E} - w_e^* = \frac{\mathbf{D} \cdot \mathbf{E}}{2} - \frac{\mathbf{P}_p \cdot \mathbf{E}}{2} = \frac{\overline{\overline{\varepsilon}}\mathbf{E} \cdot \mathbf{E}}{2}
\end{aligned} \tag{2.37}$$

and the electrostatic energy theorem becomes:

$$\begin{aligned}
&2W_e = \int_D (\mathbf{D} \cdot \mathbf{E} - \mathbf{P}_p \cdot \mathbf{E}) \ \mathrm{d}v = \int_D (\rho V - \mathbf{P}_p \cdot \mathbf{E}) \ \mathrm{d}v + \oint_\Sigma \varepsilon V \frac{\mathrm{d}V}{\mathrm{d}n} \mathrm{d}A + \sum_{k=1}^n V_k q_k, \\
&\mathrm{div}(\mathbf{D}V) = \rho V - \mathbf{P}_p \cdot \mathbf{E} \Rightarrow \oint_{\partial D = \Sigma \bigcup S_k} \mathbf{D}V \cdot \mathrm{d}\mathbf{A} = \int_D (\rho V - (\overline{\overline{\varepsilon}}\mathbf{E} + \mathbf{P}_p) \cdot \mathbf{E}) \ \mathrm{d}v \Rightarrow \\
&2W_e = \int_D \mathbf{E} \cdot \overline{\overline{\varepsilon}}\mathbf{E} \ \mathrm{d}v = \int_D (\rho V - \mathbf{P}_p \cdot \mathbf{E}) \ \mathrm{d}v + \sum_{k=1}^n V_k q_k - \oint_\Sigma V D_n \mathrm{d}A.
\end{aligned} \tag{2.38}$$

In the case that one of the n conductors is the domain boundary, and the dielectric is not charged, then the following relation is satisfied:

$$2W = \int_D \mathbf{D} \cdot \mathbf{E} \ \mathrm{d}v = \sum_{k=1}^n V_k q_k. \tag{2.39}$$

$\mathbf{D}$ and q may correspond to a state of the system of conductors, while the electric field strength and the electric potential may correspond to a different state. The only condition is that $\mathbf{D}$ be a solenoidal field and $\mathbf{E}$ be an irrotational field. So

$$(\mathbf{D}, \mathbf{E}) = \mathbf{V} \cdot \mathbf{q}, \tag{2.40}$$

where $(\mathbf{D}, \mathbf{E})$ represents the scalar product in the L^2 space, between the two field quantities, the electric flux density and the electric field strength, respectively. While $\mathbf{V} \cdot \mathbf{q}$ represents the scalar product in $\mathbb{R}^n$ space, between the vector of potentials V of the n conductors and the vector q of their charges.

The relation (2.40) represents the **Tellegen** theorem for electrostatic fields, which states that the scalar product of the irrotational electric field strength and the solenoidal field of the electric flux density is equal to the scalar product of the charges vectors and potential vectors of the n conductors, also called pseudo-energies, because they are measured in Joules (J). When the two vector fields describe the same electrostatic field, from a domain having arbitrary dielectric characteristic, then the value of the two scalar products actually represents twice of the electrostatic energy, and the result is a consequence of the electrostatic energy theorem.

Uniqueness theorems may be now formulated, one for scalar electric potential and two for electrostatic field. They are important because they describe the boundary conditions for these problems.

Uniqueness theorem of scalar electric potential. The solution of the 2^{nd} order equation of electrostatics is uniquely defined if the boundary conditions for this problem are either of Dirichlet type, specifying the value of the potential on the boundary, or Neumann type, specifying the value on the boundary of the normal derivative of the solution which is proportional to the normal component of the electric flux density.

- Dirichlet boundary conditions:

$$V(\mathbf{r}) = f_D(\mathbf{r}), \mathbf{r} \in S_D \subseteq \Sigma$$

- Neumann boundary conditions:

$$\frac{\mathrm{d}V}{\mathrm{d}n} = f_N(\mathbf{r}), \mathbf{r} \in S_N = \Sigma - S_D \neq \Sigma$$

The problem formulated using Dirichlet conditions in all boundary points has unique solution, while the problem formulated with only Neumann conditions along the frontier is not well formulated, because the potential is determined up to an arbitrary constant. Furthermore, it is possible that the problem does not have a solution at all, as it happens in the case of arbitrary Neumann conditions, whose integral on the boundary surface proportional to the total charge in the computing domain being arbitrary, does not satisfy this restriction, imposed by the Gauss theorem.

Another category of problems frequently found in practice are mixed problems, with hybrid boundary conditions, where Dirichlet conditions are imposed on a part of the frontier, and Neumann conditions are imposed on the rest of the frontier. The hybrid problems are well formulated if the Dirichlet conditions section is not empty, in order to have at least one reference point for the potential. It can also be noticed that at the surface of the conductors included in the computing domain there is a Dirichlet condition usually imposed, when we know the potential of every conductor (but the superficial charge distribution at the surface of conductors is usually unknown).

For linear problems, the uniqueness is proved by using the lemma of the null solution, according to which the linear problem has a unique solution if the homogeneous problem with null sources has a null solution.

The uniqueness theorem of electrostatic field. By formulating the fundamental problem of electrostatics in field terms it is noticed that the Dirichlet boundary condition can be obtained by integrating the electric field strength on an open curve, included in the border area of the electric field strength, and the Neumann condition can be determined from the normal component of the electric flux density:

$$\begin{aligned} &V = f_D(P) = \int_{PP_0} \mathbf{E}_t \cdot d\mathbf{r} \iff \mathbf{E}_t = -\mathrm{grad}_s V = \mathrm{grad}_s f_D \\ &\frac{\mathrm{d}V}{\mathrm{d}n} = f_N(P) = -\mathbf{E} \cdot \mathbf{n} = -\mathbf{n} \cdot \bar{\bar{\varepsilon}}^{-1}(\mathbf{D} - \mathbf{P}_p) \Rightarrow \\ &\Rightarrow f_N(P) = \frac{-\mathbf{Dn}}{\varepsilon} = \frac{-D_n}{\varepsilon}; \bar{\bar{\varepsilon}} = \varepsilon\bar{\bar{1}}, \mathbf{P}_p = \mathbf{0}. \end{aligned} \tag{2.41}$$

In the field problem, the boundary is disjointly partitioned in the section S_E where the tangential component of the field is given, identified from the previous relations with

S_D. Its complementary to Σ is S_N. Still, the reciprocal implication from the first relation is valid only if the Dirichlet condition surface S_D is a connex set, being made of a single piece and not by several disjoint pieces. This is because at the passing from one part to the other an unknown voltage jump may occurs which makes it impossible to calculate the potential in every point of the entire surface S_D only by integrating the tangential component of the electric field strength on S_D.

This is the reason why in the case that S_E on which E_t is given is not convex but composed of n disjoint parts, $S_E = \cup_{k=1}^{n} S_{E_k}, S_{E_k} \cap S_{E_j} = \emptyset$, the boundary conditions of the field problem have supplementary constants. On every disjoint part S_{E_k} of the surface S_E, either the potential in one point, either the electric flux on that surface must be known, except for the last surface which was considered as the reference for the potential (2.42).

$$\begin{aligned} U_k &= \int\limits_{PP_0} \mathbf{E}_t \, d\mathbf{r}, P_k \in S_{E_k}, P_n \in S_{E_n} \\ \Psi_k &= \int\limits_{S_{E_k}} D_n \, dS, k = 1, 2, \ldots, (n-1) \end{aligned} \tag{2.42}$$

The uniqueness theorem can be generalized to admit Robin boundary conditions, instead of the Dirichlet ones, where of a linear combination of the potential and its derivative on the normal is given (2.43):

$$V(P) + \alpha(P)\frac{\mathrm{d}V}{\mathrm{d}n} = f_R(P), P \in S_R \subset \Sigma, \tag{2.43}$$

where $\alpha \geq 0$ has the significance of the thickness of a dielectric layer deposited on an electrode of potential f_R.

The uniqueness theorems of electrostatic field and potential are direct consequences of the Tellegen's theorem of electrostatic (pseudo)energy. The variational formulation of the fundamental problem of electrostatics is known in mathematics as the weak form of the second order equation, with elliptic partial derivatives, satisfied by the electrostatic potential. This is the fundament of the finite element method [142]. In mathematical terms, the fundamental problem of electrostatics in the computing domain Ω is formulated as follows:

find $V \in H_0^1(\Omega)$ so that

$$\begin{aligned} &a(V,U) = f(U), \forall U \in H_0^1(\Omega) \text{ with} \\ &a(V,U) = \int\limits_{\Omega} \varepsilon grad V \cdot grad U dv; f(U) = \int\limits_{\Omega} U\rho dv + \int\limits_{S_N = \partial\Omega - S_D} U f_N dA, (S_D) \neq 0, \end{aligned} \tag{2.44}$$

where

$H_D^1(\Omega) = \left\{ V \in L^2(\Omega) \,|\, grad V \in L^2(\Omega), V\,|_{S_D} = f_D \right\}, H_0^1(\Omega) = H_D^1(\Omega)\,|_{f_D=0}$.

Indeed the weak formulation of the electrostatic equations is a direct consequence of the Tellegen's theorem.

This formulation is the precise mathematical description of the problem, and it establish the functional frame as it specifies the space of functions where the solution is searched

for (also called trial functions) and also the space of functions where the equations is projected (also called test functions). The two are Sobolev spaces containing functions with square gradient Lebesgue integrable, whose projections on the border satisfies the not-null and null Dirichlet condition. They are identical in null Dirichlet conditions and isomorph otherwise (when the trial functions space is the translation of the test functions space with an element that satisfies the not-null Dirichlet conditions).

According to Lax-Milgram theorem, if the bilinear form $a(.,.) : X \times X \to \mathbb{R}$ is:

- bounded $|a(u,v)| < C \|u\| \cdot \|v\|, \forall u, v \in X$ and
- coercive $|a(u,v)| > c \|u\|^2, \forall u \in X$

then the problem of determining the element v, so that $a(u,v) = f(u)$, where $f : X \to \mathbb{R}$ is a linear form is a well-formulated problem, has solution in X, the solution is unique and depends continuously on f [192, 151].

In [193] it is proved that the two conditions of the Lax-Milgram theorem are fulfilled in the case of electrostatic energy functional. The fundamental problem of electrostatics is therefore well-formulated, has a solution which is unique and which depends on the field sources continuously.

The electrostatic field acts with forces, torque, pressure, or mechanical stress on bodies that are charged and polarized temporarily or permanently, which can be dielectrics or conductors [188, 189, 190, 194, 195, 155].

The electric field strength $\mathbf{E}$ acts with Coulomb force $\mathbf{F} = q\mathbf{E}$ on a point-mass body, charged with a q. The direction of this force coincides with the field, but its orientation depends on the sign of the charge. The relationship is however inconsistent in mathematical terms as a point-mass body field is unbounded in that point. This should be understood as follows: the force of the electrical field exerted on a small body is the product of the charge of that body and the average field from the body, to the limit, the field from the body's center. This difficulty disappears when we talk about the volume density of the Coulomb force $\mathbf{f} = \rho\mathbf{E}$, which allows the calculation of the force and torque, which electrostatic field exerts upon a charged body with an arbitrary distribution of charge, volumetric or on discontinuous surfaces or of separation between bodies such as surface conductive bodies:

$$\begin{aligned} \mathbf{F} &= \int_{\Omega} \rho\mathbf{E} \, \mathrm{d}v = \int_{D} \rho_v\mathbf{E} \, \mathrm{d}v + \int_{S_d} \rho_s\mathbf{E} \, \mathrm{d}A, \\ \mathbf{C} &= \int_{\Omega} \rho\mathbf{r} \times \mathbf{E} \, \mathrm{d}v = \int_{D} \rho_v\mathbf{r} \times \mathbf{E} \, \mathrm{d}v + \int_{S_d} \rho_s\mathbf{r} \times \mathbf{E} \, \mathrm{d}A, \end{aligned} \tag{2.45}$$

the electric field that is integrated on the discontinuous surfaces is the average field from the two surfaces S_d.

Any polarized body is equivalent to a fictional polarization charge distribution $\rho_p = -\mathrm{div}\mathbf{P}$, from the produced field point of view of $(V, \mathbf{E})$ and from the point of view of mechanical effect of the field on the equivalent body, based on Maxwell stress tensor expression. The above relationships can be applied to calculate the ponderomotor forces,

on the charged and polarized bodies, if instead of the real charge density the total load is used, including the polarization $\rho_t = \rho + \rho_p = \rho - \text{div}\mathbf{P}$.

In the electrostatic regime, the charge of the conductors is linear distributed on their surface with a density

$$\rho_s = \text{div}_s\mathbf{D} = D_n = \varepsilon E_n.$$

This makes the ponderomotor forces on the conductive bodies be

$$p = \frac{\rho_s E_n}{2} = \frac{\varepsilon E_n^2}{2} = w_e \rightarrow \mathbf{F} = \oint\limits_{\Sigma} p\mathbf{n}\mathrm{d}A, \mathbf{C} = \oint\limits_{\Sigma} p(\mathbf{r}\times\mathbf{n})\mathrm{d}A.$$

Electrostatic field acts on conductors with a pressure directed outwards from the conductor, regardless of the orientation of the field, whose value equals the energy density of the electric field on the surface of the conductor. Because the field is oriented normal to the conductor's surface, this pressure expression is consistent with Maxwell stress tensor expression.

In the general case, according to the electromagnetic energy theorem in moving media and the impulse conservation theorem in linear media, the volume density of the electrostatic force has the expression:

$$\mathbf{f} = \rho_V\mathbf{E} - \frac{E^2}{2}(\text{grad }\varepsilon) + \text{grad}(\frac{E^2}{2}\cdot\tau\cdot\frac{\partial\varepsilon}{\partial\tau}) = \text{div}[\mathbf{E}\wedge\mathbf{D}^T + \bar{\bar{\mathbf{I}}}(\frac{E^2}{2}\cdot\tau\cdot\frac{\partial\varepsilon}{\partial\tau} - w_e)]. \quad (2.46)$$

In the left part the Coulomb force can be recognized, that acts upon the inhomogeneous dielectrics, due to temporal polarization and electrostrictive force. In the right part there are the Maxwell stress and electrostrictive tensor expression.

Another method to compute the mechanical effects of electrostatic fields is based on the generalized forces theorem. The generalized forces acting on the armatures of linear dipolar or multipolar capacitors have the expressions:

$$\begin{aligned} &W_e = \frac{1}{2}\mathbf{q^T S q} \Rightarrow X_k = -\frac{\partial W_e}{\partial x_k}\mid_q \Rightarrow X_k = -\frac{1}{2}\mathbf{q^T}\frac{\partial\mathbf{S}}{\partial x_k}\mathbf{q};\\ &W_e = \frac{1}{2}\mathbf{v^T C v} \Rightarrow X_k = \frac{1}{2}\mathbf{v^T}\frac{\partial\mathbf{C}}{\partial x_k}\mathbf{v}. \end{aligned} \quad (2.47)$$

The mechanical effects of the electrostatic field are determined by the fundamental problem solution of this regime. Knowing the field, the ponderomotor forces by different methods can be determine, the result being in principle the same.

2.2.2 Electrodynamic

In this section are presented the physical (conceptual) and mathematical modelling aspects of the electromagnetic field of RF-MEMS devices.

The **fundamental problem of the electrodynamic regime** consists of determining the electric field starting from its sources; so the know data is represented by the following quantities and characteristics [144, 188, 189, 155, 196]:

- The shape and size of the computing domain D.
- The dielectric, magnetic and conductivity parameters. This must be known in every point of the computing domain; for linear medium it is described by the permittivity ε, permeability μ and conductivity σ, which are positive defined values, symmetric scalars or tensors.
- The internal field sources. They must be known in every point of the computing domain; they are described in the case of affine environments by fields vector: permanent polarization $\mathbf{P}_P$, permanent magnetization $\mathbf{M}_P$, and the imposed electric current $\mathbf{J}_I$.
- The external field sources described by boundary conditions. For example $\mathbf{E}_t$ or $\mathbf{H}_t$ must be known in every point of the computational domain boundary. Most often they are null. For example $\mathbf{E}_t = \mathbf{0}$ the Perfect Electric Conductor (PEC) boundary condition corresponds to a perfect conductor (supra-conductor with $1/\sigma = 0$) placed on the boundary. $\mathbf{H}_t = \mathbf{0}$, the Perfect Magnetic Conductor (PMC) boundary condition corresponds to a perfect ferromagnetic material (with $1/\mu = 0$) placed on the boundary. But these are not the only boundary conditions that are possible.
- The previous field sources, that describe the initial conditions (vectorial fields $\mathbf{D}$ and $\mathbf{B}$), defined in every point of the computational domain at the initial time moment $t = 0$.

The equations of the fundamental problem are the Mawell's equations (2.48)-(2.54), which are the local (differential) form of the laws of electromagnetic field, characterized by vectors $\mathbf{E}$, $\mathbf{D}$, $\mathbf{B}$, $\mathbf{H}$. However the main unknowns of the problem in the electrodynamic regime of electromagnetic field are the magnetic vector potential $\mathbf{A}(\mathbf{r},\mathrm{t})$ and the electric scalar potential $\mathrm{V}(\mathbf{r},\mathrm{t})$, defined on the domain D and during the time interval of analysis $(0, T)$. They must satisfy the the second order equation (2.55), (2.56), the initial conditions and boundary conditions.

After the electromagnetic potentials have been found, the magnetic induction and electric field strength is determined from relations $\mathbf{B} = \mathrm{rot}2.55, V = -\mathrm{grad}V - \mathrm{d}2.55/\mathrm{d}t$, and other quantities of the field are determined by applying the material relationships.

There are many other methodologies of computation, the EM field may be calculated directly by solving the first order equations or their consequences thereof without being computed the electrodynamic potentials. In this procedure as the one based on potentials, the real charge density, induced in conductors and weak conductors dielectrics, is the unknown of the problem, because it results from electric flux density using electric flux law.

The initial condition for electric flux density entails knowing the initial distribution of electric charge, which determines its subsequent distribution. From magnetic field strength results the electric current density induced in conductive media, using magnetic circuit law. As a consequence of the electromagnetic induction law (2.50), magnetic flux law is satisfied for any moment of time, if it is satisfied at the initial moment by the initial condition.

The fundamental EM field problem is well formulated if the following conditions are

fulfilled [142]:

- the problem has a solution,
- the solution is unique,
- the solution depends continuously on the field sources and the problem input data.

If the solution doesn't depend continuously on the field sources and the problem input data, then small variation of the data can determine large variations of the solution, because in practice the data comes often from measurements.

The general full-wave electromagnetic field regimes the assumption is that the bodies are fixed, without any movement. In time domain, these regimes equations are hyperbolic partial differential equations of d'Alambert type. The main physical phenomena described by them is the propagation, the field in this regime being an electromagnetic wave. Two regimes can be distinguished:

- *Electrodynamic - ED full-wave - FW*, is the general regime, in media that can be conductors;
- *Electrodynamic - ED loss-less - LL*, is the general regime of the electromagnetic field in vacuum or in perfect isolated bodies.

The analysis of these regimes can be done in the frequency domain, using complex representation when quantities vary sinusoidal in time or by Fourier or Laplace transform, in transient regimes. These operational representations transform the time derivatives in algebraic operations multiplied by $j\omega$, respectively (frequency variable) complex s. The hyperbolic equations with second order derivatives in time, which may contains also first order derivatives, of damping and diffusion, turn into complex Helmholtz type equations, similar to the elliptical ones. In LL regime, which did not contain the diffusive equations, modal analysis problem can be formulated, for searching resonance modes and the eigenfrequencies.

As it was mentioned before, the electrodynamic field is described by vectorial fields **E, D, B, H**. The field sources are the electric charges ρ permanent polarization $\mathbf{P}_P$, residual magnetization $\mathbf{B}_r$ equivalent to a permanent magnetization $\mathbf{M}_p$ and the imposed electrical current $\mathbf{J}_i$ equivalent to the impressed electric field $\mathbf{E}_i$. Material constants are electric permittivity ε, magnetic permeability μ and electric conductivity σ, which are either scalars or tensors (Fig.2.9).

The **electrodynamics fundamental equations or Maxwell equations** in general full-wave regime are:

- Electric flux law:

$$\psi_\Sigma = q_{D_\Sigma} \Leftrightarrow \oint_\Sigma \mathbf{D} \cdot \mathrm{d}\mathbf{A} = \int_{D_\Sigma} \rho \mathrm{d}v \Rightarrow \mathrm{div}\mathbf{D} = \rho. \tag{2.48}$$

- Magnetic flux law:

$$\varphi_\Sigma = 0 \Leftrightarrow \oint_\Sigma \mathbf{B} \cdot \mathrm{d}\mathbf{A} = 0 \Rightarrow \mathrm{div}\mathbf{B} = 0; \mathbf{n}_{12} \cdot (\mathbf{B}_2 - \mathbf{B}_1) = 0 \Leftrightarrow \mathrm{div}_s\mathbf{B} = 0. \tag{2.49}$$

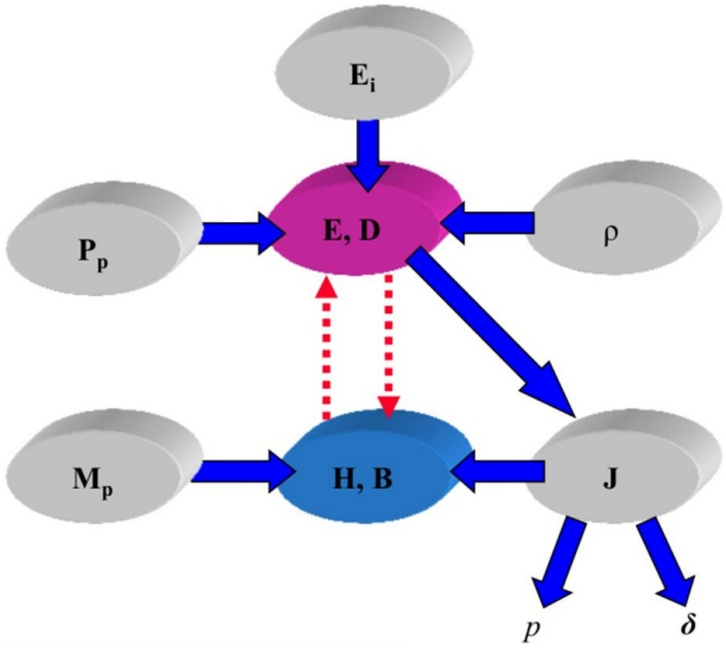

Figure 2.9: Electrodynamic regime diagram of causal relationships [142].

- Electromagnetic induction law in fixed media:

$$u_\Gamma = \frac{\mathrm{d}\varphi_{S_\Gamma}}{\mathrm{d}t} \Leftrightarrow \oint_\Gamma \mathbf{E}\cdot\mathrm{d}\mathbf{r} = \frac{\mathrm{d}}{\mathrm{d}t}\int_{S_\Gamma}\mathbf{B}\cdot\mathrm{d}\mathbf{A} \Rightarrow \mathrm{rot}\mathbf{E} = -\frac{\partial\mathbf{B}}{\mathrm{d}t};$$
$$\mathbf{n}_{12}\times(\mathbf{E}_2-\mathbf{E}_1)=\mathbf{0}\Leftrightarrow\mathbf{E}_{t2}=\mathbf{E}_{t1}. \tag{2.50}$$

- Magnetic circuit law in immobile media:

$$u_{m\Gamma} = i_{S_\Gamma} + \frac{d\psi_{S_\Gamma}}{dt} \Leftrightarrow \oint_\Gamma \mathbf{H}\cdot\mathrm{d}\mathbf{r} = \int_\Gamma \mathbf{J}\cdot\mathrm{d}\mathbf{A} + \frac{\mathrm{d}}{\mathrm{d}t}\int_{S_\Gamma}\mathbf{D}\cdot\mathrm{d}\mathbf{A} \Rightarrow \mathrm{rot}\mathbf{H} = \mathbf{J} + \frac{\partial\mathbf{D}}{\partial t};$$
$$\mathbf{n}_{12}\times(\mathbf{H}_2-\mathbf{H}_1)=\mathbf{0}\Leftrightarrow\mathbf{H}_{t2}=\mathbf{H}_{t1} \tag{2.51}$$

- Polarization law or the relationship between **D** and **E** law:

$$\mathbf{D}=\mathbf{f_1}(\mathbf{E})\Leftrightarrow\mathbf{D}=\varepsilon_0\mathbf{E}+\mathbf{P},\mathbf{P}=\mathbf{P}_t(\mathbf{E})+\mathbf{P}_p\Rightarrow\mathbf{D}=\overline{\overline{\varepsilon}}\mathbf{E}+\mathbf{P}_p. \tag{2.52}$$

- Magnetization law or the relationship between **B** and **H** law:

$$\mathbf{B}=\mathbf{f_2}(\mathbf{H})\Leftrightarrow\mathbf{B}=\mu_0(\mathbf{H}+\mathbf{M}),\mathbf{M}=\mathbf{M}_t(\mathbf{H})+\mathbf{M}_p\Rightarrow\mathbf{B}=\overline{\mu}\mathbf{H}+\mathbf{B}_r,\mathbf{B}_r=\mu_0\mathbf{M}_p. \tag{2.53}$$

- Conduction law or the relationship between **J** and **E** law:

$$\mathbf{J}=\mathbf{f_3}(\mathbf{E})\Leftrightarrow\mathbf{J}=\mathbf{J}_t(\mathbf{E})+\mathbf{J}_i\Rightarrow\mathbf{J}=\overline{\overline{\sigma}}\mathbf{J}+\mathbf{J}_i. \tag{2.54}$$

In general full-wave regimes, the electromagnetic field is described by two potentials. V the scalar electric potential and **A** the magnetic vector potential, based on:

- magnetic flux law: $\mathrm{div}\mathbf{B}=0\Rightarrow\mathbf{B}=\mathrm{rot}\mathbf{A}$
- electromagnetic induction law:

$$\mathrm{rot}\mathbf{E}=-\frac{\partial\mathbf{B}}{\partial t}\Rightarrow\mathrm{rot}\mathbf{E}=-\mathrm{rot}\frac{\partial\mathbf{A}}{\partial t}\Rightarrow\mathrm{rot}\left(\mathbf{E}+\frac{\partial\mathbf{A}}{\partial t}\right)=0\Rightarrow\mathbf{E}+\frac{\partial\mathbf{A}}{\partial t}=-\mathrm{grad}\ V.$$

The two laws generalize the magnetic vector potential and electrostatic scalar potential, but unlike these, they are time functions, and the electric field depends not only on the scalar potential (Coulombian component) but also on the time derivative of the vector potential (Faraday - induced component). Once computed, the two potentials determine the magnetic flux density and magnetic field strength, and then from the material laws the other components of the solution.

The second order equations satisfied by these potentials are obtained from magnetic circuit law and charge conservation theorem. In linear media they are:

$$\text{rot}\mathbf{H} = \mathbf{J} + \frac{\partial \mathbf{D}}{\partial t} \Rightarrow \text{rot}(\nu\ \text{rot}\mathbf{A}) + \sigma\frac{\partial \mathbf{A}}{\partial t} + \varepsilon\frac{\partial^2 \mathbf{A}}{\partial t^2} + \sigma\text{grad}\ V + \varepsilon\text{grad}\ \frac{\partial V}{\partial t} = 0, \quad (2.55)$$

$$\text{div}\mathbf{J} = -\frac{\partial \rho}{\partial t} \Rightarrow \text{div}\left(\sigma\text{grad}\ V + \sigma\frac{\partial \mathbf{A}}{\partial t}\right) = \frac{\partial \rho}{\partial t} \Rightarrow \text{div}(\sigma\text{grad}\ V) = \frac{\partial \rho}{\partial t} \quad (2.56)$$

Equation (2.56) is valid in the Coulomb type gouge condition: $\text{div}(\sigma\mathbf{A}) = 0 \Leftrightarrow \text{div}\mathbf{A} = -\text{grad}\ \sigma$, null for homogeneous conductors, imposed for the vector potential divergence, freely chosen without modifying the field.

In media in which $\mathbf{D} = \varepsilon\mathbf{E} + \mathbf{P}_p, \mathbf{B} = \mu\mathbf{H} + \mathbf{B}_r, \mathbf{B}_r = \mu_0\mathbf{M}_p \Leftrightarrow \mathbf{H} = \nu\mathbf{B} + \mathbf{I}_p, \mathbf{I}_p = -\nu\mathbf{B}_r, \mathbf{J} = \sigma\mathbf{J} + \mathbf{J}_i$, with affine characteristics, the second order equations are:

$$\begin{aligned}\text{rot}\mathbf{H} = \mathbf{J} + \frac{\partial \mathbf{D}}{\partial t} \Rightarrow \text{rot}(\nu\ \text{rot}\mathbf{A}) + \sigma\frac{\partial \mathbf{A}}{\partial t} + \varepsilon\frac{\partial^2 \mathbf{A}}{\partial t^2} + \sigma\text{grad}\ V + \varepsilon\text{grad}\frac{\partial V}{\partial t} = \\ = \mathbf{J}_i + \frac{\partial \mathbf{P}_p}{\partial t} - \text{rot}(\mathbf{I}_p),\end{aligned} \quad (2.57)$$

$$\text{div}\mathbf{J} = -\frac{\partial \rho}{\partial t} \Rightarrow \text{div}\left(\sigma\text{grad}\ V + \sigma\frac{\partial \mathbf{A}}{\partial t}\right) = \frac{\partial \rho}{\partial t} \Rightarrow \text{div}(\sigma\text{grad}\ V) = \frac{\partial \rho}{\partial t}. \quad (2.58)$$

The imposed current may induce other two field sources, the permanent polarization and magnetization, using fictitious magnetization and polarization current distributions, equivalent to these field sources. A significant simplification is achieved in domains where the scalar potential is zero, for example, the domain is isolated and not charged and potential boundary conditions are null.

Electrodynamic Energy Theorem, Tellegen's theorem. Consider a domain D, with boundary Σ characterized by the linear material constants $\varepsilon > 0, \mu > 0$ and $\sigma \geq 0$, and an imposed current density $\mathbf{J}_i$. If the local form of the electromagnetic energy theorem

$$-\text{div}(\mathbf{E} \times \mathbf{H}) = \mathbf{J} \cdot \mathbf{E} + \frac{\text{d}}{\text{d}t}\left(\frac{\mathbf{D} \cdot \mathbf{E}}{2} + \frac{\mathbf{E} \cdot \mathbf{H}}{2}\right) \quad (2.59)$$

is integrated on the spatial domain D, and then integrated on the time interval $(0, T)$ it

results:

$$
\begin{aligned}
&-\int_D \operatorname{div}(\mathbf{E}\times\mathbf{H})\mathrm{d}v = \int_D \mathbf{J}\cdot\mathbf{E}\mathrm{d}v + \frac{\mathrm{d}}{\mathrm{d}t}\int_D \left(\frac{\mathbf{D}\cdot\mathbf{E}}{2}+\frac{\mathbf{B}\cdot\mathbf{H}}{2}\right)\mathrm{d}v \Rightarrow \\
&W_{em} = \frac{1}{2}\int_D \left(\varepsilon E^2+\mu H^2\right)\mathrm{d}v = \int_D \left(\frac{D(0)^2}{\varepsilon}+\frac{B(0)^2}{\mu}\right)\mathrm{d}v - \\
&\int_0^T \left(\int_D \sigma E^2\mathrm{d}v + \int_D \mathbf{J}_i\cdot\mathbf{E}\mathrm{d}v + \int_{\partial D}(\mathbf{E}_t\times\mathbf{H}_t)\mathrm{d}\mathbf{A}\right) > 0.
\end{aligned}
\tag{2.60}
$$

It can be seen that the electromagnetic energy resulted by the integration of the energy density on the whole domain occupied by the field, has an increase equal to time integral of the power transferred by the field through domains boundaries, from outside to inside, excluding the power transferred to the bodies.

For materials with an affine electric and magnetic characteristic, to which $\mathbf{D}=\varepsilon\mathbf{E}+\mathbf{P}_p$ and $\mathbf{B}=\mu\mathbf{H}+\mathbf{B}_r$, the co-energy/energy density is:

$$
\begin{aligned}
&\mathbf{D}=\mathbf{f}(\mathbf{E})=\overline{\overline{\varepsilon}}\mathbf{E}+\mathbf{P}_p \Rightarrow w_e^* = \int_0^E \mathbf{D}'\cdot\mathrm{d}\mathbf{E}' = \int_0^E \mathbf{f}(\mathbf{E}')\cdot\mathrm{d}\mathbf{E}' = \\
&\int_0^E (\overline{\overline{\varepsilon}}\mathbf{E}+\mathbf{P}_p)\cdot\mathrm{d}\mathbf{E}' = \frac{\mathbf{E}\cdot\overline{\overline{\varepsilon}}\mathbf{E}}{2}+\mathbf{P}_p\cdot\mathbf{E} = \frac{\mathbf{DE}}{2}+\frac{\mathbf{P}_p\mathbf{E}}{2};
\end{aligned}
\tag{2.61}
$$

$$
\begin{aligned}
w_e &= \mathbf{D}\cdot\mathbf{E}-w_e^* = \frac{\mathbf{D}\cdot\mathbf{E}}{2}-\frac{\mathbf{P}_p\cdot\mathbf{E}}{2} = \frac{\mathbf{E}\overline{\overline{\varepsilon}}\mathbf{E}}{2}; \\
w_m &= \mathbf{B}\cdot\mathbf{H}-w_m^* = \frac{\mathbf{B}\cdot\mathbf{H}}{2}-\frac{\mathbf{B}_r\cdot\mathbf{H}}{2} = \frac{\mathbf{H}\cdot\overline{\overline{\mu}}\mathbf{H}}{2};
\end{aligned}
\tag{2.62}
$$

and the electromagnetic energy theorem becomes:

$$
\begin{aligned}
&W_{em}(t) = \frac{1}{2}\int_D (\mathbf{E}\cdot\overline{\overline{\varepsilon}}\mathbf{E}+\mathbf{H}\cdot\overline{\overline{\mu}}\mathbf{H})\ \mathrm{d}v = \frac{1}{2}\int_D (\mathbf{E}\cdot\overline{\overline{\varepsilon}}\mathbf{E}+\mathbf{H}\cdot\overline{\overline{\mu}}\mathbf{H})\ ||_{t=0}\ \mathrm{d}v - \int_0^T \left(\int_D \sigma E^2\mathrm{d}v + \right. \\
&\left. \int_D \mathbf{J}_i\cdot\mathbf{E}\mathrm{d}v + \int_D \left(\mu_0\mathbf{H}\cdot\frac{\partial\mathbf{M}_p}{\partial t}+\mathbf{E}\cdot\frac{\partial\mathbf{P}_p}{\partial t}\right)\mathrm{d}v + \int_{\partial D}(\mathbf{E}_t\times\mathbf{H}_t)\cdot\mathrm{d}\mathbf{A}\right) > 0.
\end{aligned}
\tag{2.63}
$$

Electrodynamic Regime Uniqueness Theorem. The correct boundary conditions of the electrodynamics problems are given by uniqueness theorems of the solution of the fundamental problem. The demonstration of the uniqueness of the solution is based on

electromagnetic energy theorem:

$$\begin{aligned}
&\int\limits_{D_\Sigma} \sigma\mathbf{E}\cdot\mathbf{E}\mathrm{d}v + \frac{\mathrm{d}}{\mathrm{d}t}\int\limits_{D_\Sigma}\left(\frac{\mu\mathbf{H}\cdot\mathbf{H}}{2}+\frac{\varepsilon\mathbf{E}\cdot\mathbf{E}}{2}\right)\mathrm{d}v = \int\limits_{D_\Sigma}\mathbf{E}\cdot\mathbf{J}_i\ \mathrm{d}v - \\
&-\int\limits_{D_\Sigma}\left(\mathbf{E}\frac{\partial\mathbf{P}_p}{\partial t}+\mu_0\mathbf{H}\frac{\partial\mathbf{M}_p}{\partial t}\right)\mathrm{d}v - \oint\limits_{\Sigma}(\mathbf{E}_t\times\mathbf{H}_t)\mathrm{d}\mathbf{A} \Rightarrow \int\limits_0^T\int\limits_{D_\Sigma}\sigma\mathbf{E}\cdot\mathbf{E}\ \mathrm{d}v\ \mathrm{d}t' + \\
&+\int\limits_{D_\Sigma}\left(\frac{\mu\mathbf{H}\cdot\mathbf{H}}{2}+\frac{\varepsilon\mathbf{E}\cdot\mathbf{E}}{2}\right)\mathrm{d}v = \int\limits_{D_\Sigma}\left(\frac{\mu\mathbf{H}\cdot\mathbf{H}}{2}\bigg|_{t=0}+\frac{\varepsilon\mathbf{E}\cdot\mathbf{E}}{2}\bigg|_{t=0}\right)\mathrm{d}v + \\
&+\int\limits_0^T\left(\mathbf{E}\cdot\mathbf{J}_i\ \mathrm{d}v - \int\limits_{D_\Sigma}\left(\mathbf{E}\cdot\frac{\partial\mathbf{P}_p}{\partial t}+\mu_0\mathbf{H}\cdot\frac{\partial\mathbf{M}_p}{\partial t}\right)\mathrm{d}v - \oint\limits_{\Sigma}(\mathbf{E}_t\times\mathbf{H}_t)\cdot\mathrm{d}\mathbf{A}\right)\mathrm{d}t'.
\end{aligned} \tag{2.64}$$

Thus, the uniqueness conditions are identified:

- The imposed current density required in all points of the computational domain during the analysis.
- The permanent polarization $\mathbf{P}_P$ in all points of the computational domain during the analysis.
- The permanent magnetization $\mathbf{M}_P$ in all points of the computational domain during the analysis.
- Tangential component of the magnetic field or electric field from all points of the boundary, during the analysis $\mathbf{E}_T$ or $\mathbf{H}_T$.
- The initial distribution of the electric field $\mathbf{E}$ in all points of the computational domain.
- The initial distribution of the magnetic field $\mathbf{H}$ in all points of the computational domain.

If all these conditions have 0 values, the right side of (2.64) vanishes:

$$0 \le \int\limits_{D_\Sigma}(\mu H^2+\varepsilon E^2)\mathrm{d}v = -2\int\limits_0^T\int\limits_{D_\Sigma}\sigma E^2\mathrm{d}v \le 0. \tag{2.65}$$

If $\sigma > 0$ in all points of the computational domain, the dissipated energy in the field by conduction is positively defined, and equality (2.65) with its restrictions can be satisfied only by null electric field $\mathbf{E} = \mathbf{0}$. If the permeability is strictly positive, then it follows that the intensity of the magnetic field $\mathbf{H} = \mathbf{0}$, even with the $\varepsilon = 0$ (in MQS regime). Dissipative condition $\sigma = 0$ imposed on all points of the domain is extremely restrictive for many of the practical problems, especially the LL regime. So it can be eliminated, replaced by $\varepsilon > 0$ to cancel the electric field. Consequently the other components of the electromagnetic field are canceled: $\mathbf{J} = \sigma\mathbf{E} = 0$, $\mathbf{B} = \mu\mathbf{H} = 0$, $\mathbf{D} = \varepsilon\mathbf{E} = 0$ and $\rho = \mathrm{div}\mathbf{D} = 0$. According to the null solution lemma, the uniqueness of all ED-FW and ED-LL field components result, under the conditions described above.

Both current and electric charge have a double status; that of the source and that of the solution (for instance the imposed current, as the known current, injected into antennas or the equivalent, virtual magnetization *amperian* current is the field source). Instead the conduction current density, which depends on the electric field strength is a component of the solution. Similarly, imposed charge, as is known, injected into antennas or the virtual equivalent of polarization Coulomb charge is the source of the field, but the real charge density, which depends on electric field strength is a component of the solution.

As it have been proven, the uniqueness conditions requires the knowledge of the tangential component of the electric field and magnetic field on the boundary. This data refers either to a system of imposed potential electrodes placed on the boundary, or to a system of currents distributed over a perfect ferromagnetic body. Or knowing the transversal field in the aperture (port) of a waveguide which supplies the computing domain, often with a known incident plane wave. Zero boundary condition correspond to enclosures, made from perfect conductors or covered by a perfect ferromagnetic layer. In many practical situations, the boundary null conditions are met on symmetry planes, on that the electric or magnetic field fall orthogonally, that is they are transversely oriented, or with zero tangential component, being longitudinally oriented.

The previous equations and problems refer to the **time domain transient regime**. In time domain most often, in the practical applications of electrodynamic regime, physical quantities have a sinusoidal time variation: $f(t) = F\sqrt{2}\sin(\omega t + \varphi)$, where F is the effective (rms) value of the quantity $\omega = 2\pi\nu = \frac{2\pi}{T}$ is the angular frequency, ν is the frequency, T is the period and φ is the initial phase. This particular variation over time allows a simplification of the equations through their **complex representation**. For each item of the set S of sinusoidal functions is assigned a complex number defined as:

$$\underline{F} = Fe^{j\varphi} = F(\cos\varphi + j\sin\varphi), \tag{2.66}$$

whose module is the rms value of the sinusoidal quantity and whose argument is its initial phase. The set S is a two-dimensional linear (vectorial) space with scalar product defined by two functions, one complex conjugate proportional to the active power if a signal is voltage and the other is current. The operator of the complex representation is bijective and has the following two characteristic properties:

- It is linear, transforming every linear combinations of the sinusoidal functions into a linear combinations of complex numbers with the same coefficients.
- It transforms the differential operations of derivation and integration into algebraic operations of multiplication and division by $j\omega$:

$$\begin{aligned}
&f(t) = F\sqrt{2}\sin(\omega t + \varphi) \in S \Leftrightarrow \underline{F} = \mathcal{C}[f(t)] = Fe^{j\varphi} \in \mathbb{C} \Rightarrow \\
&f(t) = \mathcal{C}^{-1}[\underline{F}] = \sqrt{2}\Im(\underline{F}e^{j\omega t}) = \sqrt{2}\ \Im(Fe^{j\varphi}e^{j\omega t}) = \sqrt{2}\ \Im(Fe^{j(\omega t+\varphi)}); \\
&f'(t) = F\sqrt{2}\cos(\omega t + \varphi) \Leftrightarrow \underline{F'} = j\omega\underline{F} = Fe^{j(\varphi+\pi/2)}; \\
&f(t) = \sum_{k=1}^{n} \lambda_k f_k(t) \Leftrightarrow \underline{F} = \sum_{k=1}^{n} \lambda_k \underline{F}_k.
\end{aligned} \tag{2.67}$$

The last two relations called operational and linear properties are very useful in practice because it simplifies the equations based on time derivatives, transforming them in algebraic equations. The time variable and time derivatives are removed from the equation, by this complex representation. After applying this operator, vectorial fields become complex vector:

$$\begin{aligned}&\mathbf{E}(t)=\mathbf{i}E_x(t)+\mathbf{j}E_y(t)+\mathbf{k}E_z(t);E_x,E_y,E_z\in S\Rightarrow\\&\underline{\mathbf{E}}=\mathbf{i}E_x+\mathbf{j}E_y+\mathbf{k}E_z\in\mathbb{C}^3\Rightarrow\mathbf{G}=\frac{\partial\mathbf{E}}{\partial t}\in S^3\Rightarrow\mathbf{G}=j\omega\mathbf{E}.\end{aligned}\tag{2.68}$$

Another class of problems which benefit from the complex representation is the periodic problems; i.e. the case when the quantities have a periodic temporal variation, but non-sinusoidal. Such quantities can be decomposed in Fourier series, consisting of harmonic frequencies:

$$\begin{aligned}&f(t)=f(t+T)\in\mathcal{P}\Rightarrow f(t)=\sum_{k=0}^{\infty}\left(a_k\cos\left(k\omega t\right)+b_k\sin\left(k\omega t\right)\right);\\&a_k=\frac{2}{T}\int_0^T f(t)\cos\left(k\omega t\right)\mathrm{d}t;b_k=\frac{2}{T}\int_0^T f(t)\sin\left(k\omega t\right)\mathrm{d}t;a_0=\frac{1}{T}\int_0^T f(t)\cos\left(k\omega t\right)\mathrm{d}t.\end{aligned}\tag{2.69}$$

The expressions of the Fourier coefficients are a consequence of orthogonality of *sin* and *cos* harmonics of various orders. Considering *sin* and *cos* coefficients the imaginary parts of the complex coefficients, the Fourier series takes a more elegant form:

$$\begin{aligned}&f(t)=\sum_{k=-\infty}^{\infty}c_ke^{jk\omega t};c_k=\frac{2}{T}\int_{-T/2}^{T/2}f(t)e^{-jk\omega t}\\&c_k=c_{-k}^*=\begin{cases}\frac{(a_k-jb_k)}{2};&k>0\\a_0;&k=0\\\frac{(a_k+jb_k)}{2};&k<0\end{cases}\Leftrightarrow a_k=c_k+c_{-k};b_k=c_k-c_{-k}\end{aligned}\tag{2.70}$$

which use complex numbers and negative virtual harmonics. Any periodic signal in the frequency domain is represented as a series of complex numbers, called the signal spectrum. The correspondence between the set of regular functions and their spectra is performed by Fourier transform $\mathcal{F}$. By scaling the spectrum at a finite number of harmonics defines discrete Fourier transform $\mathcal{F}_D$ (Discrete Fourier Transform - DFT):

$$\begin{aligned}&\underline{F}=\mathcal{F}[f(t)]=[c_k]_{k=\overline{0,\infty}}\in\mathbb{C}^\infty\Rightarrow\underline{F}=\mathcal{F}_d[f(t)]=[c_k]_{k=\overline{0,n}}\in\mathbb{C}^n,\\&f(t)=\mathcal{F}^{-1}[\underline{F}]=\sum_{k=-\infty}^{\infty}c_ke^{jk\omega t}=c_0\sum_{k=1}^{\infty}(c_ke^{jk\omega t}+c_k^*e^{-jk\omega t})\end{aligned}\tag{2.71}$$

If we apply the complex representation to all field components

$$\underline{\mathbf{E}}=\mathcal{C}[\mathbf{E}(t)];\underline{\mathbf{H}}=\mathcal{C}[\mathbf{H}(t)];\ldots,$$

Maxwell's equations have the following complex form:

$$\begin{cases} \nabla \cdot \mathbf{D} = \rho \\ \nabla \cdot \mathbf{B} = 0 \\ \nabla \times \mathbf{E} = -\frac{\partial \mathbf{B}}{\partial t} \\ \nabla \times \mathbf{H} = \mathbf{J} + \frac{\partial \mathbf{D}}{\partial t} \\ \mathbf{D} = \varepsilon \mathbf{E} \\ \mathbf{B} = \mu \mathbf{H} \\ \mathbf{J} = \sigma \mathbf{E} + \mathbf{J}_i \end{cases} \Rightarrow \begin{cases} \nabla \cdot \underline{\mathbf{D}} = \underline{\rho} \\ \nabla \times \underline{\mathbf{E}} = -j\omega \underline{\mathbf{B}} \\ \nabla \times \underline{\mathbf{H}} = \underline{\mathbf{J}} + j\omega \underline{\mathbf{D}} \\ \underline{\mathbf{D}} = \varepsilon \underline{\mathbf{E}} \\ \underline{\mathbf{B}} = \mu \underline{\mathbf{H}} \\ \underline{\mathbf{J}} = \sigma \underline{\mathbf{E}} + \underline{\mathbf{J}}_i \end{cases} \Rightarrow \begin{cases} \nabla \cdot (\varepsilon \underline{\mathbf{E}}) = \underline{\rho} \\ \nabla \times \underline{\mathbf{E}} = -j\omega\mu \underline{\mathbf{H}} \\ \nabla \times \mathbf{H} = (\sigma + j\omega\varepsilon)\underline{\mathbf{E}} + \underline{\mathbf{J}}_i \end{cases} \tag{2.72}$$

It can be noticed that in this regime, the complex form of the magnetic flux law is a consequence of the electromagnetic induction law and thus it is not independent whit respect to the other fundamental relationship.

For a correct analysis of the studied device and to ensure its compatibility to other circuit elements the equations of the essential phenomena must by identify. The mathematical structures that represent the physic quantities must also be identify, i.e. the algebraic and/or topological spaces, the definition domain and the functions or operators intervening in equations. Sometimes the mathematical model needs to correct the physical model to ensure correct formulation of the problem [144].

The concept of Electromagnetic Circuit Element (EMCE). Full-wave electromagnetic models can take into account all high frequency field effects, eddy currents, skin effect, dielectric loss, wave propagation, which makes the FW field solution not only necessary but also extremely useful for obtaining accurate reduced order models. For the FW analysis, the first step is to chose an appropriate electromagnetic field formulation with appropriate boundary conditions in order to describe a well defined response (input/output system). For this the Electro-Magnetic Circuit Element [197] formulation is used, which in its general form is presented in Fig.2.10. It will allow the formulation and solving of the field-circuit coupled problems.

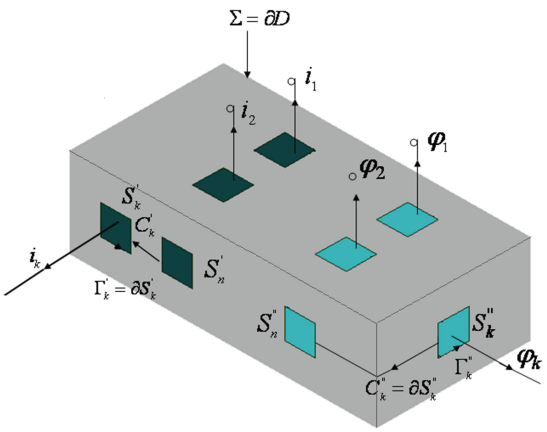

Figure 2.10: Electro-Magnetic Circuit Element (EMCE) [197]

The Electro-Magnetic Circuit Element(EMCE) is a simple connected domain Ω bounded by the surface Σ, composed form n' disjunct parts $S'_1, S'_2, \ldots, S'_n$ called *electrical terminals* and n'' disjunct parts $S''_1, S''_2, \ldots, S''_n$ called *magnetic terminals*, on which the following

boundary conditions are met:

$$\mathbf{n} \cdot [\nabla \times \mathbf{E}(P,t)] = 0, \text{ for } \forall P \in \Sigma - \cup S''_k, \tag{2.73}$$

$$\mathbf{n} \cdot [\nabla \times \mathbf{H}(P,t)] = 0, \text{ for } \forall P \in \Sigma - \cup S'_k, \tag{2.74}$$

$$\mathbf{n} \times \mathbf{E}(P,t) = 0, \text{ for } \forall P \in \Sigma - \cup S'_k, \tag{2.75}$$

$$\mathbf{n} \times \mathbf{H}(P,t) = 0, \text{ for } \forall P \in \Sigma - \cup S''_k. \tag{2.76}$$

were $\mathbf{n}$ is the surface Σ normal vector in the P point.

The EMCE conditions assures a consistently coupling with the external electrical / magnetic circuit, connected at its electric / magnetic terminals. Condition (2.73) prohibits inductive coupling with the outside, except the magnetic terminals. Condition (2.74) prohibits resistive and capacitive coupling on the boundary, except the electrical terminals. The conditions (2.75) and (2.76) are imposed to ensure the equipotential aspect of the electric and magnetic terminals.

For any electrical terminals, electrical current intensity and the electric potential of that terminal k are:

$$i_k(t) = \int_{\Gamma'_k} \mathbf{H} \cdot d\mathbf{r}, \text{ for } k = \overline{1,n}. \tag{2.77}$$

$$v_k(t) = \int_{C'_k} \mathbf{E} \cdot d\mathbf{r}, \text{ for } k = \overline{1,n}. \tag{2.78}$$

were Γ'_k is a oriented closed curve which borders the electric terminal k and C'_k is an open curve that connects k terminal to the reference terminal.

In the same manner, for any magnetic terminal, the magnetic fluxes and potentials are defined as flows:

$$\varphi_k(t) = \int_{\Gamma''_k} \mathbf{E} \cdot d\mathbf{r}, \text{ for } k = \overline{1,n}. \tag{2.79}$$

$$u_k(t) = \int_{C''_k} \mathbf{H} \cdot d\mathbf{r}, \text{ for } k = \overline{1,n}. \tag{2.80}$$

were Γ''_k is a oriented closed curve which borders the magnetic terminal k and C''_k is an open curve that connects k terminal to the reference terminal.

To ensure the well formulations of the electromagnetic field problem inside EMCE, the uniqueness theorem state that: The electromagnetic field problem associated to the Electro-Magnetic Circuit Element described by the Maxwell equations in linear materials, the (2.73)-(2.76), (2.77), (2.79) boundary conditions with null initial conditions, having the terminals excited with known values for the electric voltage or current or magnetic flux has the unique solution: $\mathbf{E}$(M,t), $\mathbf{D}$(M,t), $\mathbf{B}$(M,t), $\mathbf{H}$(M,t), $\mathbf{J}$(M,t), $\rho(M,t)$, for $\forall M \in \Omega, t > 0$. Consequently EMCE has the unique response (2.78) and (2.80).

If the electric terminals are excited with an electric potential instead of an electric current then (2.78) is the input signal and (2.77) is the output signal. Similar if the

magnetic terminals are excited with a magnetic potential instead of magnetic flux then (2.80) is the input signal and (2.79) is the output signal.

Consequently an EMCE device is a MIMO (Multiple Input Multiple Output) system having a number of input signals equal to the number of output signals, given by the number of its floating terminals (the grounded terminals are excluded). This dynamic systems with a finite numbers of inputs/outputs has however a infinite size of the state space. If it is composed by linear materials, the MIMO system is a linear one, described by linear transfer functions, which are the complex/operational circuit functions the impedance, admittance and hybrid functions.

A microwave device for which the terminals are identified can be described in terms of circuit theory quantities. The identification of terminals means the identification of disjoint simple connected surfaces on the domain boundary for which voltage and currents can be defined. Such quantities are defined in a natural way for microwave systems that operate in transversal electromagnetic mode (TEM). For any other propagating mode, the definition is a conventional one [198]. In the left hand side of Fig.2.11, which shows a device with 2 ports, the reference senses for the voltages and currents assigned to the ports are shown. Complex circuit parameters, such as the impedance matrix **Z** or the admittance matrix **Y**, are assigned to this representation (in the frequency domain), describing the linear relation between the vectors of complex terminal potentials and currents (U =ZI, I=YU), in the case of linear EMCE. Incident and reflected waves assigned to the ports are shown in the right hand side of Fig.2.11, S parameters (or **S** matrix) being associated to this representation.

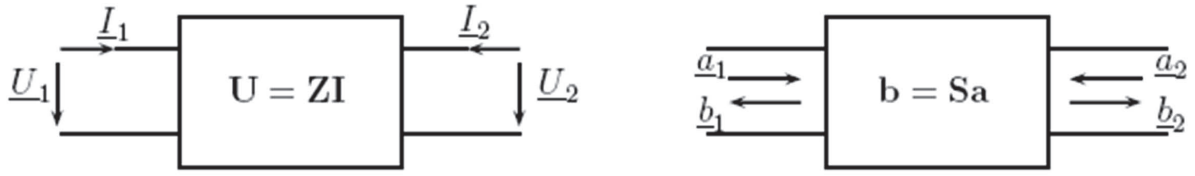

Figure 2.11: Quantities defined for a two port device: (left) voltages, currents, impedance matrix Z; (right) direct/incident waves, inverse/reflected waves, matrix of S parameters [199].

For a microwave multiport device, a characteristic impedance $\underline{Z}_{0k}$ associated to the propagation mode that corresponds to each port is defined. In general, the characteristic impedance is real [200], and it corresponds to a propagation without distortions. The voltage and the current of a port is expressed as a linear combination of the direct (incident) wave marked with plus ("+") subscript and inverse (reflected) wave marked with minus ("-") subscript, in a similar manner as for a transmission line:

$$\begin{aligned} \underline{U}_k &= \underline{U}_{k+} + \underline{U}_{k-} \\ & \qquad\qquad k = 1, 2 \\ \underline{I}_k &= \tfrac{1}{\underline{Z}_{0k}}(\underline{U}_{k+} + \underline{U}_{k-}) \end{aligned} \tag{2.81}$$

The S parameters represent a link between the transmitted or reflected voltage waves (marked with a minus subscript, and going out of the device) and the incident voltage waves (marked with plus subscript, and entering into the device). In fact, instead of

working with the quantities $\underline{U}_{k+}$ and $\underline{U}_{k-}$, are quantities are used, denoted by $\underline{a}_k$ and $\underline{b}_k$ and defined as:

$$\begin{aligned} \underline{a}_k &= \underline{U}_{k+}/\sqrt{\underline{Z}_{0k}} \\ \underline{b}_k &= \underline{U}_{k-}/\sqrt{\underline{Z}_{0k}} \end{aligned} \tag{2.82}$$

yielding

$$\begin{aligned} \underline{U}_k &= \sqrt{\underline{Z}_{0k}}(\underline{a}_k + \underline{b}_k) \\ \underline{I}_k &= (\underline{a}_k - \underline{b}_k)/\sqrt{\underline{Z}_{0k}} \end{aligned} \tag{2.83}$$

If the characteristic impedance of all ports are real and have the same value, than it makes sense to define the characteristic impedance of the multiport, denoted by Z_0, and the active power transferred to the device through the port k is expressed as:

$$P_k = a_k^2 + b_k^2 \tag{2.84}$$

where $a_k = |a_k|$ and $b_k = |b_k|$. Thus, the active power transferred through the port k is the difference between the average power injected by the incident wave and the average power extracted by the reflected wave. The S parameters (or the **S** matrix) are defined by the relationship between the reflected waves and the incident waves for all the n terminals:

$$\mathbf{b} = \mathbf{S}\mathbf{a} \tag{2.85}$$

where **a** is the column vector of the quantities $\underline{a}_k$ which represent normalized incident waves associated to the n ports, **b** is the column vector of the quantities $\underline{b}_k$ which represent normalized reflected waves, and **S** is a square complex, frequency dependent matrix of size n. The significance of each parameter is straightforward. S_{ii} is a reflection coefficient at port i, being the ratio between the reflected wave of the terminal i and the incident wave at the same terminal, provided that all the other terminals are adapted. S_{ij} is a transmission coefficient from the terminal j to the terminal i, being the ratio between the transmitted voltage wave at the terminal i and the incident wave at the terminal j provided that all the other terminals are adapted.

In [201] the S parameters are introduced directly with formulas (2.82), where the same quantity Z_0, called reference impedance, is used for all the ports.

In [200] there is a similar presentation, though the formulas are not quite identical with the ones presented above. This paper introduces also another approach, useful to realize a bridge with the definition of S parameters for A.C. circuits. Instead of using a characteristic impedance, the authors use a reference impedance Z_{ref} , with the constraint that its real part be strictly positive. *Pseudo-waves* are defined, which have no physical meaning, being only mathematical tricks with convenient properties. They are equivalent with the waves from the classical presentation when the reference impedance is equal to the characteristic impedance of the propagation mode. Although the pseudo-waves depend on the reference impedance, the voltage and the current do not depend on the reference impedance, even if this one appears explicitly in their expressions. In a similar way, pseudo-S parameters are defined. The fact that the pseudo-waves are identical with the normalized waves defined in the classical presentation if the reference impedance is

equal to the characteristic impedance, would make this choice a natural one. However, it is not always the most convenient. If the characteristic impedance depends strongly on the frequency, as it happens in the case of lossy devices, this is an inconvenient for the measurements interpretations (according to [200]).

S parameters do not have a correspondent in the electric circuit theory, for this one does not include circuit elements with propagation such as the waveguides. It does not make sense to talk about the characteristic impedance of a multiport electric circuit. And yet, similar concepts and reasoning with those defined in the microwave circuits were extended to the circuit theory. The reference impedance used is arbitrary. By analogy, quantities named waves are used, but the correct terminology would be with the prefix "pseudo" [200]. A similar statement can be formulated for the S parameters. The pseudo-waves and the pseudo-S parameters are quantities compatible with both theories. For a circuit port, a complex number, denoted by $\hat{\underline{Z}}_k$, and associated to that port is used, and the pseudo-waves are defined by [202], according to [200].

$$\begin{aligned} \underline{a}_k &= \frac{1}{2\sqrt{\Re\hat{\underline{Z}}_k}}(\underline{U}_k + \hat{\underline{Z}}_k\underline{I}_k) \\ \underline{b}_k &= \frac{1}{2\sqrt{\Re\hat{\underline{Z}}_k}}(\underline{U}_k - \hat{\underline{Z}}_k\underline{I}_k) \end{aligned} \tag{2.86}$$

The impedance $\hat{\underline{Z}}_k$ is arbitrary, the only constraint being that its real part be strictly positive. If this impedance is equal to the load impedance connected to that port, than $\underline{a}_k$ and $\underline{b}_k$ are power-waves. When $\hat{\underline{Z}}_k$ is a pure real number, the power waves become pseudo-waves with $Z_{ref} = \hat{\underline{Z}}_k$. Power waves satisfy (2.84) for any $\hat{\underline{Z}}_k$. Pseudo-waves satisfy (2.84) only if Z_{ref} is real.

In [201] conversions formulas from **S** to **Z** and from **Z** to **S** are proven, assuming that all the ports have the same reference impedance Z_0:

$$\begin{aligned} \mathbf{S} &= (\mathbf{Z} - Z_0\mathbf{I})(\mathbf{Z} + Z_0\mathbf{I})^{-1} \\ \mathbf{Z} &= (\mathbf{I} - \mathbf{S})^{-1}(\mathbf{I} + \mathbf{S})Z_0 \end{aligned} \tag{2.87}$$

where **I** is the unity matrix. It is interesting that in [203] the authors show conversions tables for complex impedance of source and load, and from the reaction [204] it follows that all those formulas based on power-waves are useless.

The matrix **S** is used for active circuits as well. In general, the active devices have non-linear characteristics, but for small signals, in the vicinity of a fixed static operating point, their characteristics can be linearized [205]. Under these conditions, the answer to small signals of active devices can be described by the matrix **S** which, in this case, depends on the static operation point.

Matrix **S** hold the following properties [205]:

- if the multiport is reciprocal, than the matrix **S** is symmetric. This is the case of devices made of linear and isotropic materials (usual circuit elements such as: resistors, inductors, capacitors, coupled inductors, interconnects);

- if the multiport is passive, than the absolute value of each component of the matrix **S** is less than or equal to 1;
- if the multiport is passive and lossless, than **S** is a unitary matrix, i.e. $\mathbf{S}^H\mathbf{S} = \mathbf{I}$. In this case, the sum of the squared values of the absolute value of the S parameters for any row or column is equal to 1, condition that reflects the power conservation in the considered device;
- for active devices, the matrix **S** is not symmetric and the S parameters may have a modulus greater than 1.

Due to these properties, the S parameters have an essential role in the description and characterization of the RF - microwave devices, circuits and systems. In our modeling procedure, the continuous MIMO (with infinite size of the state space) associated to EMCE devices is numerically modeled by FEM or FIT discretization (meshing) of Maxwell equations with EMCE boundary conditions with a finite number of states (still large). The resulted MIMO system is then reduced to compact model having a small number of states, without changing the number of terminal (number of input/output signals). The correct formulation of EM field problem with EMCCE boundary condition is therefore an important step in the multiphysic modelling of RF-MEMS devices.

2.2.3 Structural Mechanics

Solid mechanics is the branch of continuum mechanics that studies the behavior of solid materials, especially their motion and deformation under the action of forces, temperature changes, phase changes, and other external or internal agents.

Structural mechanics is the body of knowledge describing the relations between external forces, internal forces and deformation of structural materials. It is therefore necessary to clarify the various terms that are commonly used to describe these quantities. In large part, structural mechanics refers to solid mechanics because a solid is the only form of matter that can sustain loads parallel to the surface. However, some considerations of fluid-like behavior (creep) are also part of structural mechanics.

Structural mechanics or Mechanics of structures is the computation of deformations, deflections, and internal forces or stresses (stress equivalents) within structures, either for design or for performance evaluation of existing structures. It is one subset of structural analysis. Structural mechanics analysis needs input data such as structural loads, the structure's geometric representation and support conditions, and the materials properties. Output quantities may include support reactions, stresses and displacements. Advanced structural mechanics include the effects of stability and non-linear behaviors.

In structural mechanics every system contains three basic quantities: force, stiffness and deformation, which can be considered at different scale levels. The quantities used to describe space (coordinates *x,y,z*, shapes - manifolds, size, etc.), time (t), and their relation (velocity **v**, acceleration **a**, etc.) are considered as defined before, as **mass** (m) and its local repartition (mass density ρ). No distinction is made between inertial and gravitational masses.

Forces are vector quantities, thus having direction and magnitude and are measured in newtons [N]. They have different names depending upon their relationship to a reference plane (Fig.2.12): *Compressive* forces act normal and into the plane; *Tensile* forces act normal and out of the plane; and *Shear* forces act parallel to the plane.

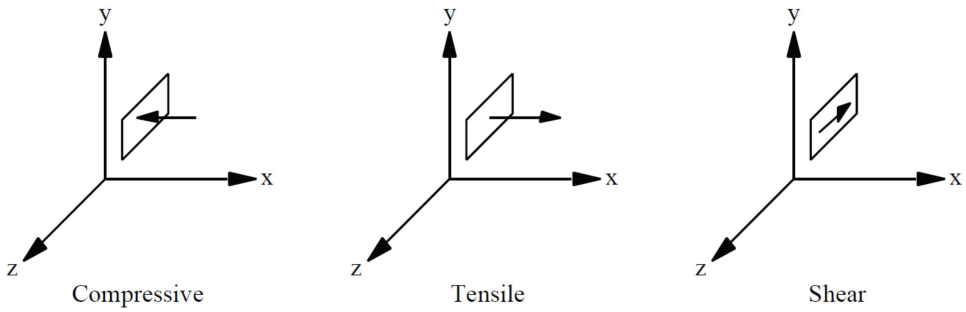

Figure 2.12: Definition of Forces [206].

To describe the local repartition the **force density** f [N/m^3]is used, which is the negative gradient of pressure $\mathbf{f} = -\text{grad}p$. The net force on a differential volume element dv of the body is:

$$\mathrm{d}\mathbf{F} = \mathbf{f}\mathrm{d}v \Leftrightarrow \mathbf{F}(t) = \int_{\Omega} \mathbf{f}(\mathbf{r}, t)\mathrm{d}v \tag{2.88}$$

Stress is the term used to define the intensity and direction of the internal forces acting at a particular point on a given plane. The stress acting at a point on a specific plane is a vector. Its direction is the limiting direction of force dF as area dA approaches zero. It is customary to resolve the stress vector into two components whose scalar magnitudes are: normal stress component σ – acting perpendicular to the plane and shear stress component τ – acting in the plane.

The selection of different cutting planes through point 0 would, in general, result in stresses differing in both direction and magnitude. Stress is thus a second-order tensor quantity, because not only are magnitude and direction involved but also the orientation of the plane on which the stress acts is involved. Writing the state of stress as tensor $\mathbf{T}$ (denoted also with σ), described in a Cartesian reference system as a symmetric 3×3 matrix:

$$\mathbf{T} = \begin{bmatrix} \sigma_x & \tau_{xy} & \tau_{xz} \\ \tau_{yx} & \sigma_y & \tau_{yz} \\ \tau_{zx} & \tau_{zy} & \sigma_z \end{bmatrix}$$

However, we have three equal pairs of shear stress: $\tau_{xy} = \tau_{yx}, \quad \tau_{xz} = \tau_{zx}, \quad \tau_{yz} = \tau_{zy}$, therefore, six quantities are sufficient to describe the stresses acting on the coordinate planes through a point, i.e., the triaxial state of stress at a point. If these six stresses are known at a point, it is possible to compute from simple equilibrium concepts the stresses on any plane passing through the point. The internal surface density of the (cohesion) force is $\mathbf{t} = \sigma\mathbf{n}$[N/m^2], where $\mathbf{n}$ is the surface normal. Fig.2.13 illustrates the general state of 3D stress at an arbitrary point by illustrating the stress components on the faces of an infinitesimal cubic element around the point.

The concept of **strain** is of fundamental importance with respect to the consideration of deflections and deformation. Strain is a directly measurable quantity, while stress is

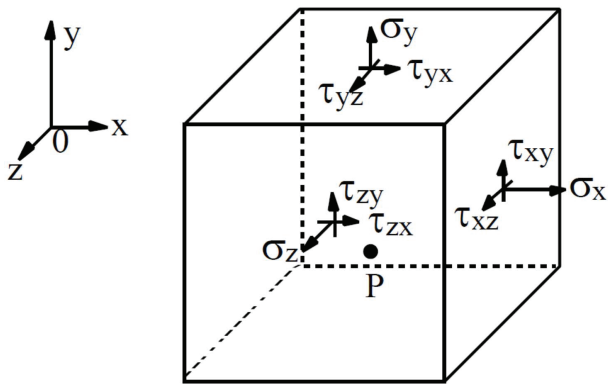

Figure 2.13: Stress element showing general state of 3D stress at a point located away from the origin [206].

not. Any physical body subjected to forces, i.e., stresses, deforms under the action of these forces. Strain describes the direction and the amplitude of the material deformation at any given point with respect to a specific plane passing through that point. *Strain is therefore a quantity analogous to stress.* Thus, state of strain is described by a tensor as state of stress is.

For convenience, strains are always resolved into normal components, ε, and shear components, γ (Fig.2.14). In these figures the original shape of the body is denoted by solid lines and the deformed shape by the dashed lines. The change in length in the x-direction is dx, while the change in the y-direction is dy. Hence, ε_x, ε_y and γ are written as indicated in these figures.

$$\varepsilon_x = \lim_{x\to 0} \frac{dx}{x}, \quad \varepsilon_y = \lim_{y\to 0} \frac{dy}{y}, \quad \gamma_{yx} = \lim_{y\to 0} \frac{dx}{y} = \tan\theta. \tag{2.89}$$

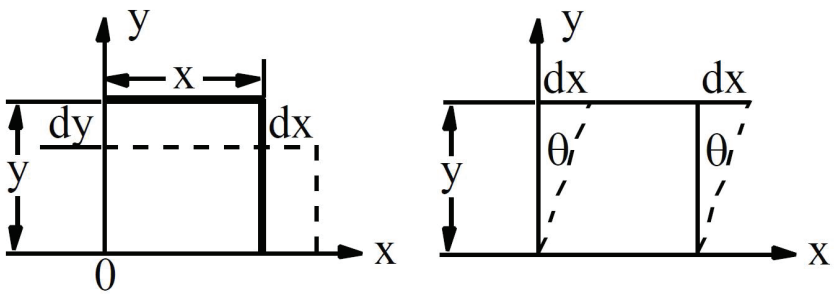

Figure 2.14: Deformation of a body where the x-dimension is extended and the y-dimension is contracted (Left). Plane shear strain (Right) [206].

Subscript notation for strains corresponds to that used with stresses. Specifically, γ_{yx} shear strain resulting from taking adjacent planes perpendicular to the y-axis and displacing them relative to each other in the x-direction (Fig.2.15); ε_x and ε_y are normal strains in x- and y-directions.

Sign conventions for strain also follow directly from those for stress: positive normal stress produces positive normal strain and vice versa. In the above example (Fig.2.14 - Left), $\varepsilon_x > 0$, whereas $\varepsilon_y > 0$. Adopting the positive clockwise convention for shear components,$\gamma_{xy} < 0$, $\gamma_{yx} > 0$. In Fig.2.14 - Right, the shear is γ_{yx} and the rotation

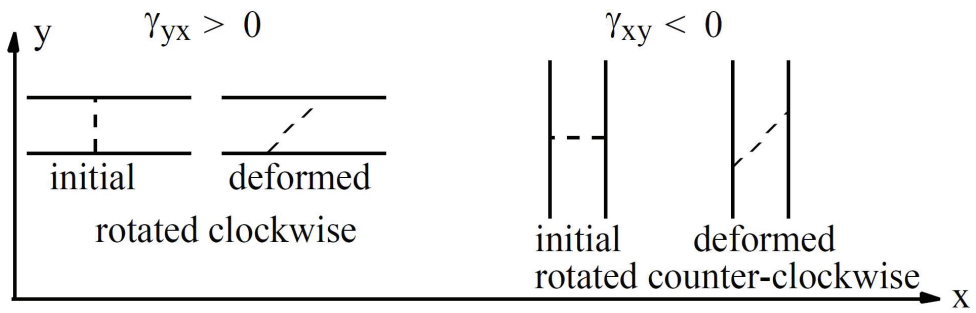

Figure 2.15: Strains resulting from Shear Stresses $\pm\gamma_{yx}$ [206].

is clockwise. Half of γ_{xy}, γ_{xz} and γ_{yz} is analogous to τ_{xy}, τ_{xz} and τ_{yz}, whereas ε_x is analogous to σ_x, resulting the state of strain as a symmetric tensor $\mathbf{E}$ (denoted also as ε) and represented by a symmetrical 3×3 matrix:

$$\mathbf{E} = \begin{bmatrix} \varepsilon_x & \frac{1}{2}\gamma_{xy} & \frac{1}{2}\gamma_{xz} \\ \frac{1}{2}\gamma_{yx} & \varepsilon_y & \frac{1}{2}\gamma_{yz} \\ \frac{1}{2}\gamma_{zx} & \frac{1}{2}\gamma_{zy} & \varepsilon_z \end{bmatrix}$$

The **law of conservation of mass** or **principle of mass conservation** states that for any system closed to all transfers of matter and energy, the mass of the system must remain constant over time, as system mass cannot change quantity if it is not added or removed. Hence, the quantity of mass is "conserved" over time.

Mass flux which cross any closed surface is equal to the minus time derivative of the internal mass. Or equivalently, the variation of any domain's mass is equal to the mass received by its boundary.

$$m(t_2) - m(t_1) = -\int_{t_1}^{t_2} Q_m(t)\mathrm{d}t = -\int_{t_1}^{t_2}\int_{\partial\Omega} \boldsymbol{\delta}(\mathbf{r},t)\cdot\mathrm{d}\mathbf{A}\mathrm{d}t \Rightarrow \int_{\partial\Omega} \boldsymbol{\delta}(\mathbf{r},t)\cdot\mathrm{d}\mathbf{A} = \frac{-\mathrm{d}m_\Omega}{\mathrm{d}t} \quad (2.90)$$

Mass is invariant (constant) if it there is no mass transfer.

The local form of the law is:

$$\mathrm{div}\boldsymbol{\delta} = -\frac{\partial\rho}{\partial t} \Leftrightarrow \mathrm{div}(\rho\mathbf{v}) = -\frac{\partial\rho}{\partial t}, \quad (2.91)$$

because $\boldsymbol{\delta} = \rho\mathbf{v}$ [kg/m$^2\cdot$ s]. This is a continuity equation, where $\mathbf{v}$ is the velocity, ρ is the mass density and $\boldsymbol{\delta}$ is mass flux density also known as the **momentum density (p)**. In incompressible materials $\rho = ct. \Rightarrow \mathrm{div}\mathbf{v} = 0$ the velocity is solenoidal (it has no sources), current lines being closed curves.

Momentum conservation law. Momentum $\mathbf{P} = m\mathbf{v}$ is defined to be the mass of an object multiplied by the velocity of the object. The conservation of momentum states that, within some problem domain, the amount of momentum remains constant; momentum is neither created nor destroyed, but only changed through the action of forces as described by Newton's laws of motion. For any bodies system, their momentum variation $\Delta\mathbf{P}$ is equal to the impulse $\mathbf{J}$ of all forces applied to them. Or equivalent, the total forces $\mathbf{F}$

applied to a body is equal to the time derivative of its momentum (which is mass m, multiplied by acceleration **a**):

$$\mathbf{P}(t_2) - \mathbf{P}(t_1) = \mathbf{J} =_{def} \int_{t_1}^{t_2} \mathbf{F}(t)\mathrm{d}t \Leftrightarrow \mathbf{F} = \frac{\mathrm{d}\mathbf{P}}{\mathrm{d}t}; \mathbf{P} = m\mathbf{v} \Rightarrow \mathbf{F} = m\frac{\mathrm{d}\mathbf{v}}{\mathrm{d}t} \Leftrightarrow \mathbf{F} = m\mathbf{a}. \quad (2.92)$$

The forces may be distributed over the volume (with a volume density $\mathbf{f}$ [N/m^3]) or/and over surface (with a surface density $\mathbf{t}$ [N/m^2]):

$$\mathbf{F} = \frac{\mathrm{d}\mathbf{P}}{\mathrm{d}t} \Leftrightarrow \int_\Omega \mathbf{f}\mathrm{d}v + \int_{\partial\Omega} \mathbf{t}\mathrm{d}A = \frac{\mathrm{d}}{\mathrm{d}t}\int_\Omega \mathbf{p}\mathrm{d}v \Rightarrow \int_\Omega \mathbf{f}\mathrm{d}v + \int_{\partial\Omega} \mathbf{t}\mathrm{d}A = \frac{\mathrm{d}}{\mathrm{d}t}\int_\Omega \rho\mathbf{v}\mathrm{d}v. \quad (2.93)$$

The local form, **motion equation**:

$$\begin{aligned}\mathbf{F} = \frac{\mathrm{d}\mathbf{P}}{\mathrm{d}t} \Leftrightarrow \int_\Omega \mathbf{f}\mathrm{d}v + \int_{\partial\Omega} \mathbf{t}\mathrm{d}A = \frac{\mathrm{d}}{\mathrm{d}t}\int_\Omega \mathbf{p}\mathrm{d}v \Rightarrow \int_\Omega \mathbf{f}\mathrm{d}v + \int_{\partial\Omega} \mathbf{t}\mathrm{d}A = \frac{\mathrm{d}}{\mathrm{d}t}\int_\Omega \rho\mathbf{v}\mathrm{d}v \Rightarrow \\ \Rightarrow \nabla\cdot\mathbf{T} + \mathbf{f} = \frac{\mathrm{d}\mathbf{p}}{\mathrm{d}t},\end{aligned} \quad (2.94)$$

where $\mathbf{T}$ is the tensor of the forces/stress/tensions applied on surfaces and $\mathbf{f}$ and $\mathbf{p}$ are the force and momentum densities, respectively.

The **equilibrium equation** its static form:

$$\nabla\cdot\mathbf{T} + \mathbf{f} = 0 \Rightarrow \int_\Omega \mathbf{f}\mathrm{d}v + \int_{\partial\Omega} \mathbf{t}\mathrm{d}A = 0. \quad (2.95)$$

Rotational Momentum Equation. The momentum of total forces applied to a body is equal to the time derivative of momentum of its momentum.

$$\int_\Omega \left[(\mathbf{r}\times\mathbf{f}) + \mathbf{c}\right]\mathrm{d}v + \int_\Omega \left[(\mathbf{r}\times\mathbf{t}) + \mathbf{m}\right]\mathrm{d}A = \frac{\mathrm{d}}{\mathrm{d}t}\int_\Omega \left[(\mathbf{r}\times\rho\mathbf{v}) + \mathbf{l}\right]\mathrm{d}v \quad (2.96)$$

Here $\mathbf{m}$ is surface density of external momentum, $\mathbf{c}$ is the volume density of external momentum, $\mathbf{l}$ is the spin volume density.

The first law of thermodynamics stats that the change in the internal energy of a closed system is equal to the amount of heat supplied to the system, minus the amount of work done by the system on its surroundings. Therefore, in any time moment, the speed of heat transferred to a system is the power transferred by the system to its surroundings plus the increasing speed of its internal energy:

$$\begin{aligned}&Q_t = p + \frac{\mathrm{d}U}{\mathrm{d}t} \Leftrightarrow \\ &-\int_{\partial\Omega} \mathbf{q}\cdot\mathrm{d}\mathbf{A} = -\int_{\partial\Omega} \nabla\cdot\mathbf{q}\mathrm{d}v = \int_\Omega p_c\mathrm{d}v + \int_{\partial\Omega} \mathbf{t}\cdot\mathbf{v}\mathrm{d}A + \int_\Omega \mathbf{f}\cdot\mathbf{v}\mathrm{d}v + \frac{\mathrm{d}}{\mathrm{d}t}\int_\Omega u\mathrm{d}v \quad \forall\Omega \Leftrightarrow \\ &\Leftrightarrow -(\nabla\cdot\mathbf{q}) = -p_c + \nabla(\mathbf{t}\cdot\mathbf{v}) + \mathbf{f}\cdot\mathbf{v} + \frac{\partial u}{\partial t} \Rightarrow \\ &\Rightarrow \frac{\partial u}{\partial t} = -(\nabla\cdot\mathbf{q}) + p_c - \nabla(\mathbf{t}\cdot\mathbf{v}) - \mathbf{f}\cdot\mathbf{v} \Rightarrow \\ &\Rightarrow \frac{\partial u}{\partial t} = -(\nabla\cdot\mathbf{q}) + p_c + \sum_{i,j}\mu_{ij}\frac{\partial w_i}{\partial x_j} + \sum_{i,j}\sigma_{ij}D_{ij},\end{aligned} \quad (2.97)$$

where $\mathbf{q}$ is the vector of heat transferred density [W/m^2], p_c is the transferred power density [W/m^3] (e.g. that of Joule-Lenz), the deformation rate $D_{ij} = v_{i,j} = \partial v_i/\partial x_j$ and couple stress $\mu_{ij}, \mathbf{w} = \mathrm{rot}(\mathbf{v}/2)$.

The second law of thermodynamics specifies the characteristic change in the entropy of a system undergoing a real process. The law accounts for the irreversibility of natural processes, and the asymmetry between future and past. For a system without exchange of matter with the surroundings, the change in system entropy exceeds the heat exchanged with the surroundings, divided by the temperature of the surroundings. In the idealized limiting case of a reversible process, the two quantities are equal, and the total entropy of system and surroundings remains unchanged. When heat exchange with the surroundings is prevented, the law states that in every real process the sum of the entropies of all participating bodies is increased.

The second law of thermodynamics has the form:

$$\frac{\mathrm{d}s}{\mathrm{d}t} = \frac{p}{T} - \frac{1}{\rho}\mathrm{div}\left(\frac{\mathbf{q}}{T}\right) + \gamma, \tag{2.98}$$

were ds/dt is the rate of increase of the system's entropy, p is distributed internal heat source per unit mass, γ is non-negative entropy production rates due to irreversible processes and $\mathbf{q}$ is the outward heat flux vector.

In the case of linear elastic solids the total strain tensor is written in terms of the displacement gradient[207]:

$$\varepsilon = \frac{1}{2}\left(\nabla\mathbf{u} + \nabla\mathbf{u}^T\right). \tag{2.99}$$

The fundamental constitutive relation, which describe the most material behavior (elasticity) is the Hooke's law which relates the stress tensor to the strain tensor and temperature:

$$\sigma = \sigma_0 + C : (\varepsilon - \varepsilon_0 - \varepsilon_{th}), \tag{2.100}$$

where C is the 4th order elasticity tensor, ":" stands for the double-dot tensor product (or double contraction), σ_0 and ε_0 are initial stresses and strains, $\varepsilon_{th} = \alpha(T - T_{ref})$ is the thermal strain, and α is the tensorial coefficient of thermal expansion. Consequently, the elastic strain energy density has the form:

$$\mathbf{W}_s = \sum_{i,j,m,n} \frac{1}{2} C^{ijmn}(\varepsilon_{ij} - \varepsilon^0_{ij} - \varepsilon^{th}_{ij})(\varepsilon_{mn} - \varepsilon^0_{mn} - \varepsilon^{th}_{mn}) \tag{2.101}$$

For linear elastic solids the relationship between stress and strain is given by: $\varepsilon_{ij} = D_{ijkl}\sigma_{kl}$ or with $\mathbf{T}$ and $\mathbf{E}$ notations : $T_{ij} = C_{ijrs}E_{rs}$ and $D = C^{-1}$. Due to the symmetry, the elasticity tensor can be completely represented by a symmetric 6×6 matrix as:

$$\begin{Bmatrix} \varepsilon_x \\ \varepsilon_y \\ \varepsilon_z \\ \gamma_{yz} \\ \gamma_{xz} \\ \gamma_{xy} \end{Bmatrix} = \begin{bmatrix} D_{11} & D_{12} & D_{13} & D_{14} & D_{15} & D_{16} \\ D_{21} & D_{22} & D_{23} & D_{24} & D_{25} & D_{26} \\ D_{31} & D_{32} & D_{33} & D_{34} & D_{35} & D_{36} \\ D_{41} & D_{42} & D_{43} & D_{44} & D_{45} & D_{46} \\ D_{51} & D_{52} & D_{53} & D_{54} & D_{55} & D_{56} \\ D_{61} & D_{62} & D_{63} & D_{64} & D_{65} & D_{66} \end{bmatrix} \begin{Bmatrix} \sigma_x \\ \sigma_y \\ \sigma_z \\ \tau_{yz} \\ \tau_{xz} \\ \tau_{xy} \end{Bmatrix}$$

D is known as the *elasticity matrix*. Its inverse C is called the compliance matrix.

For isotropic material only two constants are enough to describe the material elasticity. Using E – Youngs elastic modulus, and ν – Poisson rate of lateral to axial strains, the elasticity matrix becomes:

$$D = \frac{E}{(1+\nu)(1-2\nu)} \begin{bmatrix} 1-\nu & \nu & \nu & 0 & 0 & 0 \\ \nu & 1-\nu & \nu & 0 & 0 & 0 \\ \nu & \nu & 1-\nu & 0 & 0 & 0 \\ 0 & 0 & 0 & \frac{1-2\nu}{2} & 0 & 0 \\ 0 & 0 & 0 & 0 & \frac{1-2\nu}{2} & 0 \\ 0 & 0 & 0 & 0 & 0 & \frac{1-2\nu}{2} \end{bmatrix}.$$

Different pairs of elastic moduli can be used, and as long as two moduli are defined, the others can be computed [207].

Viscoelastic materials have a time-dependent response even if the loading is constant in time. Many polymers and biological tissues exhibit this behavior. Linear viscoelasticity is a commonly used approximation where the stress depends linearly on the strain and its time derivatives (strain rate). Also, linear viscoelasticity deals with the additive decomposition of stresses and strains. It is usually assumed that the viscous part of the deformation is incompressible so that the volumetric deformation is purely elastic. Viscoelasitc materials have post-effect, therefore their constitutive relation is a convolution integral:

$$T_{ij}(t) = \int_{-\infty}^{t} G_{ijkl}(t-\tau)\frac{\mathrm{d}E_{kl}(\tau)}{\mathrm{d}\tau}\mathrm{d}\tau \tag{2.102}$$

here G is the shear modulus, $G = E/2(1+\nu)$.

Plasticity may be modeled by a differential equation:

$$\dot{E}_{ij} = \frac{1}{2\mu}\dot{T}_{ij} - \frac{\lambda}{2\mu(3\lambda+2\mu)}\dot{T}_{kk}\gamma_{ij} + \dot{\Lambda}\frac{\partial f(T_{ij})}{\partial T_{ij}}; \tag{2.103}$$

Newtonian fluids by

$$\begin{aligned} T_{ij} &= (-p(\rho,\theta) + \lambda(\rho,\theta)S_{kk}\delta_{ij}) + 2\mu(\rho,\theta)S_{ij} \\ \mathbf{T} &= (\mathbf{S}^T\lambda - p)\mathbf{I} + 2\mu\mathbf{S} \end{aligned} \tag{2.104}$$

where μ is the shear viscosity of the fluid and $S_{ij} = \partial v_i/\partial x_j + \partial v_j/\partial x_i$ is the shear tensor.

Incompressible viscous fluid:

$$\begin{aligned} T_{ij} &= -p\delta_{ij} + 2\mu(\theta)S_{ij} \\ \mathbf{T} &= -p\mathbf{I} + 2\mu(\theta)\mathbf{S} \end{aligned} \tag{2.105}$$

Ideal fluid (without viscosity):

$$\begin{aligned} T_{ij} &= -p\delta_{ij} \\ \mathbf{T} &= -p\mathbf{I} \end{aligned} \tag{2.106}$$

To formulate the elastic field problem the field equations of linearized isotropic isothermal elasticity that has to be solved is composed from (related to Lagrange coordonates X_i, linked to the material points):

- 3 equations of motion:
$$\frac{\partial T_{ij}}{\partial X_j} + \rho \mathbf{b} = \rho \frac{\partial^2 u_i}{\partial t^2};$$

- 6 Hooke's law equations:
$$T_{ij} = \lambda E_{kk} \delta_{ij} + 2\mu E_{ij};$$

- 6 geometric equations:
$$E_{ij} = \frac{1}{2}\left(\frac{\partial u_i}{\partial X_j} + \frac{\partial u_j}{\partial X_i}\right);$$

in total 15 equations to determine 6 stresses (T_{ij}), 6 strains (E_{ij}) and 3 displacements (u_i). The two Lamé elastic constants λ and μ, are related to the shear modulus G, Youngs modulus E, and Poissons ν ratio by:

$$\mu = G = \frac{E}{2(1+\nu)} \quad \text{and} \quad \lambda = \frac{\nu E}{(1+\nu)(1-2\nu)},$$

$\mathbf{b}_i$ [N/kg] are densities of forces.

In each point of the domain's boundary, the boundary conditions are prescribed one of follows:

- **Displacement boundary conditions**, with the three components u_i prescribed on the boundary.
- **Traction boundary conditions**, with the three traction components $t_i = T_{ji} n_j$ prescribed at a boundary point.
- **Mixed/hybrid boundary conditions** that include cases where the displacement boundary conditions are prescribed on a part of the bounding surface, while traction boundary conditions are prescribed on the remainder, or at each point of the boundary local rectangular Cartesian axes $\bar{X}_i$ can be chosen and then prescribe $\bar{u}_1$ or $\bar{t}_1$, but not both, $\bar{u}_2$ or $\bar{t}_2$, but not both and $\bar{u}_3$ or $\bar{t}_3$, but not both.

The governing equations can be simplified by eliminating stress and strain from the governing equations, and solving directly for the displacements:

$$(\lambda + \mu)\nabla(\nabla \cdot \mathbf{u}) + \mu \nabla^2 \mathbf{u} + \rho \mathbf{b} = \rho \frac{\partial^2 \mathbf{u}}{\partial t^2}; \tag{2.107}$$

whit deformation or traction boundary conditions:

$$\lambda(\nabla + \mathbf{u})\hat{\mathbf{n}} + \mu(\mathbf{u}\bar{\nabla} \cdot \hat{\mathbf{n}} + \bar{\nabla}\mathbf{u}) \cdot \hat{\mathbf{n}} = \text{prescribed function}; \tag{2.108}$$

In the elasto-static case the left hand term of (2.107) is zero and the fundamental equation became:

$$(\lambda + \mu)\nabla(\nabla \cdot \mathbf{u}) + \mu \nabla^2 \mathbf{u} + \rho \mathbf{b} = 0. \tag{2.109}$$

The transient problem, described by the equation (2.107) and the static problem described by equation (2.109) are usually solved numerically by FEM. The initial conditions of the transient problem are related to initial displacements and their time derivative (initial speeds) in any point of computing domain [208].

In order to illustrate the process of mechanical modeling, will be considered a simple study case of a rigid body (Fig.2.16), a plate suspended by 4 springs, having only 6 degree of freedom (3 translations and 3 rotations). A mechanical system with n degrees of freedom may be described in terms of n generalized coordinates, $q_1, q_2, \cdots, q_n$ and time t. A general method of determining the equation of motion is the use of Lagrange's equation [209, 210, 211, 212, 124].

$$\frac{d}{dt}\left(\frac{\partial L}{\partial \dot{q}_i}\right) - \left(\frac{\partial L}{\partial q_i}\right) = Q_{nc,i};\ i = \bar{1,n}, \tag{2.110}$$

where $L = T - V$ is the Lagrangian operator, T is the total kinetic energy of the system and V is the total potential energy of the system arising because of the conservative forces. Non-conservative forces such as dissipative forces, are lumped in the terms $Q_{nc,i}$. If only viscous damping terms (damping proportional to velocity) are present, then the Lagrange's equation can be written as:

$$\frac{d}{dt}\left(\frac{\partial L}{\partial \dot{q}_i}\right) - \left(\frac{\partial L}{\partial q_i}\right) + \left(\frac{\partial F}{\partial q_i}\right) = Q_{ext,i}; \quad i = \bar{1,n} \tag{2.111}$$

where F is the Raleigh dissipation function and $Q_{ext,i}$ is an external generalized force associated with the coordinate q_i. In the general case, the kinetic energy, potential energy and the dissipation function have the forms:

$$T = \frac{1}{2}\sum_{i=1}^{n}\sum_{j=1}^{n} m_{ij}\dot{q}_i\dot{q}_j, \tag{2.112}$$

$$V = \frac{1}{2}\sum_{i=1}^{n}\sum_{j=1}^{n} k_{ij}\dot{q}_i\dot{q}_j, \tag{2.113}$$

$$F = \frac{1}{2}\sum_{i=1}^{n}\sum_{j=1}^{n} B_{ij}\dot{q}_i\dot{q}_j, \tag{2.114}$$

where m_{ij}, k_{ij} and B_{ij} are the inertia, stiffness and damping coefficients, respectively.

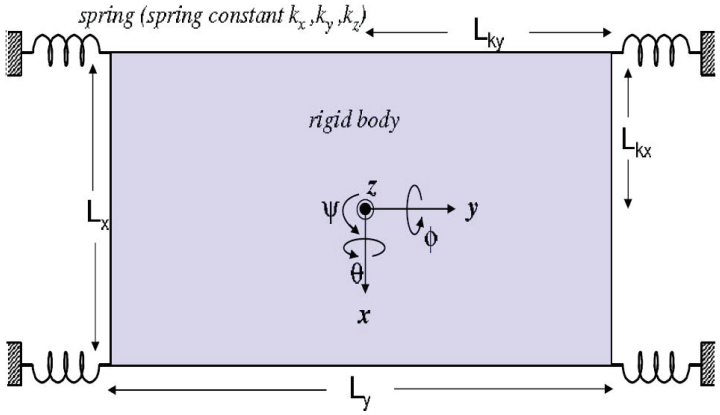

Figure 2.16: Schematic of a rigid plate with dimensions $L_x \times L_y$, springs are attached at distances L_{kx} and L_{ky} along the x-axis and y-axis, respectively from the centroid of the plate[213].

The Cartesian coordinates x, y and z and three angles of rotation θ, ϕ and ψ are chosen to be the generalized coordinates with the plate center as the origin. However, in specific cases such as bridges and cantilevers the z-axis origin is chosen to be the substrate

below anchor points. The variable Δz in such a case represents the vertical displacement of the plate from its rest (zero mechanical potential) position. Potential energy stored in the springs is determined by the contributions of each spring. Making small angle approximations, it results

$$V = 2(k_x x^2 + k_y y^2 + k_z z^2 + k_z L_{ky}^2 \theta^2 + k_z L_{kx}^2 \phi^2 + k_z L_{kx}^2 \psi^2), \tag{2.115}$$

where k_x, k_y and k_z are the spring constants in the x, y and z directions respectively. The dimensions L_{kx} and L_{ky} are the distances along the x and y axis from the centroid of the plate to the springs, the springs in Fig.2.16 are located at $L_{kx} = L_x/2$ and $L_{ky} = L_y/2$. The spring force is assumed to vary linearly with the displacement, however nonlinear spring forces can be modeled by substituting stiffness coefficients that are functions of the position into (2.115). Assuming mass-less springs the kinetic energy T is:

$$V = 2(m\dot{x}^2 + m\dot{y}^2 + m\dot{z}^2 + I_\theta \dot{\theta}^2 + I_\phi \dot{\phi}^2 + I_\psi \dot{\psi}^2), \tag{2.116}$$

where m is the plate mass and the mass moments of inertia of the plate are:

$$I_\theta = \frac{m}{12} L_y^2, \tag{2.117}$$

$$I_\phi = \frac{m}{12} L_x^2, \tag{2.118}$$

$$I_\psi = \frac{m}{12} (L_x^2 + L_y^2). \tag{2.119}$$

The viscous damping of the plate can be expressed by the damping function:

$$V = \frac{1}{2}(B_x \dot{x}^2 + B_y \dot{y}^2 + B_z \dot{z}^2 + B_\theta \dot{\theta}^2 + B_\phi \dot{\phi}^2 + B_\psi \dot{\psi}^2) \tag{2.120}$$

where $B_x, B_y, B_z, B_\theta, B_\phi, B_\psi$, are the damping coefficients of the six modes. The expression for kinetic energy, potential energy and the dissipation function of the mass-spring-damper system are substituted into (2.110) and then solved for each of the six coordinates resulting in the following equations of motion:

$$F_x = m\ddot{x} + B_x \dot{x} + k_x x, \tag{2.121}$$

$$F_y = m\ddot{y} + B_y \dot{y} + k_y y, \tag{2.122}$$

$$F_z = m\ddot{z} + B_z \dot{z} + k_z z, \tag{2.123}$$

$$\tau_\theta = I_\theta \ddot{\theta} + B_\theta \dot{\theta} + k_z L_{ky}^2 \theta, \tag{2.124}$$

$$\tau_\phi = I_\phi \ddot{\phi} + B_\phi \dot{\phi} + k_z L_{ky}^2 \phi, \tag{2.125}$$

$$\tau_\psi = I_\psi \ddot{\psi} + B_\psi \dot{\psi} + k_z L_{ky}^2 \psi, \tag{2.126}$$

where $F_x, F_y, F_z, \tau_\theta, \tau_\phi, \tau_\psi$, are the external forces and torques that act on the plate. By solving these 6 ODEs are obtained the time evolutions of the 6 DoFs of the modeled system. However, the movement of the bridge of a MEMS device involves in the most cases only the vertical (or horizontal) motion. Therefore, in the models of MEMS bridge as a rigid body, reference is made to the vertical (horizontal) equations of motion, which can be expressed in the alternative form as:

$$F_z = m(\ddot{z} + 2\zeta_z\omega_z\dot{z} + \omega_z^2 z), \tag{2.127}$$

$$\tau_\theta = I_\theta(\ddot{\theta} + 2\zeta_\theta\omega_\theta\dot{\theta} + \omega_\theta^2\theta), \tag{2.128}$$

$$\tau_\phi = I_\phi(\ddot{\phi} + 2\zeta_\phi\omega_\phi\dot{\phi} + \omega_\phi^2\phi), \tag{2.129}$$

where ω_z, ω_θ, and ω_{phi}, are the resonant frequencies and ζ_z, ζ_θ and ζ_ϕ, are the dimensionless damping factors of the z, θ, and ϕ modes, respectively. In general, the resonant frequency, ω_i, and damping factor, ζ_i, of the mode, i, are given by:

$$\omega_i = \sqrt{\frac{k_i}{m_i}}, \tag{2.130}$$

$$\zeta_i = \frac{B_i}{2\sqrt{k_i m_i}}, \tag{2.131}$$

where k_i is the stiffness coefficient and m_i is the inertia coefficient (mass for translational modes or moment of inertia for rotational modes) of mode i. Effects of the spring mass can be included by introducing effective inertia coefficients to adjust the resonant frequency.

The **impedance analogy** is a method of representing a mechanical system by an analogous electrical system [214]. The advantage of doing this is that there is a large body of theory and analysis techniques concerning complex electrical systems, especially in the theory of filters. By converting to an electrical representation, these tools in the electrical domain can be directly applied to a mechanical system without modification. A further advantage occurs in **electro-mechanical systems** is that converting the mechanical part of such a system into the electrical domain allows the entire system to be analyzed as a unified whole.

The mathematical behavior of the simulated electrical system is identical to the mathematical behavior of the represented mechanical system. Each element in the electrical domain has a corresponding element in the mechanical domain with an analogous constitutive equation. Every law of circuit analysis, such as Kirchhoff's laws, that apply in the electrical domain also applies to the mechanical impedance analogy.

The impedance analogy is one of the two main mechanical-electrical analogies used for representing mechanical systems in the electrical domain, the other being the mobility analogy. The roles of voltage and current are reversed in these two approaches, and the electrical representations produced are the dual circuits of each other. The impedance analogy preserves the analogy between electrical impedance and mechanical impedance whereas the mobility analogy does not. On the other hand, the mobility analogy preserves the topology of the mechanical system when transferred to the electrical domain whereas

the impedance analogy does not. Table 2.1 contains the analogies between electric and mechanic quantities and equations and the constitutive equations of elements in electric and mechanic similar networks.

Table 2.1: Analogies between electric and mechanic quantities and equations.

Electric qt.	El. Equation	Mc. Equation	Mechanic qt.
u [V]			F [N] – force
i [A]			v [m/s] – velocity
R [Ohm]	u = R i	F = b v	b [Ns/m] – dumper
L [H]	u = L di/dt	F = m dv/dt	m [N] – mass
C [F]	i = C du/dt	v = k dF/dt	k [N/m] – spring

2.2.4 Fluid Mechanics

Fluid flow mechanics is the study of fluids in terms of their mechanical behavior. Specifically, they are studied the equilibrium (static) and motion (dynamics) of fluids and the interactions between them and solid surfaces that are in contact. It is a branch of continuum mechanics, a field that shape matter at the macroscopic level, ignoring the atomic and nuclear behavior. Fluid mechanics, especially fluid dynamics, is an area of active research with many unsolved or partially solved problems. Fluid mechanics can be formulated through advanced mathematical equations based on differential equations and algebraic theory. The mathematical model is obtained by employing numerical calculation implemented in various CFD (Computational Fluid Dynamics) simulation software. Also, using special flow visibility property, fluids can be analyzed by the method of viewing the behavior of particle trajectories [215, 157, 156].

Like any real-world mathematical model, fluid mechanics takes into account several considerations regarding the studied material. These assumptions are translated into equations, which are valid only on condition that the assumptions made is real. The fluid, defined as continuously perfect environment in its structure can be deformed continuously and infinitely (so it can flow) to a shear action.

Fluids may exist in these states of aggregation:

- liquids that are less compressible in contact with a gas possesses a free surface;
- gases that are very compressible, can fill the entire space, steady only in confined spaces;
- plasmas, though can be considered as ionized gas, overall electrically neutral, yet they are a distinct aggregate condition having specific properties.

Fluid flow is a complex phenomenon whose study required for each application, a number of simplifying assumptions. The fundamental assumption in fluid mechanics is that of continuity: scale study of the phenomenon, which is a macroscopic, all attached functions to the flow property (speed, pressure, density, etc.) are continuous and the derivable on the considered domain, except for some areas of discontinuity.

Fluids are deemed continue deformable environments and isotropic, that possess a set of properties that characterize their actual behavior. The forces that manifest in fluid mechanics are classified in two categories: body and surface forces. Inside the fluid can exert only compressive forces.

The flow is described by 7 fundamental quantities, 4 scalars, 2 vectors and 1 symmetric (3×3) tensor, in total 16 scalar components, local and instantaneous: $\mathbf{v}$ is the velocity, ρ is the mass density, p is the pressure, u is the internal energy density, θ is the temperature, $\mathbf{T}$ is the stress tensor and $\mathbf{q}$ is the heat flux vector.

Three conservation laws are used to solve fluid dynamics problems, and may be written in integral or differential form. Mathematical formulations of these conservation laws may be interpreted by considering the concept of a control volume. A control volume is a specified volume in space through which air can flow in and out. Integral formulations of the conservation laws consider the change in mass, momentum, or energy within the control volume. Differential formulations of the conservation laws apply Stokes' theorem to yield an expression which may be interpreted as the integral form of the law applied to an infinitesimal volume at a point within the flow.

Mass continuity (conservation of mass) states that the rate of change of fluid mass inside a control volume must be equal to the net rate of fluid flow into the volume. Physically, this statement requires that mass is neither created nor destroyed in the control volume [216], and can be translated into the integral form of the continuity equation [145]:

$$\operatorname{div}(\rho \mathbf{v}) = -\frac{\partial \rho}{\partial t} \Leftrightarrow \int_{\partial\Omega} \rho \mathbf{v} \cdot \mathrm{d}\mathbf{A} = -\frac{\mathrm{d}m_{\Omega}}{\mathrm{d}t}. \tag{2.132}$$

where ρ is the fluid density, $\mathbf{v}$ is the flow velocity vector and t is time.

Conservation of momentum. This equation applies Newton's second law of motion to the control volume, requiring that any change in momentum of the air within a control volume be due to the net flow of air into the volume and the action of external forces on the air within the volume:

$$\nabla \cdot \mathbf{T} + \mathbf{f} = \frac{\mathrm{d}\mathbf{p}}{\mathrm{d}t} \Leftrightarrow \int_{\Omega} \mathbf{f} \mathrm{d}v + \int_{\partial\Omega} \mathbf{t} \mathrm{d}A = \frac{\mathrm{d}}{\mathrm{d}t} \int_{\Omega} \mathbf{p} \mathrm{d}v. \tag{2.133}$$

In aerodynamics, air is assumed to be a Newtonian fluid, which posits a linear relationship between the shear stress (due to internal friction forces) and the rate of strain of the fluid.

Conservation of energy. Although energy can be converted from one form to another, the total energy in a given closed system remains constant.

$$\begin{aligned} &\frac{\partial u}{\partial t} + (\nabla \cdot \mathbf{q}) = \phi + \sum_{i,j} \sigma_{ij} D_{ij} \Leftrightarrow \\ &\int_{\partial\Omega} \mathbf{q} \cdot \mathrm{d}\mathbf{A} = \int_{\Omega} p_c \mathrm{d}v - \int_{\partial\Omega} \mathbf{t} \cdot \mathbf{v} \mathrm{d}A - \int_{\Omega} \mathbf{f} \cdot \mathbf{v} \mathrm{d}v - \frac{\mathrm{d}}{\mathrm{d}t} \int_{\Omega} u \mathrm{d}v. \end{aligned} \tag{2.134}$$

To formulate the fluid flow problem the constitutive equations are added:

1. Gas/liquid law: $F(p, \rho, \theta) = 0$;
2. Stress tensor expression: $\mathbf{T} = (\mathbf{S}^T\lambda - p)\mathbf{I} + 2\mu\mathbf{S}$;
3. Fouriers conduction law: $\mathbf{q} = -k\nabla\theta$;
4. Internal energy expression: $u = f(\theta, \rho)$.

There are 5 conservation equations for 14 unknowns: ρ, $\mathbf{v}$, $\mathbf{T}$, u, $\mathbf{q}$. Constitutive and state relations provide another 11 equations and introduce 2 additional state variables: p and θ. That gives the total number of 16 equations for 16 unknown field variables.

The most general description of a fluid flow is obtained from the full system of Navier-Stokes equation. Substituting $\mathbf{T}$ and $\mathbf{q}$ from constitutive to general equations, remains only 7 unknowns:

$$\frac{\mathrm{d}\mathbf{p}}{\mathrm{d}t} = \nabla((\mathbf{S}^T\lambda - p)\mathbf{I} + 2\mu\mathbf{S}) + \mathbf{f} \Rightarrow \begin{cases} \rho\frac{\mathrm{d}\mathbf{v}}{\mathrm{d}t} = -\nabla p + (\lambda + \mu)\nabla(\nabla \cdot \mathbf{v}) + \mu\Delta\mathbf{v} + \mathbf{f}; \\ \rho\frac{\partial u}{\partial t} = (\nabla \cdot (k\nabla\theta)) - p\nabla \cdot \mathbf{v} + \phi + 2W_D; \\ \mathrm{div}(\rho\mathbf{v}) = -\frac{\partial\rho}{\partial t}; \\ \text{with } F(p, \rho, \theta) = 0; \text{ and } u = f(\theta, \rho). \end{cases} \tag{2.135}$$

The nonlinearity appears in convection term:

$$\rho\frac{\mathrm{d}\mathbf{v}}{\mathrm{d}t} = \rho\frac{\partial\mathbf{v}}{\partial t} + \rho(\mathbf{v} \cdot \nabla)\mathbf{v}.$$

In incompressible fluids $\lambda = 0$ and it is obtained the most used form of Navier-Stockes equations, having as unknown the velocity field $\mathbf{v}$ and pressure p, 4 scalar components in total:

$$\rho\left(\frac{\partial\mathbf{v}}{\partial t} + (\mathbf{v} \cdot \nabla)\,\mathbf{v}\right) = -\nabla p + \mu\Delta\mathbf{v} + \mathbf{f} \Leftrightarrow \frac{\partial\mathbf{v}}{\partial t} + (\mathbf{v} \cdot \nabla)\,\mathbf{v} - \nu\Delta\mathbf{v} = -\nabla w + \mathbf{g}; \tag{2.136}$$

where the velocity has $\nabla \cdot \mathbf{v} = 0$, $\mathbf{v} \cdot \nabla\mathbf{v}$ is the convection term, $\nu\Delta\mathbf{v}$ is the diffusion term ($\nu = \mu/\rho$ is cinematic viscosity), $-\nabla w$ internal sources ($w = p/\rho$ is the specific thermodynamic work) and $\mathbf{g} = \mathbf{f}/\rho$ represents the external sources [215, 157, 156].

The fundamental problems (solved by CFD = Computational Fluid Dynamics [217]) are in steady state, when $\mathbf{v}$ is constant in time and in transient regime when $\mathbf{v}(\mathbf{r},\mathrm{t})$. They are usually solved numerically by Finite Elements (FEM) or by Finite Volumes (FVM).

They have has appropriate boundary conditions [218]:

- **Mass density boundary conditions**: $\rho = \hat{\rho}$ on S_ρ, where $\hat{\rho}$ is the mass density prescribed on the boundary.
- **Velocity or traction boundary conditions**: $\mathbf{v} = \hat{\mathbf{v}}$ on S_u or $\mathbf{T} \cdot \mathbf{n} = \hat{\mathbf{t}}$ on S_t or mixed, where $\hat{\mathbf{v}}$ is the velocity vector and $\hat{\mathbf{t}}$ is the traction vector prescribed on the boundary.
- **Temperature or heat flux boundary conditions**: $\theta = \hat{\theta}$ on S_θ or $\mathbf{q} \cdot \mathbf{n} = \hat{q}$ on S_q or mixed, where $\hat{\theta}$ is the temperature and $\hat{q}$ is the inward heat flux prescribed on the boundary.

A particular aspect, important in the MEMS modelling is the Fluid-Solid-Interface (FSI). At this particular interface, both interacting bodies have the same velocity and same action/reaction traction vector on interface. In the case of numerical modelling, based on strong FSI coupling, the 3D structural (2.107) and flow (2.136) equations are solved together, simultaneously, usually by FEM. A simpler modeling approach, called Squeeze Film Air Damping in MEMS is based on a 2D flow modelling [219].

The damping in a fluid depends on the fluid properties and the size, shape and speed of the object. One approximate way to express this is through a fluid friction equation:

$$F_D = \frac{1}{2}\rho v^2 C_D A \tag{2.137}$$

where F_D is the damping force, ρ is the fluid density, v is the relative velocity of the object with the fluid, A is the transversal section, C_D is the damping coefficient [220].

The damping coefficient depends on object shape and the Reynolds number: $R_e = vD/\nu$, where D may have geometric characteristics (diameter or linear dimensions), ν is the dynamic viscosity of the fluid equal viscosity μ divided by the density. For low Reynolds numbers, the damping coefficient is proportional to the inverse asymptotic Reynolds number, which means that friction is proportional to velocity. For high Reynolds numbers damping coefficient is more or less constant.

At high velocity (or more precisely, the high Reynolds number), the damping with the fluid will vary with the square of velocity. The resultant power required to overcome this fluid damping will vary with the cube of velocity. For standard equation of fluid friction is equal to the damping coefficient divided by 2, multiplied by the density of the fluid mass, the cross section of the specified item, and the square of velocity.

The power required to overcome friction of a fluid is given by:

$$P_d = \mathbf{F}_d \cdot \mathbf{v} = \frac{1}{2}\rho v^3 A C_d. \tag{2.138}$$

It can be seen that the power needed to push an object through a fluid increases with the cube of speed.

2.3 Conclusions

This chapter presented the description of the multiphysics modelling procedure which comprises the following steps: Conceptual modelling, Mathematical modelling, The approximate analytic modelling, Numerical modelling, Verification and validation of the model, Extracting reduced order parametric models and in the end the Optimization.

In the general operation of MEMS devices, occur several physical phenomena that must be studied. Each physical discipline has its primitive quantities and laws. They are structural (general) and constitutive (describe material behavior). Nonlinear materials generate nonlinear equations. Local forms of laws are PDEs complied by the local and instantaneous quantities. Depending on regime, they are elliptic, parabolic or hyperbolic. Dynamical aspects and specific phenomena are described by time variations and time

derivative terms in equations. Space distribution is described by spatial derivatives (rot, div, grad). Removing the metric structure of space, several systems may be described as networks, defined by their topology (So complexity is reduced!). The fundamental equations of these networks are of ODE type, w.r.t time. Spatial coordinates does not appear, having a finite complexity (SS size). Between fundamental equations of several disciplines there are a series of analogies (Table 2.2), in both continuous (PDE) and discrete/circuits (ODE). So the electric circuits, described by Kirchhoff's and constitutive equations are similar to structural (mechanical, as in Table 2.1), flow and thermal networks.

Table 2.2: Multiphysics Networks (circuits) Analogies [206] (Disp. - Displacement).

General	Electrical	Mechanical	Fluidic	Thermal
Effort, e	Voltage, V	Force, F	Pressure, P	Temp. diff., ΔT
Flow, f	Current, I	Velocity, v	Vol. flow rate, Q	Heat flow
Disp., q	Charge, Q	Disp., x	Volume, V	Heat, Q
Momentum p	-	Momentum, p	Pressure Momentum, Γ	-
Resistance	Resistor, R	Damper, b	Fluidic resistance, R	Thermal resistance, R
Capacitance	Capacitor, C	Spring, k	Fluid capacitance, C	Heat capacity, mcp
Inertance	Inductor, L	Mass, m	Inertance, M	-
Node law	KCL	Continuity of space	Mass conservation	Heat energy conservation
Mesh law	KVL	Newton's 2^d law	Pressure is relative	Temperature is relative

The objective of the RF-MEMS switch is to control the flow of the RF signal, therefore its electromagnetic analysis is essential. As we expected it is dependent on the mechanical/geometrical state of the switch. The actuation of the device is done by applying an actuation voltage, that generates an electrostatic force, this is why an electrostatic problem must be formulated and solved. For the deformation and movement of the flexible switch's membrane a structural-mechanical problem must be formulated and solved. If the device is not not packaged in vacuum, the movement suffers air damping. For this a fluid-flow problem must be formulated and solved. Because all the phenomena influence each other, their interactions must be also formulated as a coupled multiphysics problem. Thereby, the correct mathematically formulation of the electrostatic, electrodynamic, structural mechanics and fluid flow field problems and their couplings must to be described, based of deep understanding of the device operation. The theoretical background of this procedure was presented in this chapter. The knowledge presented here allows a proper formulation of multiphysics models and their description to the computational environments and dedicated CAD/CAE software packages, as well as their simulation by several numerical methods and techniques.

Chapter 3

One Dimensional Models of MEMS Switches

The aim of this step of research is the dynamic and static analysis of the simplest models that we can imagine for RF-MEMS Switches, the 1D one of a *parallel plane capacitor with a mobile armature suspended by a spring.*

I will recall the main steps of modelling, according to [143]:

- **Conceptual modelling**: decide on the simplifying hypotheses and the neglected aspects;
- **Mathematical modelling**: use the mathematics language to formulate a well defined problem;
- **The approximate analytical modelling**: determine the relationships between the input and output quantities, in an analytical form, by solving a simplified variant of the model equations;
- **Numerical and computational modelling**: build an algorithm for solving the problem defined in the mathematical model and implement it on the computer;
- **Model order reduction**: extract from the numerical model a reduced one, which has a smallest order but approximate in an acceptable manner the behavior of the original system;
- **Verification and validation of the model**: do a series of simulations, aiming to verify the solution and to validate the model, by comparison, the simulation results with the experimental results.

Even if this example is extremely simple, it will allow the understanding of the concepts and the physical phenomena as well as the practical aspects that are of maxim interest in engineering.

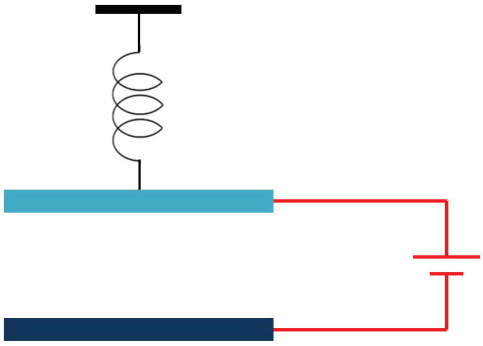

Figure 3.1: Electrostatic actuated switch model.

3.1 Conceptual Modelling

This is the first step of modelling that consists of setting the geometrical model and the (multi)physical one. The build of the geometrical model requires the perfect understanding of the structure of the modelled object, whereas the physical model requires the understanding of the operating principle and the most relevant phenomena in it. During this step, aspects of the geometrical modelling cannot be totally decoupled from the physical modelling aspects, as it will be shown in what follows.

3.1.1 Description of the Modelled Object (Geometrical Modelling)

Regardless the exact geometry of the MEMS switch, there is a mobile, elastic plate, which is deformed by electrostatic forces. If the exact shape of the plate is neglected we may consider it as plane capacitor. This parallel plate capacitor has the armatures (made from a rigid conducting material) placed horizontally, the bottom armature being fixed, and the top armature being suspended by means of a virtual elastic spring (Fig.3.2). The device is placed in vacuum or in a gas. Supplementary, on the bottom armature there may be a thin dielectric layer (Fig.3.3). An electric actuation voltage is applied between the two plates (Fig.3.1). These figures describe the geometric object, this is why no forces are drawn.

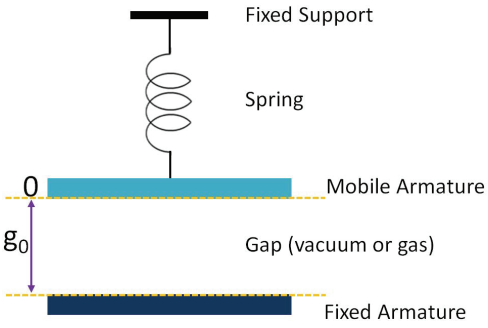

Figure 3.2: Resistive Switch.

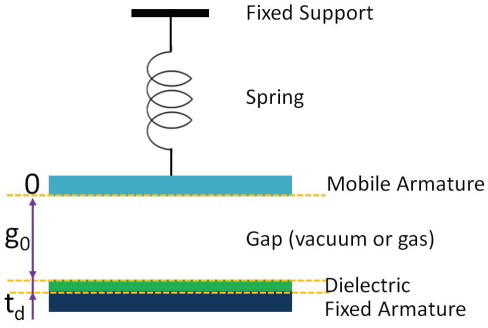

Figure 3.3: Capacitive Switch.

When a voltage is applied between the capacitor plates (electrostatic actuation - Fig.3.1), an electric force appears which moves the mobile plate. If the force is big enough

the movement will take until a mechanical contact between the two plates take place (DOWN stable state). When the voltage is zeroed, the system moves back to the initial position (UP stable state) due to the elastic forces of the spring. During the movement which is considered rectilinear, there is a drag force due to the relative movement of the mobile plate with respect to the gas that surrounds it. It is obvious that the movement is non-uniform (the velocity is not constant, the acceleration is non-zero, so when writing the equilibrium equations in a reference system attached to the mobile plate, an inertial force has to be considered).

In order to describe the geometrical data we will use a right Cartesian system of coordinates. The OZ axis is vertical (perpendicular to the plates) and has the origin placed in the plane that corresponds to the bottom face of the top plate, in the UP position the positive values of the OZ axis are under this plane. The reference system is fixed, it is not moving, being not stuck to the mobile armature.

Due to hypotheses made on the physical model, some of the coordinate axes might be non-relevant, for instance only two coordinates might be used (e.g. XOZ in Fig.3.4 left) or even only one (e.g. in Fig.3.4 right).

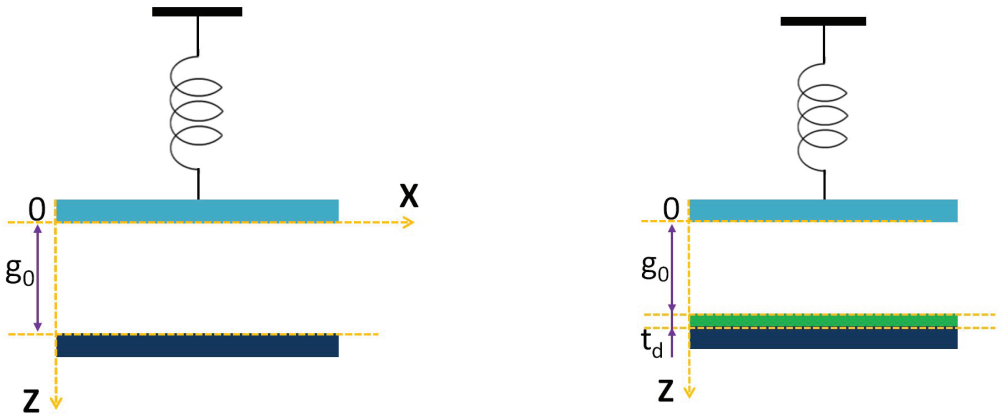

Figure 3.4: Coordinate system.

3.1.2 Simplifying Hypotheses (Physical Modelling)

The most important hypothesis refers to the variation assumed for the local characteristic quantities (given and unknown) with respect to the coordinates. The setting of this hypothesis cannot be done solely by looking at the geometry. For instance, for the geometric description of the plates we need two coordinates (the problem is 2D), marked as X and Z in Fig.3.4 - left, but if we will assume that the electric field between the plates is uniform, then its potential depends only on one coordinate, namely the Z coordinate shown in Fig.3.4 - right. Note again that the geometrical modelling cannot be separated from the physical modelling.

Assuming that the movement of the mobile plate is only along the OZ axis, so from the mechanical point of view the model is 1D (MEC1D). The displacement being 1D, the velocity of the plate and the drag force (due to the fluid dynamics FD) will be 1D as well (FD1D). The electrostatic field that appears between the capacitor plates will be

assumed uniform, so it will depend only on the distance between the plates, so only on the Z coordinate as well. Consequently, the electrostatic model is also 1D (ES1D).

In order to study the stray electric field (the edge effect), this model might be refined as MEC1D + FD1D + ES2D (case in which the electric field problem needs two coordinate axes as in Fig.3.4 - right) or MEC1D + FD1D + ES3D. Next refinements that make sense are MEC2D + FD2D + ES2D and MEC3D + FD3D + ES3D, when the mobile part is an elastic plate anchored on its boundary.

To begin with, all the geometric shapes are considered ideal, as the surface roughness is not considered. The model analyzed in what follows is MEC1D + FD1D + ES1D and the only required axis is OZ (Fig.3.4 - right).

For the MEC+FD analysis we will assume that the mobile plate is a dimensionless point concentrated in its mass center, which moves along a line. The MEC+FD domain is thus of dimension 1, the 1D interval of Z variation: $(0,\ g_0)$.

For the ES analysis, the domain is two-dimensional, the problem being 2D and the stray field being neglected. The shape of the domain is a rectangle but since the electric field is assumed uniform, the ES domain may be considered 1D, a vertical segment of length equal to the distance between the armatures, its ends being the mass centers of the plates.

The main goal of the multiphysics modelling consists of identifying the regimes for each physical field, the sources of these fields, the coupling relationships, i.e. the transition from the qualitative, phenomenological understanding, towards a quantitative one. The ways in which the quantities depend on time establish the operating regime. The possible types are:

- **Static/Steady-state**, in which the quantities do not depend on time (or the dependence of these effects is neglected); In particular, a steady-state regime may be static if there are no energetic transfers (elastostatic/electrostatic).
- **Modal analysis (harmonic balance)**, in which are identified the resonant eigenmodes that may appear in the structure after the excitations are off.
- **Dynamic (Transient)**, in which the quantities have an unspecified variation in time, on the time interval of interest.

The description of the physical quantities depends on the presumed regime, this is why the analysis will be carried out for each regime separately.

3.2 Dynamic Regime

3.2.1 Multiphysics Modeling in the Dynamic Regime

In order to develop the physical model of the device one must carefully analyze the operating principle and identify the main phenomena occurring and describing the fundamental relationships. The mobile armature moves due to electrostatic forces, but move-

ment is influenced also by other aspects such as inertial force, elastic force, damping due to internal friction or air, as well as interaction with the contact. Weight may be neglected because its gravitational effect is nonessential. Because the model of the switch is dynamic, mechanical movement is the main phenomenon that occurs, its equations underlying the model. So we start from the fundamental equation of mechanics, Newton's second law:

$$F = ma \Rightarrow F = m\frac{\mathrm{d}v}{\mathrm{d}t}; \quad v = \frac{\mathrm{d}z}{\mathrm{d}t} \tag{3.1}$$

where: m is the mass of the body in motion, F is the total force acting on the body and a is the acceleration of the body.

State equations of motion are therefore:

$$\frac{\mathrm{d}z}{\mathrm{d}t} = v; \quad \frac{\mathrm{d}v}{\mathrm{d}t} = \frac{F}{m}; \tag{3.2}$$

The equation highlights the state vector $[z,\ v]$, whose components are the position and the velocity of the mobile armature. The values of these state variables must be known at the initial moment, in order to have a unique solution of state equations. As noted, both have zero initial values.

The excitation of the system is the force *F(t)* which is time-dependent. If it also depends to the state variables *F(z, v, t)* in a nonlinear way, then we have a nonlinear system. The main components of the force are $F = F_{ES} + F_c + F_e + F_a$, where:

- $F_{\mathrm{ES}}(u,z) = \frac{1}{2}\frac{\mathrm{d}W}{\mathrm{d}z} = \frac{u^2}{2}\frac{\mathrm{d}C}{\mathrm{d}z} = \frac{1}{2}\frac{\varepsilon_0 A u^2}{(g_0 - z + \frac{t_d}{\varepsilon_0})^2}$ is the electrostatic force.
- $F_c(z,v)$ is the contact force, which describes the interaction with the contact. A viscoelastic model can be used for it, similar to those of the mobile armature, but with different values of the constants, ie $F_c = k'(z - g_0) - b'v$, model that only applies if the armature is in contact, $z > g_0$, otherwise $F_c = 0$.
- $F_e = -kz - k_s z^3$ is the elastic force, depending in the simplest model to the displacement z, where k is the linear elasticity coefficient and k_s is a non-linear (cubic) elasticity coefficient.
- $F_a = -bv$ is the damping force, proportional in the simplest model to the velocity v, where b is the damping coefficient.

Consequently, the following motion state equations are obtained:

$$\begin{cases} \frac{\mathrm{d}z}{\mathrm{d}t} = v; \\ \\ m\frac{\mathrm{d}v}{\mathrm{d}t} = F_{\mathrm{ES}}(u,z) + F_c(z,v) - kz - kz^3 - bv. \end{cases} \tag{3.3}$$

3.2.2 Mathematical Modelling in the Dynamic Regime

Mathematical modelling aims to formulate the problem solely in mathematical terms exclusively and verify that the problem is well formulated.

What is given

First the geometry of the computational domain has to be set. For the mechanical domain the geometry is reduced to a material point whose position is described by the Z coordinate included in the interval $0 < Z < g_0 - t_d$, which defines the spatial computational domain. For the electrostatic domain there are the initial distance between the armature g_0 [m], the thickness of the isolator t_d [m], the area of the armature A [m^2] and the distance z between the armature that is a unknown for the mechanical problem and an input data for the electrostatic problem. All the lengths are measured in meters.

The materials used are described for the mechanical domain by the mass m [kg] of the mobile armature, the elastic constant k [N/m] of the spring and the damping coefficient b [Ns/m], and for the electrostatic domain by ε_r - the relative permittivity of the isolator.

As internal field sources, for the mechanical domain there is the gravity force and for the electrostatic domain there are no internal field sources.

The boundary conditions of the mechanical problems, indeed the initial conditions are both zero as we noticed above. For the electrostatic domain, the boundary conditions are given by electric potential V of the top armature, as the bottom armature is considered grounded ($V = 0$).

What to find

The unknowns of the coupled problem is represented by the displacement $z(t)$ for $0 < t < t_{max}$ of the mobile armature.

Relationships between data and results

The relationship between data and results is given by the equation of motion of a mobile plate of mass m (3.4), where we can distinguish (from left to right) the inertial force F_m, the damping force F_a, the elastic force F_e, the electric force F_{ES} and the contact force F_c:

$$m\frac{\mathrm{d}^2 z}{\mathrm{d}t^2} + b\frac{\mathrm{d}z}{\mathrm{d}t} + kz + k_s z^3 = F_{\text{ES}} + F_c \tag{3.4}$$

with initial conditions:

$$z(0) = 0, \frac{\mathrm{d}z}{\mathrm{d}t\ |_0} = 0.$$

From the mathematical point of view, this is a nonlinear ODE of second order, because F_e my have a nonlinear variation, with a cubic terms, $F_{\text{ES}} = \frac{1}{2}\frac{\varepsilon_0 A u^2}{(g_0 - z + \frac{t_d}{\varepsilon_0})^2}$ depends on z^2, b and the contact force F_c depends on z. The solution of this equation is the real function $z = f(t)$, defined on the time interval $0 < t < t_{max}$ of practical interest.

3.2.3 Analytical Modelling in the Dynamic Regime

Analytical solutions may be obtained in the following simplifying hypothesis: $k_s = 0, F_c = 0$ (study of the movement until it reaches the contact), b is constant and F_{ES} is constant (e.g. equal to the value for $z = 0$). Under the assumption $F_{\text{ES}} = E_{\text{ES-ct}}$, we can solve linear second order ordinary differential the equation and get an idea of the order

of magnitude of the involved quantities:

$$\begin{cases} m\frac{\mathrm{d}^2z}{\mathrm{d}t^2} + b\frac{\mathrm{d}z}{\mathrm{d}t} + kz = F_{\mathrm{ES-ct}} \\ z(0) = 0, \frac{\mathrm{d}z}{\mathrm{d}t|_0} = 0 \end{cases} \tag{3.5}$$

The solution of this linear equation is obtained by superposition of the "free" solution of the homogeneous equation (with 0 right hand side) and a particular, "forced" solution of non-homogeneous one $z(t) = z_o(t) + z_p$. Since the right hand side is a constant, the particular solution may be considered a constant equal to: $z_p = \frac{F_{\mathrm{ES-ct}}}{k}$, resulting in the characteristic equation: $mr^2 + br + k = 0$ and the free solution depends on $\Delta = b^2 - 4mk$.

CASE 1) If $\Delta > 0$ i.e. $b^2 > 4mk$, then the characteristic equation has 2 real solutions and the solution of the homogeneous ODE is:

$$z_0(t) = C_1 e^{r_1 t} + C_2 e^{r_2 t} \tag{3.6}$$

where r_1 and r_2 are the real solutions of the characteristic equations.

$$r_1 2 = (-b \pm \sqrt{\Delta})/4m \tag{3.7}$$

CASE 2) If $\Delta = 0$ i.e. $b^2 = 4mk$, then the characteristic equation has 1 real solution: $r = -b/2a$ and the solution of the homogeneous ODE is:

$$z_0(t) = C_1 e^{rt} + C_2 e^{rt} \tag{3.8}$$

CASE 3) If $\Delta < 0$ i.e. $b^2 < 4mk$, then the characteristic equation has 2 complex conjugate solutions: $r_1 = \alpha + j\beta$ and $r_1 = \alpha - j\beta$ and the solution of the homogeneous equation is:

$$z_0(t) = e^{\alpha}(C_1 \cos(\beta t) + C_2 \sin(\beta t)). \tag{3.9}$$

As in the case of an RLC series / parallel circuit, the three cases above are known as:

- $\Delta > 0$ - over-damped
- $\Delta = 0$ - critically damped
- $\Delta < 0$ - under-damped

The units in equation:

$$m\frac{\mathrm{d}^2z}{\mathrm{d}t^2} + b\frac{\mathrm{d}z}{\mathrm{d}t} + kz = F_{\mathrm{ES-ct}}, \tag{3.10}$$

are as follows:

$$(Kg)\frac{(m)}{(s)^2} + \frac{(N)(s)}{(m)}\frac{(m)}{(s)} + \frac{(N)}{(m)}(m) = \frac{\frac{(F)}{(m)}(m)^2(V)^2}{(m)^2}, \tag{3.11}$$

which can be scaled as:

$$(mg)\frac{(\mu m)}{(ms^2)} + \frac{(N)(ms)}{(m)}\frac{(\mu m)}{(ms)} + \frac{(N)}{(m)}(\mu m) = \frac{\frac{(pF)}{(m)}(mm)^2(V)^2}{(\mu m)^2}, \tag{3.12}$$

indeed,

$$(10^{-6})\frac{(10^{-6})}{(10^{-3})^2}+\frac{1(10^{-3})}{1}\frac{(10^{-6})}{(10^{-3})}+\frac{1}{1}(10^{-6})=\frac{\frac{(10^{-12})}{1}(10^{-3})^2 1^2}{(10^{-6})^2}. \tag{3.13}$$

So, in the scaled equation we will use the following units in order to keep at the minimal level the truncation errors and to increase the numerical stability:

- k - in N/m, as in S.I.;
- Electric permittivity ε in pF/m. This means that $\varepsilon_0 = 10^3/(36\pi)pF/m$;
- Length and width of the plates in mm;
- The gap in microns;
- Voltage in volts;
- Mass in mg;
- Damping coefficient b in mN/m;
- Acceleration in $m/s^2 (= \mu m/ms^2)$;
- Velocity in mm/s;
- Forces will be expressed in μN.

3.2.4 Numerical Modelling in the Dynamic Regime

The study case presented above will be analyzed by using *MATLAB*, *APLAC* and *SPICE*. The numerical values we consider are these given in the APLAC documentation [221]. The problem formulation as in the APLAC documentation refers to a mechanical resonator (Fig.3.5) whose physical appearance is not important, having the mass M of 10 mg, spring coefficient of $k = 3553$ N/m and quality factor Q of 3. A stub limits the maximum displacement of the mass $z_{\max}(d_{\max}) = 5 \quad \mu m$, the air gap $g_0(d) = 10 \quad \mu m$ and the surface area $A(l \times w)$ is $100 \quad mm^2$.

The mechanical resonant frequency is:

$$f_0 = \frac{1}{2\pi}\sqrt{\frac{k}{m}} = \frac{1}{2\pi}\sqrt{\frac{3553\frac{\mathrm{N}}{\mathrm{m}}}{10\cdot 10^{-6}\mathrm{kg}}} = \frac{1}{2\pi}\sqrt{\frac{3553}{10}}\frac{1}{\mathrm{ms}} = 3 \text{ kHz}; \tag{3.14}$$

and the damping coefficient is:

$$b = \frac{k}{\omega_0 Q} = \frac{3553\frac{\mathrm{N}}{\mathrm{m}}}{6\pi\frac{1}{\mathrm{ms}}\cdot 3} = 62.8313 \quad \frac{(\mathrm{mN})(\mathrm{s})}{\mathrm{m}} = 62.8313 \quad \frac{(\mu\mathrm{N})(\mathrm{ms})}{\mu\mathrm{m}} = 62.8313 \quad \frac{\mathrm{mg}}{\mathrm{ms}}. \tag{3.15}$$

In *MATLAB*, the ODE numerical procedures accept only first order equations or systems of equations. This is why our second order ODE equation has to be reformulated in

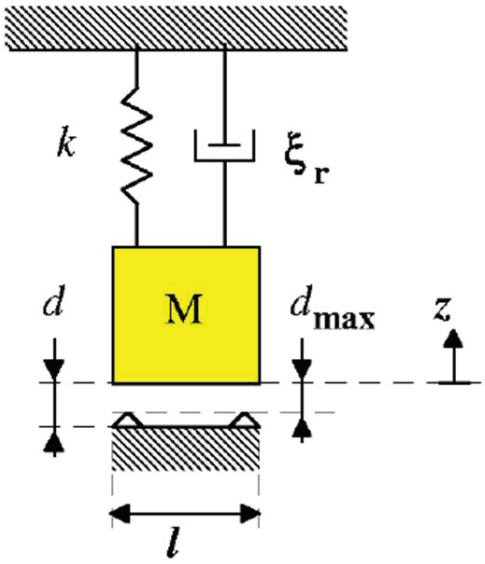

Figure 3.5: Study case schematic diagram [221].

the state form, as a first order system:

$$m\frac{\mathrm{d}^2z}{\mathrm{d}t^2}+b\frac{\mathrm{d}z}{\mathrm{d}t}+kz+k_sz^3=F_{\mathrm{ES}}+F_c\Rightarrow\begin{cases}\frac{\mathrm{d}z}{\mathrm{d}t}=v;\\ \frac{\mathrm{d}v}{\mathrm{d}t}=-\frac{b}{m}v-\frac{k}{m}z-\frac{k_s}{m}z^3-\frac{F_{\mathrm{ES}}}{m}-\frac{F_c}{m}.\end{cases}\tag{3.16}$$

The results obtained are shown in Fig.3.6, on the right side is presented the velocity dependence on time and on the left side is presented the displacement dependence on time.

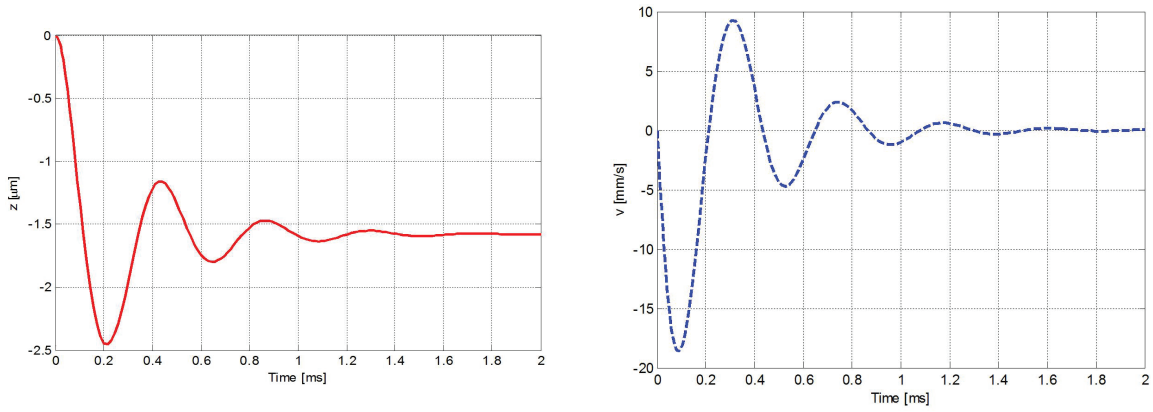

Figure 3.6: Time dependence of the displacement and velocity resulted from MATLAB analysis[222].

In Fig.3.7 is presented the APLAC schematic, where the mass-spring system is implemented as in the schematic from Fig.3.8. The results from the simulation in APLAC are presented in Fig.3.9.

In Fig.3.10 is presented the SPICE circuit model and the time dependence *V(n003)* which represents the displacement z in μm.

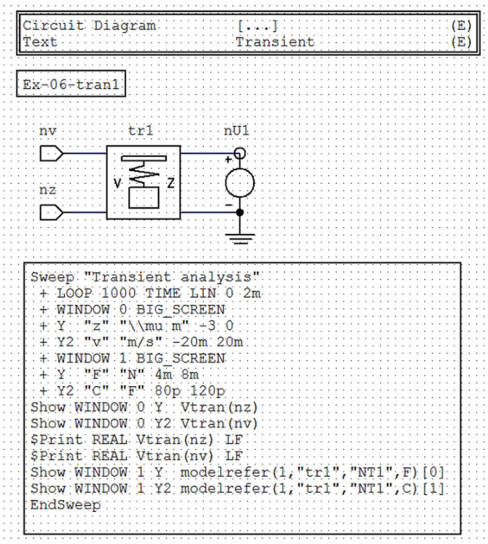

Figure 3.7: APLAC schematic [221].

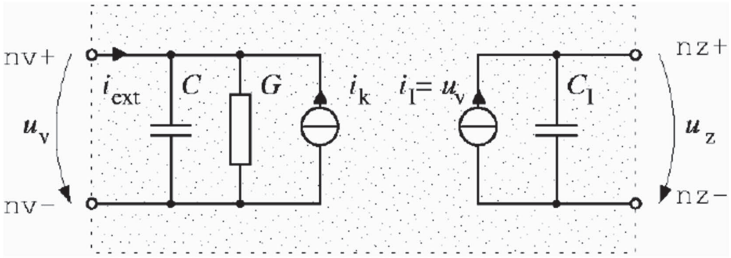

Figure 3.8: APLAC Equivalent circuit for the mass-spring system [221].

In order to be compatible with the APLAC notation, $-z$ will be displayed instead of z. So *-V(n003)* is the displacement in the APLAC notation and *-V(n002)* is the velocity (Fig.3.11).

In conclusion if we compare it with the analytical solution (Fig.3.12), the graphs match well near the initial position and the displacement with constant force is smaller than the real one, which it makes sense. Such an approximation is useful to check the numerical procedure at the beginning of the movement.

3.2.5 Parametric Analysis

Since we validated the SPICE models and MATLAB procedures, we can use them to better understand the influence of various parameters. We will take again the simple APLAC example and change one parameter at a time, under a voltage step excitation of 30 V (which is less than pull-in voltage, so the system moves from the initial state, but the contact will not be reached).

Mass

In this study the mass of the resonator is halved and, respectively, doubled. The mass influences the inertial force. The system will reach the same equilibrium position, but quicker in the case of a smaller mass and with an increased velocity (Fig.3.13).

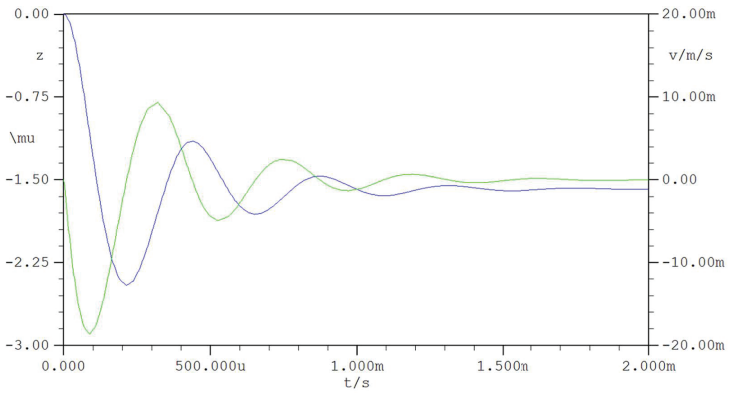

Figure 3.9: Time dependence of the displacement and velocity resulted from APLAC analysis [222].

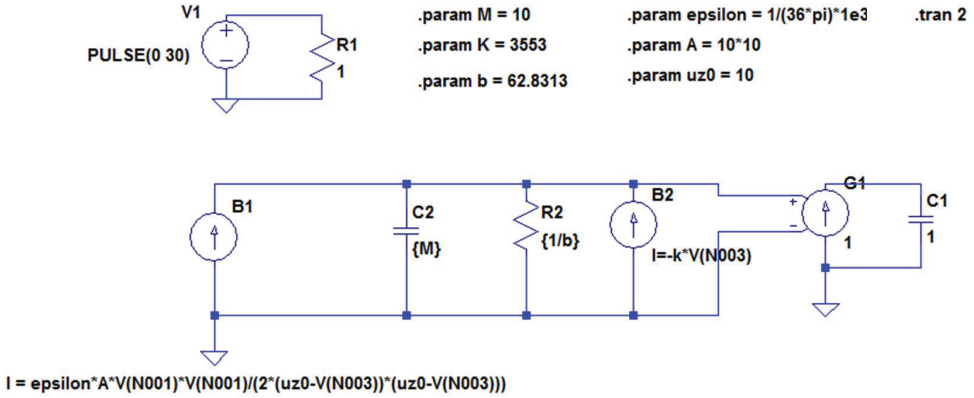

Figure 3.10: SPICE circuit model [222].

Neglecting the inertial force in a dynamic simulation would be unphysical. Here (Fig.3.14) there is an example of simulation with a very small mass instead of 0.

Damping

The damping force is sought as being linear with respect to the velocity $F_d(v) = bv$, where $b = k/(\omega_0 Q)$ is a damping coefficient, $\omega_0 = \sqrt{k/m}$ representing the resonant frequency.

As expected, a higher damping (smaller Q) decreases the amplitude of oscillations (Fig. 3.15).

It is interesting to see how the system behaves when there is no damping. As expected, the oscillations are undamped (Fig. 3.16).

No damping results in undamped oscillations of the system, with a period $T = 1/3 \quad \text{kHz} = 0.33 \quad \text{ms}$, which correspond to the resonant frequency $\omega_0 = \sqrt{k/m}$, which is not physical. Therefore a model for damping should always be taken into account.

In conclusion, in the dynamic simulations, both inertial force and the damping force have to be considered.

Spring constant

To imagine a spring with half the elastic constant of the initial example seems to

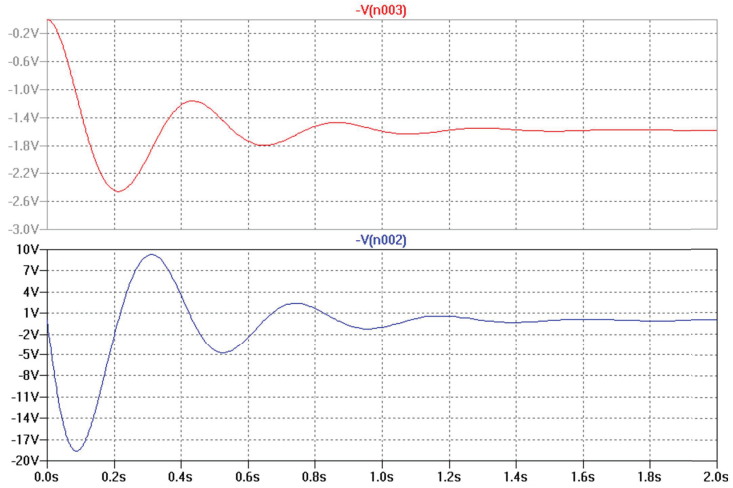

Figure 3.11: Time dependence of the displacement (UP) and velocity (DOWN) resulted from SPICE analysis [222].

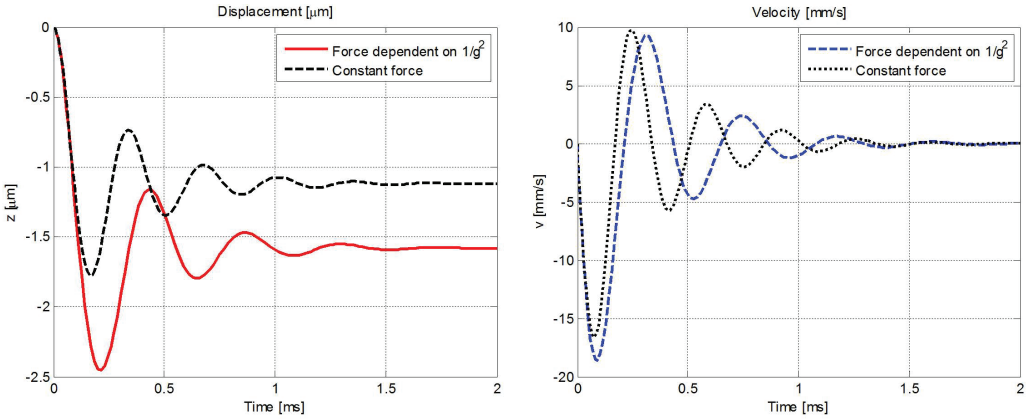

Figure 3.12: Time dependence of the displacement (left) and velocity (right) [222].

be exaggerated in this case, the elastic constant has a strong influence upon the pull-in voltage resulting one smaller than the applied voltage of 30 V, that is the reason for the behavior in Fig.3.17.

In Fig.3.18 the time dependency of the displacement and velocity for a small variation of the elastic constant is presented.

3.2.6 Parameters Computed by the Dynamic Analysis

Switching time

Switching time [s] which describe the "speed" of the device is computed from the pull-down simulation as the duration needed to reach the contact. The initial conditions are $z(0) = 0$, $v(0) = 0$, and the switching time t_s is the time for which $z(t_s) = g_0$, equivalent to $g(t_s) = 0$. For instance, Fig.3.19 presents this dependencies for applied voltages higher than V_{pi}, and various quality factors. The switching time increases with the decrease of quality factor Q, in this example t_s is about 0.2 ms for $Q = 2$ and it is more than double for $Q = 0.5$. This is why it is recommended that $Q >= 0.5$

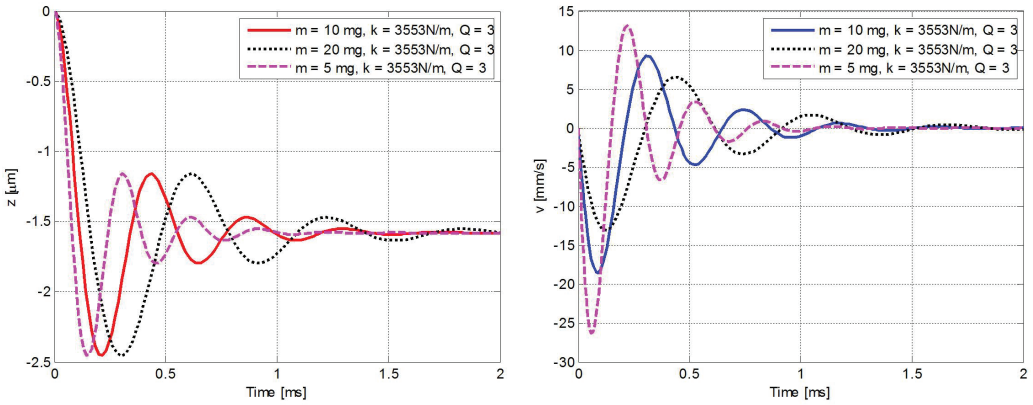

Figure 3.13: Time dependence of the displacement (left) and velocity (right) for different values of the mass [222].

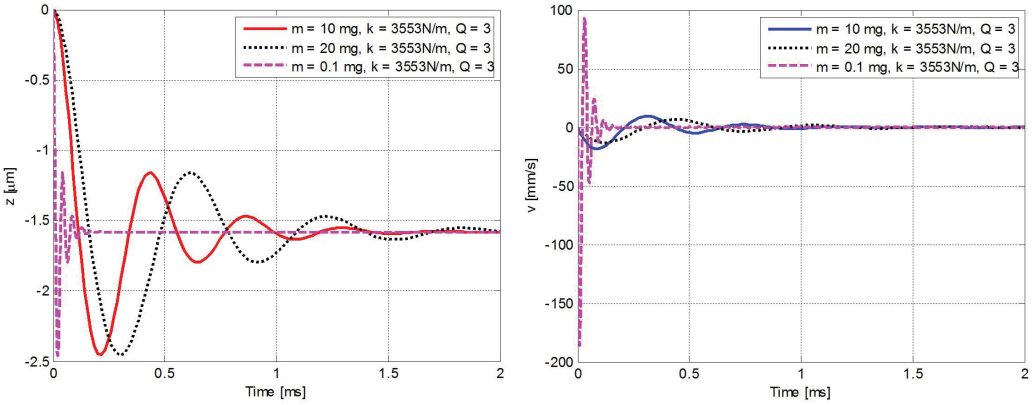

Figure 3.14: Time dependence of the displacement (left) and velocity (right) for a very small mass [222].

A closed-form expression [21] for the switching time can be obtained for inertia limited systems that happen in beams with a small damping coefficient and $Q \geq 2$. The equation of motion becomes ($b \approx 0$):

$$m\frac{\mathrm{d}^2 z}{\mathrm{d}t^2} + kz = -\frac{1}{2}\frac{\varepsilon_0 A V^2}{g_0^2}, \tag{3.17}$$

where the force is taken to be constant and equal to the initial applied force. The solution is:

$$t_s \approx 3.67\frac{V_{\mathrm{pi}}}{V_s \omega_0}, \tag{3.18}$$

where V_s represents the applied voltage and V_{pi} represents the pull-in voltage. According to [21], in most cases, the applied voltage is between 1.3 and 1.4 of the pull-in voltage V_p to result in a fast switching time at a reasonable voltage level.

If the system is damping limited ($Q \leq 0.5$), then a similar equation can be derived, with the assumption of constant damping with gap height and neglecting the acceleration and spring component. The equation of motion becomes

$$b\frac{\mathrm{d}z}{\mathrm{d}t} = F_e \tag{3.19}$$

and can be solved with integral methods or estimated with difference methods. The

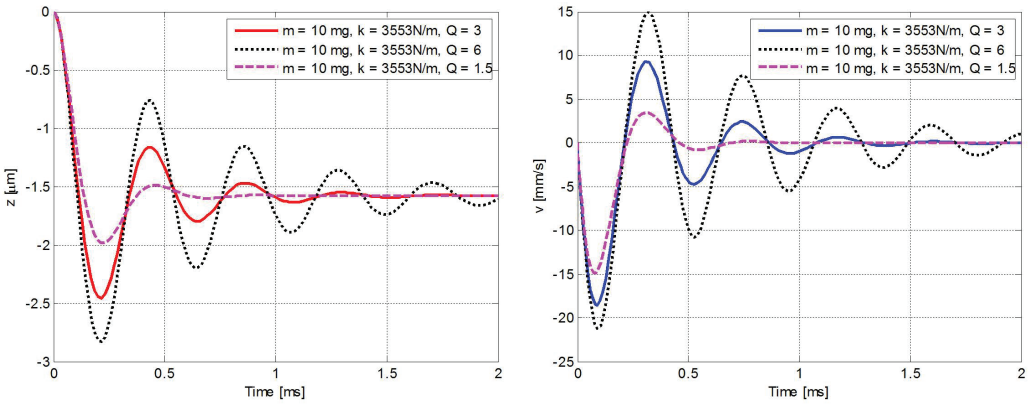

Figure 3.15: Time dependence of the displacement (left) and velocity (right) for different values of the damping coefficient [222].

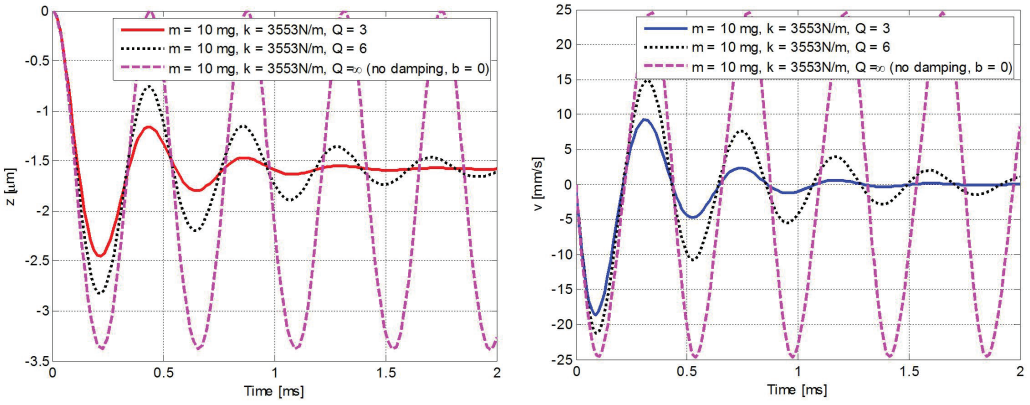

Figure 3.16: Time dependence of the displacement (left) and velocity (right) for null damping coefficient [222].

solution using integral methods and $F_e = \varepsilon_0 A V^2/g^2$ results in:

$$t_s = \frac{2bg_0^3}{3 * \varepsilon_0 A V_s^2} \approx \frac{9V_{\text{pi}}^2}{4\omega_0 Q V_s^2} \text{ for } V_s \gg V_{\text{pi}}. \tag{3.20}$$

Another estimate can be made assuming that the electrostatic force F_e is constant plus a constant approximation for the velocity ($dz/dt = g_0/t_s$). This switching time estimate is given by

$$t_s = \frac{2bg_0^3}{\varepsilon_0 V_s^2} \approx \frac{27V_{\text{pi}}^2}{4\omega_0 Q V_s^2} \text{ for } V_s \gg V_{\text{pi}}. \tag{3.21}$$

We can look also at the dependence of the switching time w.r.t the actuation voltage, assuming that the actuation voltage is 1.2 - 2 times greater than the pull-in voltage. Knowing the pull-in voltage V_{pi} and the displacement g_{pi} at V_{pi} as:

$$g_{\text{pi}} = \frac{2g_0}{3}, \; V_{\text{pi}} = \sqrt{\frac{8kg_0^3}{27\varepsilon_0 A}} \tag{3.22}$$

for $k = 3553$ N/m, $g_0 = 10$ $\mu m, A = 100$ mm^2 and $V_{\text{pi}} = 34.5054$ V in Table 3.1, the switching time is presented for different applied voltages V and different quality factors Q and Fig.3.20 holds the qualitative representation.

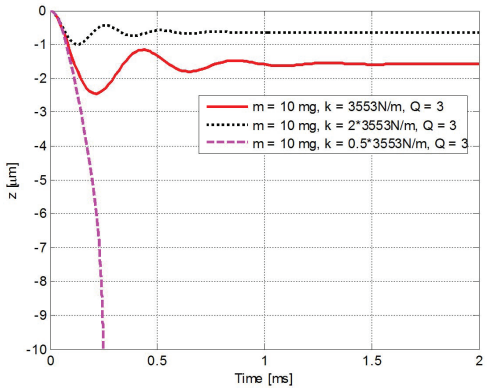

Figure 3.17: Time dependence of the displacement for values of the elastic constant [222].

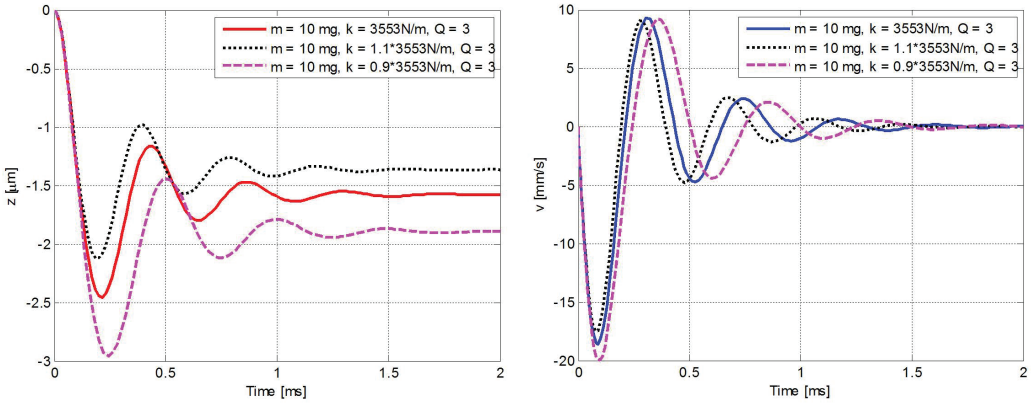

Figure 3.18: Time dependence of the displacement (left) and velocity (right) for small variation of the elastic constant [222].

Release time

The release time is computed by using the same ODE equation, but without electric force (the applied voltage is zero) and with the initial condition $z(0) = g_0, V(0) = 0$. The release time t_r is the time for which $z(t_r) = 0$, equivalent to $g(t_r) = g_0$ and $z(t) = 0$ for any $t > t_r$.

Fig.3.21 shows the time behavior of the gap height for different quality factors. At release of the mass, for $Q = 2$ oscillations form, and this may have a negative effect on the RF response of the line. That is why $Q \geq 2$ is not recommended. In general, a $Q = 1$ is recommended for the best release response.

Switching current

Switching current is injected in the actuation electrode, during its actuation: $i = \mathrm{d}q/\mathrm{d}t$, where q is the electric charge of a plate, that can be computed by the surface integral

Table 3.1: Switching time for different applied voltages and different quality factors.

V/V_{pi}	1.2	1.4	1.6	1.8
Q = 0.5	0.4178	0.2545	0.1865	0.1481
Q = 1	0.2617	0.1788	0.1399	0.1160
Q = 2	0.2006	0.1489	0.12	0.1028

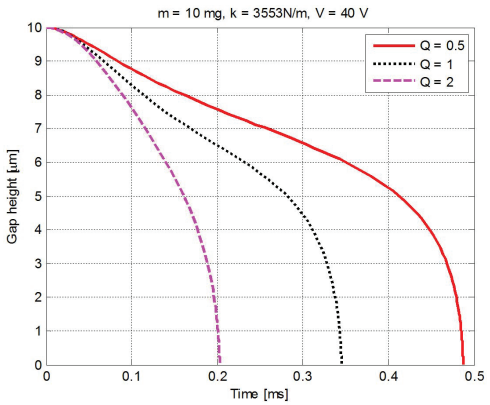

Figure 3.19: Curves that reveal the switching time and its dependence w.r.t to the quality factor Q, for the same applied voltage [222].

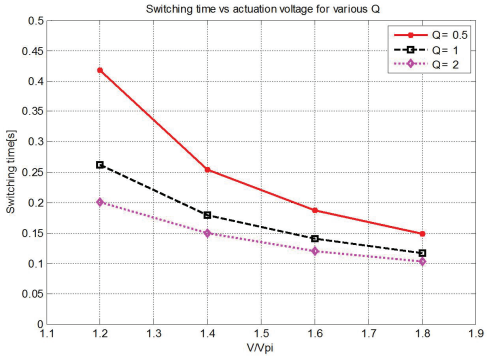

Figure 3.20: Switching time w.r.t. applied voltage for several values of Q.[222]

of the **D** field over a closed surface that surrounds the plate. If we assume an uniform electrostatic field, than we can write:

$$\begin{cases} q = CU = \frac{\varepsilon_0 AU}{g_0 - z} \\ i = \frac{\mathrm{d}(CU)}{\mathrm{d}t} = C\frac{\mathrm{d}U}{\mathrm{d}t} + U\frac{\mathrm{d}C}{\mathrm{d}t}. \end{cases} \tag{3.23}$$

and we obtain a relationship that involves $\mathrm{d}U/\mathrm{d}t$ which is known and $\mathrm{d}z/\mathrm{d}t$ which is already computed.

The peak switching current appears when the gap tends to zero. In more realistic

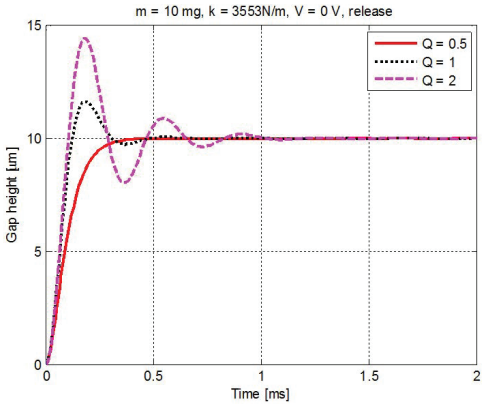

Figure 3.21: Time behavior of the gap height for various Q.[222]

models (2D and 3D) the difficulty will come from the contact, because this is not done in a planar fashion. For example, in the case of a beam the initial contact is at the center of the beam, followed by a quick spreading of the contact area to cover the entire beam.

Energy consumed in the switching process

The energy consumed in the switching process is the sum of electrical and mechanical energies:

- electrical energy stored in the capacitor;
- mechanical spring energy ($kz^2/2$ in the 1D model);
- kinetic energy ($mv^2/2$ in the 1D model);
- energy lost in damping ($\int bv^2 \mathrm{d}t$ from 0 to the considered moment);
- Joule energy dissipated in the conductors, due to the switching current that appears.

Influence of the switch on the RF parameters

When the switch is in the up position (not actuated), the radio frequency (RF) signal may influence its position and thus the S parameters may be affected (which is not desirable). We could do a study case by considering $V(t)$ in the right hand side of the equation, where $V(t)$ is the RF signal.

When the switch is in the down position, the RF signal may influence only the release time in the case of capacitive switches. In the other situations, it has no effect.

Effect of the dielectric charging

Several well-known properties of dielectric charging are detailed in [21] and are as follows:

- The charging of dielectrics is due to the application of stress, whatever its nature: mechanical, ionizing, thermal, or electric field stress.
- Electrons are trapped at low fields (25 MV/cm) and de-trapped at high fields, while trapped positive charges are typically observed at high fields (710 MV/cm).
- Surfaces and interfaces, which are areas where defects are concentrated, will be areas where charges are preferentially trapped.
- There is no direct relationship between an insulator conductivity and its charging properties. The trapped electrostatic charge is not only due to the insulating nature of the material (ionic or covalent), but is due to defects, either from its crystallographic structure or from defects due to tooling (dislocation, nonstoichiometry), or due to radiation under ionizing beams (electron, photon, or ion bombardment of SiO_2).
- Dielectrics will break down at any high electric field, provided that they are stressed long enough. The breakdown will always occur beyond a certain amount of injected charge.

For an actuation voltage of 30 to 60 V and a dielectric thickness of 1500 Å, the electric field can be as high as 2 to 4 MV/cm in the dielectric layer. Under these high field conditions, it is possible for charges to tunnel into the dielectric under a phenomenon similar to FrankelPoole emissions or using a whole set of other mechanisms. It is for this reason that the hold-down voltage must be decreased at the value of 8 to 12 V once the switch is in the down-state position [21].

3.3 Static Regime

In this regime the time dependencies of the quantities are neglected ($\mathrm{d}/\mathrm{d}t = 0$) and is assumed that energies transfers are non existent, neither electrostatic nor elastostatic, i.e. top armature is in a equilibrium position, is immobile.

3.3.1 Multiphysics Modeling in the Static Regime

The condition of equilibrium of the mobile armature in static regime requires that $\mathbf{G} + \mathbf{F}_k + \mathbf{F}_\varepsilon = 0$, i.e. $G\mathbf{k} - k(z - z_0)\mathbf{k} + \mathbf{F}_\varepsilon = 0$ or $G\mathbf{k} - k(z + G/k)\mathbf{k} + \mathbf{F}_\varepsilon = 0$ resulting that the gravity force is not relevant in the static regime.

In static regime, assuming that the elastic constant is linear, the movement equation takes the form:

$$-kz\mathbf{k} + \mathbf{F}_\varepsilon = 0, \tag{3.24}$$

where, using the notation $F_{\mathrm{ES}} = \mathbf{F}_\varepsilon \cdot \mathbf{k} = -F_\varepsilon$,

$$F_{\mathrm{ES}} = \frac{\varepsilon_0 A V^2}{2\left(g + \frac{t_d}{\varepsilon_r}\right)^2}, \tag{3.25}$$

and the relationship between the distance between the armature and the displacement coordinate is $g = g_0 - z$.

It is obvious that the coupling quantity between the two problems thus formulated is the electrostatic force. For the electrostatic domain the problem is explicit: it is given the geometry, materials, actuation voltage and force calculation is done according to them explicitly. For the mechanical domain the problem is implicit: it is given the force, materials, the starting position and is required the position g of the mobile armature.

The equations being algebraic, there is no need to impose any boundary conditions and initial conditions. Obviously by substituting the expression of the electrostatic forces, it results a third order algebraic equation, having the form:

$$k(g_0 - g) = \frac{\varepsilon_0 A V^2}{2\left(g + \frac{t_d}{\varepsilon_r}\right)^2}, \tag{3.26}$$

The coupled equation can have mathematically three real solutions, out of which only one will have a physical meaning. In this case there are two restrictions. It is obvious

that the physical solution must satisfy $g \in [0, g_0]$, because an attraction force acts on the armature, and the movement cannot exceed the point where contact occurs. Also, the steady state reached must be a stable one.

From the mathematical point of view, the relation (3.26) can be put in the form of a nonlinear equation $f(g) = 0$, where:

$$f(g) = g\left(g + \frac{t_d}{\varepsilon_r}\right)^2 - g_0\left(g + \frac{t_d}{\varepsilon_r}\right)^2 + \frac{\varepsilon_0 A V^2}{2k}, \tag{3.27}$$

for the capacitive case; for the resistive case $t_d = 0$.

3.3.2 Resistive type Micro-Switch

In the case of the resistive type micro-switch the dielectric domain between the armatures is homogeneous. The electric field is uniform (Fig.3.22), where its strength is $\mathbf{E} = E\mathbf{k}$ and $E = V/g$ relationship results from applying the electric voltage definition.

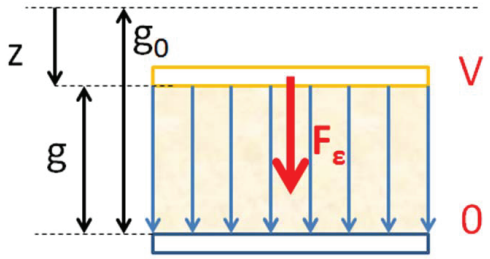

Figure 3.22: Electric field lines for parallel plane capacitor with homogeneous dielectric.[222]

If $V > 0$ the electric field is oriented in the positive directions of the Oz axes, otherwise is oriented in opposite direction. E [V/m] is the projection on the Oz axes of the electric field strength component of the field, resulting that the electric flux density component is $\mathbf{D} = \varepsilon_0 E\mathbf{k}$ were ε_0 is the relative permittivity of vacuum.

The armatures are conductive, the electrostatic field inside them is null and consequently they are charged with electric charge; the size can be determined by applying the electric flux law on a closed surface surrounding them tightly. The top armature has the charge $q = \mathbf{D} \cdot \mathbf{k}A = DA = (\varepsilon_0 AV)/g$, were $D = (\varepsilon_0 V)/g$ is the projection upon the Oz axes of the electric flux density component. The bottom armature is charged with $\mathbf{D} \cdot (-\mathbf{k})A = -q$ equal and opposite with the charge from the top armature. The capacitance is $C = q/v = \varepsilon_0 A/g$ and the electric energy gathered in the dielectric is:

$$W_e = \frac{\mathbf{D} \cdot \mathbf{E}}{2} Ag = \frac{CV^2}{2} = \frac{q^2}{2C}. \tag{3.28}$$

By applying the generalized forces theorem, where the generalized coordinate is the distance between armatures, the electrostatic force acting on the mobile armature is:

$$F_{\text{ES}} = \left.\frac{\mathrm{d}W_e}{\mathrm{d}g}\right|_{V=ct} = \frac{V^2}{2}\frac{\mathrm{d}C}{\mathrm{d}g} = -\frac{\varepsilon_0 A V^2}{2g^2}. \tag{3.29}$$

The minus sign from equation (3.29) indicates that the electrostatic force acts in the downward direction of the generalized coordinate, meaning this is an attraction force. Consequently, the vectors should be written: $\mathbf{F}_{\text{ES}} = -F_{\text{ES}}\mathbf{k}$. The direction of the force is independent on the sign of the applied voltage.

3.3.3 Capacitive type Micro-Switch

In the case of a capacitive micro-switch the reasoning is similar. The difference comes from the fact that only the electric flux density component is uniform throughout the computational electrostatic domain, imposed by the continuity of the normal component according to the form of electric flux law on discontinuity surfaces. The electric field strength is uniform on the two sub-domains, the air and the dielectric (Fig.3.23).

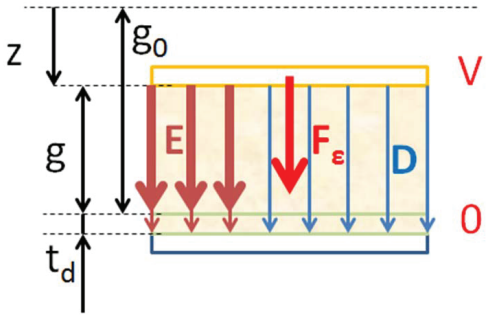

Figure 3.23: Electric field lines for parallel plane capacitor with piecewise homogeneous dielectric.[222]

We will denote with ε_r the relative electric permittivity pf the dielectric and with t_d its thickness. The continuity of the normal component of electric field density imposes that $D = \varepsilon_0 E = \varepsilon_0 \varepsilon_r E_d$, where E is the electric field strength in air and E_d the electric field strength in the insulator. From the electric voltage definition it results that $V = Eg + E_d T_d$, hence:

$$D = \frac{\varepsilon_0 V}{g + \frac{t_d}{\varepsilon_r}} \tag{3.30}$$

and the capacitance of the formed capacitor is:

$$C = \frac{\varepsilon_0 A}{g + \frac{t_d}{\varepsilon_r}}. \tag{3.31}$$

The electrostatic force that acts upon the mobile armature is: $\mathbf{F}_{\text{ES}} = -F_{\text{ES}}\mathbf{k}$, where:

$$F_{\text{ES}} = \frac{\mathrm{d}W_e}{\mathrm{d}g}\bigg|_{V=ct} = \frac{V^2}{2}\frac{\mathrm{d}C}{\mathrm{d}g} = -\frac{\varepsilon_0 A V^2}{2(g + \frac{t_d}{\varepsilon_r})^2}. \tag{3.32}$$

3.3.4 Analytical Modelling in Static Regime

The considered study case [21] is a capacitor with area of the armature $A = LW$, where $L = 100\mu$m is the length and $W = 100\mu$m is the width of the armature. The initial distance is $g_0 = 3\mu$m and the elastic constant of the spring is $k = 10$N/m. The actuation

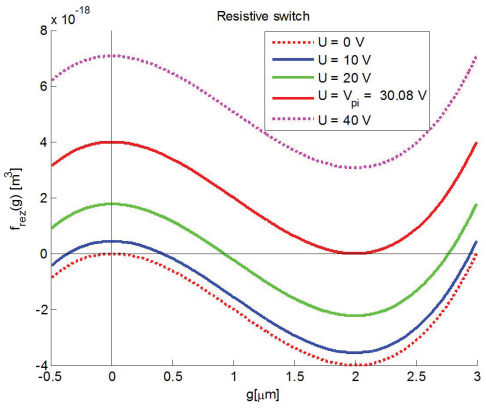

Figure 3.24: Dependency of the nonlinear function on the distance between armatures for different values of the applied voltage.[222]

voltage used is in the range of 0 to 40 volts. The simplicity of the problem allows an exact analytical modelling of the problem.

3.3.4.1 Resistive Case

For this case there is no isolation layer between the armatures $t_d = 0$, the nonlinear equation has the form:

$$f_{rez}(g) = g^3 - g_0 g^2 + \frac{\varepsilon_0 A V^2}{2k}. \tag{3.33}$$

The nonlinear equation will always have a negative solution, which has no physical significance and other two solutions, from which one or non real solutions, everything depends on the actuation voltage. The graphical representation of this function for the values specified above for different applied voltages is presented in Fig.3.24. A pull-in voltage $V_{\text{pi}} = 30.08$ V and the displacement of $g_{\text{pi}} = 2\mu$n.

If the value of the local minimum function is strictly positive, then there is no real solution of the equation in the range considered, the armature can not stay in the equilibrium position, applying such a voltage will collapse the upper armature. If the value of the local minimum function is zero then there is only a real solution of this equation, and this solution corresponds to the pull-in voltage and the displacement at this voltage has the values:

$$V_{\text{pi}} = \sqrt{\frac{8kg_0^3}{27\varepsilon_0 A}} \text{ and } g_{\text{pi}} = \frac{2g_0}{3}. \tag{3.34}$$

If the function value in local minimum is less than zero, then the equation has two real solutions. From these two mathematical solutions, only one has the proper physical significance, namely a stable system. If the applied voltage has a small increase compared to the position of the equilibrium state, then the new static equilibrium position must correspond to a bit smaller distance between the electrodes (Fig.3.25) because the electrostatic force of attraction increases. By analyzing the curve and what happens to high actuation voltage, it results that if the nonlinear equation has two positive real solutions, the stable is the one that is in the range $g \in [2g_0/3, g_0]$.

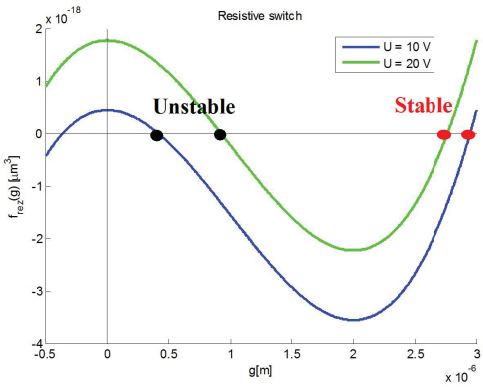

Figure 3.25: Dependency nonlinear function of the distance between armatures stable and unstable positions.[222]

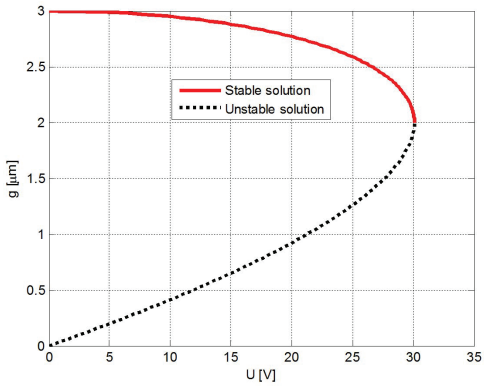

Figure 3.26: Dependency of the gap between the armatures of the applied voltage.[222]

Another result that is of interest is the dependence of the stable and unstable solution with the applied voltage. An alternative is to use analytical formulas for solutions of the third order equation, but a simpler representation is to consider the inverse function and calculate the voltage depending on the movement. From (3.33) equal to 0 it results that:

$$V = \sqrt{\frac{2k}{\varepsilon_0 A} g^2 (g_0 - g)}, \tag{3.35}$$

formula when computed for $g \in [0, 2g_0/3)$ results in unstable values and when computed for $g \in [2g_0/3, g_0]$ results in stable values of the displacement (Fig.3.26). It is meaningless to apply this formula for values of the distance between the plates outside this range.

3.3.4.2 Capacitive Case

For this case the isolation layer between the armatures has a thickness $t_d \neq 0$, the nonlinear equation has the form:

$$f_{cap}(g) = (g - g_0)\left(g + \frac{t_d}{\varepsilon_r}\right)^2 + \frac{\varepsilon_0 A V^2}{2k}, \tag{3.36}$$

The local minimum point that gives the value of the pull-in voltage is smaller then two thirds of the initial gap. The expressions for the pull-in voltage and the displacement at

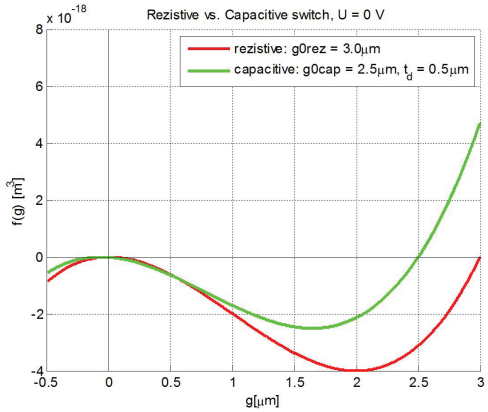

Figure 3.27: Resistive switch vs. capacitive switches. Nonlinear dependency on the gap in the absence of the actuation voltage [222].

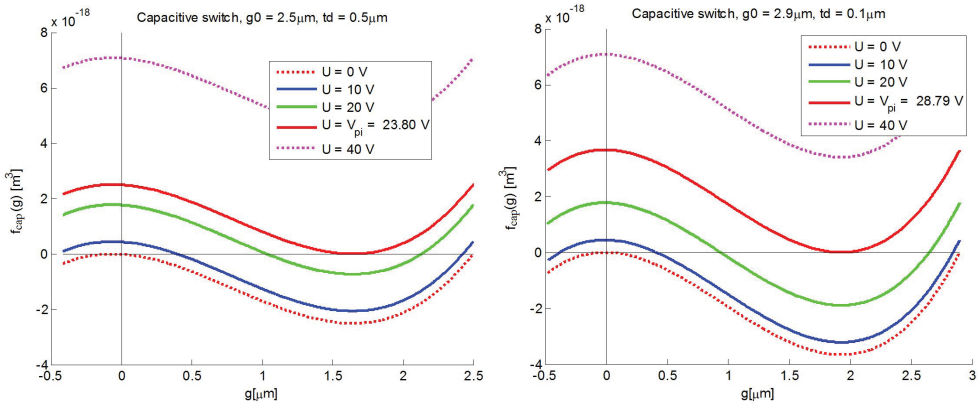

Figure 3.28: Dependence of nonlinear function f_{cap} of the distance between armatures for different values of the applied voltage. Right - Configuration with $g_0 = 2.5\mu$m and $t_d = 0.5\mu$m. Left - Configuration with $g_0 = 2.9\mu$m and $t_d = 0.1\mu$m [222].

this value are:

$$V_{pi} = \sqrt{\frac{8k}{27\varepsilon_0 A}\left(g_0 + \frac{t_d}{\varepsilon_r}\right)^3} \text{ and } g_{pi} = \frac{2g_0}{3} - \frac{t_d}{3\varepsilon_r}. \tag{3.37}$$

To make a comparison with the resistive case, in the 3μm initial gap of the resistive switch an isolation layer is inserted whose relative permittivity has the value of 7.5 typical for Si_3N_4

Therefore the comparison from Fig.3.27 between the resistive and capacitive case requires that the initial gap from resistive case to be the sum of initially gap from the capacitive case and the thickness of the dielectric, which can be seen from the non linear function representation, if this is represented a zero voltage.

The analysis of the nonlinear dependence of actuation voltage shows that the insertion of the dielectric between the armature has the effect of lowering pull-in voltage (Fig.3.28 - Left). For this configuration with $g_0 = 2.5\mu$m and $t_d = 0.5\mu$m results $V_{\text{pi}} = 23.8$ V with a displacement $g_{\text{pi}} = 1.64\mu$m. For this example the thickness of the isolator is a bit exaggerated, usually $t_d = 0.1 \quad \mu$m, resulting a initial gap $g_0 = 2.9\mu$m and $V_{\text{pi}} = 28.79$ V with a displacement $g_{\text{pi}} = 1.93\mu$m (Fig.3.28 - Right).

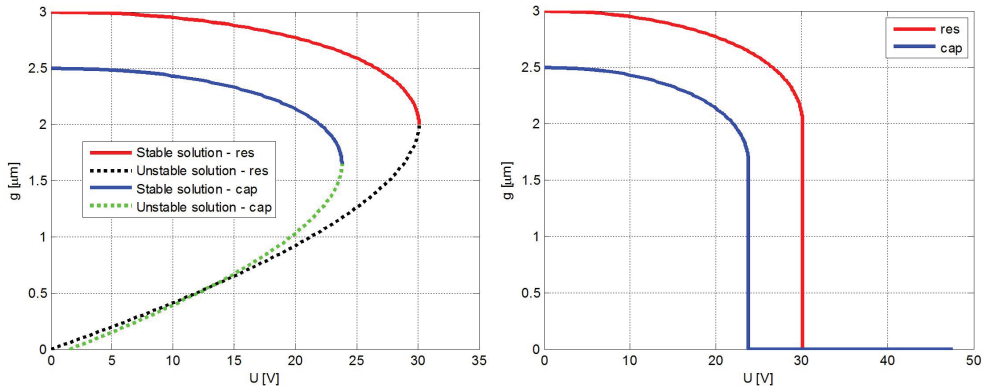

Figure 3.29: Left: Dependency of the gap between the armatures of the applied voltage [222]. Right: Real dependency of the gap.

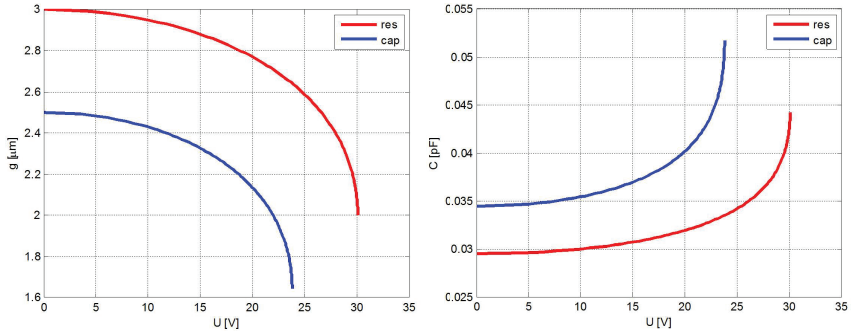

Figure 3.30: Dependency of the gap between the armatures (left) and capacitance (right) w.r.t. applied voltage [222].

The dependence of the stable and unstable solutions with the applied voltage (Fig.3.29 - Left) was similar to the resistive case applying the expression:

$$V = \sqrt{\frac{2k}{\varepsilon_0 A}(g_0 - g)}\left(g + \frac{t_d}{\varepsilon_r}\right)^2. \tag{3.38}$$

A more correct representation is given in Fig.3.29 - Right, for an applied voltage greater then V_{pi}; the switch is actuated and the gap between the armatures is null.

Another quantity that is of interest is the capacity of the capacitor formed by the two armatures. For the resistive switch the expression of the capacity is:

$$C_{\text{res}} = \frac{\varepsilon_0 A}{g}, \tag{3.39}$$

and for the capacitive switch is:

$$C_{\text{cap}} = \frac{1}{\frac{g}{\varepsilon_0 A} + \frac{t_d}{\varepsilon_0 \varepsilon_r A}}, \tag{3.40}$$

the dependence of the capacitance with the applied voltage, until it reaches V_{pi}, is presented in Fig.3.30.

In the case of the capacitive switch, the capacitance can be computed for voltages higher than V_{pi} (Fig.3.31), this being the capacitance of a capacitor with the distance

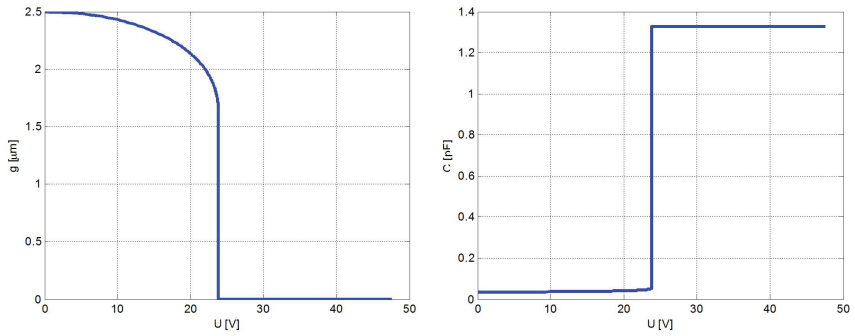

Figure 3.31: Dependency of the gap between the armatures (left) and capacitance (right) w.r.t. applied voltage that passes V_{pi} [222].

between the armatures equal to t_d, filled with dielectric. Obviously this can be done for the resistive switch, its capacitance in actuated position will be infinite.

For this representation the the C-V curve aspect in the stable zone can not be distinguished because the capacity in down position is between 30 to 40 times higher then the capacity in up position. For this example the computed capacitance are:

$$C_{\text{down}} = 1.326 \quad pF, C_{\text{up}} = 0.034 \quad pF, C_{\text{pi}} = 0.051 \quad pF, C_{\text{down}}/C_{\text{up}} = 38.5, C_{\text{down}}/C_{\text{pi}} = 25.6.$$

All judgments so far have been done, as is it natural, by imagining that initially there was no applied voltage and that a voltage is applied to the terminals. Of course, this cannot be done suddenly and if we imagine that the growth rate is slow enough, then for every moment in time we can assume that the system is in a static state. But what happens between V_{pi} and the moment when the armatures are in contact is no longer static. When the switch is in down position, according to the curve of Figure Fig.3.31, the voltage is beyond V_{pi} and there is no reason to increase it.

If we imagine now that the voltage slowly decreases, the phenomena are not reversible because now the problem is different, we have different initial conditions. We now have a capacitor which has only dielectric between the armatures. A capacitor in down position, with only dielectric, requires a lower voltage than Vpi to be maintained in this state.

The condition is that the elastic force corresponding to the stretching of the spring with g_0 distance, force that is directed up, to be lower than the corresponding electrostatic force formed between the armatures, without any air gap at which the weight of the armature is added, both oriented in down direction.

The condition mentioned to keep the switch actuated is:

$$kg_0 \leq \frac{\varepsilon_0 A V^2}{2} \left(\frac{t_d}{\varepsilon_r}\right)^2 + G \tag{3.41}$$

resulting that the voltage that has to be applied is:

$$V \geq \frac{t_d}{\varepsilon_r} \sqrt{\frac{2}{\varepsilon_0 A}(kg_0 - G)}. \tag{3.42}$$

Obviously, if the weight is greater than the corresponding elastic force of g_0 elongation, there is no need to have a voltage applied between the armatures to keep the switch actuated. Moreover, this kind of switch will never be not actuated.

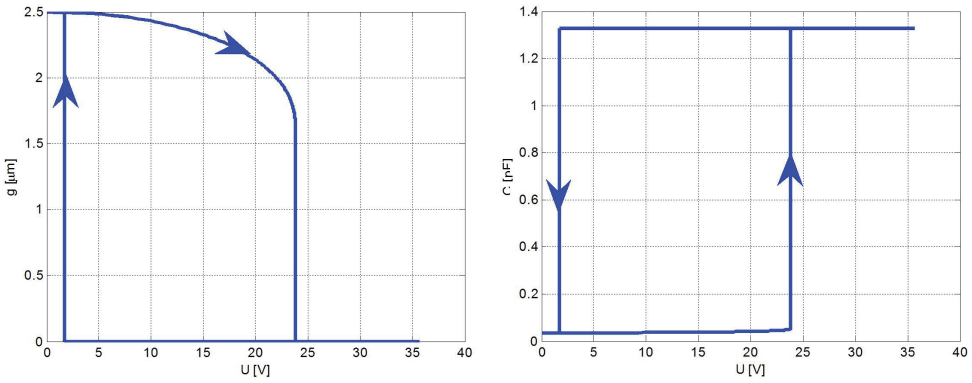

Figure 3.32: Dependency of the gap between the armatures (left) and capacitance (right) w.r.t. applied voltage [222].

To estimate the mass of the considered numerical example we suppose that the armatures are made from aluminum, which has a mass density of 2.7 g/cm^3, and assume a 0.5 μm thickness of the armature, resulting a gravity force of $1.3 \cdot 10^{-10}$ N, against the elastic force of the spring corresponding to the maximum elongation which is $kg_0 = 3 \cdot 10^{-5}$ N. Consequently, the mass can be neglected.

The minimum value of this expression (3.42) is called the pull-out voltage and has the value:

$$V_{po} \geq \frac{t_d}{\varepsilon_r}\sqrt{\frac{2}{\varepsilon_0 A}kg_0}. \tag{3.43}$$

If the applied voltage becomes smaller then V_{po} the upper armature is released, the representation of the actuation and deactuation processes for the dependence of the gap between the armatures and the capacitance with the applied voltage is presented in Fig.3.32.

3.3.5 Numerical Modelling in Static Regime

Numerical modeling consists of conceiving an algorithm dedicated to solving the model equations. What is interesting is that every issue taken separately is linear in terms of constitutive relations (material). In electrostatic domain, materials are linear and in mechanic domain the spring is linear (constant k is not dependent on the force applied). However the coupling between the domains is nonlinear, so even this simple problem is nonlinear.

Numerical computation in static regime means finding the g-V point in the stable state segment, ie $g \in [2g_0/3, g_0]$, the problem has unique solution, and is well conditioned, according to previous studies.

Natural formulation (from the physical point of view) is for a given V is required $g \in [2g_0/3, g_0]$ this being the direct problem. But considering the bijectivity of the function, an inverse problem can be formulated, for a given $g \in [2g_0/3, g_0]$ is required V so the system can be in static equilibrium.

Given all the previous judgments, the problem is difficult to solve directly, a third order nonlinear algebraic equation, while the inverse problem solution has already the

dependency on the problem data expressed explicitly.

Using MATLAB software the problem can be solved simply by writing a code to solve the nonlinear equation (3.26).

Using Spice software the describing circuit (3.26) is shown in Fig.3.33, where *B1* and *B2* are behavioral sources. G is a voltage controlled current source. The element *R1* does not have any significance.

The units of the input parameters were scaled this way as the simulation is more robust. For equation (3.26) the SI units are:

$$\frac{N}{m}(m) = \frac{\frac{F}{m} m^2 V^2}{m^2}, \tag{3.44}$$

which can be scaled as:

$$\frac{N}{m}(\mu m) = \frac{\frac{pF}{m} m m^2 V^2}{\mu m^2}, \text{ indeed: } \frac{1}{1}(10^{-6}) = \frac{\frac{10^{-12}}{1}\left(10^{-3}\right)^2 1^2}{\left(10^{-6}\right)^2}. \tag{3.45}$$

So, in the scaled equation we will use the following units:

- elastic constant k - in N/m, as in S.I.;
- the permittivity in pF/m, this means that $\varepsilon_0 = 10^3/(36 * \pi) pF/m$;
- the length and the width of the plates in mm;
- the gap in μ;
- the voltage in volts;
- forces will be expressed in μN.

In Fig.3.34 the dependency of the displacement w.r.t. the applied voltage obtained by simulating the circuit is presented. To do the validation, the values computed in MATLAB are compared with the values obtained by simulating the circuit in Table 3.2. The small difference between the data validates the models.

Table 3.2: Comparison between values computed in MATLAB and values obtained by simulating the SPICE circuit [222].

MATLAB Values		SPICE Values	
V = 23.8036	g = $1.644{\cdot}10^{-6}$	V = 23.8500	g = $1.660{\cdot}10^{-6}$
V = 23.1914	g = $1.858{\cdot}10^{-6}$	V = 23.1900	g = $1.858{\cdot}10^{-6}$
V = 21.0397	g = $2.072{\cdot}10^{-6}$	V = 21.0300	g = $2.072{\cdot}10^{-6}$
		V = 21.0400	g = $2.072{\cdot}10^{-6}$
V = 16.3650	g = $2.286{\cdot}10^{-6}$	V = 16.3399	g = $2.286{\cdot}10^{-6}$
		V = 16.3499	g = $2.286{\cdot}10^{-6}$
		V = 16.3599	g = $2.286{\cdot}10^{-6}$

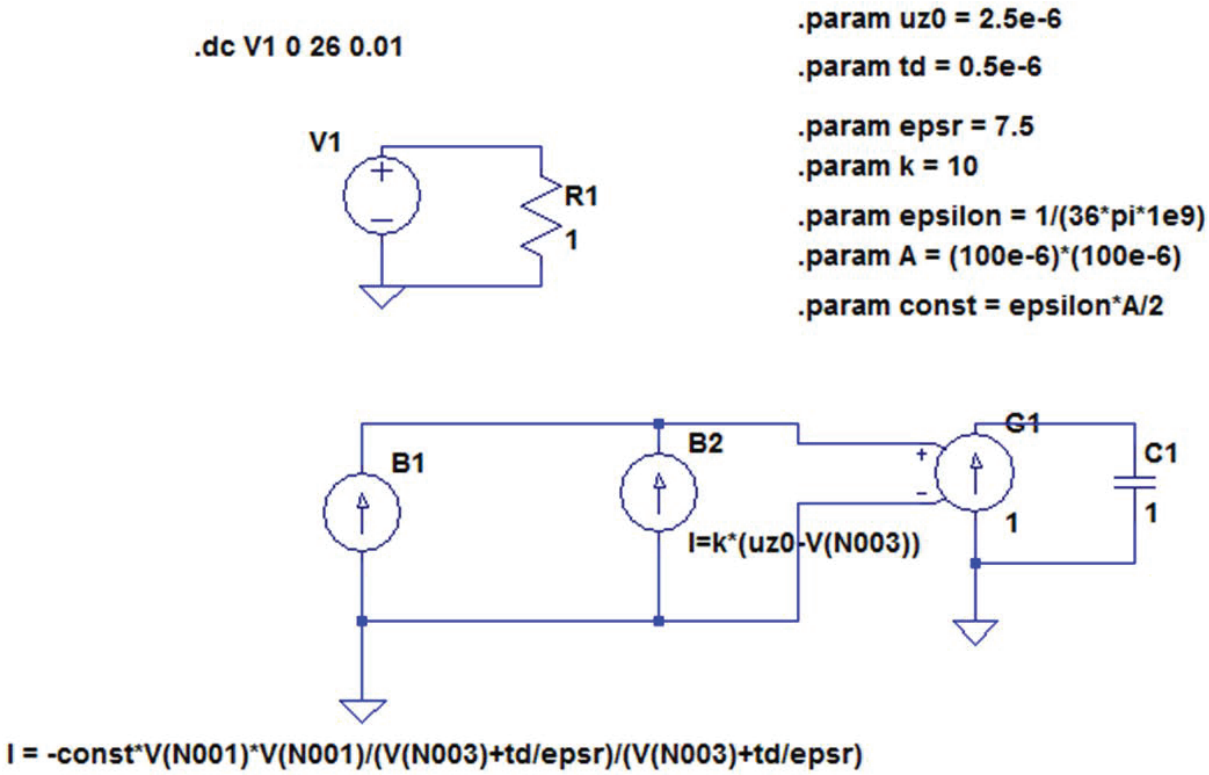

Figure 3.33: Spice circuit used to solve the nonlinear equation [222].

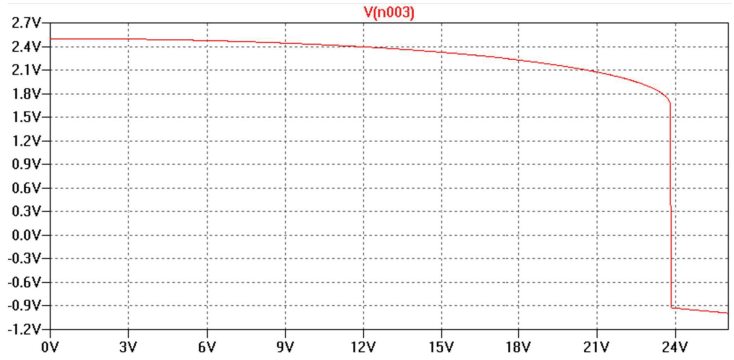

Figure 3.34: Dependency of the displacement with applied voltage obtained from SPICE [222].

3.4 Conclusions

This chapter presents the analytical and numerical modelling of the most simple 1D model than can be imagine for a RF-MEMS device, the one of a parallel plane capacitor with one armature suspended from a spring. The analysis starts from the most general case, the dynamic analysis, were electrostatic, structural mechanic and fluid flow (represented in this study by the damping force) are coupled together. As a particular case making $\mathrm{d}/\mathrm{d}t = 0$ the static model was performed. For both regimes the modelling steps set in the previous chapter were checked for two constructive types of switches, capacitive and resistive.

The analytic analysis was done by solving the nonlinear differential equation. For the numerical modelling the problem was studied in three ways. MATLAB by a script that solves the nonlinear differential equation, APPLAC using a model that is implemented in the program and SPICE creating a *netlist* circuit that also solves the nonlinear differential equation. The SPICE equivalent circuit is indeed a similar circuit, the based on the electric-mechanic similitude table. It was concluded that, in the dynamic simulations, both inertial force and the damping force have to be considered and in the static regime only the electrostatic force influence the structure. The gravitational force is never relevant.

Parametric analysis was conducted upon the lumped quantities extracted from the solutions, studding the effective elastic (stiffness) constants k, k_s, damping (that depends on the quality factor Q) coefficient b and effective mass (resonant frequency $\omega_0 = 2\pi f_0$) m_{eff}.

The static simulation of the model (including the MATLAB, APLAC or SPICE equivalent circuit) allows the extraction of the pull-in voltage, while its dynamic simulation allows the extraction of the switching time. Even the analysis model is the simplest one, the simulation results are meaningful and very valuable for the designers, allowing a better quantitative understanding of the switch operation. Although more accurate results will be obtained below, by using more complex models, the qualitative understanding of the essential aspect of RF MEMS switches operation may be easier reached by the analysis made above in this chapter. The conclusions and knowledge acquired by this analysis became a skeleton for the next more detailed and more accurate models. The main idea is to improve the Spice model, by using more accurate circuit parameters, without increasing its complexity or changing its topology.

Chapter 4

Multiphysics Modelling of MEMS Switches and their Validation

This section presents the multiphysics modelling of a MEMS switch. As study case, two switches (QIAN and IMT) will be analyzed, which differ by the geometrical configuration and the way that the contact between the membrane and transmission line is made. One has a capacitive contact (QIAN) and the other a resistive one (IMT). For both configuration will be computed the pull-down voltage and their RF behavior (S parameters at the RF ports) in their stable states, UP and DOWN.

For both MEMS switches the 2D and 3D numerical models were developed, and then they were simulated in the static and dynamic regimes by using Finite Element Method (FEM) within COMSOL Multiphysics software package, coupling the Electrostatic, Structural Mechanic and Fluid Dynamic phenomena that occur in the operation of these devices. The full wave electromagnetic field was analysed by using the Finite Integration Technique to solve Maxwell equations with electromagnetic circuit element (EMCE) boundary conditions.

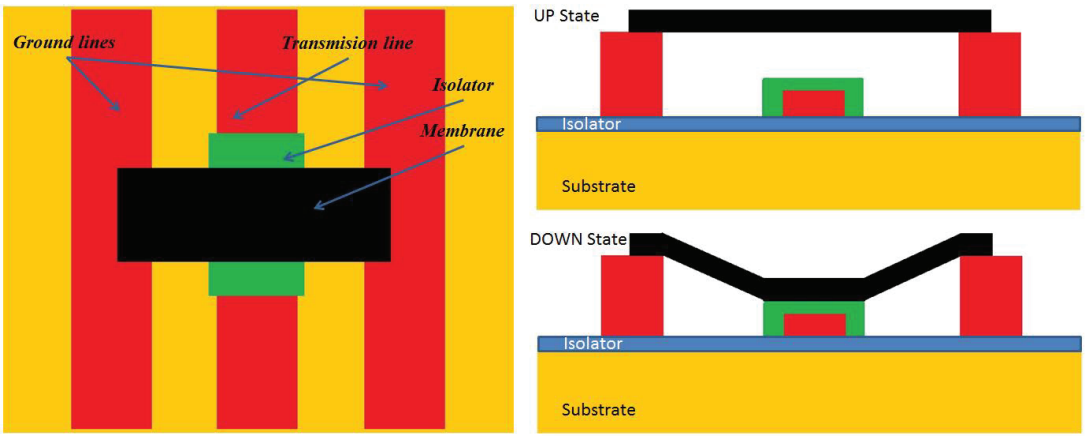

Figure 4.1: Qian Structure. Left upper view of the geometry. Right transversal section, Up and Down stable positions.

The QIAN structure [56], presented in Fig.4.1, consists of a CPW made by two grounded conductors on which the membrane (bridge) is placed, suspended over a signal

line, along which the RF signal is propagated, if the membrane is in the UP state. In the DOWN state of the membrane, the RF signal is blocked due to the high capacitance between the two conductive plates (which makes a short circuit to ground). The signal line is thinner in the middle; this part is serving as the actuation electrode having the same width as the signal line, coated with an isolator layer. The RF signal has a level much lower than those of actuation voltage, generating as consequence a neglected attraction force.

The IMT structure, presented in Fig.4.2 which shows the practical realization of this switch, consisting of two grounded conductors on which the membrane is placed, suspended over a signal line, along which the RF signal is propagated if the membrane is in UP state. The construction with two actuation pads is preferred to the classical one which has the dielectric placed on the RF signal line, due to the fact that in this case the dielectric degradation problem that appears in down state is avoided [10].

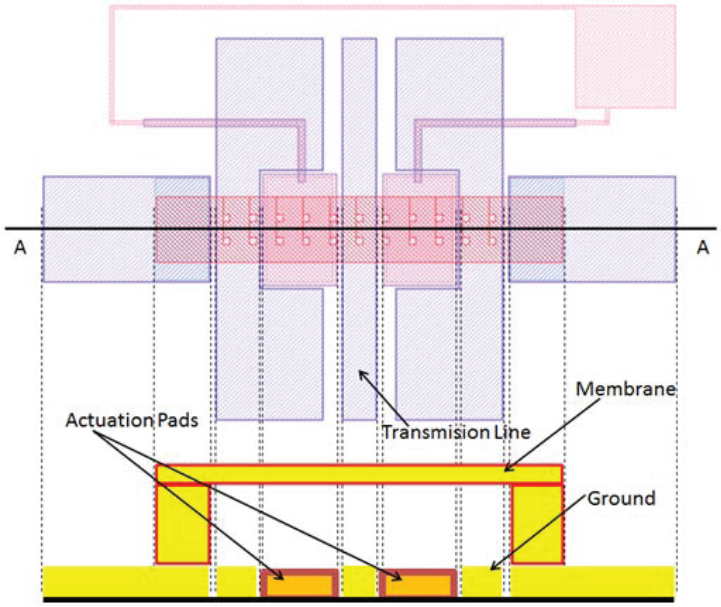

Figure 4.2: IMT Structure. The transversal section is not to scale.

4.1 2D Multiphysics Static Models of MEMS Switches

To reduce the computational effort, for beginning it is considered a two-dimensional, plan parallel model, in which the edge effects of the mobile membrane are neglected. Due to the symmetry with central, longitudinal ZOY vertical plane, the analysis is done only for a half of the structure (Fig.4.3). The transmission line, the insulating layer and the silicon substrate are excluded from the computational domain, being replaced by physical boundary conditions.

In the static regime the time variation is neglected ($d/dt = 0$) for any quantity and it is assumed that there is not any energy transfer (either electrostatic or elastostatic) i.e. top armature is in a equilibrium position, an immobile body. Therefore a pair of coupled electrostatic (ES) and structural mechanical (MEC) problems have to be solved.

4.1.1 First Study Case: Static Analysis of the QIAN Structure

The parametrized geometric model of the QIAN structure is presented in Fig.4.3. Here is indicate also the materials of the switch components. The numeric values of the geometric parameters are presented in Table4.1 and of the material constants are listed in Table4.2 where E is the Young's elastic modulus, ν is the coefficient of transversal contraction (Poisson's ratio) and ρ is the mass density.

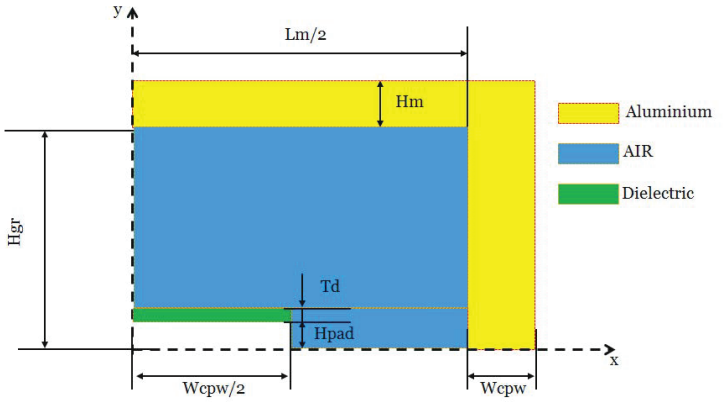

Figure 4.3: Qian Structure. Parametric model.

Table 4.1: QIAN structure geometric parameters. Value and significance

Parameter	Value	Significance
L_m	$280\mu m$	length of the membrane
H_m	$0.4\mu m$	height of the membrane
H_{gr}	$4\mu m$	height of the ground line
H_{pad}	$0.4\mu m$	height of the central part of the transmission line
T_d	$0.1\mu m$	height of dielectric
W_{cpw}	$120\mu m$	width of the transmission and ground line

Table 4.2: QIAN structure material parameters.

Parameter	Material	ε_r	μ_r	$\sigma[S/m]$	$\nu[-]$	E [Pa]	$\rho[Kg/m^3]$
$ALUM$	Aluminum	1	1	$6.6 \cdot 10^7$	0.35	$70 \cdot 10^9$	2700
AIR	Air	1	-	-	0	10^{-6}	1.23
$Dielectric$	Silicon nitride Si_3N_5	7	1	10^{-3}	0.25	$300 \cdot 10^7$	2600

The computational domain of the mechanic (structural) problem (MEC) is composed from the membrane and ground line, delimited by $X_{max} = L_m/2 + W_{cpw}$ and $Y_{max} = H_{gr} + H_m$ (Fig.4.4 - left). The boundary conditions of the structural problem (Fig.4.4 - right) provided by the symmetry conditions imposed on the symmetry axis ($x = 0$) on which the displacement are only vertical i.e. $\mathbf{n} \cdot \mathbf{u} = 0$, where $\mathbf{n}$ is the normal at the boundary; null displacement (fixed constraint) $\mathbf{u} = \mathbf{0}$ is imposed on the ground line ($y = 0$), where the membrane is embedded. On the rest of the MEC natural boundary conditions (free movement) are imposed. A plane strain model is considered, in which the

unknown is the displacement 2D vector **u**, defined in every point of the computational MEC domain.

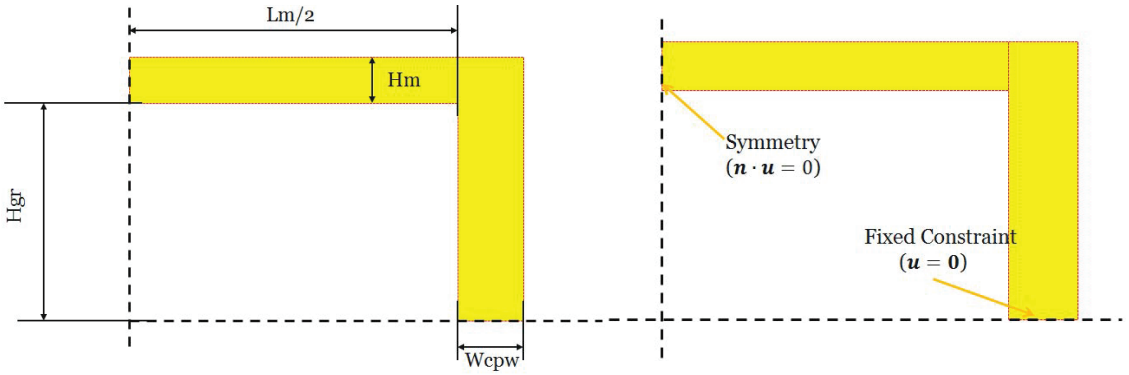

Figure 4.4: The computational MEC domain (left) and the imposed boundary conditions (right).

The computational domain ES of the electrostatic problem is composed by the air beneath the membrane and the dielectric above actuation pad, delimited by $X_{max} = L_m/2$ and $Y_{max} = H_{gr}$ (Fig.4.5 - left). In order to avoid the presents of singularity points and the problem to be not well formulated, on the vertical face of the actuation pad was placed a dielectric of thikness T_d. The electrostatic field described by the electric scalar potential V, defined in every point of the ES domain. For it, Dirichlet boundary conditions are imposed as shown in (Fig.4.5 - right); an imposed voltage U on the bottom of the isolator layer (where the actuation electrode is placed) and null potential on the membrane and on ground line, whereas the rest of the ES boundary is left with natural boundary conditions $dV/dn = 0$.

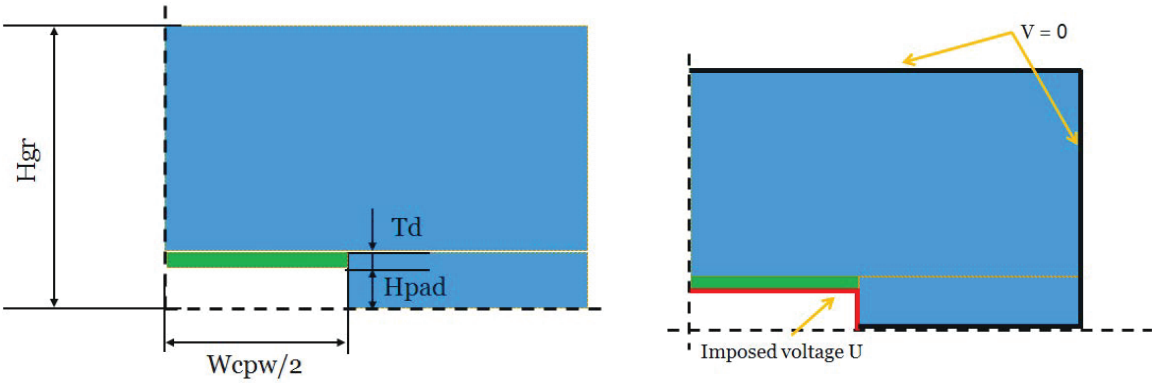

Figure 4.5: The computational ES domain (left) and imposed boundary conditions (right).

The coupling can be treated in two ways. The first possibility is to carry out iterations between the ES and MEC simulations. This is also known as co-simulation or staggered solution procedures for a weak coupling. A second possibility is to couple the models in a strong manner, in which the equations of the ES and MEC formulations, together with their boundary conditions and coupling conditions, are solved simultaneously.

The two MEC and ES domains have a common boundary (Fig.4.6), where coupling conditions will be imposed. Indeed, the electric field applied between the grounded membrane and the actuation electrode produces a force that makes the MEC domain to change

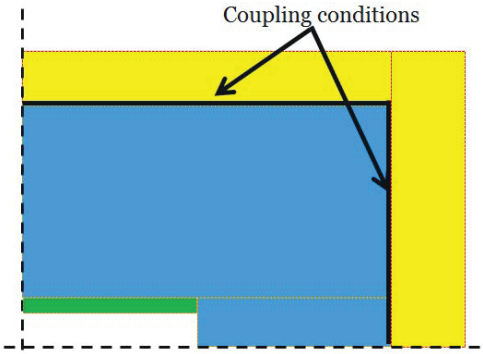

Figure 4.6: Qian Structure. Coupling boundary conditions.

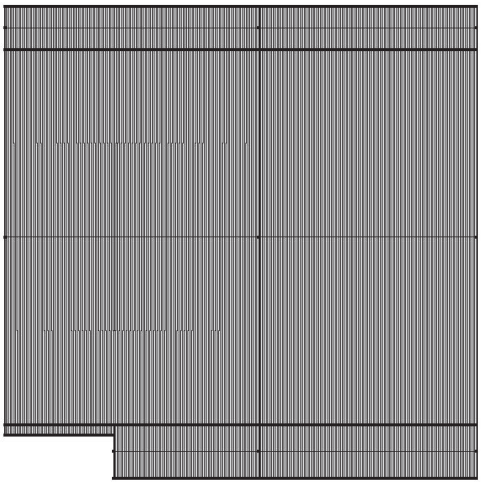

Figure 4.7: Discretization grid of the computational domain (not at same x-y scale).

its shape, and thus it is modified by the ES domain and the electric field. More precisely, the Maxwell stress tensor computed from the ES field (4.1) is a negative pressure acting on the beam surface:

$$\mathbf{n}_1 T_2 = \frac{1}{2}\mathbf{n}_1(\mathbf{E}\cdot\mathbf{D}) + (\mathbf{n}_1\cdot\mathbf{E})\mathbf{D}^T \tag{4.1}$$

The numerical simulation was performed by COMSOL Multiphysics V 4.4 computing environment [137]. The MEC+ES computational domain was discretized by a Cartesian grid that consists of 1506 domain elements and 1065 boundary elements, which generated 16007 degrees of freedom. Along the x-axis, the domain was divided into elements of approximately 1μm. Along axis y axis, the membrane was divided into two elements, the air space and ground line into 4 parts and the dielectric in one element (Fig.4.7).

Two static mutually coupled problems have been solved, one electrostatic and one elastostatic (Fig.4.8). To solve the multiphysics problem a nonlinear solver was used. The applied voltage U on the electrode was varied from 0 to 40 V. The pull-in voltage (V_{pi}) was assumed as the last value of the applied voltage U for which the procedure is convergent. The value $V_{pi} = 30.045$ V is obtained. The shape of the membrane at V_{pi} is presented in Fig.4.9 which shows the cross section of the device at scale, in the initial position (UP state, for $U = 0$) and the last computed position before instability. For the latter, Fig.4.10 shows the color map of the displacements and Fig.4.11 shows the color

map of the electric potential.

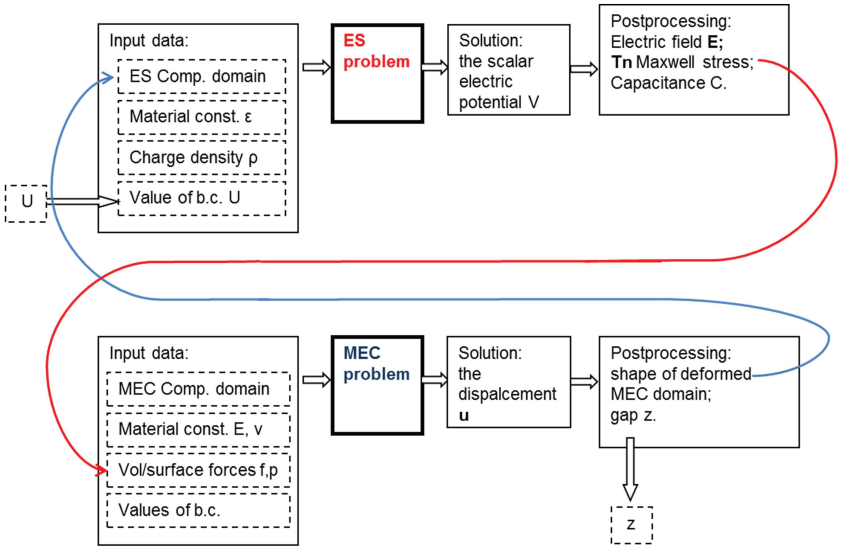

Figure 4.8: The mutual coupling of the electrostatic (ES) and the structural-elastostatic (MEC) problems

The variation of the membrane position vs. applied voltage is presented in Fig.4.12, the central displacement z for a point situated in the middle of the membrane on the bottom surface, were the maximum displacement should occur. The verification was done by comparing the simulation results obtained with COMSOL with results of ANSYS [138], which gives the result depicted in Fig.4.13. In this case, the last actuation voltage at which the algorithm converges is $U = 29.07$ V.

The relative difference of the latest pull-in voltage calculated by COMSOL and ANSYS is about 3%, which is quite acceptable. The maximum displacement of the membrane computed by COMSOL is $z_{pi} = 2.26\mu$m, and with ANSYS is $z_{pi} = 2.19\mu$m, having also a deviation below 3%.

4.1.2 Second Study Case: Static Analysis of the IMT Structure

The parametrized geometry of the IMT structure, is presented in Fig.4.14, where are identified the materials values of the the switch's components. The values of the geometric parameters are presented in Table4.3 and the values of the material parameters in the Table4.4.

As in the previous case, the structural (MEC) domain includes only the membrane, its maximal limits being $x_{\max} = L_m/2 + W_p$ and $y_{\max} = H_{\text{cpw}} + H_{\text{gap}} + H_m$. A plane strain

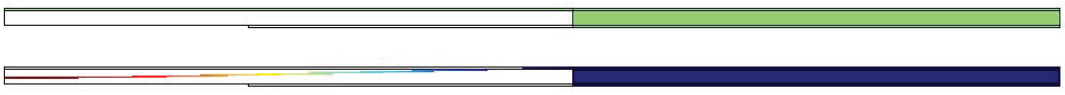

Figure 4.9: The shape of the membrane at V_{pi}, representation at scale.

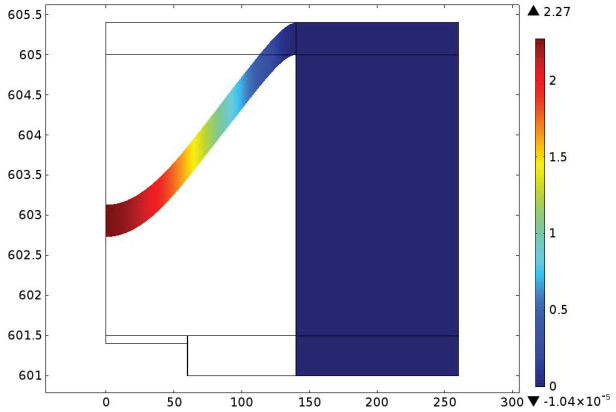

Figure 4.10: The shape of the membrane at V_{pi}.

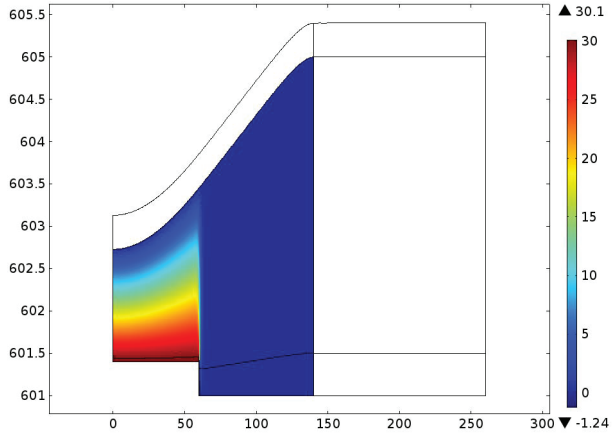

Figure 4.11: Color map of the electric potential for the last stable position. Figure not to scale.

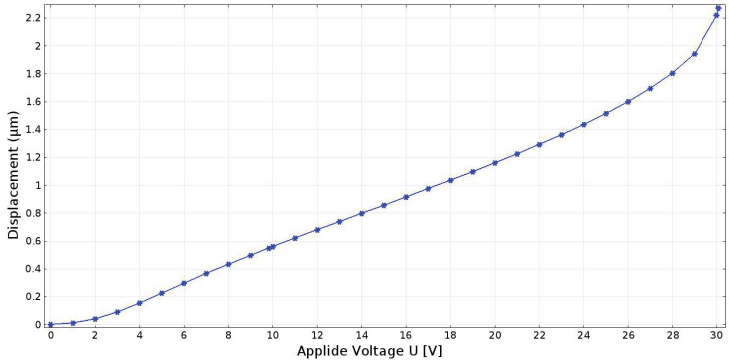

Figure 4.12: The central displacement z vs. applied voltage U (COMSOL simulation).

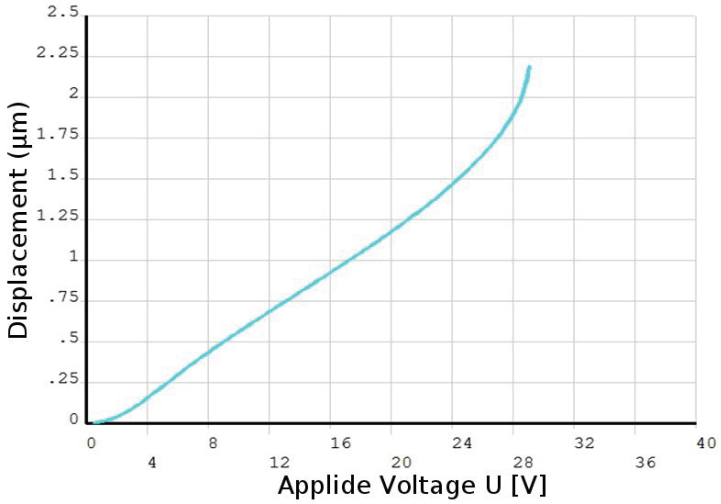

Figure 4.13: The central displacement z vs. applied voltage U (ANSYS simulation).

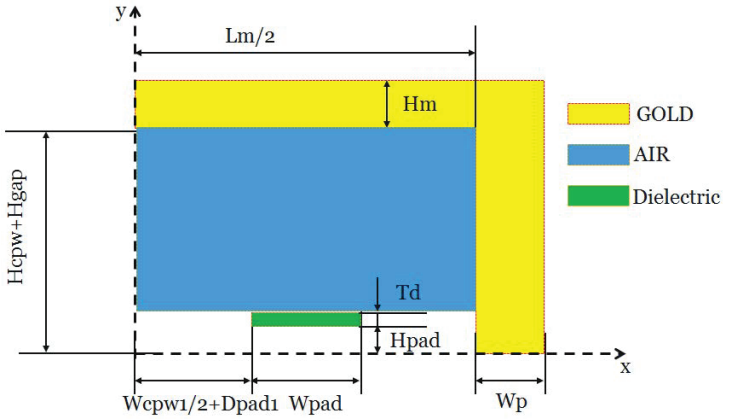

Figure 4.14: Parametrized geometry of the IMT structure.

Table 4.3: Geometric parameters.

Parameter	Value (μm)	Significance
L_m	910	Length of the membrane
W_m	200	Width of the membrane
H_m	2	Height of the membrane
H_{cpw}	0.6	Height of the signal line
H_{gap}	2.5	Height of the gap
H_{pad}	0.45	Height of the electrode
W_{cpw}	100	Width of the signal line
W_{pad}	200	Width of the electrode
W_p	160	Width of the membrane support
D_1	30	Distance between the CPW and electrode
T_d	0.1	Height of the dielectric

Table 4.4: Material parameters used in the model.

Material	Gold	Air	Dielectric
Relative permittivity ε_r	-	1	3.9
Poisson's ratio ν	0.44	-	-
Elasticity (Young's) modulus E [Pa]	$78 \cdot 10^9$	-	-
Mass density ρ [kg/m^3]	19280	-	-

model is considered, in which the unknown is the 2D displacement vector $\mathbf{u}$ defined in every point of the computational MEC domain. The boundary conditions of the structural problem (Fig.4.15 – left) provided by the symmetry conditions imposed on the symmetry axis ($x = 0$) on which the displacement are only vertical i.e. $\mathbf{n} \cdot \mathbf{u} = 0$, where $\mathbf{n}$ is the normal at the boundary; null displacement (fixed constraint) $\mathbf{u} = \mathbf{0}$ is imposed on the ground line ($y = 0$), where the membrane is embedded. On the rest of the MEC natural boundary conditions (free movement) are imposed. An important aspect to consider in the mechanical modeling is the residual stress σ. Ideally $\sigma = 0$, since in our case this stress is not desirable, however it may be present in the membrane, as a result of the fabrication process.

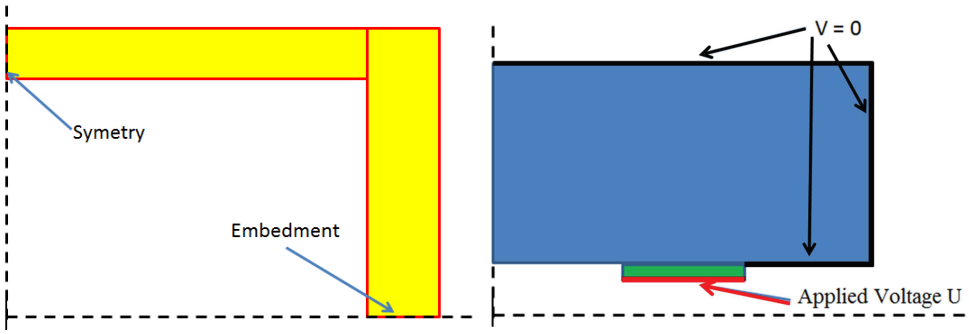

Figure 4.15: MEC Boundary Conditions – Left; ES boundary conditions – Right.

The electrostatic (ES) domain includes the dielectric and the air just under the membrane, its maximal limits being $x_{\max} = L_m/2$ and $y_{\max} = H_{\text{cpw}} + H_{\text{gap}} - H_{\text{pad}}$. The electrostatic field described by the electric scalar potential V, defined in every point of the ES domain. For it, Dirichlet boundary conditions are imposed as shown in (Fig.4.15 – right); an imposed voltage U on the bottom of the isolator layer (where the actuation electrode is placed) and null potential on the membrane and on ground line, whereas the rest of the ES boundary is left with natural boundary conditions $dV/dn = 0$.

As in the previous study case, the MEC and ES domains have two curves of common boundary (Fig.4.16), where coupling conditions have to be imposed. Indeed, the electric field between the membrane and the actuation electrode produces a forces that makes the MEC domain to change its shape, and thus it modifies the shape of the ES domain and consequently the electric field. As a consequence, a multiphysics (ES-MEC) with the mutual coupling described in Fig.4.8 have to be solved.

The numerical modeling was carried out the finite element method implemented in COMSOL Multiphysics software. A strong MEC-ES coupling was used. The computational domain was meshed with quadrilateral elements. Along the OX axis, the domain

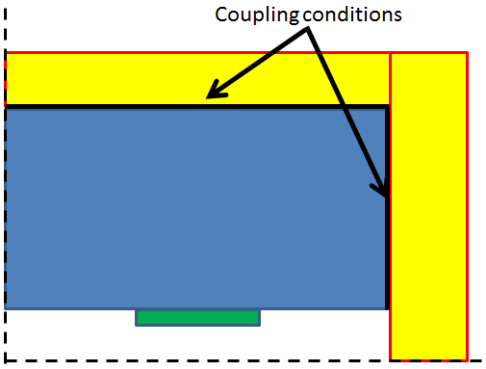

Figure 4.16: MEC and ES fields are coupled along two curves.

was divided into elements with the length of 1μm and along the OY axis, the membrane was divided into two parts, the air space and the dielectric in one element and the support of the membrane in 4 elements. In order to check the independence of the numerical solution with respect to the mesh, a series of refinements were considered. The largest model has 4335 elements and 49989 unknowns (Fig.4.17). For each configuration, for any applied voltage, a non-linear solver was used, and the solution was obtained in about 3 minutes, on a laptop with Intel Processor of 2.4 GHz and 8.00 GB RAM.

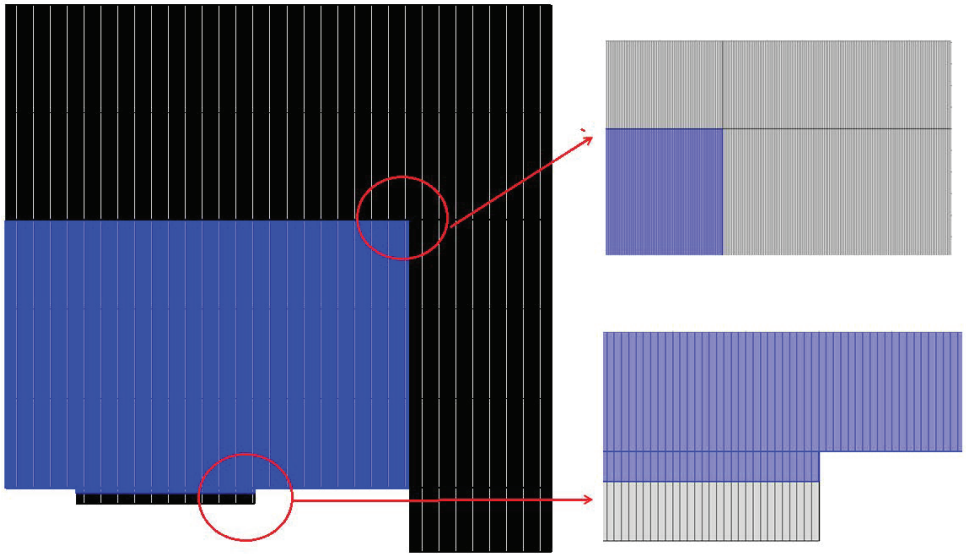

Figure 4.17: Discretization of the domain. Figure is not to scale, the vertical dimensions have been multiplied about 100 times.

The shape of the membrane at V_{pi} is presented in Fig.4.18 which shows the cross section of the device at scale, in the initial position (UP state, for $U = 0$) and the last computed position before instability. For the latter, Fig.4.19 shows the color map of the displacements and Fig.4.20 shows the color map of the electric potential.

The applied voltage U on the electrode was changed from 0 to 10 V. The pull-in voltage (V_{pi}) was assumed to be the last value of the applied voltage U, for which the procedure is convergent, and it has the value $V_{pi} = 7.896$ V and the maximum displacement has the value $g_{pi} = 1.42\mu$m. The variation of the membrane position vs. applied voltage is presented in Fig.4.21, the central displacement z for a point situated in the middle of the

Figure 4.18: Cross-section at scale: up - up position, down - last computed position before instability.

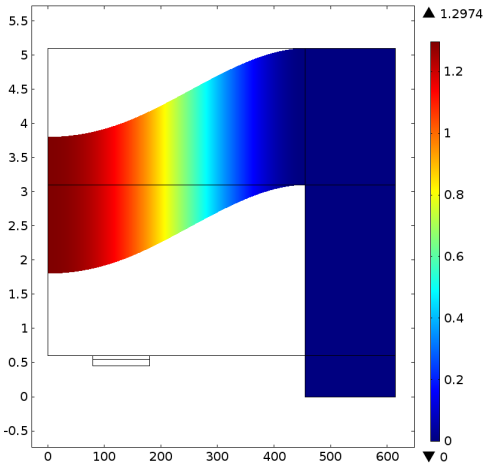

Figure 4.19: Color map of the displacement for the last stable position. Figure not to scale. Dimensions are in μm.

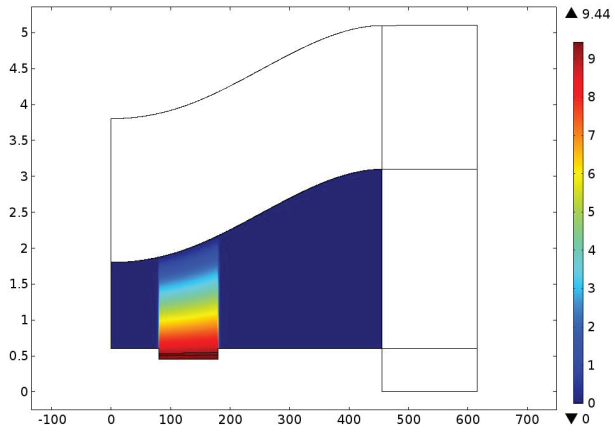

Figure 4.20: Color map of the electric potential for the last stable position. Figure not to scale.

membrane on the bottom surface, were the maximum displacement should occur.

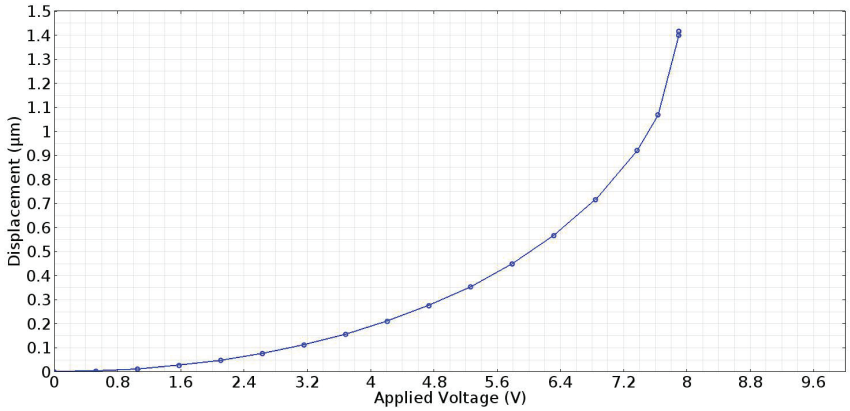

Figure 4.21: The central displacement z vs. applied voltage U (COMSOL simulation).

4.1.3 Parametric 2D Multiphysics Analysis

In this section is analyzed the IMT switch (Fig.4.144) from the point of view of designer, who is interested to understand how the pull-in voltage is influenced. A parametric study was carried out, considering several changes, such as dimensions of the actuation pads and the bridge length.

The width of the actuation pads W_{pad} was changed from 100μM to 300μm with a step of 50μm. The length of the membrane L_m was varied from 910μm to 1110μm with a step of 100μm.

An important aspect to consider is the residual stress σ. Ideally $\sigma = 0$, since in our case this stress is not desirable, however it may be present in the membrane, as a result of the fabrication process. The residual stress σ was varied from 0 MPa to 60 MPa with a step of 10 MPa.

The numerical modelling was carried out by the finite element method implemented in COMSOL Multiphysics software package. The strong MEC-ES coupling was used (Fig.4.8). The computational domain was meshed with quadrilateral elements. Along the OX axis, the domain was divided into elements with the length of $1\mu m$ and along the OY axis, the membrane was divided into two parts, the air space and the dielectric in one element and the support of the membrane in 4 elements. The largest model has 4335 elements and 49989 unknowns (Fig.4.22). For each configuration, a non-linear solver was used, the solving time being about 3 minutes, on a laptop with Intel Processor of 2.4 GHz and 8.00 GB RAM.

The first set of simulations focused on the static pull-in voltage, for different configurations and different residual stresses in the membrane. In each run, the load characteristic curve was obtained, the instability of the nonlinear solver occurring at the pull-in voltage V_{pi}.

In order to validate the models, coupled MEC-ES models have been simulated both in COMSOL and in ANSYS. The models have identical grids and identical boundary

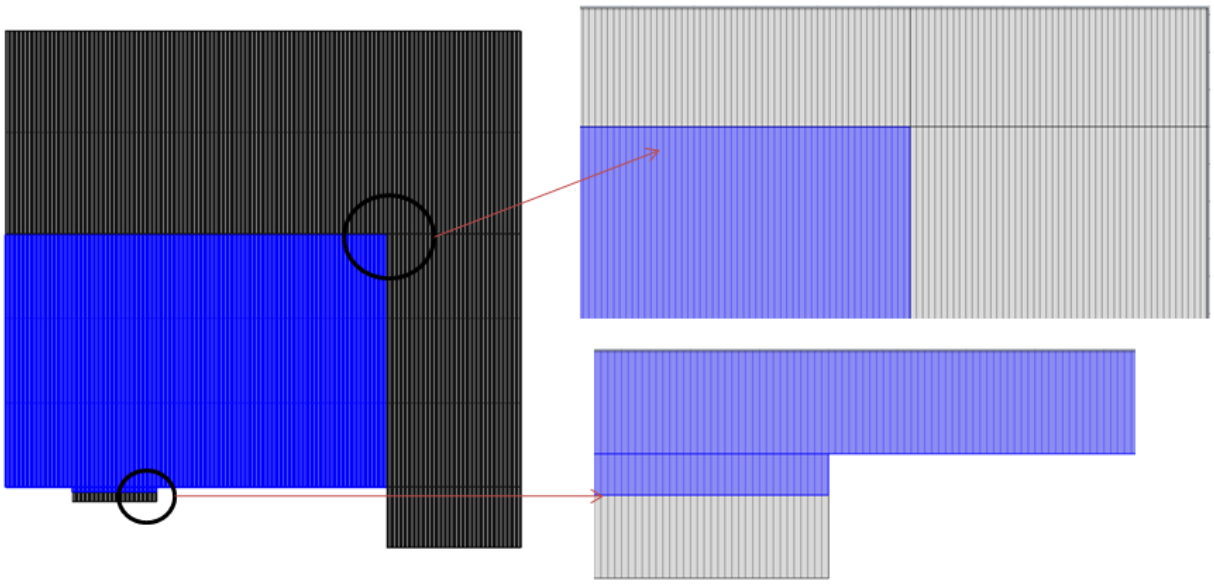

Figure 4.22: Discretization of the domain. Figure is not to scale, the vertical dimensions have been multiplied about 100 times.

conditions, but the formulations, as well as the used nonlinear solvers, are different. Even so, the relative differences in the resulted pull-in voltage is under 3% (Table 4.5).

Table 4.5: Dependence of the Pull-In Voltage vs. the Pad Width and Residual Stress.

W_{pad}	σ	V_{pi} [V]		Rel.dif.
μm	MPa	ANSYS	COMSOL	%
100	0	9.2	9.4	2.17
	20	29.7	29.9	0.67
	40	40.6	40.7	0.25
200	0	7.7	7.9	2.6
	20	23.8	23.9	0.42
	40	32.3	32.4	0.31
300	0	7.4	7.6	2.7
	20	22.3	22.4	0.45
	40	30.2	30.3	0.33

Fig.4.23 shows the dependence of the pull-in voltage with respect to the pad width, for different residual stress values. It can be noticed that it decreases with the increase of the pad width, which is expected since the capacitance increase and thus the actuation force obtained for the same voltage. It is important to notice that this pull-in voltage is very sensitive to the residual stresses in the membrane.

Fig.4.24 shows the dependence of the pull-in voltage with respect to the pad width, for different lengths of the membrane, when no residual stress is assumed. For a constant pad width, the pull-in voltage decreases with the membrane length, and this is due to the decreasing of the effective spring constant.

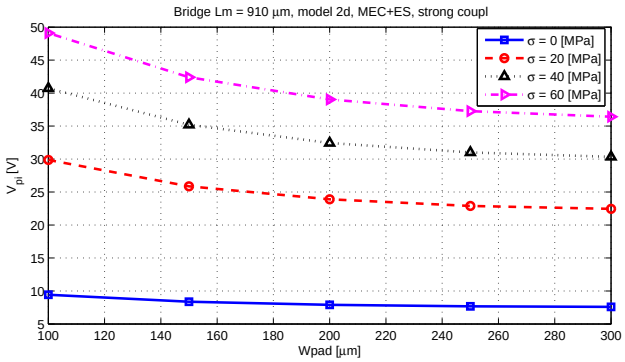

Figure 4.23: Dependence of the pull-in voltage vs. the pad width, for different residual stress values.

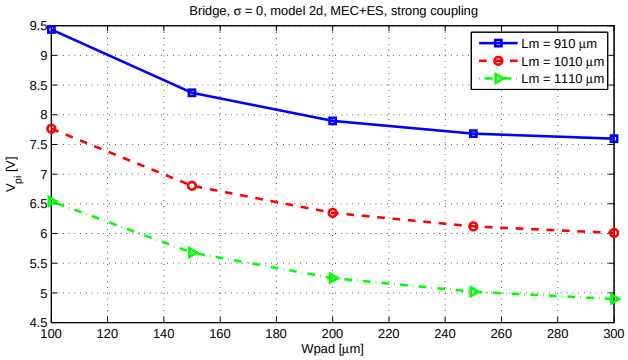

Figure 4.24: Dependence of the pull-in voltage vs. the pad width, for different lengths of the membrane.

4.2 3D Multiphysics Models of MEMS Switches

To retrieve relevant quantities related to the switching action from one stable state to the other, the investigation of the dynamic behavior needs simulations that take into account several physical effects: electrostatic actuation, mechanical motion as well as the air damping [49], [133]. The fluid flow damping phenomena, which is essential for accurate computations of dynamic characterisitics (e.g. commutation time, pull-out voltage, etc.) can be simulated only by using 3D models. An accurate dynamic behavior can be extracted only if three field problems are coupled as in Fig.4.25.

This section is dedicated to the dynamic, transient analysis. The evolution in time of the membrane deformation is simulated, aiming to compute the dynamic pull-in voltage, which is the lowest voltage that can be applied so that the switch is actuated (the membrane crashes on the actuation pad). From the transient response, may be extracted also the actuation time as well as the capacitance variation in time, including the corresponding capacities of the two stable states UP and DOWN.

4.2.1 Study Case: Dynamic Analysis of the QIAN Structure

Due to the structural symmetry, only a quarter of the geometry is modeled. The signal line, the ground lines and the actuation pads are not relevant for the multiphysics models

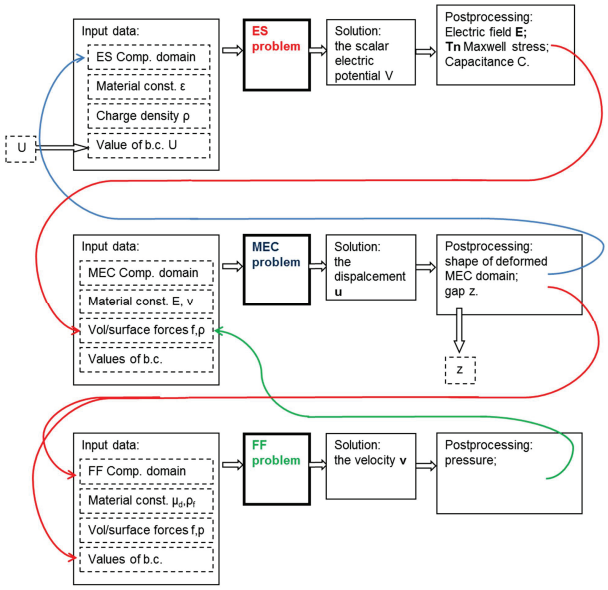

Figure 4.25: The mutual coupling of the electrostatic (ES), the dynamic-structural (MEC) and Fluid Flow (FF) problems

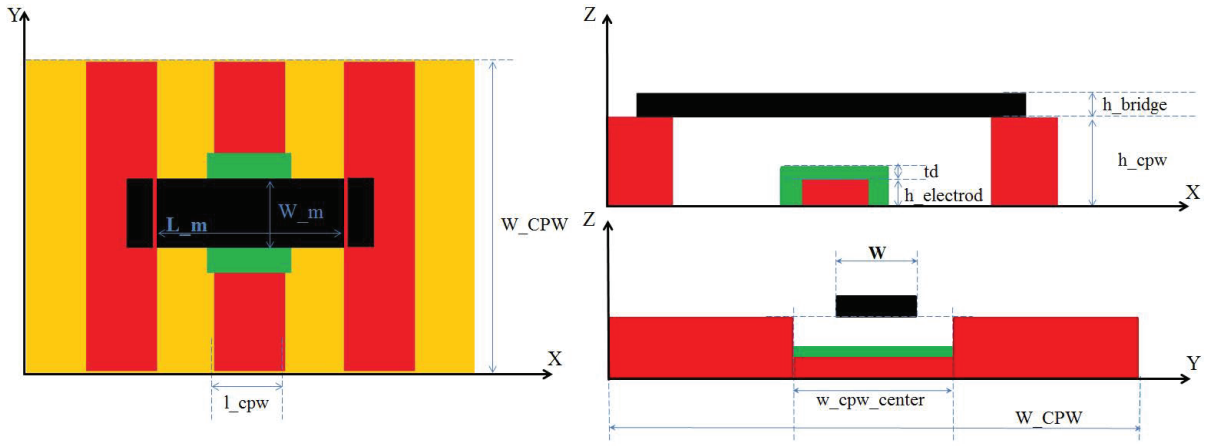

Figure 4.26: Qian Structure. Left - upper view of the geometry. Right - transversal cuts view, Up - ZX plane, Down - ZY plane.

that focus on the switching between the up and down positions, when there is no signal passing through the signal lines.

The parameterized geometry of the model is shown in Fig.4.26. The geometric information is given in Table 4.6, whereas material properties used, aluminum for the membrane and the CPW lines and Silicon nitride for the isolator deposited over the central part of the signal line, can be found in Table 4.7 (only the information relevant for the simulations described is given).

The structural (MEC) domain includes only the membrane of the structure, its maximal limits being $x_{max} = L_m/2, y_{max} = W_m/2$ and $z_{min} = h_{cpw}, z_{max} = h_{cpw} + h_{bridge}$. A plane strain model is considered, in which the unknown is the 3D displacement vector **u** defined in every point of the computational MEC domain, obtained by solving the

Table 4.6: QIAN structure geometric parameters. Value and significance

Parameter	Value	Significance
L_m	$280\mu m$	length of the membrane
W_m	$120\mu m$	width of the membrane
W_{CPW}	$280\mu m$	length of the CPW lines
W_{wcpw_center}	$120\mu m$	length of the CPW central part
h_{bridge}	$0.4\mu m$	height of the membrane
h_{cpw}	$4\mu m$	height of the ground line
$H_{electrod}$	$0.4\mu m$	height of the central part of the transmission line
t_d	$0.1\mu m$	height of dielectric
l_{cpw}	$120\mu m$	width of the transmission and ground line

Table 4.7: QIAN structure material parameters.

Parameter Material	Aluminum	Air	Silicon nitride Si_3N_4
Relative permittivity ε_r	-	1	7
Poisson's ratio ν	0.35	-	-
Young's modulus E [Pa]	$70 \cdot 10^9$	-	-
Mass density $\rho[kg/m^3]$	2700		

momentum (Newton-equilibrium) equation:

$$\rho \frac{\partial^2 \mathbf{u}}{\partial t^2} - \nabla \cdot \mathbf{T} = \mathbf{f} \tag{4.2}$$

where ρ is the mass density, $\mathbf{T}$ is the stress tensor, and $\mathbf{f}$ is the external body force density. The constitutive relationship is $\mathbf{E} = \mathbf{D}\ \mathbf{T}$, where $\mathbf{E}$ is the strain tensor and $\boldsymbol{D} = \boldsymbol{C}^{-1}$ is a compliance matrix that depends on E and ν, $\boldsymbol{C}$ is the elasticity (stiffness) matrix. An additional condition that ensures the geometrical compatibility between strains and deformations is added for completeness:

$$\begin{aligned} T_{ij} &= \lambda E_{kk} \gamma_{ij} + 2\mu E_{ij}, \\ E_{ij} &= \frac{1}{2}\left(\frac{\partial u_i}{\partial X_j} + \frac{\partial u_j}{\partial X_i}\right), \end{aligned} \tag{4.3}$$

μ and λ are the two Lame elastic constant:

$$\mu = \frac{E}{2(1+\nu)} \text{ and } \lambda = \frac{\nu E}{(1+\nu)(1-2\nu)}$$

.

The boundary conditions of the structural problem (Fig.4.27) are provided by the symmetry conditions on the symmetry planes (x=0, y=0), ensuring only the vertical displacement, i.e. $\mathbf{n} \cdot \mathbf{u} = 0$, the null displacement imposed on the surface where the membrane is embedded $\mathbf{u} = 0$. On the rest of the MEC boundary, the natural conditions (free movement) are imposed.

The electrostatic (ES) domain includes the dielectric and the air just under the membrane, its maximal limits being $x_{max} = L_m/2, y_{max} = w_{cpw\_center}/2$ and $z_{max} = h_{cpw} +$

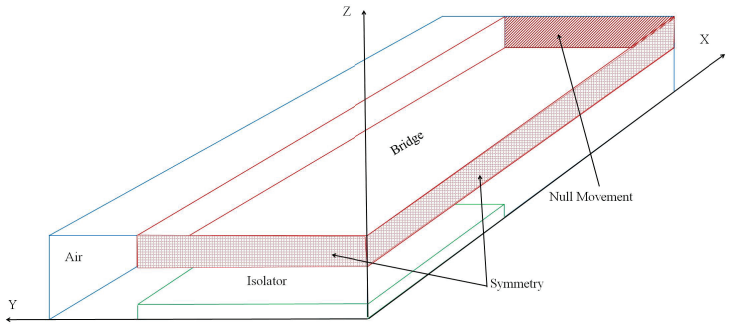

Figure 4.27: The structural domain and the boundary conditions.

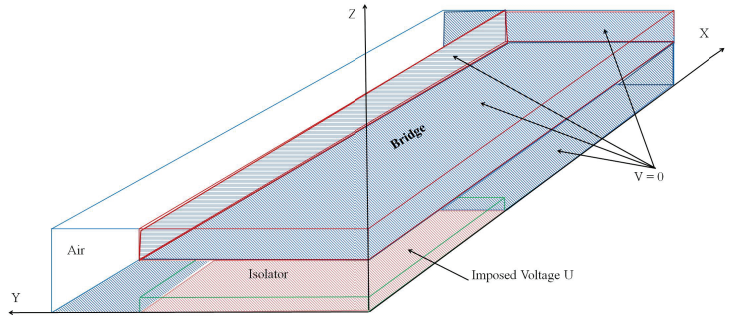

Figure 4.28: The electrostatic domain and the boundary conditions.

h_{bridge}. The ES field by the the electric scalar potential V, defined in every point of the computational ES domain, which satisfies the Laplace equation $\Delta V = 0$, actually $div(\varepsilon gradV) = 0$. For it, boundary conditions are imposed as shown in Fig.4.28. They are of Dirichlet type, an imposed voltage U on the bottom of the isolator and null potential on the membrane surface and on the air domain on the bottom and on one side where the ground line should be, whereas the rest of the ES boundary is left with natural boundary conditions $dV/dn = 0$.

The two MEC and ES domains have a common boundary (Fig.4.29), where coupling conditions will be imposed, in order to transfer the changes of the MEC shape produced by its displacement to the ES problem, by changing accordingly its computation domain. Indeed, the electric field applied between the grounded membrane and the actuation electrode produces a force that makes the MEC domain to change its shape, and thus modify the ES domain and the electric field. More precisely, the Maxwell stress tensor computed from the ES field is a pressure imposed on the beam surface, for the structural field. The multiphysics coupling is described by the diagram depicted in Fig.4.8.

For the numerical simulation the finite element method and a strong coupling between the ES and MEC formulations were used. The computational domain was meshed with quadrilateral elements. Along the OX and OY axis, the domain was divided into elements with the length of $10\mu m$ and along the OZ axis, the membrane was divided into two parts, the air space and the dielectric in one element. The complete mesh consists of 448 domain elements, 712 boundary elements, and 300 edge elements resulting a total of 17835 unknowns (Fig.4.30).

The simulation flow starts with a static simulation aiming to compute the static pull-in voltage V_{pi} that represents the highest voltage for which the bridge is in a stable position

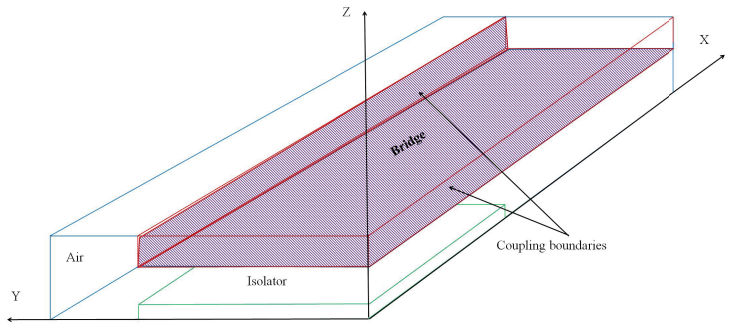

Figure 4.29: Coupling condition between the two domains.

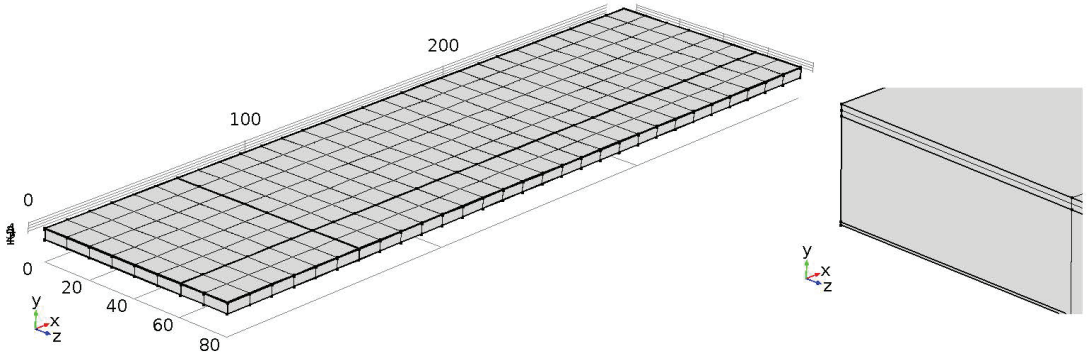

Figure 4.30: Discretization of the computational domain. Right - discretization detail on the membrane.

and the maximum displacement z_{pi} of the bridge at an actuation voltage equal to V_{pi}.

The computing time needed to complete the entire static simulation was 1555 seconds, and it required 3.45 GB RAM. The applied Voltage was varied from 0V to 30V with a step of 5V. The resulted static pull-in voltage is $V_{pi} = 29.53$ V and the maximum displacement $z_{pi} = 2.22\mu$m. Fig.4.31 holds the solution obtain and Fig.4.32 contains the full representation of the bridge, reconstructed from symmetries, at maximum displacement. In Fig.4.33 represented the dependency of the displacement of the middle bridge point with respect to the applied voltage U.

The relative difference between the static pull-in voltage extracted from the 2D model and the one from the 3D model is less than 2%.

In order to extract the switching duration, a dynamic analysis have to be done. The numerical model and the discretization grid used for the dynamic analysis was the same as

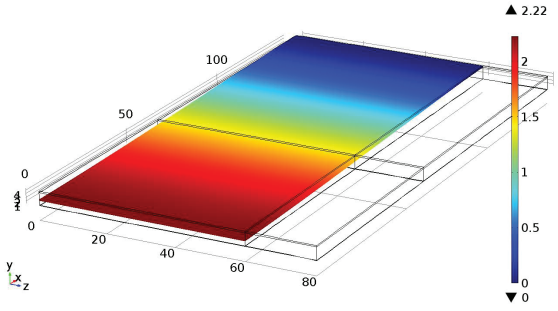

Figure 4.31: Displacement of the bridge at pull-in voltage.

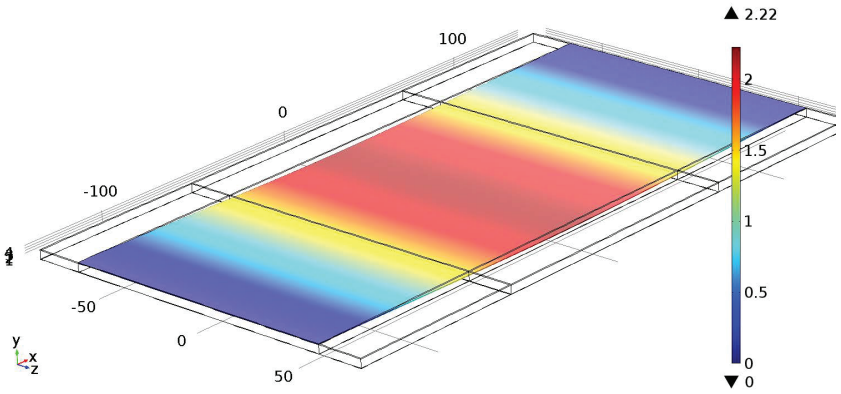

Figure 4.32: Displacement of the bridge at pull-in voltage. Full representation is reconstructed by symmetry.

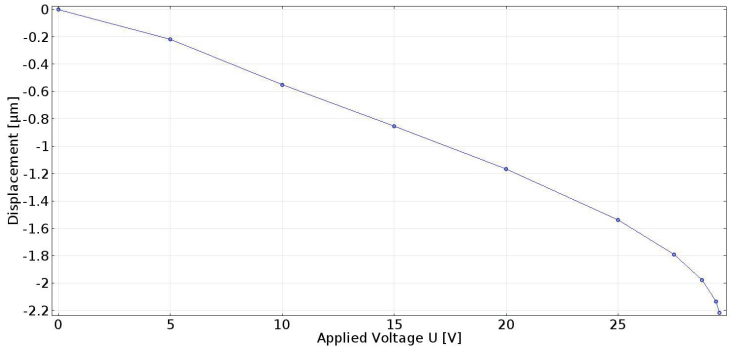

Figure 4.33: Displacement of the bridge middle point w.r.t. applied voltage U.

in the static case. It was simulated the transient regime under a constant (step) actuation voltage up to 60μs. To obtain the time evolution of 17835 unknowns the simulation time was 1005 s, on a laptop with Intel Processor of 2.4 GHz and 8.00 GB RAM.

The time evolution of the maxim displacements of the membrane, for several constant actuation voltages are represented in Fig.4.34. As we expected, without considering air damping, the oscillations are continuous undamped. The dynamic pull-in voltage is $V_{dpi} =$ 25.8 V and the actuation time is 7μs.

The time variation of the switch capacitance when the applied voltage has the value V_{dpi} is presented in Fig.4.35. The capacitance has the minim value of 0.037 pF corresponding to the Up position and its maxim values is 0.13 pF corresponds to the Down position.

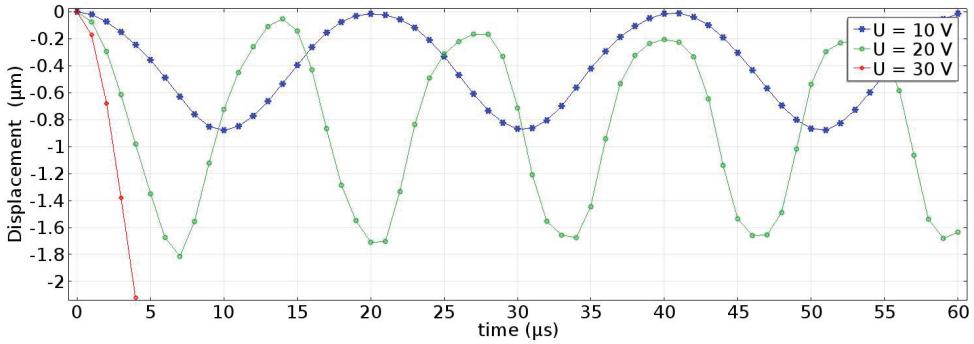

Figure 4.34: Maxim displacement of the bridge in time, for different applied voltage U.

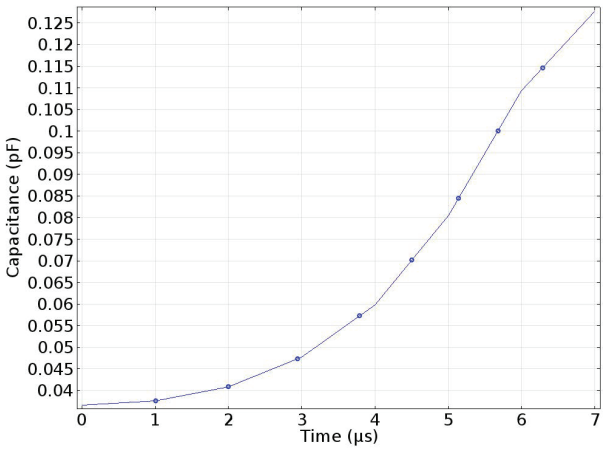

Figure 4.35: Time evolution of the Capacitance during actuation.

Their ratio $C_{max}/C_{min} = 3.5$ describe the efficiency of the switch.

The relative difference between the static and dynamic pull-in voltage is reaching almost 13% which is quite high, meaning that Fluid-Structure-Interaction (FSI) has to be taken in consideration, in order to model the dumped effect of the air during the transient regime.

To solve the three field multiphysics problem (ES+MEC+FSI), the numerical model has to be adjusted. A layer of air is placed upon the membrane, aiming to fully capture the movement of the air flow around it (4.36).

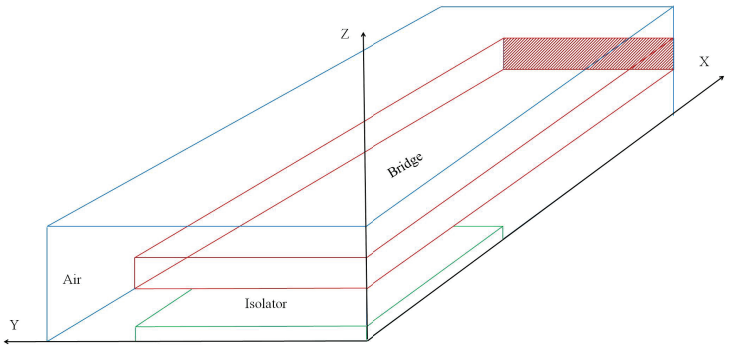

Figure 4.36: QIAN 3D model for FSI analysis.

The surrounding air has fluidic properties i.e. a dynamic viscosity of $\mu_d = 18.2 \cdot 10^{-6}$Pa·s, and a density $\rho_f = 1.22$ Kg/m^3. Beneath the bridge, the viscosity depends on the Knudsen number. The flow regime is a mild slip regime, which enables the using the Navier-Stokes equations for momentum:

$$\rho\frac{\partial \boldsymbol{\nu}}{\partial t} + \rho(\boldsymbol{\nu}\cdot\nabla)\boldsymbol{\nu} = \nabla[-p\mathbf{I} + \mu_d\nabla(\boldsymbol{\nu}+\boldsymbol{\nu})^t], \tag{4.4}$$

and the mass conservation equation $\nabla v = 0$. Here ν is the velocity of fluid, p is the fluid pressure, and $\mathbf{I}$ is the unity matrix.

According to [223], beneath the cantilever we use the effective viscosity in Eq.4.4 given by

$$\mu_{eff}(t) = \frac{\mu}{1 + 9.638[Kn(t)]^{1.159}} \tag{4.5}$$

where,

$$Kn(t) = Kn_{ref}\frac{p_{ref}}{p(t)}\sqrt{\frac{T(t)}{T_{ref}}}\frac{h_0}{h_0 + h(t)} \tag{4.6}$$

whit $Kn_{ref} = 0.03$ and $p_{ref} = 1$ atm.

Assuming isothermal conditions, one can notice that the increase of Knudsen number with the gap is somehow balanced by its decrease with pressure variation beneath. At the interface between the air and the cantilever, the velocity of the fluid has to be equal with the velocity of the solid $\boldsymbol{\nu_f} = d\boldsymbol{u_s}/dt$.

Appropriate conditions are imposed on the symmetry plane. On the bottom surface where the substrates should exist and on the side where the ground line should be, wall boundary conditions are assumed. On the rest of the boundary, open boundary for the fluid flow is set. Figure 4.37 shows the interaction surfaces between the MEC domain and Fluid Flow domain. The coupling diagram of several multiphysics sub-problems is represented in the Fig.4.25.

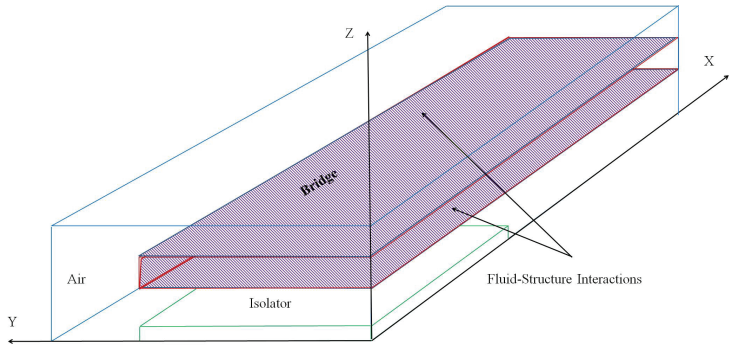

Figure 4.37: Fluid Flow – MEC domains interaction surfaces.

Fig.4.38 contains a typical solution of the ES+MEC+FSI problem is presented for an applied voltage of 30 V and in Fig.4.39 the full structure of the switch was reconstructed from symmetry. The vectors in these images represent the fluid speed.

Considering air damping, which correspond to a model closer to the reality, the found dynamic pull-in voltage is around 31 V (Fig.4.40). The relative difference between static

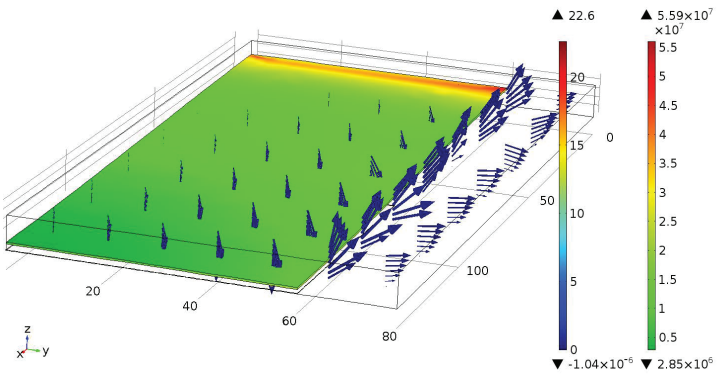

Figure 4.38: Typical solution of the ES+MEC+FSI problem is presented for an applied voltage of 30 V.

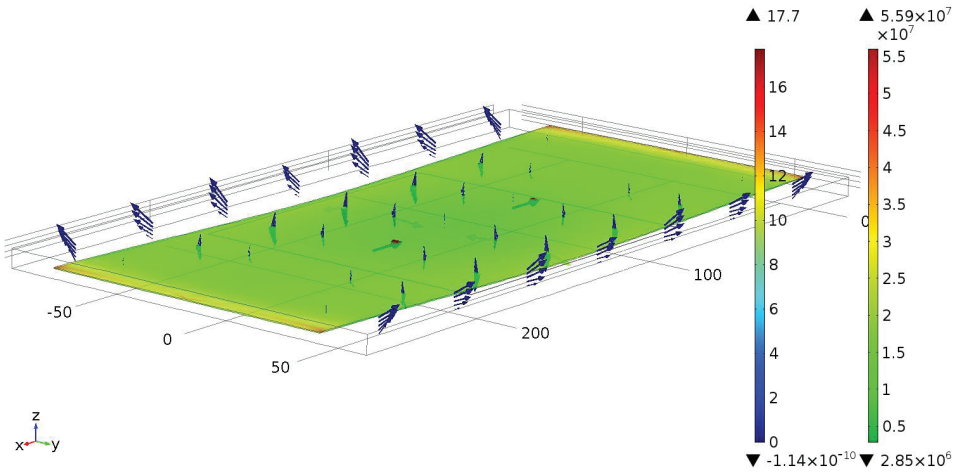

Figure 4.39: Full structure of the switch reconstructed from symmetry.

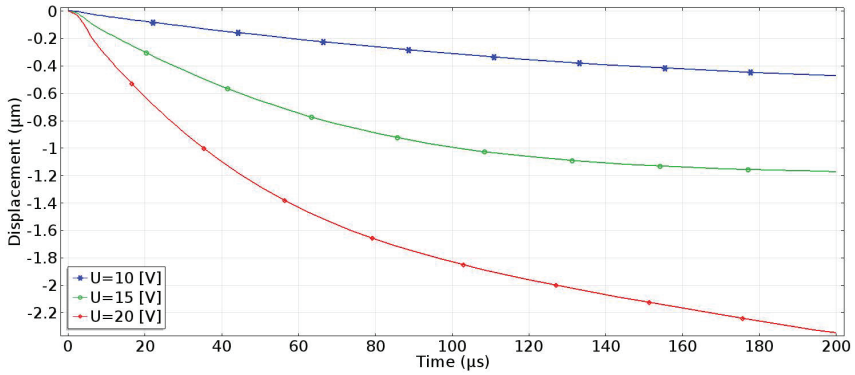

Figure 4.40: Evolution in time of the displacement of the bridge for different applied voltages with air damping.

and dynamic analysis with air-dumping is around 3%, which is quite acceptable. Comparing the Fig.4.34 and Fig.4.40 it is obvious the fundamental importance of the air dumping in the MEMS modelling.

In conclusion for a more accurate extraction of the dynamic pull-in voltage, the air damping has to be taking in consideration. It can not be neglected in any conditions.

A series of difficulties experienced in the modelling with COMSOL package. Using COMSOL default settings, the simulations fail and to obtain reliable results, attention must be paid to the model building and to the solver settings. When dynamic analysis is conducted, consideration should be given to the time stepping method [224].

4.2.2 Contact Modelling

In order to model the full dynamic response of the movement of the switch's membrane (to simulate a compete switching cycle UP-DOWN-UP), the contact force must be included in the numerical model. In order to model the contact interaction, the Penalty/Barrier Method [225] is used. This method combines elements of the penalty procedure with elements from the barrier method. The normal contact force, t_N, is ex-

pressed as:

$$\begin{aligned} t_N &= \hat{t}_N + \varepsilon_N g_N; \text{ for } g_N \ll 0; \\ t_N &= \hat{t}_N exp\left(\frac{\varepsilon_N}{\hat{t}_N} g_N\right) \text{ for } g_N \geq 0; \end{aligned} \tag{4.7}$$

where ε_N is the earlier penalty stiffness and $\hat{t}_N$ is an input estimate of the contact force.

When the gap g_N is greater than zero, the total force rapidly decays to zero while, with penetration, it builds up from $\hat{t}_N$ via the penetration and the linear stiffness, ε_N. From (4.7) the tangential stiffness, are given by

$$\begin{aligned} \varepsilon_{\tan} &= \varepsilon_N g_N; \text{ for } g_N < 0 \\ \varepsilon_{\tan} &= \varepsilon_N \exp\left(\frac{\varepsilon_N}{\hat{t}_N} g_N\right) \text{ for } g_N \geq 0 \end{aligned} \tag{4.8}$$

and there is no sudden jump.

The model of QIAN structure was excited by a smooth step voltage of 35 V (above V_{pi}), having a rise time of 5 μs as in Fig.4.41. The transient analysis was performed for 40 μs, considering the contact force.

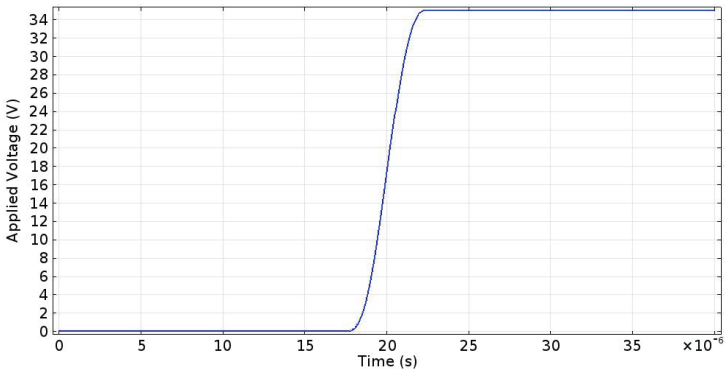

Figure 4.41: Time dependence of the Applied Voltage.

Without taking in consideration the air damping, is obtained the time variation of the displacement of the bridge center presented in Fig.4.42. Fig.4.43 holds the shape of the bridge that is in contact with the isolator layer, for a quarter of the model and in Fig.4.44 the full model is represented. Fig.4.45 presents the electric potential distribution underneath the bridge for the contact position, detailed in Fig.4.46.

Now it is applied to the same model a voltage signal having a rectangular pulse shape with a rise and fall of 5 μs (Fig.4.47). Without taking in consideration the air damping, the time dependence of the displacement of the bridge center, resulted from transient simulation is presented in Fig.4.48. The analysis was performed for 60 μs. Unrealistic oscillations may be observed when the bridge is released.

Including the air dumping, the time dependence of the displacement of the bridge center, resulted from the transient simulation under step excitation is presented in Fig.4.49. In Fig.4.50 is presented the time dependence of the displacement of the bridge center for the applied voltage of rectangular signal type. As we expected the switching time is clearly increased.

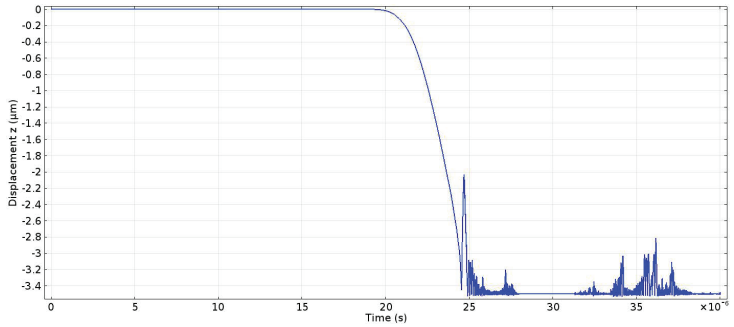

Figure 4.42: Time dependence of the displacement of a point from the center of the bridge.

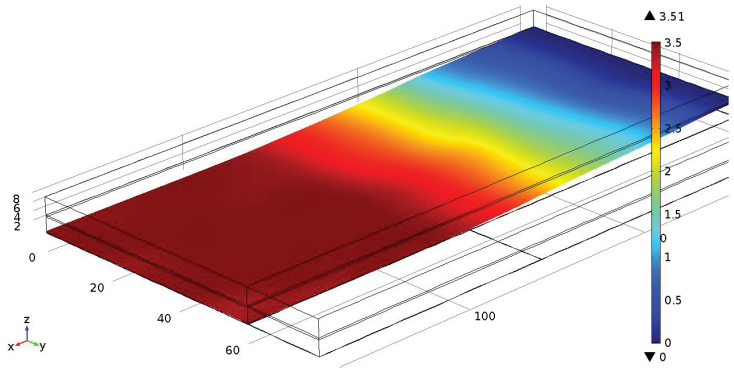

Figure 4.43: Shape of the membrane at contact with the isolator layer.

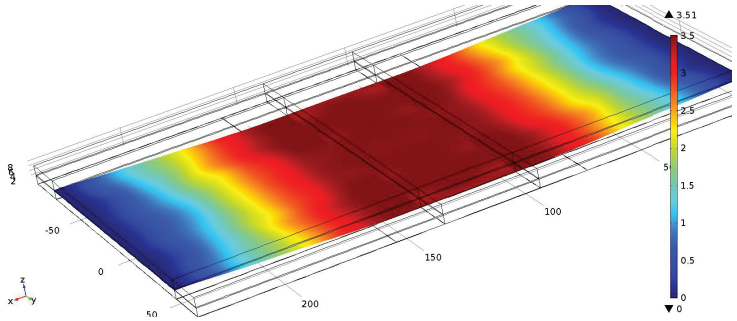

Figure 4.44: Shape of the membrane at contact with the isolator layer. Full representation reconstructed from symmetry.

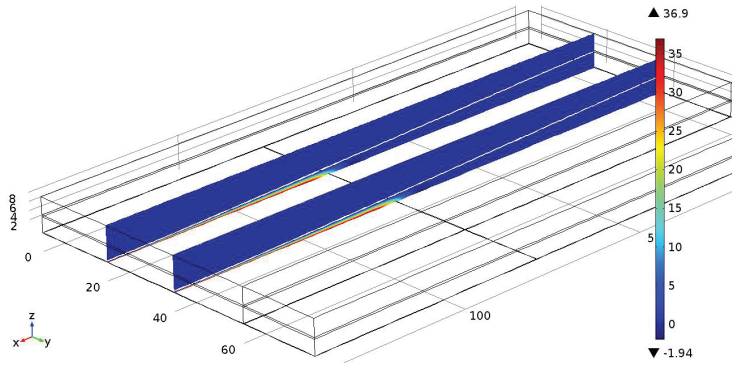

Figure 4.45: Electric potential distribution underneath the bridge for the contact position.

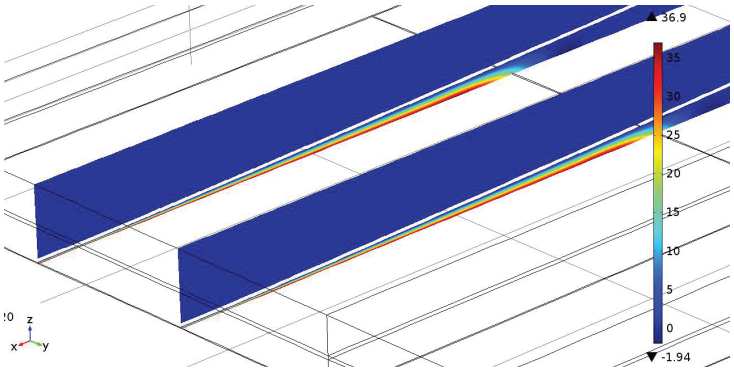

Figure 4.46: Detail on the electric potential distribution underneath the bridge for the contact position.

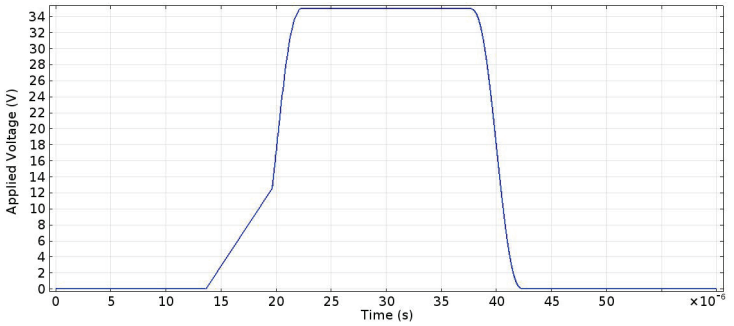

Figure 4.47: Time dependence of the Applied Voltage.

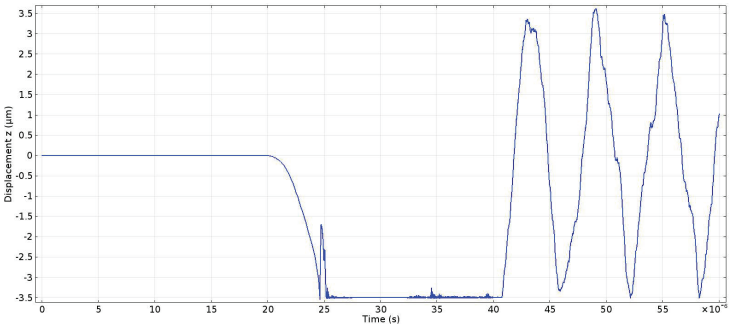

Figure 4.48: Time dependence of the displacement of the bridge center.

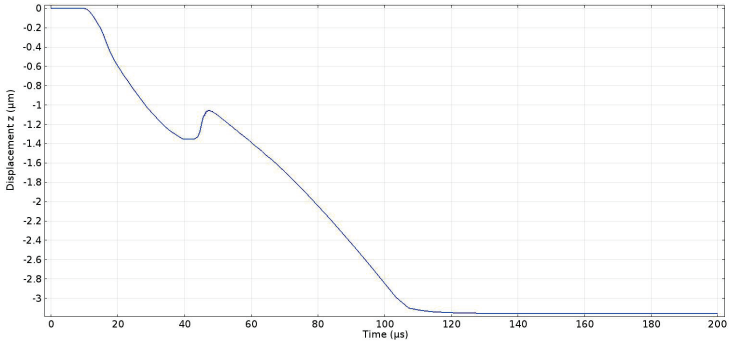

Figure 4.49: Time dependence of the displacement of the bridge center for a step input signal.

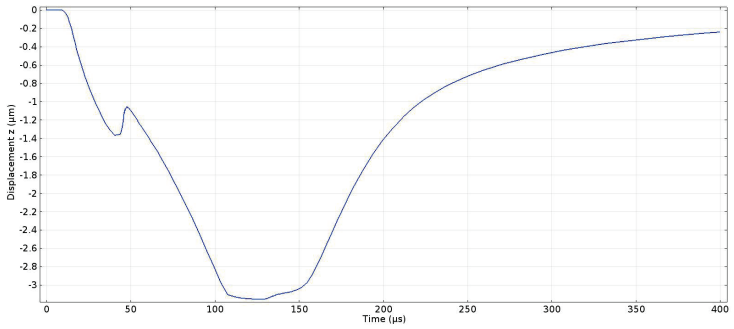

Figure 4.50: Time dependence of the displacement of the bridge center for a 20μs pulse signal.

4.2.3 Influence of Membrane's Perforations

In order to facilitate the extraction of the sacrificial layer, during their technological process, the MEMS membranes have perforations. From structural point of view, the existence of holes has the advantage that some of the residual stress in the bridge are reduced, thus reducing the Youngs modulus of the RF-MEMS structure. Another advantage of membrane perforation is that it can reduced the pull-in voltage and increase the switching speed due to the easier fluid flow.

In this section it will be analyzed the influence of membrane perforations on the dynamic behavior of the membrane, taking in consideration the air damping. The model used in this analysis is presented in Fig.4.51. In the membrane 3 perforations have been placed, having the area of 400 μm^2. The model represents only a quarter of the switch, thus the full model will contain 12 perforations in the membrane.

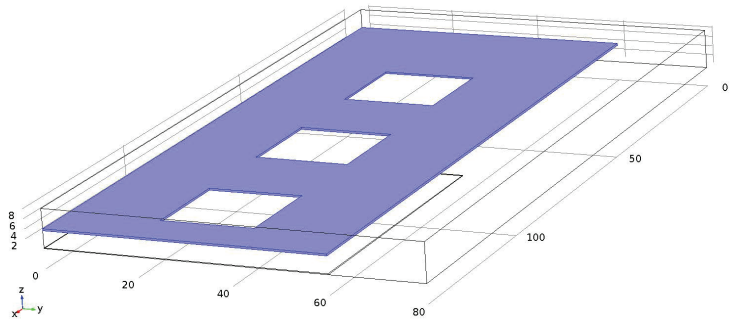

Figure 4.51: QIAN 3D model with perforations in the membrane.

The computational domain ES+MEC+FSI was discretized by using tetrahedral elements. The mesh (Fig.4.52) generated by COMSOL consists of 41179 domain elements, 15682 boundary elements, and 1651 edge elements. The number of degrees of freedom is 150751. The multiphysics transient problem was solved by using a fully coupled nonlinear solver. The time needed to find the solutions was 2624 s on a laptop with Intel Processor of 2.4 GHz and 8.00 GB RAM. The COMSOL model is presented in the annex A3 and the COMSOL solution report is presented in the annex A4.

Figure 4.53 contains a typical solution of the ES+MEC+FSI problem, presented for an applied voltage of 25 V. In Fig.4.54 a YZ plane view is presented and in Fig.4.55 the full structure of the switch was reconstructed from symmetry. The vectors in these images

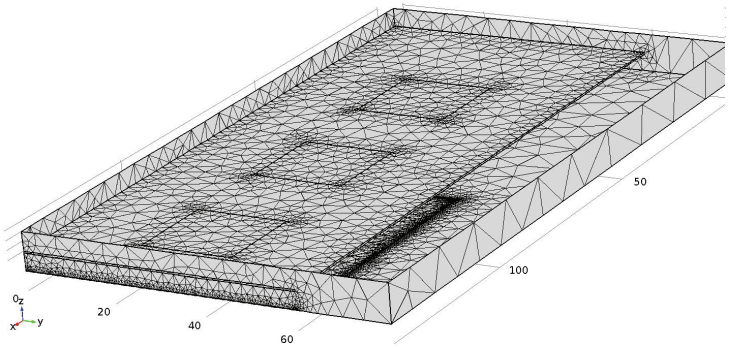

Figure 4.52: Mesh of the QIAN 3D model with perforations in the membrane.

represent the fluid speed. The dynamic pull-in voltage is found around 26.5 V. Adding perforation in the membrane caused a drop of V_{dpi} with approximately 15 %. The time dependence of the position of the bridge center, exited by an applied voltage of 25 V, is presented in Fig.4.56. We noticed a smoother monotonic movement.

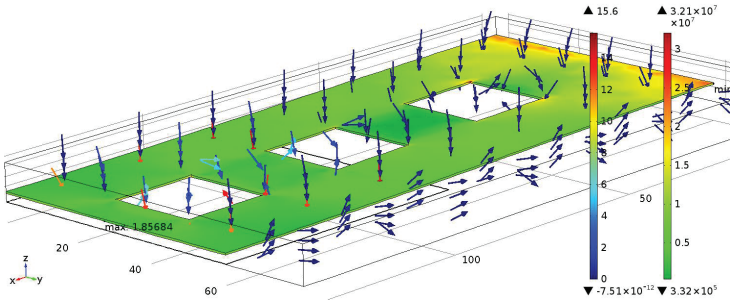

Figure 4.53: Typical solution of the ES+MEC+FSI problem for an applied voltage of 25 V

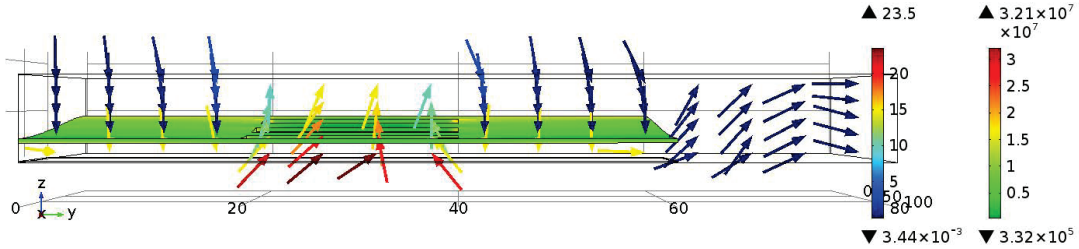

Figure 4.54: Typical solution of the ES+MEC+FSI problem for an applied voltage of 25 V. YZ plane view.

4.2.4 Parametric 3D Multiphysics Modelling

Modelling of MEMS devices is a challenging task due to the coupling of multiphysics phenomena that have to be considered. In these conditions, parametric modelling is even more challenging and it is a compulsory step before the optimization. Some papers such as [56] are referred to this challenge, but only the RF behavior is investigated In this current section is investigated also its multiphysics parametric behavior.

In the case of the QIAN structure, there are three parameters that may vary: the width of the central line of the CPW l_{cpw} was varied from 60 μm to 200 μm with a

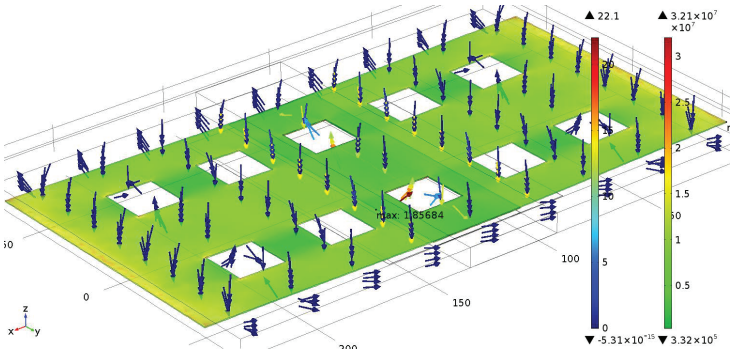

Figure 4.55: Typical solution of the ES+MEC+FSI problem for an applied voltage of 25 V. Full geometry reconstructed from symmetry.

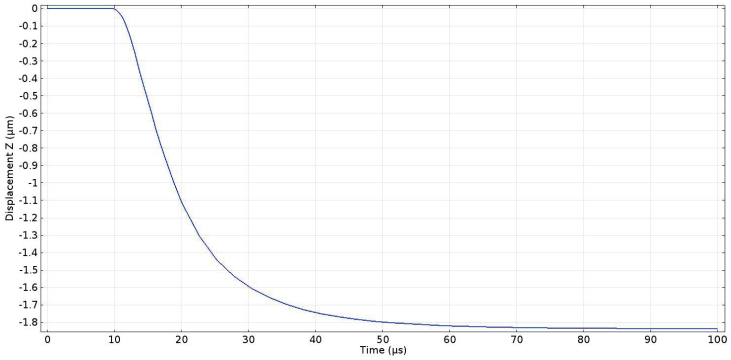

Figure 4.56: Time dependence of the bridge center position, when the applied voltage is 25 V.

step of 40 μm, the length of the membrane L_m was varied from 280 μm to 580 μm with a step of 100 μm and the width of the membrane W_m was varied from 60 μm to 120 μm with a step of 20 μm.

The static simulation of the multiphysics model was done by using the finite element method and a strong coupling between the ES and MEC problem. The computational domain was meshed with quadrilateral elements. Along the OX and OY axis, the domain was divided into elements with the length of 10 μm and along the OZ axis, the membrane was divided into two parts, the air space and the dielectric in one element. For the largest model the complete mesh consists of 928 domain elements, 1372 boundary elements, and 480 edge elements with 36285 unknowns.

Table 4.8 contains the results of the parametric study of the pull-in voltage w.r.t. the length of the membrane for $l_{cpw} = 120$ μm. From this analysis V_{pi} and z_{pi} was extracted. The table also contains the number of unknowns, time and computational resources needed to solve the problems. It can be observed as the pull-in voltage decreases with the length of the membrane, while the maximum displacement remains approximately constant. The computational time is influenced by the voltage steps that were computed, a lower pull-in voltage leads to fewer steps.

The influence of the discretization was also investigated. Table 4.9 grasps the results obtained using a denser mesh with double the number of discretization nodes. For the largest model, the complete mesh consists of 3840 domain elements, 4032 boundary elements, and 813 edge elements and it has 139971 unknowns. The relative difference between the two meshes for V_{pi} and z_{pi} is less than 5%, therefore, the initial mesh is

Table 4.8: Parametric study results of V_{pi} [V] for different values of L_m.

L_m [μ m]	DoF	Time [s]	Physical memory [GB]	$V_{pi}[V]$	z_{pi} [μ m]
280	17835	1555	1.68	29.53	2.22
380	23985	2025	2.06	18.19	2.17
480	30135	1235	2.54	11.56	2.18
580	36285	863	2.71	8.44	2.14

acceptable, providing an enough accurate numerical result.

Table 4.9: Parametric study results of V_{pi} [V] for different values of L_m with a refined mesh.

L_m	DoF	Time	Physical memory	V_{pi}	z_{pi}	err [%]	
[μm]	-	[s]	[GB]	[V]	[μm]	V_{pi}	z_{pi}
280	82251	4552	4.76	29.16	2.26	1.253	1.802
380	111111	3950	5.82	16.98	2.17	4.673	0.2
480	139971	5958	6.7	11.25	2.01	2.683	7.8

Table 4.10 contains the results of the parametric study on the width of the electrode that was varied from 60 μm to 200 μm for different lengths of the membrane. Fig.4.57 shows the dependency of the pull-in voltage with the length of the membrane for different widths of the electrode, while Fig.4.58 represents the dependency of the pull-in voltage with the width of the electrode for different lengths of the membrane. It can be seen that the pull-in voltage also decreases with the increases of the electrode width.

Table 4.10: Parametric study results of V_{pi} [V] for different values of L_m and l_{cpw}.

L_m	$l_{cpw}[\mu m]$					DoF
[μm]	60	100	120	160	200	-
280	36.35	30.78	29.53	28.13	27.5	17835
380	22.03	18.3	18.19	15.94	15.31	23985
480	15.16	12.34	11.56	10.57	10	30135

In Table 4.11 the influence of the width of the membrane upon the pull-in voltage was investigated; the length of the electrode was kept fix at 120μm. Table 4.12 contains the results of the analysis when both width of the membrane W_m and the length of the electrode were varied. In both cases the pull-in voltage remains approximately constant.

The dynamic simulation was performed in order to estimate the dynamic pull-in voltage, the actuation time and time variation of the switch capacitance. All information is presented in Table 4.13 together with the minimum and maximum values of the capacitance and the relative difference between dynamic and static pull-in voltage.

In conclusions, the results of parametric analysis show that the static pull-in voltage depends on the switch dimensions and material characteristics, decreasing with the length of the membrane and width of the electrode, while the maximum displacement remains

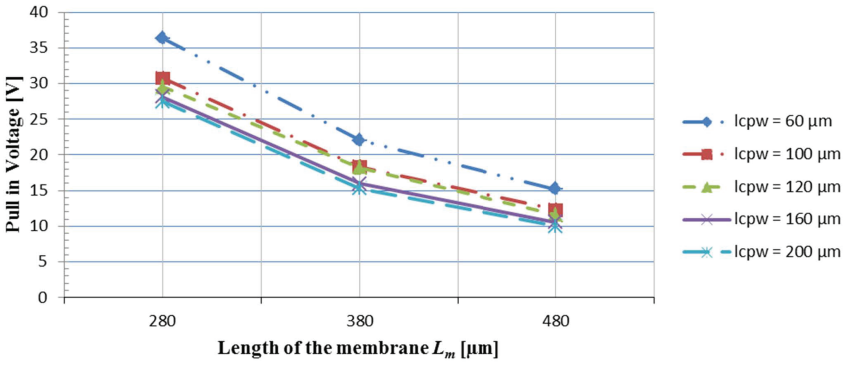

Figure 4.57: Variation of the V_{pi} w.r.t L_m for different values of the width of the signal line.

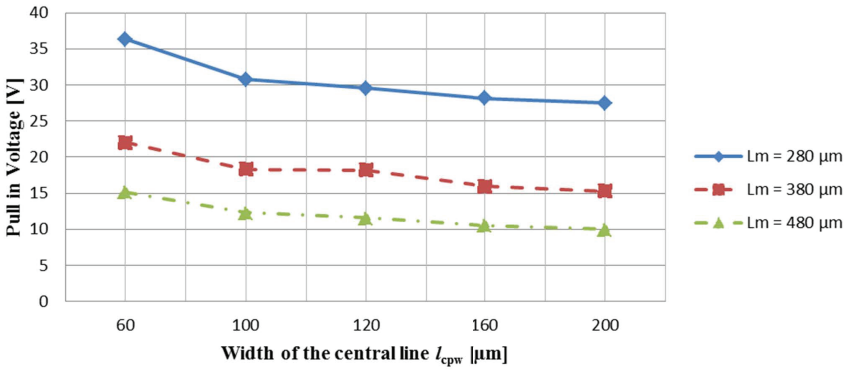

Figure 4.58: Variation of the V_{pi} w.r.t the width of the signal line for different values of L_m.

Table 4.11: Parametric study results of V_{pi} [V] for different values of W_m.

L_m	DoF	Time	Physical memory	V_{pi}	z_{pi}
$[\mu m]$	-	[s]	[GB]	[V]	$[\mu m]$
60	18009	1099	2.07	28.85	2.27
80	17951	1353	2.07	28.91	2.27
100	17893	906	1.95	28.91	2.26
120	17835	1555	1.68	29.53	2.22

Table 4.12: Parametric study results of V_{pi} [V] for different values of W_m and actuation electrode length l_{cpw}.

l_cpw	W_m	DoF	Time	Physical memory	V_{pi}	z_{pi}
$[\mu m]$	$[\mu m]$	-	[s]	[GB]	[V]	$[\mu m]$
80	13775	2028	1.53	1.58	29.69	2.26
120	17835	1555	1.68	1.77	29.53	2.22
160	21895	847	1.94	2.06	29.53	2.27

Table 4.13: Dynamic analysis, parametric study results, for different values of L_m.

L_m	DoF	V_{dpi}	Actuation time	$Capacitance[pF]$		err [%]
$[\mu m]$	V	-	[s]	UP	DOWN	V_{pi} - V_{dpi}
280	17835	25.8	7	0.037	0.23	12.63
380	23985	20.1	9	0.035	0.24	10.5
480	30135	14.9	11	0.037	0.26	28.9
580	36285	10.4	18	0.037	0.21	23.22

approximately constant. For a more accurate extraction of the dynamic pull-in voltage the air damping has to be taking in consideration.

The switching time is also linked to the geometric parameters, decreasing with the increasing in the length of the membrane, otherwise the corresponding capacities of the two stable states UP and DOWN remains approximately constant.

4.3 3D Electromagnetic Modelling of MEMS Switches

Radio frequency micro-electro-mechanical switches (RF-MEMS) are miniature devices that use mechanical movement to change the configuration of a radio frequency circuit. The simplest devices are used to perform a short circuit or an open circuit in a transmission line. The RF-MEMS switch analyzed in this section is the QIAN structure presented in Fig.4.1.

Between the membrane and central line there is a space, which creates a capacity, the membrane being placed transversely to the line. When not actuated, the value of this capacity is quite small, so that the RF signal that crosses the line is not disrupted. When a sufficient high voltage is applied to the actuation electrode placed under the membrane, the switch is actuated and the RF signal is blocked, because the capacitance between the signal line and the ground became high.

Scattering parameters (S Parameters) are frequency dependent complex functions, which describe the behavior of a multiport system. Initially, they were used in electrical transmission line theory, for their definition being used the incident voltage waves reflected or transmitted. More generally, they can be defined in microwave circuits and even the electrical circuits. There are a multitude of possibilities for introduce them [201, 205, 198], which makes their physical interpretation and understanding their significance often difficult.

S parameters don't have a direct interpretation in electrical circuit theory, because they do not contain circuit elements where propagation phenomena exists as waveguides. Yet in circuit theory have expanded similar judgments to those made for microwave circuits, introducing the concept of "power wave", terminology that comes from their meaning which is related to the dependence of active power consumed by a load connected to a port and operating frequency [200].

Understanding S parameters is particularly important for high frequency applications

including active and passive components from integrated circuits [197], including micro-electro-mechanical systems (MEMS) and wireless transfer power systems[226].

When propagation phenomena are present, the significance of S parameters is linked to a port waves reflection or wave propagation from one port to another. S parameters are important for high frequency applications because they are the ones that are measured at these frequencies and because they do not need open or short circuit conditions, which are needed to measure impedance or admittance matrix elements, conditions which would be difficult to achieved at high frequencies.

The S_{11} parameter represents the reflection losses corresponding to the signal, because the load is not suited to the transmission line. S_{21} parameter represents the line losses, including losses due to skin effect. S_{21} describes the isolation between the input and output port.

It is desirable that a switch has small insertion loss, its value in dB is close to 0 dB and high isolation its value in dB as high as possible in absolute value. An ideal switch would have 0 dB insertion loss and infinite isolation [199].

4.3.1 Study Case: the QIAN Structure

RF simulation of this device was performed by using of the *chamy* package, which is a in house software toolbox dedicated to the computational modeling of the passive high-frequency integrated circuit components and their interaction with the electromagnetic environment, aiming to calculate the frequency characteristics of the examined devices [227, 197, 228].

Once the problem was defined, by using the input file, the program generates state matrices of the modeled device using Finite integrals techniques (FIT) to discretize the Maxwell's equations in the full wave electromagnetic regime with Electromagnetic Circuit Elements (EMCE) type boundary conditions:

$$\begin{aligned} \mathbf{C}\frac{dx(t)}{dt} + \mathbf{G}\mathbf{u}(t) &= \mathbf{B}\mathbf{u}(t), \\ \mathbf{y}(t) &= \mathbf{L}\mathbf{x}(t), \end{aligned} \tag{4.9}$$

where $\mathbf{x}$ is the state vector of dimension n, $\mathbf{u}$ is the input signals vector of dimension m and $\mathbf{y}$ is the output signals vector of dimension m. $\mathbf{C}$ and $\mathbf{G}$ matrices of size $n \times n$, $\mathbf{B}$ of size $n \times m$, $\mathbf{L}$ size $m \times n$ are the state matrices, where n is the number of state variables and m is a number of the input terminals that is equal to the output terminals. In the frequency domain, the relationship between the input and the output signals is obtained by solving a system of complex linear algebraic equations for each frequency obtained by complex representation of (4.9). The input/output relation in the frequency domain is described by the transfer matrix:

$$\begin{aligned} \mathbf{H}_{FIT}(\omega) &= \mathbf{L}(\mathbf{G} + j\omega\mathbf{C})^{-1}\mathbf{B}, \\ \mathbf{y} &= \mathbf{H}_{FIT}\mathbf{u}. \end{aligned} \tag{4.10}$$

This step is achieved by using the Adaptive Frequency Sampling (AFS) algotihm combined with Vector Fitting (VF) [229, 230, 231, 232]. VF procedure uses as input a set

of pairs $(\omega_k, \mathbf{H}(\omega_k))$, $k = \overline{1, F}$ where F is the number of frequency samples. Its purpose is to identify poles p_i, waste matrices $\mathbf{K}_i$ and constant terms $\mathbf{K}$, $\mathbf{K}_0$ of $\mathbf{H}_{FIT}(\omega)$ rational approximation:

$$\mathbf{H}_{VF}(\omega) = \sum_{q}^{i=1} \frac{\mathbf{K}_i}{j\omega - p_i} + \mathbf{K}_{\text{inf}} + j\omega\mathbf{K}_0. \tag{4.11}$$

This section describes the step of reducing the model and it is essential for the extraction of a circuit model [232], which can be used further in the design or redesign of more efficient micro-electro-mechanical devices.

The parametric geometric model of QIAN structure is presented in Fig.4.59, Fig.4.60. It is composed of three metal lines, made from aluminum (ALUM), placed on an buffer layer, made from silicon dioxide (SiO_2), deposited on a silicon (Si) substrate. The transmission line is thinned in the middle part, where a dielectric layer of silicon nitride (Si_3N_4) is deposited. The membrane, made also from from aluminum, resting on the two ground lines is suspended above the center line. The geometric parameters are presented in Table 4.14 and the material parameters in Table 4.15.

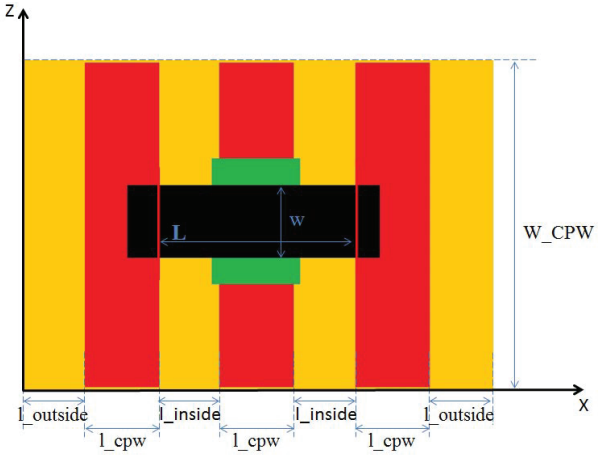

Figure 4.59: RF MEMS switch, up view. Geometric parameters

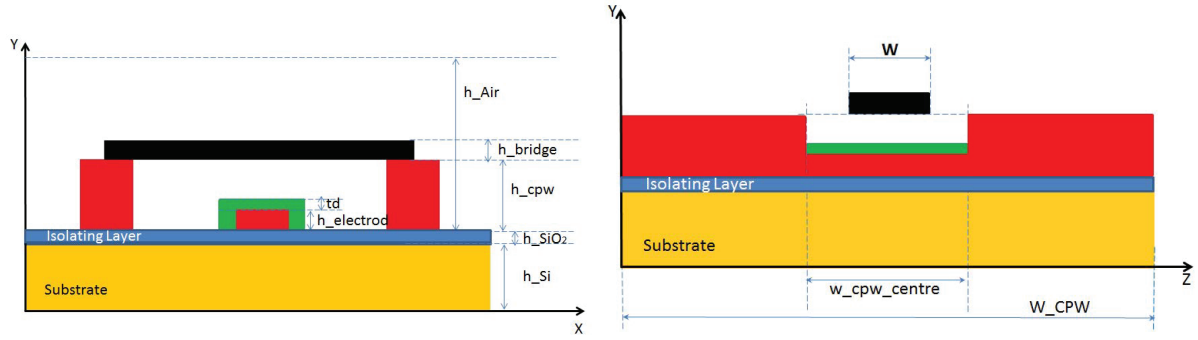

Figure 4.60: QIAN structure geometric parameters: transversal section – Left; longitudinal section – Right

The computational domain for this problem has maximum coordinates along OX axes $X_{max} = 2 \cdot l_{outside} + 2 \cdot l_{inside} + 3 \cdot l_{CPW}$ along OY $Y_{max} = h_{Si} + h_{SiO_2} + h_{Air}$, and the dept of the computational domain along OZ axes is $Z_{max} = W_{CPW}$.

Table 4.14: RF MEMS switch geometric parameters. Value and significance

Parameter	Value	Significance
$l_{outside}$	100 μm	space between domain edge and ground line
l_{cpw}	120 μm	length of the line
l_{inside}	80 μm	space between lines
L	280 μm	length of the membrane
h_{Si}	600 μm	height of the silicon layer
h_{SiO2}	1 μm	height of the silicon dioxide layer
h_{Air}	600 μm	height of the air layer
h_{cpw}	4 μm	height of the line
h_{bridge}	0.4 μm	height of the bridge
$h_{electrod}$	0.4 μm	height of the electrode
t_d	0.1 μm	height of the isolating layer
w_{cpw}	600 μm	width of the transmission and ground line
w_{cpw_centre}	240 μm	width of the thinned central part line
W	120 μm	width of the bridge

Table 4.15: RF MEMS switch material parameters and properties.

Component part	Parameter	Material	ε_r	μ_r	$\sigma[S/m]$
Substrate	Si	Silicon	1	1	10^{-5}
Buffer layer	$SiO2$	Silicon Oxide	4.1	1	10^{-7}
Isolator	$Si3N4$	Silicon Nitrate	7	1	10^{-3}
CPW lines	$ALUM$	Aluminum	1	1	$6.6 \cdot 10^7$
Bridge	$ALUM$	Aluminum	1	1	$6.6 \cdot 10^7$

In Fig.4.61 is presented the model of capacitive switch generated by *chamy*. It highlights the boundary conditions expressed by the two types of terminals, electric voltage terminal “ev” and electrical ground terminal “eg”.

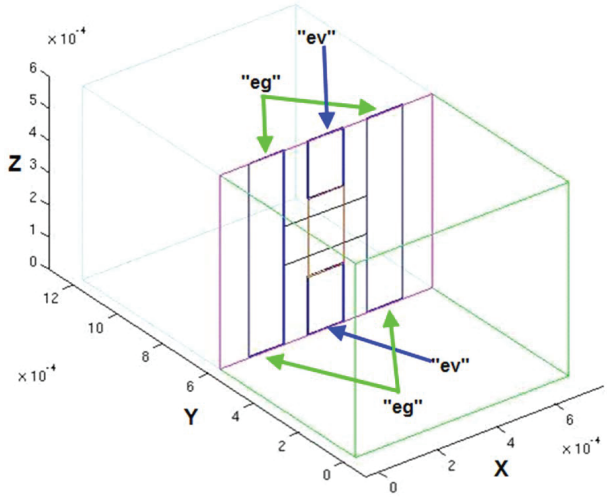

Figure 4.61: RF-MEMS switch model and its boundary conditions

The Cartesian discretization grid used by the numerical model (Fig.4.62) has 31x38x17 nodes with a number of 108644 DOFs.

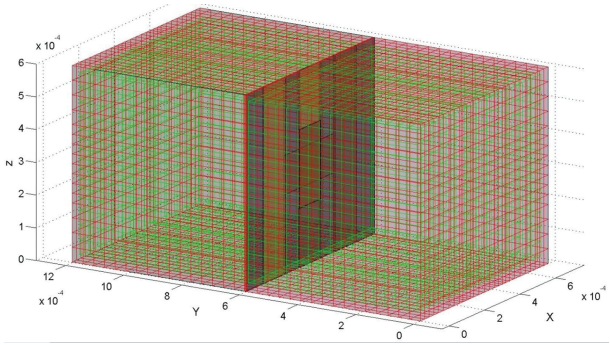

Figure 4.62: Domain discretization.

For the UP state of the RF-MEMS device, the time required to extract the FIT matrices was 84.65 seconds. Using AFS with VF, time needed to compute the frequency answer was $2.325 \cdot 10^3$ seconds, the answer in 11 frequencies was computed for a range from 1GHz to 60GHz. Fig.4.63 and Fig.4.64 shows the amplitude and phase of S_{11} respective S_{21} parameters, obtained by EM simulation with *chamy*.

For the DOWN state of the RF-MEMS device, the time required to extract the FIT matrices was 84.65 seconds. Using AFS with VF, time needed to compute the frequency answer was $3.307 \cdot 10^3$ seconds, the answer in 15 frequencies was computed for a range from 1 GHz to 60 GHz. Fig.4.65 and Fig.4.66 shows the amplitude and phase of S_{11} respective S_{21} parameters, obtained by EM simulation with *chamy*.

To validate the results obtained with *chamy*, a comparison was made with the results from the literature [56] (Fig.4.67 and Fig.4.68), in this paper the author creates a efficient electromagnetic model of a MEMS switch, operating in RF characterized using

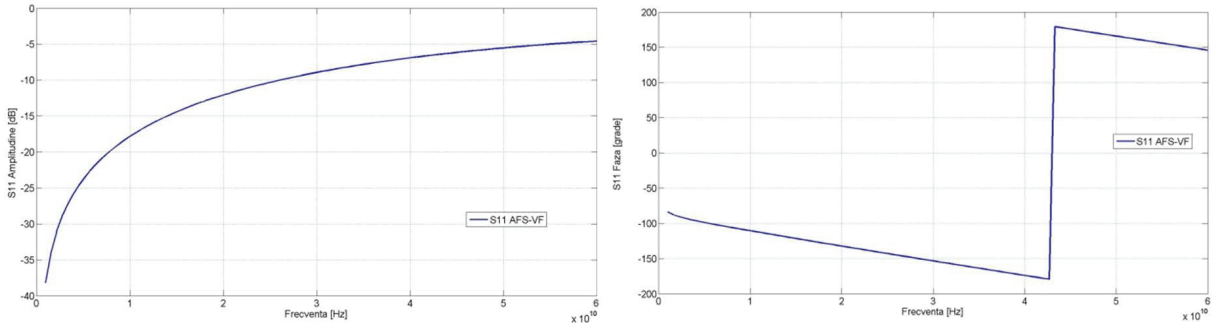

Figure 4.63: S_{11} Parameter for Up position. Amplitude and phase.

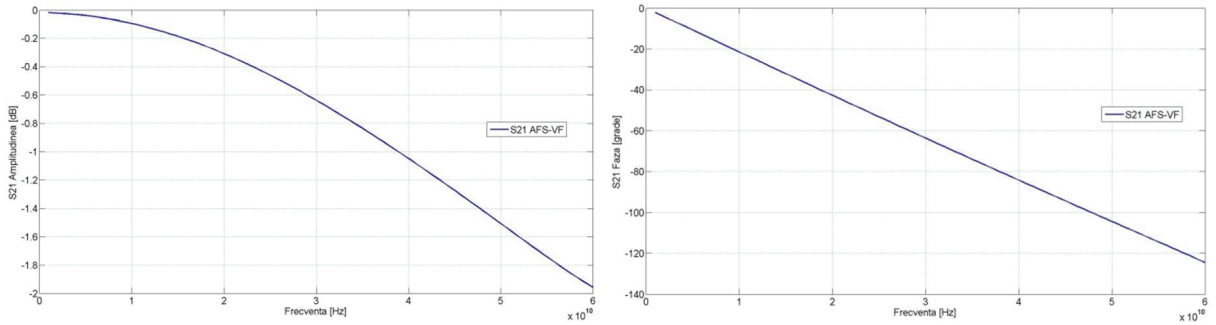

Figure 4.64: S_{21} Parameter for Up position. Amplitude and phase.

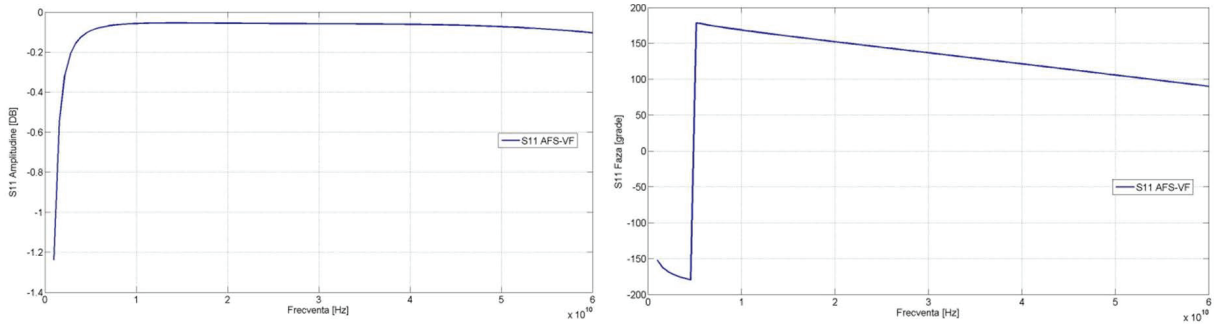

Figure 4.65: S_{11} Parameter for Down position. Amplitude and phase.

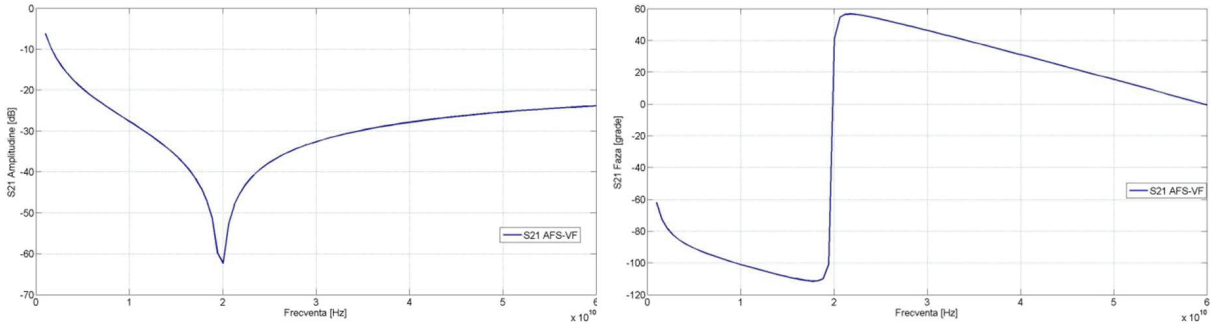

Figure 4.66: S_{21} Parameter for Down position. Amplitude and phase.

electromagnetic analysis based on FEM (with ANSYS HFSS) to extract S parameters at different geometric dimensions. Finally, this numerical model was validate using the comparison between simulated and measured data. However, in these figures, "Model" means the simulation result of the compact TL-RLC-TL model.

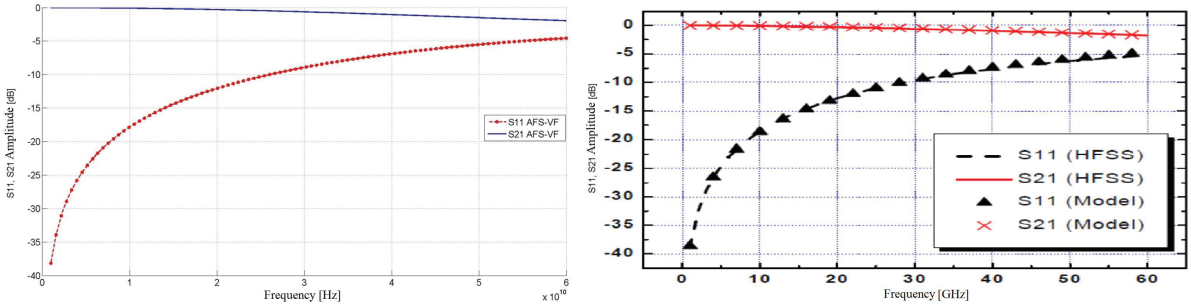

Figure 4.67: S Parameter for Up position. Comparison with results from the literature [56].

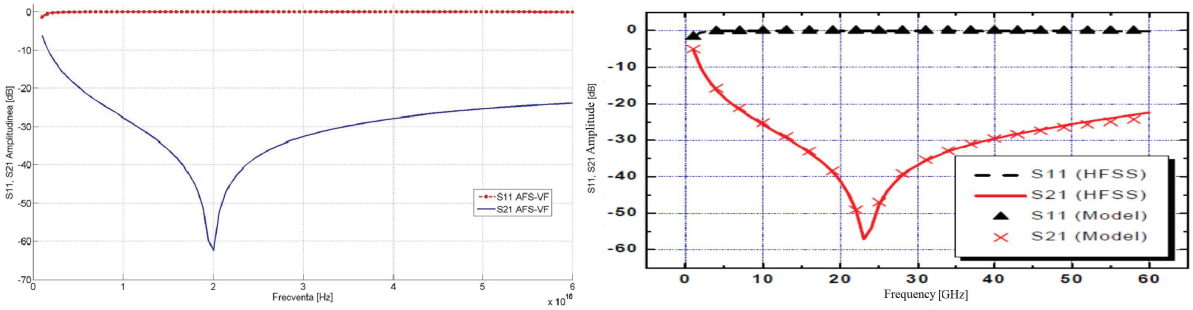

Figure 4.68: S Parameter for DOWN position. Comparison with results from the literature [56].

Comparing the results, one can observe a good agreement of results obtained by *chamy* software with the results presented in [56] obtained with a commercial software and, which was experimentally validated (less than 4 dB error). Consequently, the numerical model proposed in this section is validated.

To observe the influence on the frequency response of the width of the membrane, a parametric analysis was conducted, varying it in the range of 60 μm to 180 μm. In Fig.4.69 the amplitudes of S_{11} and S_{21} is presented related to the five widths of membrane in the DOWN state.

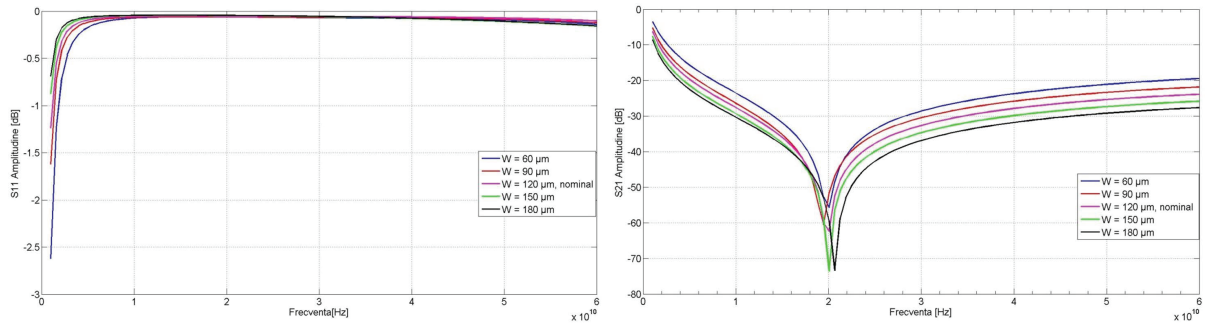

Figure 4.69: Amplitude of S_{11} and S_{21} parameter in DOWN position for five widths of membrane.

Below will be analyzed the influence of membrane perforations on the RF characteristic expressed by means of S parameters. Different types and configurations of the perforations applied to the membrane are investigated, both from the S parameters point of view and the computational time, needed for each simulation.

The test structures considered for this study are presented in Fig.4.59, in which the membrane has one of 4 types of perforations depicted in Fig.4.70. The first configuration (a) has 5×13 perforations (holes) of $100\mu m^2$ area (Fig.4.71). The second configuration (b) has 3×7 perforations of $400\mu m^2$ area. The third test (c) is an extreme case of only 2 large holes in the membrane. And finally (d) is a bridge without perforations.

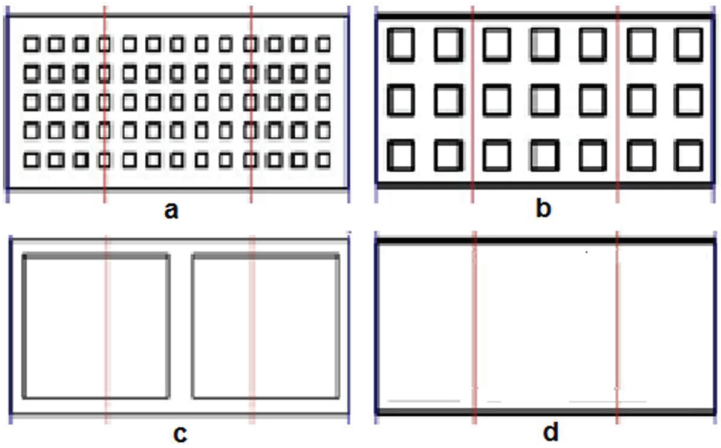

Figure 4.70: Perforation configurations (a) 5×13, (b) 3×7, (c) 1×2, (d) unperforated.

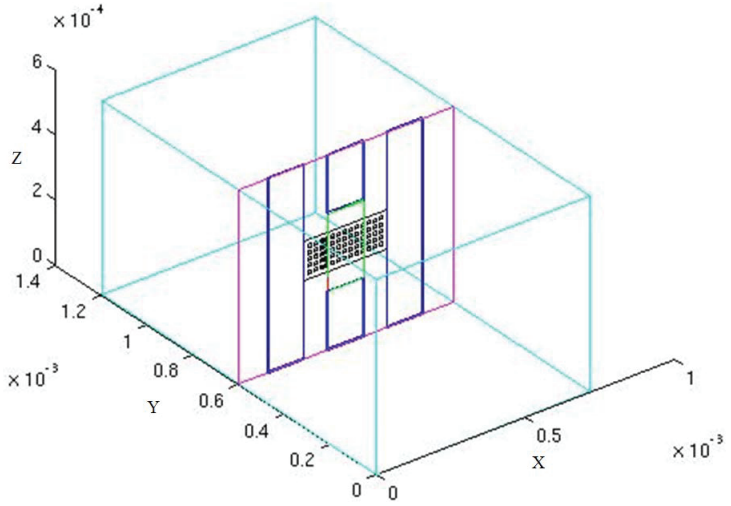

Figure 4.71: *chamy* model with membrane having 5×13 perforations.

The study case (a) has the finest FIT grid with $36 \times 22 \times 16$ nodes (Fig.4.72), refined in the middle of the domain, in order to catch the geometry of holes. The same grid was used for a test without holes ("d-a" means "case d with the same grid as case a"). In the study cases (b) a medium discretization grid with $24 \times 22 \times 13$ nodes was used. The same grid was used also to model the membrane without holes ("d-b" means "case d with the same grid as case b"). Finally for the case (c) it was used a coarser discretization grid, having only $17 \times 22 \times 13$ nodes. The study case "d-c" means "case d with the same grid as case c".

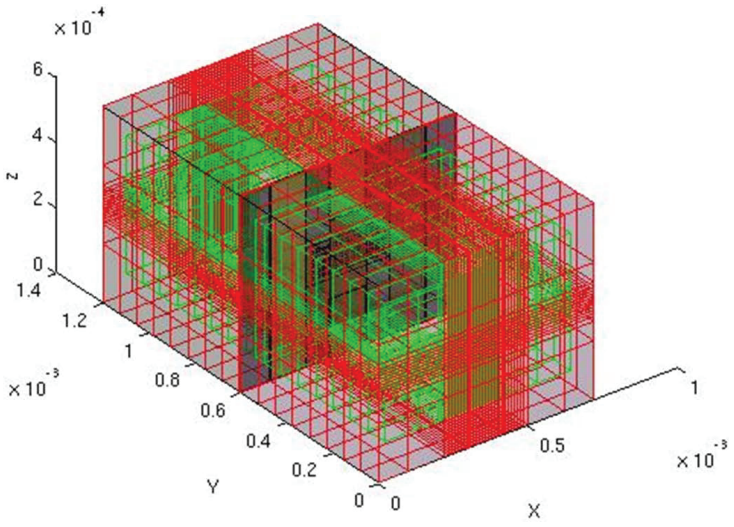

Figure 4.72: $36 \times 22 \times 16$ Grid generated by *chamy*.

All simulations were carried out for both UP and DOWN State positions of the membrane. The simulation results obtained in the UP State position are given in Table 4.16, and that obtained in the DOWN State position are given in Table 4.17.

Table 4.16: The results for the UP position RF analysis.

	Grid	DOF(n)	FIT matrices generation time [s]	Computing time for one frequency [s]	Variation [%]
(Case d-a)	$36 \times 22 \times 16$	67573	**80.28**	**23.9**	0
(Case a)	$36 \times 22 \times 16$	67573	77.61	26.1	**0.011**
(Case d-b)	$24 \times 22 \times 13$	35704	20.38	7.65	1.33
(Case b)	$24 \times 22 \times 13$	35704	19.46	7.81	8.29 3.8 1.24
(Case d-c)	$17 \times 22 \times 13$	24910	8.43	4.08	8.09
(Case c)	$17 \times 22 \times 13$	24910	**8.21**	**4.1**	5.03

Considering the d-a as a reference, the relative variation of S parameters, for the cases (a) and (b), generated by the material change (perforation filling) is very low, around 0.02 % for UP State position and around 0.04 % for DOWN State position. The relative variation of the result, generated by changes of the discretization grid (case d-b) is also very low, only 1.33 % for UP State position and around 1.0 % for DOWN State position.

It is interesting to note that the results variation of the extreme case (c) is unexpectedly low, about 5.0 % for UP State position and around 1.2 % for DOWN State position. Fig.4.73 and Fig.4.74 hold the absolute value of S parameters for several membrane positions. The results are similar to the measurements reported in [56].

In conclusion, this study shows that there is no need to take the perforations of the membrane into account in the RF models of capacitive MEMS switches, because the relative variation of the simulation results of the RF models with and without holes is around 0.04 % both in the UP and DOWN states. This is a great advantage for the RF model since it allows the meshing of the membrane with a coarser grid. This leads to

Table 4.17: The results for the DOWN position RF analysis.

	Grid	DOF(n)	FIT matrices generation time [s]	Computing time for one frequency [s]	Variation [%]
(Case d-a)	$36 \times 22 \times 16$	67573	**77.73**	**22.4**	0
(Case a)	$36 \times 22 \times 16$	67573	81.32	24.8	**0.01**
(Case d-b)	$24 \times 22 \times 13$	35704	19.8	8	1.03
(Case b)	$24 \times 22 \times 13$	35704	19.8	8	**0.04**
(Case d-c)	$17 \times 22 \times 13$	24910	8.41	3.8	5.12
(Case c)	$17 \times 22 \times 13$	24910	**8.29**	**3.8**	1.24

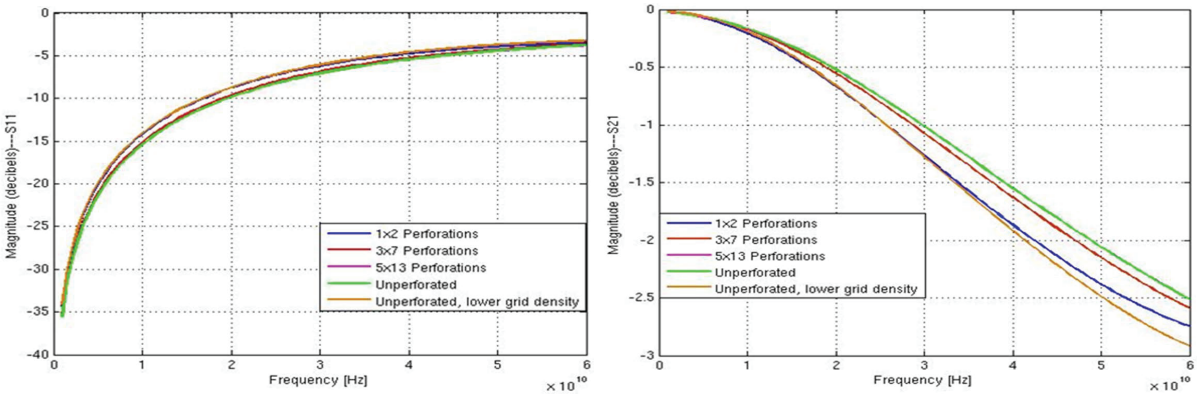

Figure 4.73: Absolute value for S_{11} (return loss) and S_{21} (isolation) parameters in UP stable position.

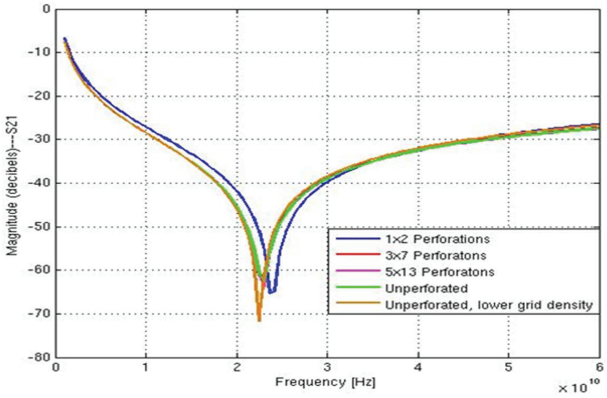

Figure 4.74: Absolute value for S_{21} parameter in Down stable position (isolation).

an important decrease of the computational resources: the model has a lower order (in our example 3 times lower) and the computational effort decreases both in pre-processing (matrix generation times is about 10 times lower) and in solving (5-6 times lower), while the error is acceptable.

4.3.2 Study Case: the IMT2.5 Structure

The conceptual model of this study case is presented in Fig.4.75. It is composed of three metal lines, from gold (GOLD), placed on a titanium layer (TI), deposited on a silicon (Si) substrate. The actuation of the device is made by two action pads, made from gold, placed on each side of the signal line (middle line) coated by a silicon oxide (SiO_2) layer. The membrane, also from gold, resting on the two ground lines, is suspended above the central line. The geometric parameters are presented in Table 4.18 and the material parameters in Table 4.19.

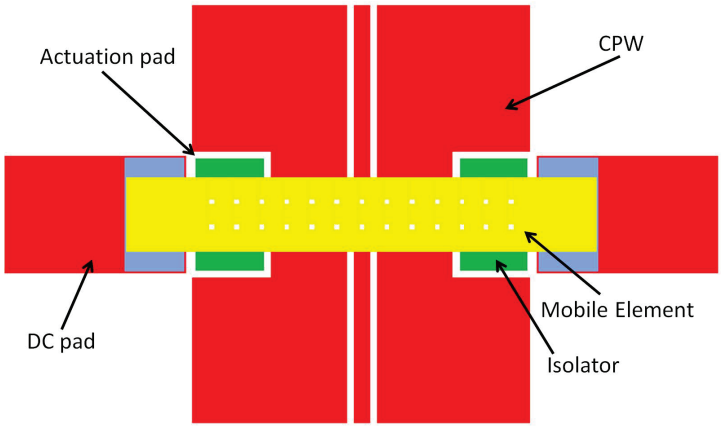

Figure 4.75: RF MEMS switch, up view.

The computational domain for this problem has the following maximum coordinates: along OX axes $X_{max} = 2 \cdot w_{leg} + l_{Lm}$, along OY $Y_{max} = h_{Si} + h_{Ti} + h_{Air}$ and the dept of the computational domain along OZ axes $Z_{max} = l_{cpw\_mid}$.

In Fig.4.76 is presented the geometrical model of this switch, as it is described to *chamy*.

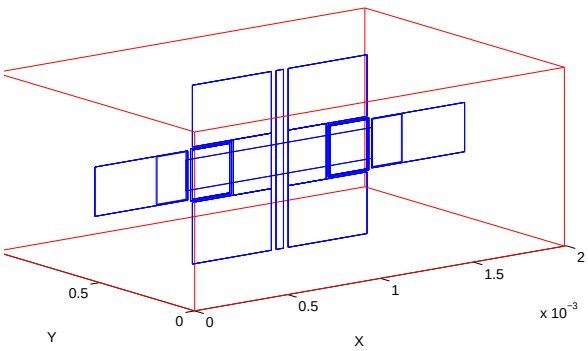

Figure 4.76: The geometrical model of IMT2.5 described to *chamy*.

Table 4.18: The geometric parameters of IMT2.5 structure. Value and significance.

Parameter	Value	Significance
w_{cpw_mid}	40 μm	width of the RF line
w_{cpw_gnd}	425 μm	width of the ground lines
w_{cpw_nar}	80 μm	width of the middle part of ground lines
w_{act_pad}	200 μm	width of the actuation pad
w_{leg}	600 μm	width of the bridge support
w_{SiO2}	1 μm	width of the isolating layer
w_{Wm}	200 μm	width of the bridge
h_{Si}	525 μm	height of the Si substrate
h_{Air}	525 μm	height of air layer
h_{Hti}	0.05 μm	height of titanium layer
h_{cpw}	0.5 μm	height of RF line
h_{Td}	0.1 μm	height of isolating layer
h_{gap}	2.5 μm	height of gap
h_{act_pad}	2.5 μm	height of actuation pad
h_{Hm}	1 μm	height of the bridge
l_{cpw_mid}	1160 μm	length of the RF line
l_{cpw_gnd}	400 μm	length of the ground lines
l_{cpw_nar}	360 μm	length of the middle part of ground lines
l_{act_pad}	320 μm	length of actuation pad
l_{leg}	310 μm	length of the bridge support
l_{Lm}	1000 μm	length of the bridge

Table 4.19: The material parameters of IMT2.5.

Component part	Parameter	Material	ε_r	μ_r	$\sigma[S/m]$
Substrate	Si	Silicon	1	1	10^{-5}
Titanium layer	Ti	Titanium	1	1	$2.38 \cdot 10^6$
Isolator	$SiO2$	Silicon oxide	3.9	1	10^{-7}
CPW lines	$GOLD$	Gold	1	1	$4.1 \cdot 10^7$
Bridge	$GOLD$	Gold	1	1	$4.1 \cdot 10^7$

The discretization grid (Fig.4.77) has 63x35x32 nodes with a number of 713873 DOFs.

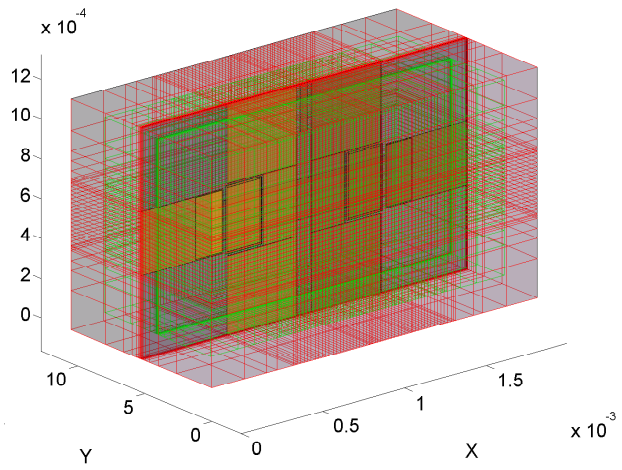

Figure 4.77: $63 \times 35 \times 32$ Grid generated by *chamy*

For UP state of the RF-MEMS device, the time required to extract the FIT matrices was 3714.41 seconds. By using AFS with VF, the time needed to compute the frequency answer in 13 frequency in the range from 1GHz to 60GHz was $7.67 \cdot 10^4$ seconds. Fig.4.78 and Fig.4.79 shows the amplitude and phase of S_{11} respective S_{21} parameters.

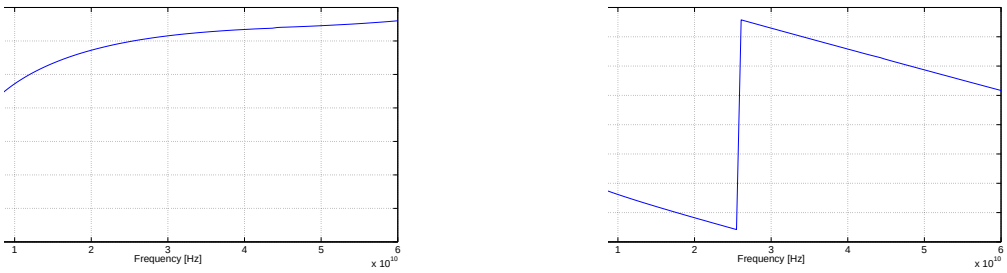

Figure 4.78: S_{11} Parameter for Up position. Amplitude and phase.

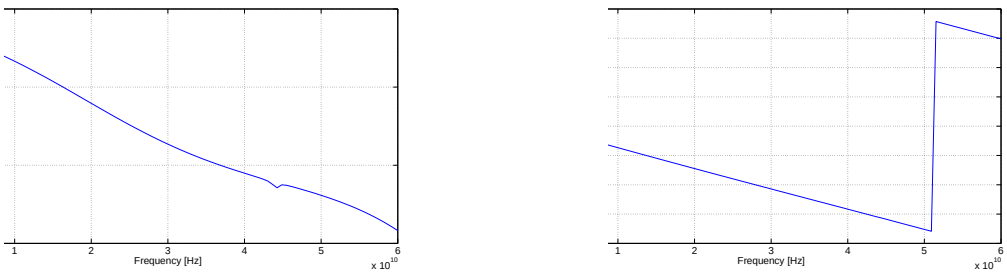

Figure 4.79: S_{21} Parameter for Up position. Amplitude and phase.

For DOWN state of the RF-MEMS device, the time required to extract the FIT matrices was 3714.41 seconds, and to compute the frequency answer was $3.15 \cdot 10^5$ seconds. Fig.4.80 and Fig.4.81 shows the amplitude and phase of S_{11} respective S_{21} parameters.

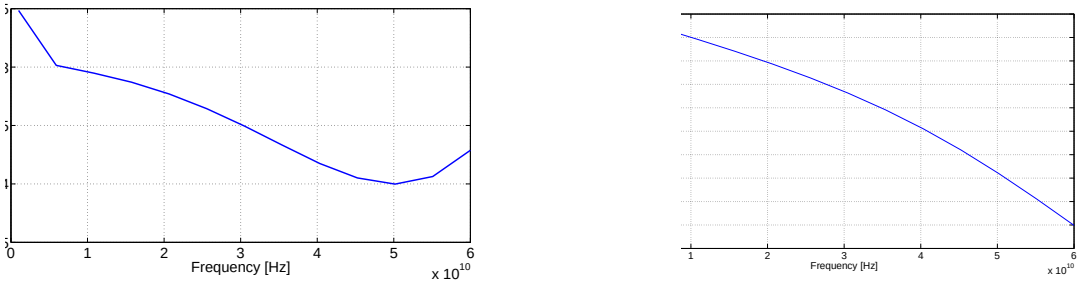

Figure 4.80: S_{11} Parameter for Down position. Amplitude and phase.

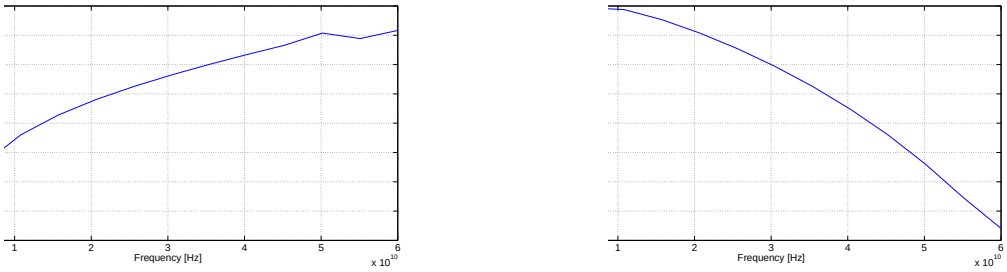

Figure 4.81: S_{21} Parameter for Down position. Amplitude and phase.

In the case of CPW (without switch membrane), the time required to extract the FIT matrices was 3714.41 seconds, and the time to compute the frequency answer was $3.15 \cdot 10^5$ seconds. Fig.4.82 and Fig.4.83 shows the amplitude and phase of S_{11} and S_{21} parameters.

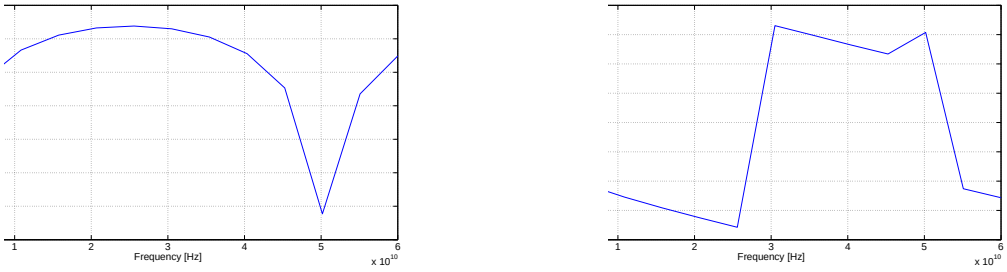

Figure 4.82: S_{11} Parameter for Down position. Amplitude and phase.

4.4 Experimental Characterization of the IMT2.5 Structure

The practical realization of the IMT2.5 structure and its RF characterization was done at National Institute for Research and Development in Microtechnologies (IMT) - Bucharest, Romania (`www.imt.ro`).

Two wafers of high resistivity silicon were processed and several types of structures were added:

- CPW lines;
- RF-MEMS switches with a construction of bridge type for which the following pa-

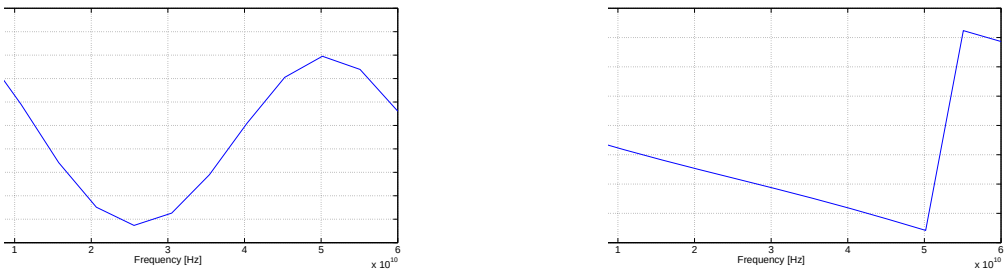

Figure 4.83: S_{21} Parameter for Down position. Amplitude and phase.

rameters were varied: width of the bridge w_{Wm} (80 and 200 μm), length of the bridge l_{Wm} (910, 1110 and 1210 μm), width of the actuation pad w_{act_pad} (200 and 300 μm);

- RF-MEMS switches with a construction of cantilever type for which the following parameters were varied: length of the cantilever (910, 1110 and 1210 μm), width of the actuation pad (100, 200 and 300 μm);

The characterization and testing of the devices was achieved by using a Vector Network Analyzer (VNA) 37397D type from *Anritsu*, able to measure a frequency up to 110 GHz, by a sub-system for measuring the components directly on the wafer, by using coplanar probes, PM5 model from *Suss Microtec* (Fig.4.84).

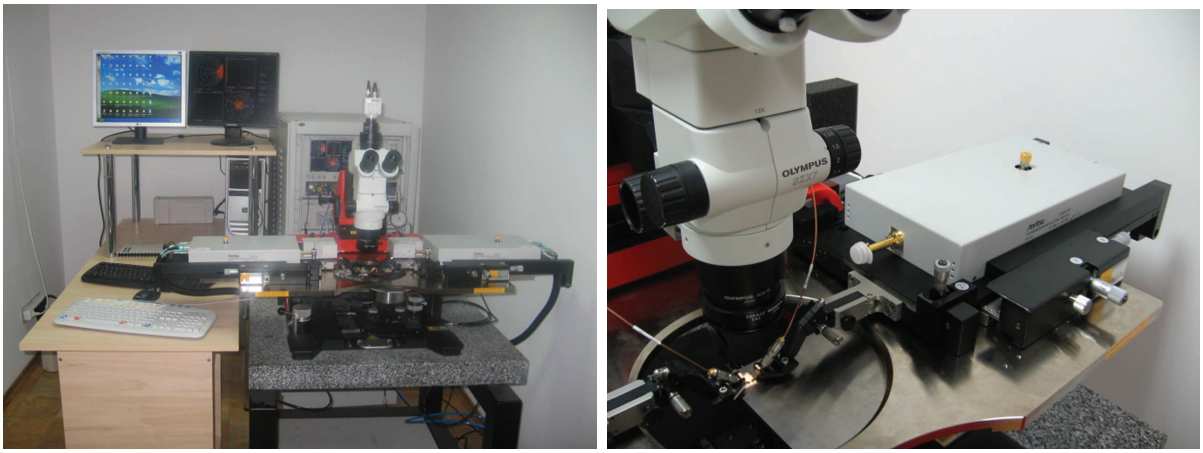

Figure 4.84: Measurement Setup.

The Fig.4.85 - Left presents a photography of the IMT2.5 structure, by optical microscope, Fig.4.85 - Right of the IMT structure, Fig.4.86 - Left the QIAN structure and Fig.4.86 - Right only the CPW lines. The comparison of the measured RF response on both of the wafers for the Up position of the switches with the same configuration as IMT2.5 structure is presented in Fig.4.87 and Fig.4.88. The amplitude and phase of S_{11} respective S_{21} parameter is illustrated. An insertion loss between -0.03 dB and -5 dB was obtained.

The relative difference of the RF response from the wafers is approximately 10%.

The validation of the numerical model is done by comparison of the simulation results with the results of the experimental measurements. Fig.4.89 and Fig.4.90 contain this

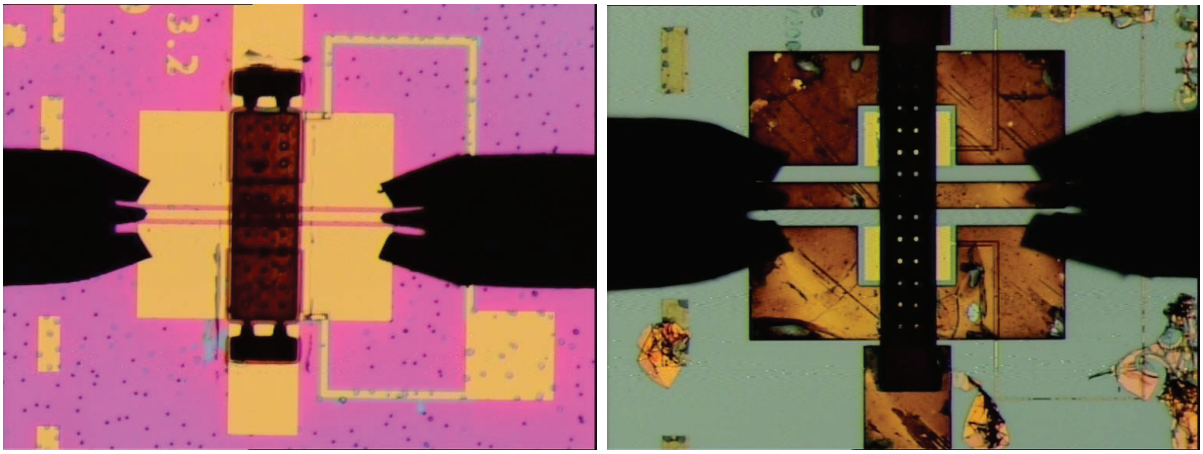

Figure 4.85: Left - Microscope view of the IMT2.5 Structure. Right - Microscope view of the IMT Structure.

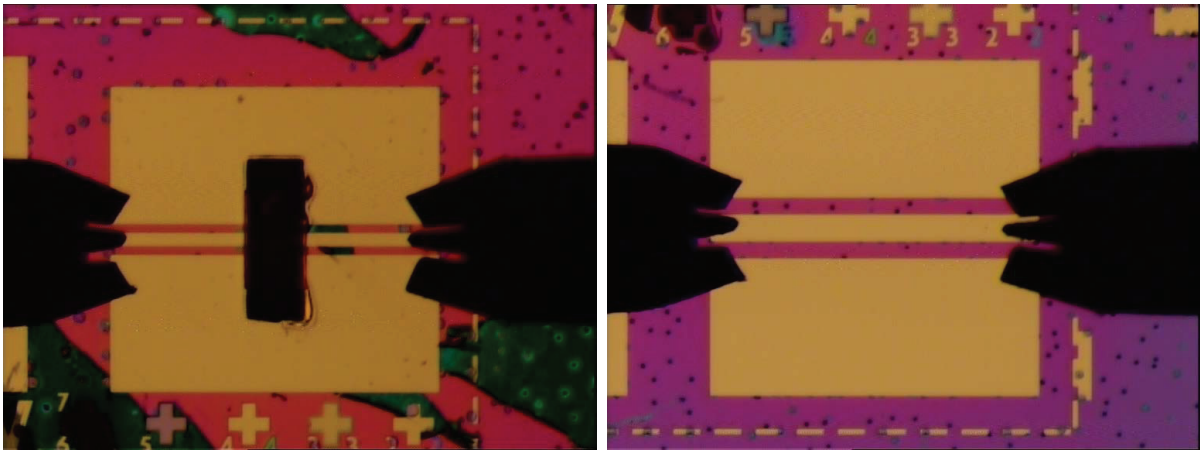

Figure 4.86: Left - Microscope view of the QIAN Structure. Right - Microscope view of the CPW lines.

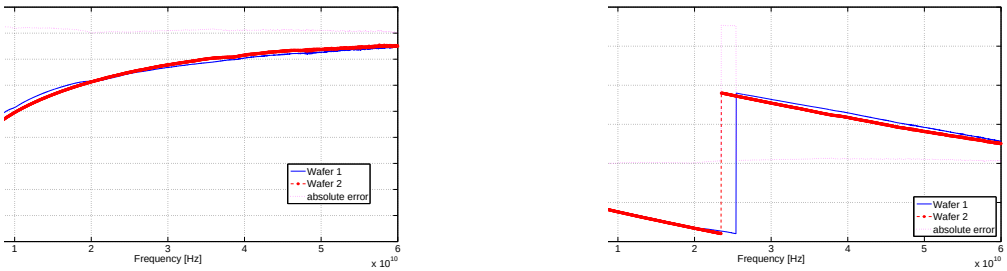

Figure 4.87: S_{11} Parameter for Up position. Comparison between the measured RF response of the 2 wafers

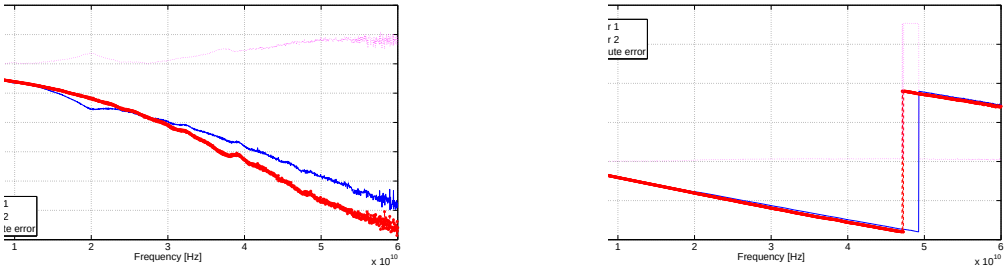

Figure 4.88: S_{21} Parameter for Up position. Comparison between the measured RF response of the 2 wafers

comparison applied to S_{11} and S_{21} for wafer n. In Fig.4.91 and Fig.4.92 are represented the same comparisons, but for another version of the IMT switch, on wafer 2.

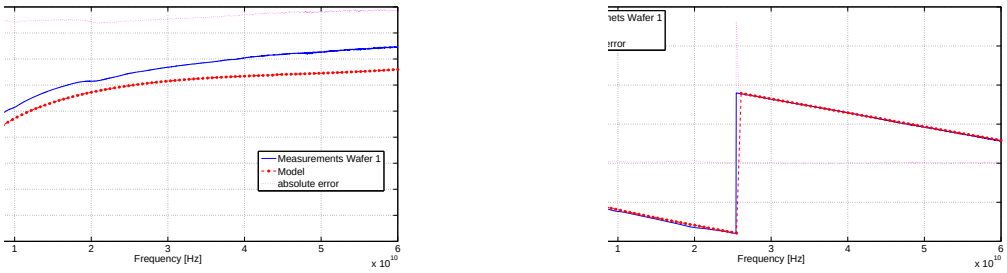

Figure 4.89: S_{11} Parameter for Up position. Comparison between the computed RF response and measured RF response from wafer 1.

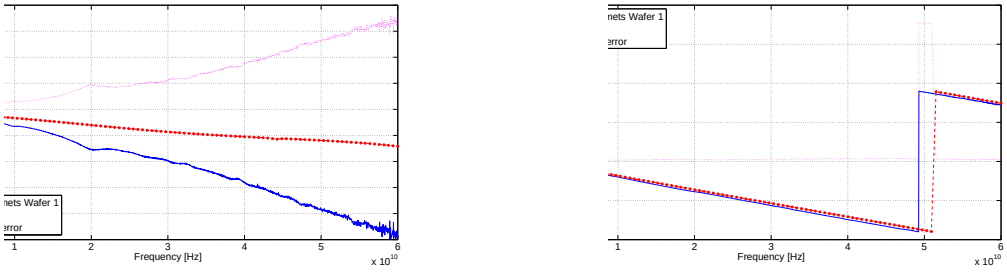

Figure 4.90: S_{21} Parameter for Up position. Comparison between the computed RF response and measured RF response from wafer 1.

One can notice a good agreement between numerical results and measurements, thus validating the numerical model.

4.5 Conclusions

This chapter is dedicated to the development of numerical multiphysics and RF models for RF-MEMS study cases. Static, dynamic and EM analysis were performed, in order to compute the field-solution of these three problems. Electric and magnetic problems (ES and RF) are strongly coupled with mechanical problems (MEC - Structural and FD - Fluid dynamics). The verification of the results was made by using several software packages

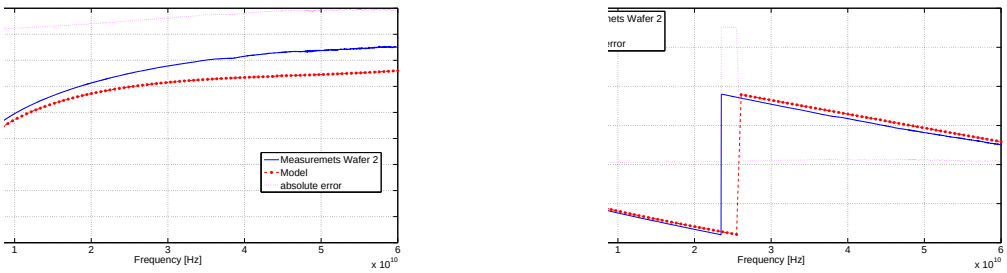

Figure 4.91: S_{11} Parameter for Up position. Comparison between the computed RF response and measured RF response from wafer 2.

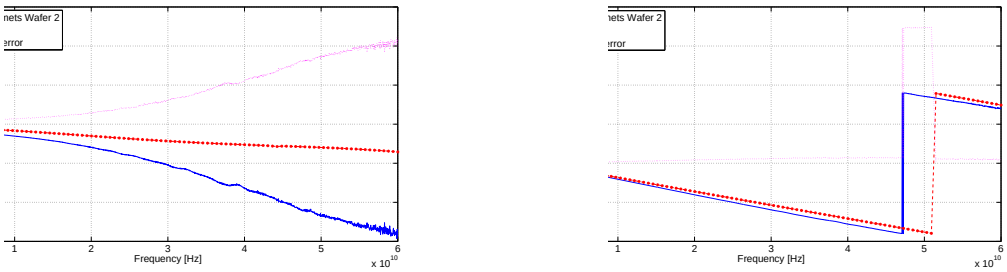

Figure 4.92: S_{21} Parameter for Up position. Comparison between the computed RF response and measured RF response from wafer 2.

(COMSOL and ANSYS based on FEM for multiphysics; *chamy* based on FIT and HFSS based on FEM for RF numerical modelling). The validation of the developed numerical models is done by experimental means. The experimental results describing the RF behavior of two RF MEMS switches are obtained from literature and from measurement made by IMT.

After the static analysis of the QIAN structure the difference between numerical solutions, computed by COMSOL and ANSYS is about 3%. The maximum displacement of the membrane computed by COMSOL is $z_{pi} = 2.26\mu m$. The difference under 3% proves the correctness of the numerical solving procedure. From the parametric study, it can be noticed that the pull-down voltage decrease with the increase of the pad width and length of the membrane, being very sensitive to the residual stresses in the membrane. The 2D models are enough accurate for the static analysis, consequently they are suitable for computing of the static pull-in voltage.

For a more accurate extraction of the dynamic pull-in voltage, the air damping has to be take in consideration. The relative difference between the static and dynamic pull-in voltage decreasing in this manner from 13% to 3%. In order to model the air dumping, a 3D model is necessary. Consequently, in order to compute the switching time, a dynamic, 3D multiphysics analysis (ES-MEC-FSI, strongly coupled) have to be done. To simulate a switching cycle (OFF-ON-OFF) a contact model must be included.

From RF point of view, comparing the results, one can observe a good agreement between our results obtained using *chamy* software and the results presented in [56], obtained with a commercial software and validated by measurements. As consequence, the numerical method proposed in this thesis is validated.

To obtain reliable simulation results, many aspects must be considered. Each field problem (ES, MEC, FF, RF, contact) have to be very careful described to the computer (the geometry, material constants, field sources, and boundary conditions), the couplings between problems and the solving methods, as well as their parameters (appropriate meshing, linear and nonlinear solvers, time integration).

The study conducted on the effects of membrane perforations upon the RF characteristics shows that there is no need to take the perforations of the membrane into account in the electromagnetic modeling of capacitive MEMS switches, because the relative error between the models with and without holes is around 0.4 % both in the UP and DOWN states. This is a great advantage for the RF modelling since it allows the meshing of the membrane with a coarser grid.

The human and computational effort to simulate in an accurate manner the mechanical and RF behavior of RF-MEMS switches, based on their numerical field models is quite substantial. Therefore for an efficient (re)design of these devices, another approach should be used. This is why, in this chapter an important attention was dedicated to the parametric modelling and in the next chapter the model reduction will be addressed.

Chapter 5

Reduced Models for RF MEMS Switches

The modeling of MEMS devices is an important issue in their design loop [133, 49], that has to provide eventually a compact model, described as a circuit netlist. This will allow the designer to easily simulate the whole system in which the switch is embedded.

5.1 Extraction of Lumped Parameters

The switch's behavior is characterized by several parameters. The compact models mentioned above (as that in Fig.5.1) need equivalent (effective) lumped parameters that characterize their components. The transversal variable capacitor is an essential component for understanding the switch behavior.

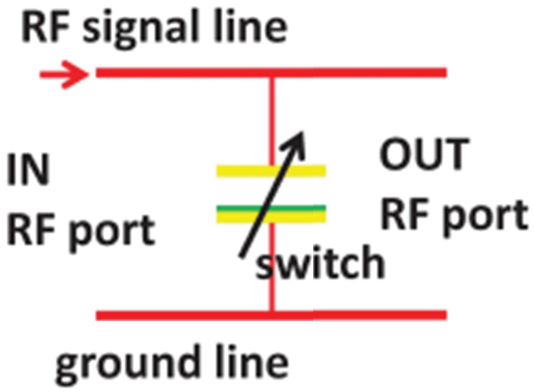

Figure 5.1: Conceptual macro-model of a RF MEMS switch

The most simple model of a RF-MEMS switch consists of a parallel plate capacitor, having one plate (armature) fixed and the other plate suspended by a spring. It was presented and analyzed in the Chaper 2. When an actuation voltage $u(t)$ is applied between the two plates, the mobile armature begins to move. If, for instance, the applied voltage is a step signal $u(t) = V_0 1(t)$, with V_0 small enough, the mobile armature oscillates

and finally reaches an equilibrium position for which the electrostatic force is equal and opposite to the elastic force of the string.

If the applied voltage V_0 is high enough, the mobile armature may collapse onto the fixed armature. The smallest value of V_0 for which this instability occurs is an important parameter of the switch, called pull-in voltage V_{pi}. This pull-in voltage can be extracted, by both static and dynamic simulations [133].

The movement of the mobile armature is described in this simple model by only one degree of freedom which is the displacement z of the rigid armature, with respect to its equilibrium position. The equation that governs this 1D movement , particular form of (3.4) is based on Newtons law, which becomes after projection on the Oz direction:

$$m \cdot \frac{d^2 z}{dt^2} + b \cdot \frac{dz}{dt} + kz = F_{ES}(z, V_0) \tag{5.1}$$

where m is the mass of the mobile armature, k is the spring stiffness constant and b is a damping coefficient. The right hand side is the electrostatic force ($F_{\mathrm{ES}} = \frac{1}{2}\frac{\varepsilon_0 A V_0^2}{(g_0 - z + \frac{t_d}{\varepsilon_0})^2}$) that depends on the applied voltage and on the displacement. Thus, (5.1) is a nonlinear ODE, describing a strong coupling between the MEC and the ES fields.

The behavior of this dynamic system (an invariant linear second order I/O system, for small variations of z, which do not change too much the electrostatic force) depends on the values of the m, b, k parameters. As we know from the classical theory of the second order linear dynamic systems, if we denote by $\alpha = b/(2m)$ the attenuation coefficient and by $\omega_0 = \sqrt{k/m}$ the resonance angular frequency, then the solution depends on the value of the damping ratio $\zeta = \alpha/\omega_0$. The system can be: *un-damped* if $\zeta = 0$ (i.e. the damping coefficient is zero $b = 0$), *under-damped* if $\zeta < 1$ in which case the solution to a step function excitation consists of damped oscillations, *over-damped* if $\zeta > 1$ and *critically-damped* if $\zeta = 1$. The damping ratio is strongly related to the quality factor of an oscillator, i.e. $\zeta = 1/(2Q)$. In a system with high Q the oscillations last for a long time.

The main idea of this chapter is to consider the 1D MEMS model as a compact - reduced model of the more accurate 3D model. That means we have to extract the characteristic lumped parameters of 1D model from the simulation results of the 3D model. For example, starting from the solutions of the 3D simulations, one can identify equivalent ("effective"') values for the effective stiffness, mass and damping coefficients. The effective stiffness k_{eff} may be extracted also from simulations of 2D model. Below is presented a complete and coherent procedure to extract the multiphysics reduced model and its SPICE equivalent circuit based on the accurate 3D multiphysics and RF-EM simulations of the modeled device. Its MALTAB code is presented in the annex A1.

5.1.1 Extraction of Effective Elastic Coefficients

In the static case, it is assumed that the actuation voltage $u(t)$ increases progressively, but very slow, to V_{pi}, so that the inertial forces and the damping forces can be neglected.

Assuming that V_0 is less than the pull-in voltage, then the elastic force equals the electrostatic force at equilibrium position and (5.1) becomes

$$kz = F_{ES}(z, V_0), \tag{5.2}$$

and, more generally:

$$F_{elastic}(z) = F_{ES}(z, V_0), \tag{5.3}$$

since the elastic force might not be linear with respect to the displacement.

Inspired by the case of fixed-fixed beams where there is a stretching effect and the elastic force is nonlinear with respect to the displacement [21], we will assume that the elastic force may include a cubic dependence on z, as well as in (3.4):

$$F_{elastic}(z) = kz + k_s z^3. \tag{5.4}$$

The real switches as well as above models, analyzed in the previous chapter have a complex deformation of the membrane and an apriori estimation of the equivalent stiffness coefficients k or $\{k, k_s\}$, is difficult. Some analytical formulas exist for these coefficients, but their applicability is limited.

The goal of this section is to find a general algorithm to extract an equivalent stiffness coefficient k, or an equivalent pair of stiffness coefficients $\{k, k_s\}$ for a given MEMS switch, starting from a set of static simulations of the numerical model based on coupled MEC and ES fields. The validation of this procedure will be done by comparing the static pull-in voltage extracted from the circuit simulation of the compact model with the static pull-in voltage obtained by the FEM simulation.

In order to extract the effective elastic coefficients, a coupled MEC+ES multiphysics model is analyzed in static regime. To obtain a reliable result, the model must includes a proper coupled field formulation and it should be analyzed with appropriate numerical simulation techniques. To illustrate this aspects, QIAN and IMT test structures will be analyzed.

Several attempts to extract the effective elastic coefficient were tried, one based on analytical formula and four based on numerical computations that use the results given by the coupled model described in the previous section.

A. Analytical Method

An analytical formula for an effective elastic coefficient $k_{analytic}$, derived for a fixed-fixed beam with distributed loads is available in the literature [10]. If residual stress is neglected, the value depends solely on the material characteristics (Youngs modulus E and moment of inertia I), and geometrical dimensions. Using the notations of the parametrized model from Fig.4.14, the analytical expression of the effective elastic coefficient is:

$$k_{analytic} = \frac{4EW_m H_m^3}{L_m[(l_1 + W_p ad)^2 + l_1(l_1 + W_{pad}) + l_1^2] - (2l_1 + W_{pad})[(l_1 + W_{pad})2 + l_1^2]}, \tag{5.5}$$

where: $l_1 = L_m/2W_{pad}(W_{cpw1}/2 + D_1)$.

B. Numerical Method

From the set of static simulations, triples (V_0, z, W_{ES}) are extracted. The ES force acting on a membrane can be computed by means of the generalized force theorem $F_{ES} = \frac{\partial W_{ES}}{\partial g}$, where $g = g_0 - z$ is the generalized coordinate, i.e. the gap between the plates. Given the dependency of the displacement w.r.t. the imposed voltage (Fig.4.21) and knowing that the electric energy is proportional to the capacitance created between the plates:

$$W_{ES}(z, V_0) = C(z)\frac{V_0^2}{2} \tag{5.6}$$

a rational approximation of the capacitance with respect to the displacement was computed

$$C(z) = 1/(\alpha z + \beta) \tag{5.7}$$

by using a first order linear square approximation of the dependence $1/C$ with respect to the displacement z (Fig.5.2).

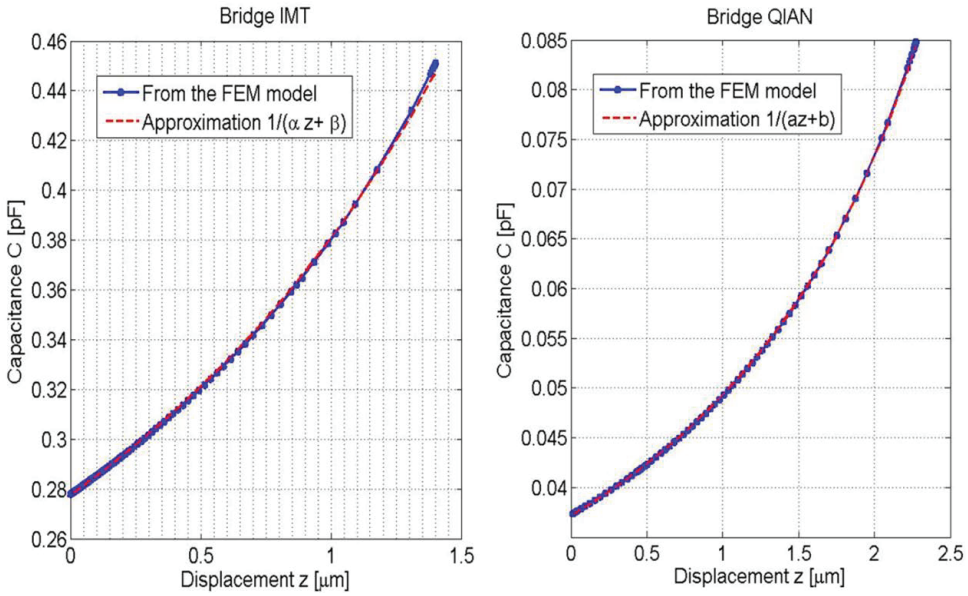

Figure 5.2: Dependance of the capacitance w.r.t displacement.

Consequently, the electrostatic force is approximated as:

$$F_{ES}(z, V_0) = \frac{1}{\alpha z + \beta}\frac{V_0^2}{2} \tag{5.8}$$

Method B1 - "*averaged (F/z)*".

Since at equilibrium, the ES force is equal to the elastic force, we divide it by the displacement z, as suggested by (5.2), and an equivalent elastic coefficient may be computed:

$$k_{B1}(z) = \frac{F_{ES}}{z}. \tag{5.9}$$

This value is dependent on the position, and thus a further averaging is needed, e.g. given by:

$$k_{averaged(F/z)} = \frac{\int_0^{z_{pi}} k_{B1}(z)dz}{z_{pi}}. \tag{5.10}$$

Method B2 - "*(averaged F)/z*".

Another numerical attempt is to take the average of the force with respect to the displacement and divide it by the pull-in displacement:

$$k_{elastic\_energy} = \frac{\int_0^{z_{pi}} F_{ES} dz}{z_{pi}^2}. \tag{5.11}$$

Method B3 - "*LS order 1*".

Assuming that the elastic force varies linearly with the displacement as given by (5.2), a first order linear approximation is sought by Least Squares approach, for the z, F_{ES} pairs, and a value denoted by k in what follows is obtained.

Method B4 - "*LS order 3*".

Assuming that the elastic force varies cubically with the displacement as given by (5.4), a third order approximation is sought by Least Squares approach, for the $\{z, F_{ES}\}$ pairs, and $\{k, k_s\}$ values are obtained.

In Fig.5.3 the elastic force computed with 5.2 or (5.4) using the effective elastic constant extracted with the numerical methods is compared with the elastic force computed with FEM.

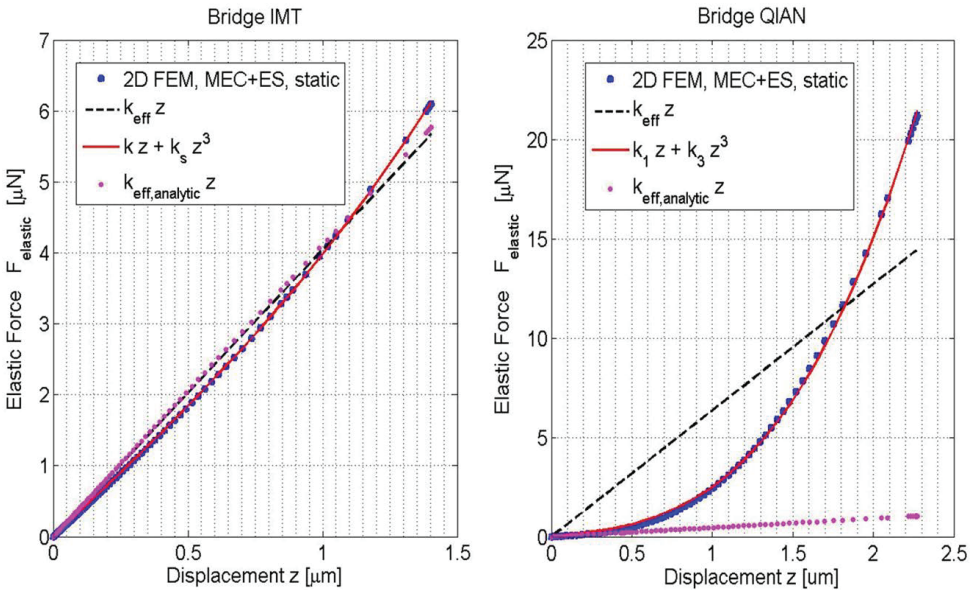

Figure 5.3: Dependance of the elastic force F_{el} w.r.t displacement.

In conclusion, we may say that the nonlinear (cubic) approximation of the elastic force is more appropriate, at least for the QIAN study case.

5.1.2 Extraction of Effective Mass

The effective mass of the bridge may be extracted from the results of dynamic analysis performed for the coupled 3D electrostatic-structural problem. Applying a voltage less

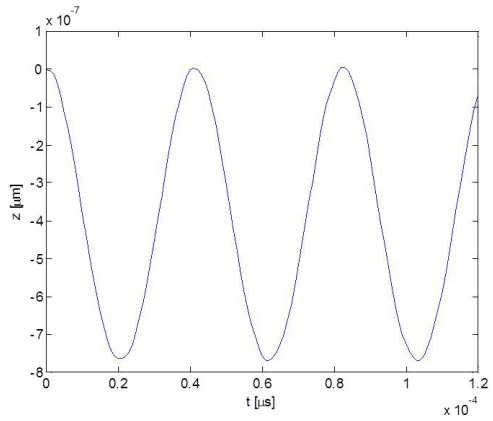

Figure 5.4: Time oscillations of the membrane for an applied step voltage.

than V_{pi}, un-damped oscillations of the bridges displacement was obtained, as the ones shown in Fig.5.4.

Applying Fast Fourier Transform on the resulted signal $z(t)$ (Fig.5.5) the first resonant frequency f_0 is extracted and the effective mass is computed:

$$m_{eff} = \frac{k_{eff}}{\omega_0^2}, \text{ where } \omega_0^2 = 2\pi f_0. \tag{5.12}$$

Because (5.12) is valid only for a 2^{nd} order linear systems, we suppose that z is very small signal, so the nonlinear ODE may be linearized. Therefore, the elastic coefficient is that corresponding to the linear term of elastic force.

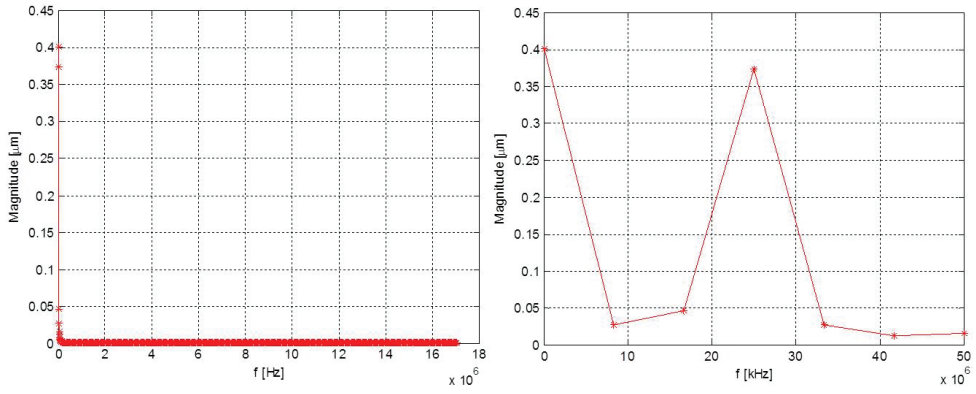

Figure 5.5: FFT of the membrane oscillation and zoomed for f_0.

The effective mass is expected to be lower than the real mass of the membrane, because the several inside points have lower oscillations than the central point of the membrane.

5.1.3 Extraction of Damping Coefficient

Because the dumping is produced mainly by the air resistance, the damping coefficient may be extracted from coupled 3D electrostatic-structural-fluid flow problem solved numerically by FEM. Applying a voltage less than V_{pi} a damped displacement of the bridges was obtained, as in Fig.5.6. The membrane movement is monotonic, totally damped, without any oscillation.

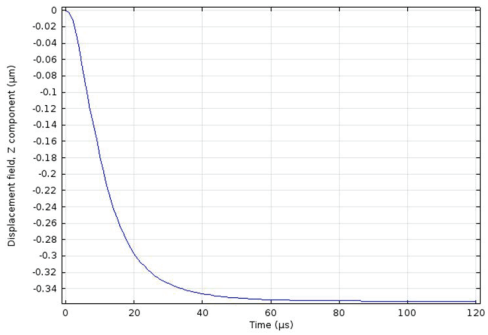

Figure 5.6: Position of the bridge vs time, considering air dumping.

Post-processing the results of the FEM analysis,the position $z(t)$ and electrostatic energy $W_{ES}(u)$ is recorded. Next the dependence of the capacitance with respect to the position is computed and it is approximated with the expression $1/(c_1 z + c_2)$, then the electrostatic force is computed by using the the generalized force theorem.

The velocity is computed by the first derivative of the displacement $v(t) = dz(t)/dt$ and acceleration is computed by the first derivative of the velocity $a(t) = dv(t)/dt$.

The corresponding damping force $F_d = b \cdot v$ and is computed by:

$$F_d = F_{ES} - F_{el} - F_{in} \Longrightarrow b \cdot v = F_{ES} - kz - k_s z^3 - m_{eff} \cdot a. \tag{5.13}$$

In the end, the effective damping coefficient is computed by a first order least square approximation of the damping force dependence with respect to the velocity (Fig. 5.7). In Fig.5.8 a representation of the forces w.r.t. the displacement is presented. As we can see in that figure, the extraction of the dumping coefficient is less reliable than previous extraction. One explanation may be the numerical instability generated by the double derivative, which is estimated with numeric methods (a procedure known as very instable one). The numerical errors of the Computational Fluid Dynamics procedure worse the extraction process.

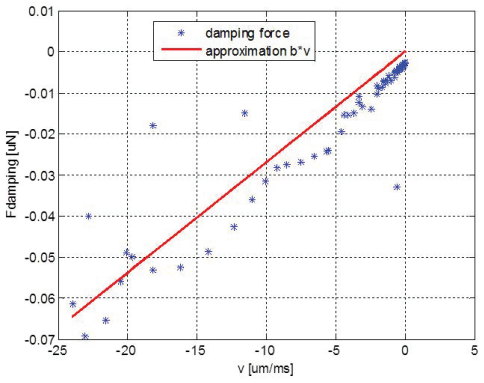

Figure 5.7: Fitting of the damping force extracted from the FEM simulations.

5.1.4 The Multiphysics Reduction Procedure

In conclusion, the procedure of extraction of the effective m, b and k coefficients, consists by the following 10 steps:

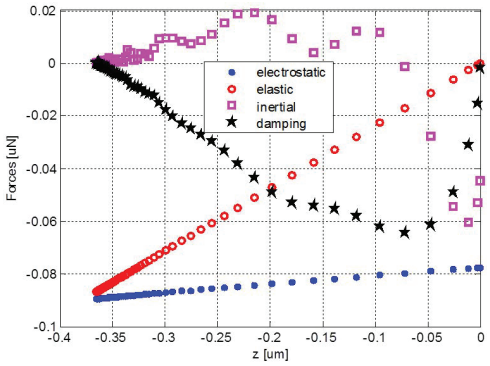

Figure 5.8: Electrostatic, Elastic, Damping and Inertial forces dependency of the displacement.

- Step 1. Do coupled static numerical ES+MEC simulations (e.g with FEM) for increasing values of the actuation voltage V_0. Record position z and electrostatic energy W_{ES}.
- Step 2. Compute the dependence of the switch capacitance $C(z) = 2W_{ES}/V_0^2$ on the membrane displacement and approximate the capacitance inverse $1/C(z)$ with $\alpha z + \beta$ by affine regression (find coefficient α and β by the least square method).
- Step 3. Compute the dependence of the electrostatic force $F_{ES}(z)$ vs. displacement z by applying the generalized force theorem $F_{ES}(z) = V_0^2/2 \cdot dC(z)/dz$.
- Step 4. Do a cubic least square approximation of the dependence found at step 3 in order to find k and k_s.
- Step 5. Do a coupled dynamic transient structural-electrostatic analysis (e.g. by FEM), under a step voltage very less than the pull-in voltage. Extract the resonance frequency from the un-damped obtained oscillation of the membrane, by FFT. Compute the effective mass as $m = k/\omega^2$.
- Step 6. Do a coupled transient analysis (structural-electrostatic-fluid flow) for a step actuation voltage. Record position $z(t)$ and electrostatic energy $W_{ES}(u)$.
- Step 7. Apply again the parameter identification for the second order linear system, by computing the dependence of the capacitance with respect to the position $C(z)$ and approximate it with an expression $1/(c_1 z + c_2)$. Based on it, compute the electrostatic force $F_{ES}(z)$ by using the generalized force theorem.
- Step 8. Compute the velocity $v = dz/dt$ and the acceleration $a = dv/dt$.
- Step 9. Compute damping force $F_d = F_{ES} - F_{el} - F_{in}$, where F_{el} uses the effective stiffness coefficients and found at step 4 and $F_{in} = m \cdot a$ uses the effective mass found at step 5 and the acceleration computed at step 8.
- Step 10. Do a first order least square approximation of the damping force dependence with respect to the velocity and compute the effective damping coefficient b.

The complexity reduction procedure of the nonlinear multiphysics RF-MEMS switches model is based not only on mathematical principles but rather on some essential physical

principles. This makes the reduced model to preserve more essential characteristics of the real device.

5.2 Lumped Parameters of the RF Model

As we may see in Fig.5.1. the conceptual model of RF MEMS switch contains two transmission lines and a transversal dipolar microwave circuit element. These structure might be approximated by a compact circuit with lumped parameters, but more accurate results may be obtained if we adopt a hybrid approach, combining lumped with distributed elements. The two lines are modeled as 1D transmission lines while for the transversal dipole, an equivalent circuits with lumped parameters is considered (Fig.5.9). The simplest choice is to model the transversal element as a RLC series circuit with lumped parameters (having values dependent w.r.t. z- the membrane position, as a continuous function, or at least known for the two stable position UP and DOWN.

Closed-form relationships for this TL-lumped compact model of a RF MEMS switch can be derived by using TLs theory. Considering the topological constraints:

$$\underline{U}_2^{(1)} = \underline{U}_1^{(2)}, \tag{5.14}$$

$$\underline{I}_2^{(1)} = \underline{I}_1^{(2)} + \underline{Y}\underline{U}_1^{(2)}, \tag{5.15}$$

where, according to the TLs theory

$$\begin{cases} \underline{U}_2^{(1)} = \underline{U}_1 \cosh(\gamma l/2) - \underline{Z}_c \underline{I}_1 \sinh(\gamma l/2), \\ \\ \underline{I}_2^{(1)} = \underline{I}_1 \cosh(\gamma l/2) - \underline{U}_1/\underline{Z}_c \sinh(\gamma l/2), \end{cases} \tag{5.16}$$

$$\begin{cases} \underline{U}_1^{(2)} = \underline{U}_2 \cosh(\gamma l/2) - \underline{Z}_c \underline{I}_2 \sinh(\gamma l/2), \\ \\ \underline{I}_1^{(2)} = \underline{I}_2 \cosh(\gamma l/2) - \underline{U}_2/\underline{Z}_c \sinh(\gamma l/2), \end{cases} \tag{5.17}$$

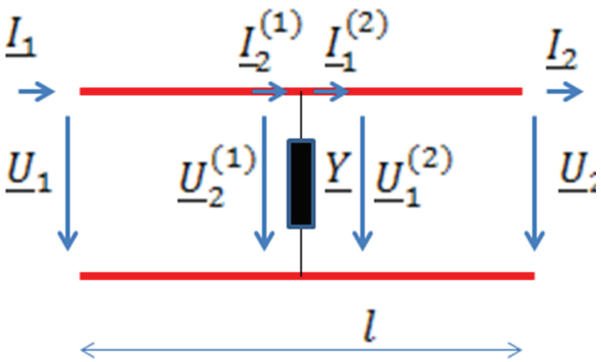

Figure 5.9: General RF compact model of the switch

If we denote by $\underline{Z}$ the transfer complex impedance of the quadripolar compact model:

$$\begin{bmatrix} \underline{U}_1 \\ \underline{U}_2 \end{bmatrix} = \underline{\boldsymbol{Z}} \begin{bmatrix} \underline{I}_1 \\ -\underline{I}_2 \end{bmatrix}, \tag{5.18}$$

by some algebraic computations, the components of this complex, symmetric, impedance matrix can be derived:

$$\begin{cases} \underline{Z}_{ii} = \frac{\sinh^2(\gamma l)+\underline{Z}_c\underline{Y}\sinh(\gamma l)\cosh(\gamma l)+\cosh^2(\gamma l)}{\Delta} \\ \\ \underline{Z}_{ij} = \frac{1}{\Delta} \end{cases} \tag{5.19}$$

where $i, j \in 1, 2, i \neq j$ and

$$\Delta = \frac{2\sinh(\gamma l)2\cosh(\gamma l)}{\underline{Z}_c + \underline{Y}\cosh^2(\gamma l)}. \tag{5.20}$$

Equations (5.19) and (5.20) will be used in three ways:

1. the computation of the frequency response for a compact model (explicit),
2. from the frequency response and the transmission line parameters we may identify the complex admittance $\underline{Y}$ (implicit) and
3. from the frequency response and the admittance $\underline{Y}$ we may identify the line parameters γ and $\underline{Z_c}$ and thus to derive the transmission per unit length parameters.

TL-lumped RF compact models of MEMS switches can be extracted with a robust procedure from the numerical solution of Maxwell equations with ECE boundary conditions. To to do it, the simulations are made in three cases: lines alone, UP and DOWN positions.

As a consequence, the proposed algorithm dedicated to extraction of the TL-lumped of the RF compact model's parameters has 4 steps:

- Step 1. Browsing frequency, do simulations of the line alone (e.g. by numerical solving of Maxwel's equations) and extract the frequency dependence line's S parameters.
- Step 2. Do simulation of the Full Wave EM field in the MEMS device in the UP position. By using (5.19) and (5.20), extract Y_{up} and compute C_{up}.
- Step 3. Improve the line parameters using the average value of C_{up} over the frequency range.
- Step 4. Do simulation for the DOWN position. Extract Y_{down} compute R_{mem}, C_{down} and L_{mem}.

Using closed form relationships has the benefit to do a fast fitting and correction of parameters of the compact model. The proposed algorithm has the advantage that it may incorporate easily the frequency dependence of parameters, either for the TLs or for the switch inductivity.

5.3 Validation of the Reduction Procedure

5.3.1 Multiphysics Compact Model

To validate the method of extracting the effective elastic coefficient, the nonlinear equation (5.3) in z is solved for several applied voltages and the instability point is recorded. The solving was done in SPICE. In this respect, an equivalent (actually based on mechanic-electric similitude) circuit that synthesizes these equations can be easily built and simulated for an increasing of values of the actuation voltage. The schematic of this circuit is shown in Fig.5.10. It contains behavioral current sources, the currents representing forces. The actuation voltage is modeled by the independent voltage source V_1, the ES force "flows" through the behavioral current source B_1 and the elastic force is modeled by the behavioral source B_2. The values are scaled for a more robust numerical analysis. Consequently the simulation result provides the solution of the (5.3) - (5.8) system of ODE.

Table 5.1 holds the simulation results for the IMT structure and Table 5.2 holds the results for the QIAN structure, obtained with several methods used to model the elastic behavior.

Table 5.1: Pull-in voltage obtained from the simulation of the macro-model

Pull-in voltage obtained from the simulation of the equivalent macro-model.

Method	Extracted effective elastic coefficients	Vpi from the macro-model	Relative error of V_{pi}
A Analytical	k = 4.113 N/m	7.73 V	2.02 %
B1 Averaged (F/z)	k = 3.838 N/m	7.46 V	5.45 %
B2 (Averaged F)/z	k = 1.989 N/m	5.37 V	31.9 %
B3 LS order 1	k = 4.041 N/m	7.66 V	2.92 %
B4 LS order 3	k = 3.582 N/m $k_s = 0.387 \cdot 10^{12}$ N/m^3	7.93 V	0.51 %

For the IMT structure the relative error of the pull-in voltage is computed with respect to the reference value of 7.89 V obtained from the static FEM simulation. A better image is obtained if displacement-voltage curves are compared for increasing values of the actuation voltage, as in Fig.5.11. It can be noticed that the averaging approaches behave worse than the analytical approach, and the cubic least square is able to recover not only a very accurate pull-in voltage (relative error less than 0.5 %), but the whole behavior of the displacement curve.

To extract the effective mass and damping coefficient, a 3D numerical model has to be analysed. The extraction method is tested on a simple benchmark (Fig.5.12), a cantilever switch, actuated by a voltage that is applied between it and a ground that ensures an

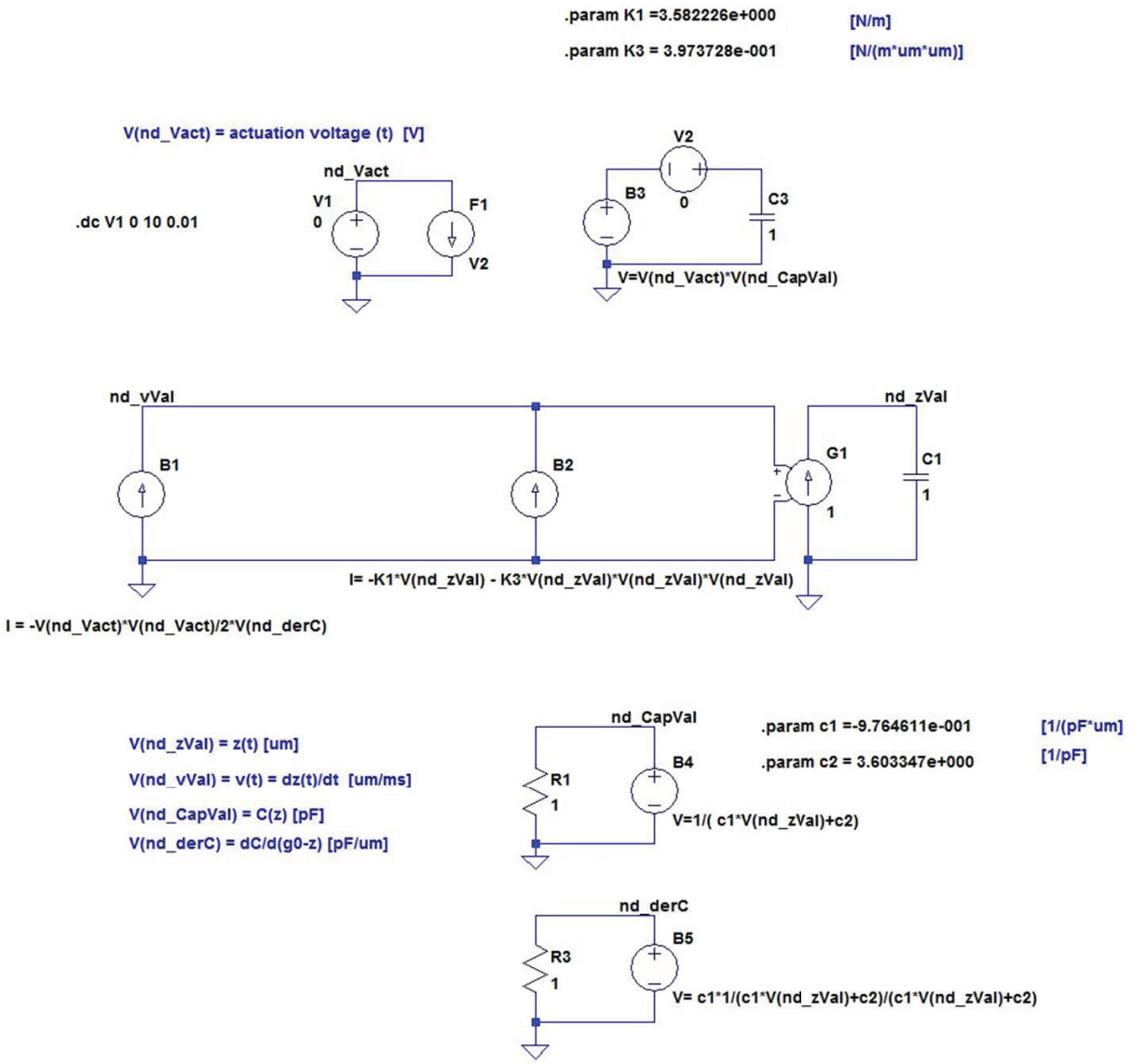

Figure 5.10: Static macro-model: Spice circuit that models several relationships that include the global mechanical end electrostatic phenomena in the coupled static simulation. (Here: $k_1 = k, k_3 = k_s, c_1 = \alpha, c_2 = \beta$).

Table 5.2: Effective coefficients obtained for the QIAN structure. Pull-in voltage obtained from the simulation of the equivalent macro-model.

Method	Extracted effective elastic coefficients	Vpi from the macro-model	Relative error of V_{pi}
A Analytical	k = $4.579 \cdot 10^{-1}$ N/m	7.73 V	74.18 %
B1 Averaged (F/z)	k = 2.581 N/m	18.38 V	38.70 %
B2 (Averaged F)/z	k = 3.629 N/m	21.79 V	27.32 %
B3 LS order 1	k = 6.357 N/m	28.92 V	3.5 %
B4 LS order 3	k = $8.493 \cdot 10^{-1} N/m$ ks = 1.66 N/m^3	30.23 V	0.82 %

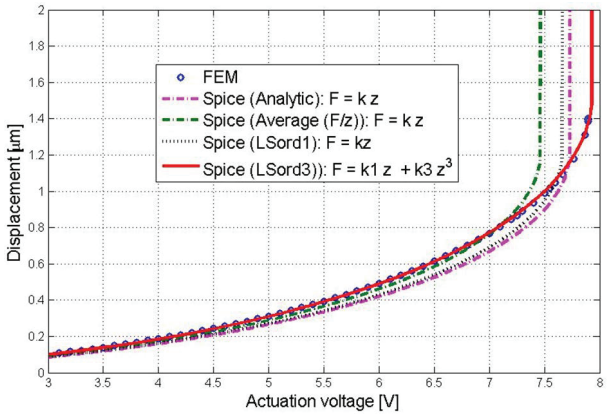

Figure 5.11: Displacement-actuation curves: reference (FEM) vs. SPICE macro-model simulations with values of effective coefficients obtained from various methods.

initial airgap of g_0. The cantilever is of parallelepiped shape, with length $l = 300\mu m$, width $w = 20\mu$, and thickness $t = 2\mu m$.

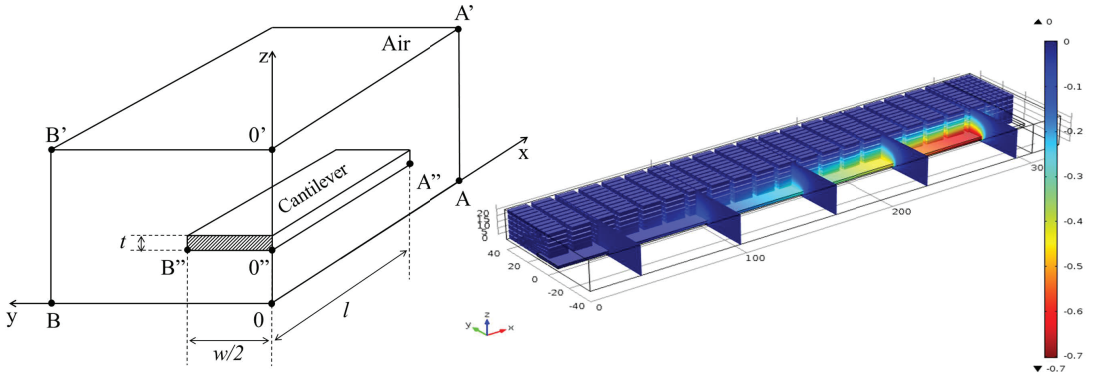

Figure 5.12: Left: Benchmark problem: the computational domain includes half of the cantilever. (Size of domain: $320\mu m \times 15\mu m \times 8\mu m$. Drawing is not at scale). Right: typical distribution of the electrostatic field norm.

The Spice circuit that describes the macro-model is shown in Fig.5.13. The actuation voltage is modeled by the independent voltage source V_1. The ES force "flows" through the behavioral current source B_1. The elastic force is modeled by the behavioral source B_2. The effective mass is a capacitance and the "current" flowing through it is the inertial force. The displacement, is the voltage at the node labeled "nd_zVal".

The effective elastic coefficient is extracted in the same way as for the 2D model. The results are: $k = 23[N/m], k_1 = 0.27[N/m], k_3 = -0.084[N/m(\mu m)^2], c_1 = -6[(pF \cdot \mu m)^{-1}], c_2 = 30[(pF)^{-1}]$.

By transient simulation of ES-MEC coupled problems under small applied voltage, an oscillating frequency $f_0 = 25[kHz]$ is obtained, resulting an effective mass of $m = 9.6 \cdot 10^{-6}[Kg]$. Even if only linear model was used to extract the mass, the macro-model response is better when it implements the cubic dependence of the elastic force.

The final validation is carried out for a three field coupled problem electrostatic-structural-fluid flow. As a result of the damping force - velocity fitting obtained the value of the dumped coefficient $b = 2.710^{-6}[Kg/s]$. This value is used as a conductance

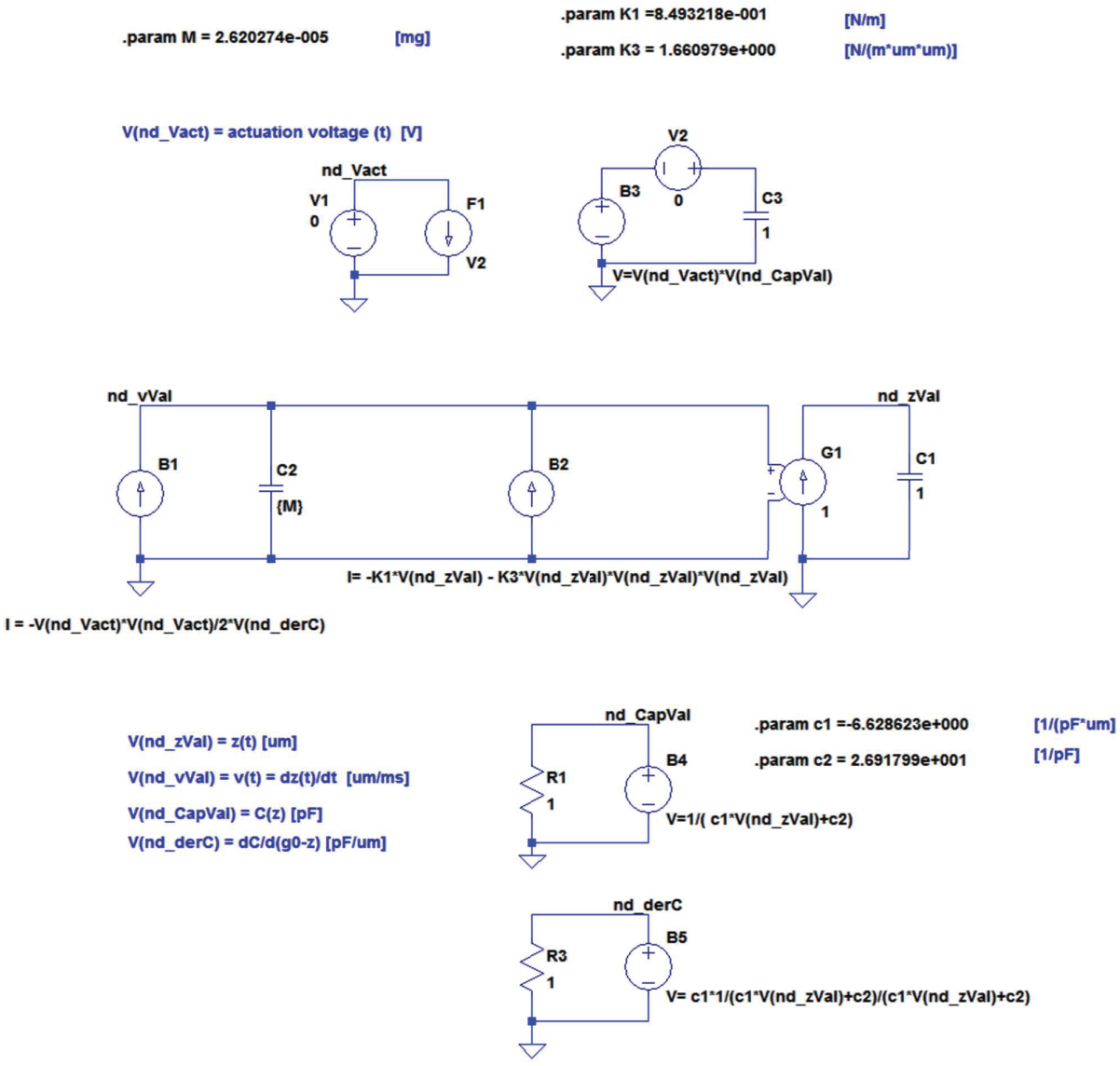

Figure 5.13: Multiphysics Macro-model. Scaled values are used.

in the SPICE equivalent model circuit (Fig.5.13). The dynamic answer of the macro-model as well as the reference answer obtained from the field simulation are shown in Fig.5.14. For the step excitation of $5V$ the relative error is 0.19 %, while for an excitation of $6V$ step the relative error is 0.35%.

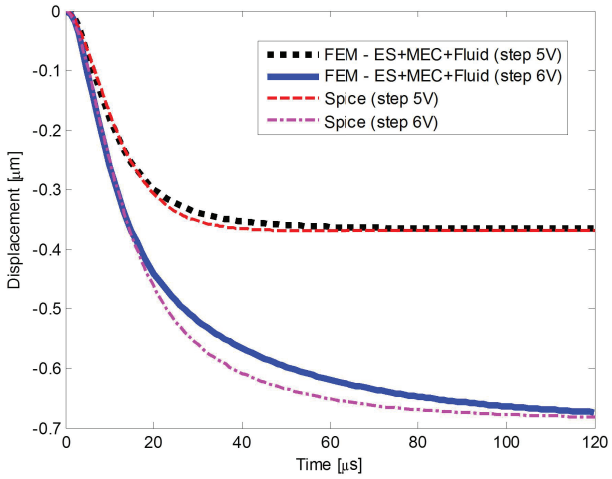

Figure 5.14: Multiphysics compact model. Scaled values are used.

The deviation of the behavior of compact model from the reference FEM-field model is quite acceptable, validating the extraction procedure of the SPICE multiphysics model presented above.

5.3.2 Compact RF Model

The compact model is inspired by the geometry of the device and it consists of a transmission line that model the RF signal line and an equivalent lumped parameter circuit model for the switch itself. In the UP position the lumped parameter model of the switch is merely a capacitance, whereas in the DOWN state position, the lumped parameter model is a R, L, C series connection. The values of the RF compact model are derived from the RF simulations, and therefore it is important to have accurate RF models of the device. In order to extract the lumped parameters of switch itself, a kind of de-imbedding, must be done, in order to eliminate the effects the the input and output connection lines.

Two test configurations were studied, QIAN and IMT structures, and acceptable relative errors in the S-parameters were obtained. Improvements are possible if a frequency dependent model is adopted for the switch's inductivity.

The QIAN benchmark is useful since [56] provides also measurements for the S parameters in the UP and DOWN positions, and thus, any RF model we use to illustrate the proposed extraction algorithm is validated.

A. Simulation of Lines Alone. Extraction of Line Parameters.

From the simulations of the line alone, easily obtained if in the RF model the material of the bridge is changed to air, the frequency dependence of the line parameters are

obtained and from here the line parameters. For this problem, an average value of the line parameters can take for the frequency range of interest, since the relative error in the reconstruction of the frequency response is less than 1 % (Fig.5.15).

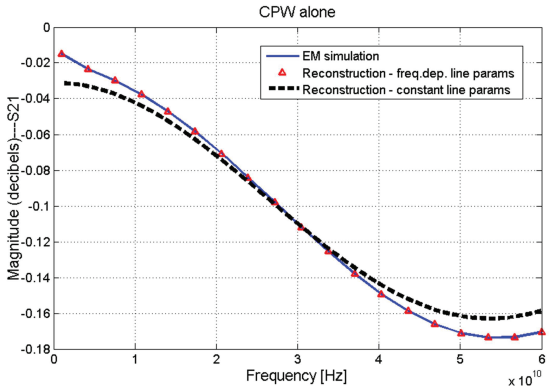

Figure 5.15: Frequency dependence of S_{21} for CPW alone

B. Simulation in the UP Position. Extraction of C_{UP}. Correction of Line Parameters

From the simulation in the up position, we can extract $\underline{Y}_{\mathrm{UP}}$ either from (5.19) or from (5.20). The results obtained (Fig.5.16) validate that for the up position a pure capacitive component

$$C_{\mathrm{UP}} = \frac{\Im(\underline{Y}_{\mathrm{UP}})}{\omega}. \tag{5.21}$$

can be used.

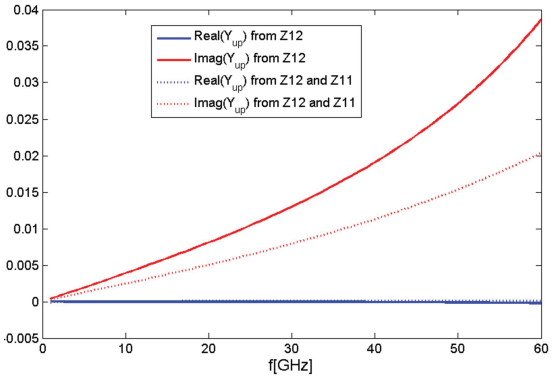

Figure 5.16: Dependence of Y_{UP} with respect to the frequency

A specific value is obtained by averaging it over the frequency range (Fig.5.17). But with this value of the capacitance, the line parameters can be recomputed (improved), by using again the implicit dependence in (5.19) and (5.20).

The final simulation of this compact model for the Up position S_{11} is shown in Fig.5.18 and S_{21} in Fig.5.19. The relative errors obtained are given in Table 5.3.

C. Simulation in the Down Position

From the simulation in the down position, we can extract $\underline{Y}_{\mathrm{DOWN}}$ either from (5.19) or from (5.20). The results obtained for QIAN (Fig5.20) and IMT (Fig.5.21) structures,

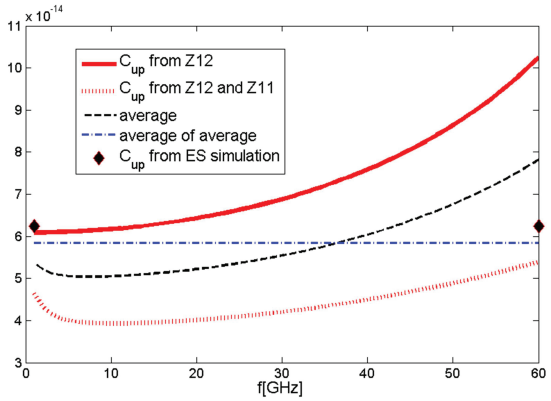

Figure 5.17: UP position, the capacitance extraction

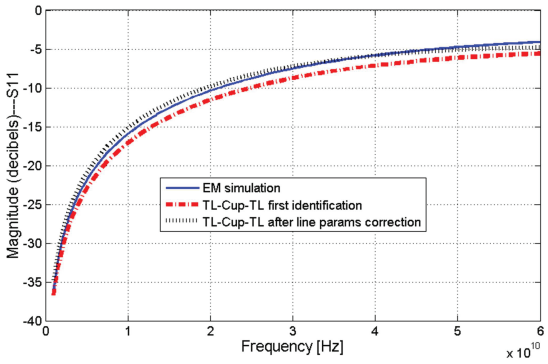

Figure 5.18: QIAN: UP position, EM results vs. macro-model results: Reflection loss S_{11}.

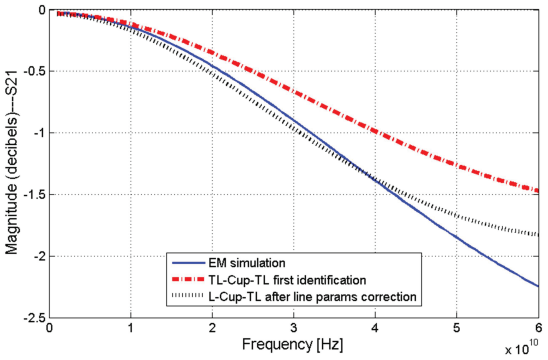

Figure 5.19: QIAN: UP position, EM results vs. macro-model results: Insertion loss S_{21}.

Table 5.3: Relative Errors in S Parameters.

	DOWN, first approx.	DOWN, after line params correction	UP with const. L_{mem}	UP with freq.dep. L_{mem}
QIAN	8.5 %	2.8 %	8.1 %	2.5 %
IMT	13 %	4.2 %	7.1 %	7.1 %

validate that for QIAN switch in the DOWN position a series $R-L-C$ configuration is needed due to the resonance frequency ω_0 that can be identified, whereas for the IMT switch an inductive behavior can be noticed, so that a $R-L$ modeling is appropriate. In this case the differences in the values obtained are much less relevant than in the UP position.

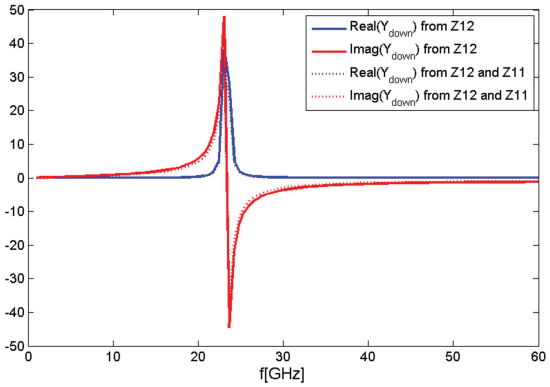

Figure 5.20: QIAN: Dependence of Y_{DOWN} with respect to the frequency. $R-L-C$ behavior.

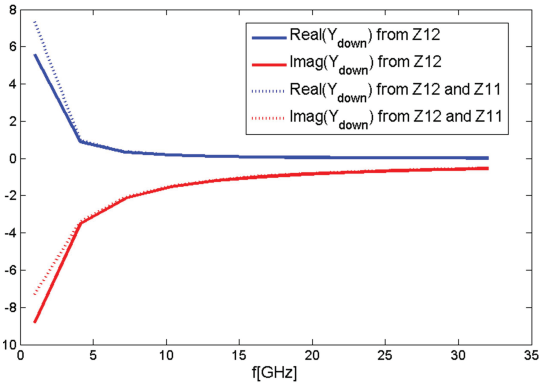

Figure 5.21: IMT: Dependence of Y_{DOWN} with respect to the frequency. $R-L$ behavior

The resistance of the membrane is computed as

$$R_{\mathrm{mem}} = \Re(1/Y_{\mathrm{DOWN}}). \tag{5.22}$$

The result is shown in Fig.5.22, and the average value over the frequency range was taken.

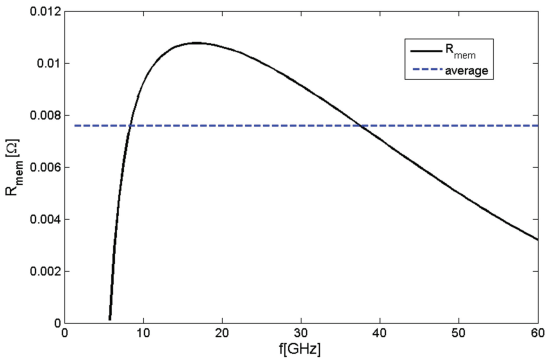

Figure 5.22: QIAN: Extraction of the membrane resistance R_{mem}.

Having identified the resonance frequency, the down capacitance can be computed as

$$C_{\mathrm{DOWN}} = \frac{\omega^2/\omega_0^2 - 1}{\Im(1/Y_{\mathrm{DOWN}})}. \tag{5.23}$$

The result is shown in Fig.5.23 and an average value was considered.

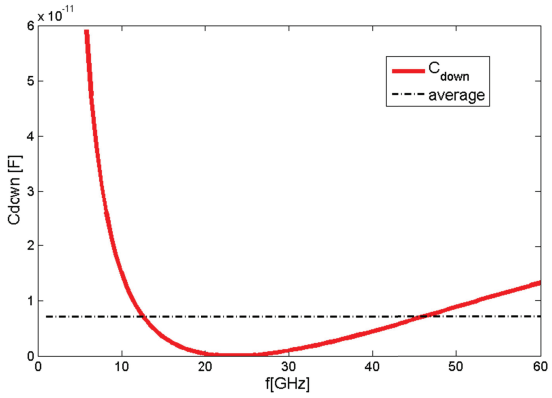

Figure 5.23: QIAN: Extraction of DOWN position capacitance C_{DOWN}.

Finally, either a constant value of the inductivity can be computed as

$$L_{\mathrm{mem}} = \frac{1}{\omega_0^2 C_{\mathrm{DOWN}}}, \tag{5.24}$$

or, a frequency dependent inductivity can be identified as (Fig.5.24)

$$L_{\mathrm{mem}} = \frac{1/(\omega C_{\mathrm{DOWN}}) + \Im(1/Y_{\mathrm{DOWN}})}{\omega}. \tag{5.25}$$

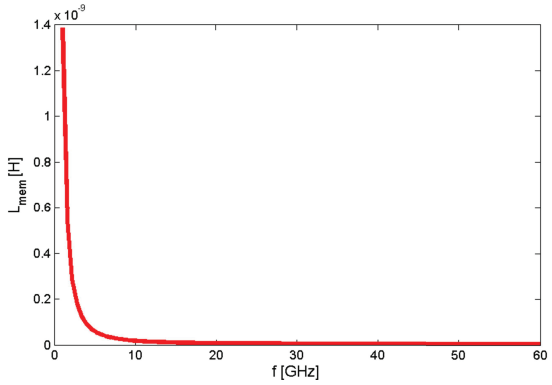

Figure 5.24: QIAN: Frequency dependent L_{mem} can be extracted.

For the IMT resistive switch, the identification is simpler (Fig.5.21),

$$L_{\mathrm{mem}} = \frac{\Im(1/Y_{\mathrm{DOWN}})}{\omega}. \tag{5.26}$$

The final simulation of the compact model for the QIAN benchmark in the DOWN position is shown in Fig.5.25 and reveals an error of 8.1 % in the case of constant inductivity for the switch and 2.5 % when a frequency dependent inductivity is used. In

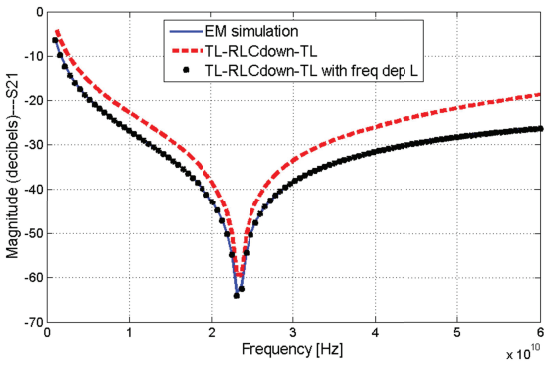

Figure 5.25: QIAN: Isolation S_{21} for the DOWN position: EM results vs. macro-model results

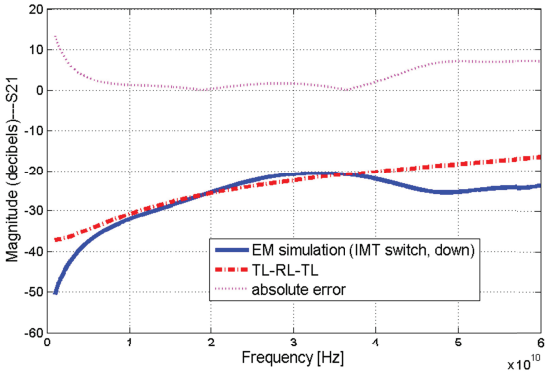

Figure 5.26: IMT: Isolation S_{21} for the DOWN position: EM results vs. macro-model results

the case of the IMT benchmark, result shown in Fig.5.25, there is no improvement if a frequency dependent inductivity is used, the relative error is 7.1 %.

The proposed algorithm was illustrated for a shunt switch but no conceptual difficulties are foreseen for series (inline) switches. For the QIAN structure, the modeling of the frequency dependence for the line parameters is not so important, but the modeling of the frequency dependence for the switch inductivity is relevant, the relative error in the S parameters decreasing from 8 % to 2.5 %. For the IMT Structure, which is a resistive one, the compact model is good but not as accurate as the QIAN results.

5.3.3 Compact Parametric RF Model

The method proposed in the previous section extracts the TL macro-model solely from three simulated frequency responses: one for the signal line alone, one for the switch in the passing through state and one for the switch in the blocking state. The characteristic parameters of the TL-lumped model are extracted by fitting. It is based on closed form expressions derived from the transmission lines theory, and it has the advantage that very few steps are required to obtain a relatively accurate RF macro-model. Moreover, the method allows naturally the inclusion of frequency dependence behavior, either in the transmission line parameters, or in the switch inductivity.

This section is an expanded version of the above method, in which the extraction procedure is modified so that a parametrized TL-lumped macro-model be obtained. To do this, not only the frequency response is computed from an RF simulation, but also

its sensitivity with respect to the parameter that varies, which is consequently used to compute the sensitivity of the lumped components of the macro-model.

In this section two test problems are studied: QIAN structure, which is a capacitive switch of bridge type, placed transversely with respect to the RF signal line, and another configuration, IMT2.5 structure, which is a resistive switch, with two actuation pads.

A MIMO distributed system with $(n-1)$ inputs and $(n-1)$ outputs may be properly defined to characterize the behavior of a device with n terminals. If a terminal is excited by current (voltage), then its voltage (current) is the output signal. Therefore, according to its excitation, the ECE is described by a frequency dependent, hybrid matrix. In particular, impedance $\underline{\mathbf{Z}}$ or admittance $\underline{\mathbf{Y}}$ matrices may be properly defined and extracted from the field solution.

To assembly the discrete state space system of a switch configuration, we use the Finite Integration Technique (FIT) to discretize the Maxwell equations [233].

When the variation of some parameters $\mathbf{p}$ is of interest, the MIMO system discretized above can be parameterized, a parametric time-domain model being obtained:

$$\mathbf{C}(\mathbf{p})\,\frac{\mathrm{d}\mathbf{x}(t)}{\mathrm{d}t} + \mathbf{G}(\mathbf{p})\mathbf{x}(t) = \mathbf{B}\mathbf{u}(t), \qquad \mathbf{y}(t) = \mathbf{L}\mathbf{x}(t), \tag{5.27}$$

where $\mathbf{x}(t)$ is the state space vector, consisting of electric voltages defined on the electric grid used by FIT, magnetic voltages defined on the magnetic grid and output quantities $\mathbf{y}$. Equations can be written such that only two semi-state space matrices ($\mathbf{C}$ and $\mathbf{G}$) are affected by the parameters $\mathbf{p}$. The input quantities $\mathbf{u}$ and the output quantities $\mathbf{y}$ are solely related to the terminals.

In the frequency domain, the complex representation of the output quantity can be expressed as

$$\underline{\mathbf{y}}(\mathbf{p}) = \mathbf{L}(j\omega\mathbf{C}(\mathbf{p}) + \mathbf{G}(\mathbf{p}))^{-1}\mathbf{B}\underline{\mathbf{u}}. \tag{5.28}$$

The computation of the sensitivities of the matrices $\mathbf{C}$ and $\mathbf{G}$ is straightforward into a FIT implementation since only the cells that are affected by the parameter that varies contribute to them [234].

The sensitivity of the output quantity with respect to one parameter p can be computed from the sensitivities of the state space matrices as

$$\frac{\partial\underline{\mathbf{y}}}{\partial p} = \mathbf{L}\frac{\partial\underline{\mathbf{x}}}{\partial p} \tag{5.29}$$

where

$$\frac{\partial\underline{\mathbf{x}}}{\partial p} = -(j\omega\mathbf{C} + \mathbf{G})^{-1}\left[\left(j\omega\frac{\partial\mathbf{C}}{\partial p} + \frac{\partial\mathbf{G}}{\partial p}\right)\underline{\mathbf{x}}\right] \tag{5.30}$$

and

$$\underline{\mathbf{x}} = (j\omega\mathbf{C} + \mathbf{G})^{-1}\mathbf{B}\underline{\mathbf{u}}. \tag{5.31}$$

All terminals are excited in voltage, and thus, the input-output transfer matrix is an admittance matrix $\underline{\mathbf{Y}}$, where

$$\underline{\mathbf{y}} = \underline{\mathbf{Y}}\,\underline{\mathbf{u}}. \tag{5.32}$$

Once the sensitivity $\partial\underline{\mathbf{Y}}/\partial p$ of the admittance is computed, the sensitivity of the impedance matrix can be derived as

$$\frac{\partial\underline{\mathbf{Z}}}{\partial p} = -\underline{\mathbf{Z}}\frac{\partial\underline{\mathbf{Y}}}{\partial p}\underline{\mathbf{Z}}. \tag{5.33}$$

Moreover, if the scattering parameters are defined as $\underline{\mathbf{S}} = (\underline{\mathbf{Z}} - Z_0\mathbf{I})(\underline{\mathbf{Z}} + Z_0\mathbf{I})^{-1}$ then their sensitivity is

$$\frac{\partial\underline{\mathbf{S}}}{\partial p} = (\underline{\mathbf{S}} - \mathbf{I})\frac{\partial\underline{\mathbf{Z}}}{\partial p}(\underline{\mathbf{Z}} + Z_0\mathbf{I})^{-1}. \tag{5.34}$$

Closed-form relationships for the TL-lumped macro-model of the switch can be derived by using transmission lines theory, as shown in the previous section.

By combining topological constraints with the relationships from the TLs theory and if we denote by $\underline{\mathbf{Z}}$ the transfer complex impedance

$$\begin{bmatrix} \underline{U}_1 \\ \underline{U}_2 \end{bmatrix} = \underline{\mathbf{Z}} \begin{bmatrix} \underline{I}_1 \\ -\underline{I}_2 \end{bmatrix}, \tag{5.35}$$

then, by some algebraic computations, the components of this complex, symmetric, impedance matrix can be derived:

$$\begin{array}{rcl} \underline{Z}_{ii} & = & \frac{\sinh^2(\gamma l)+\underline{Z}_c\underline{Y}\sinh(\gamma l)\cosh(\gamma l)+\cosh^2(\gamma l)}{\Delta} \\ \underline{Z}_{ij} & = & \frac{1}{\Delta}, \end{array} \tag{5.36}$$

where $i, j \in \{1, 2\}, i \neq j$ and

$$\Delta = \frac{2}{\underline{Z}_c}\sinh(\gamma l)\cosh(\gamma l) + \underline{Y}\cosh^2(\gamma l). \tag{5.37}$$

Equations (5.36) and (5.37) can be used for the computation of the frequency response for a known compact model. Moreover, if the frequency response and the line parameters are known, the complex admittance $\underline{Y}$ can be computed either as

$$\underline{Y} = \frac{1}{\underline{Z}_c\sinh(\gamma l)\cosh(\gamma l)}\left(\frac{\underline{Z}_{ii}}{\underline{Z}_{ij}} - \sinh^2(\gamma l) - \cosh^2(\gamma l)\right), \tag{5.38}$$

or as

$$\underline{Y} = \frac{1}{\cosh^2(\gamma l)}\left(\frac{1}{\underline{Z}_{ij}} - \frac{2}{\underline{Z}_c}\sinh(\gamma l)\cosh(\gamma l)\right). \tag{5.39}$$

In the previous method relationships (5.36) and (5.37) are also used to correct the per unit length parameters knowing the frequency response and the switch admittance $\underline{Y}$, but this correction is not appropriate for a parametric model, since in this case the parameter p will influence the line parameters as well. That is why, in this paper we have modified the extraction algorithm so that its parametrization affects only the switch admittance $\underline{Y}$.

If we take the derivative of (5.38) and (5.39) with respect to the parameter p, it follows that the sensitivity of the switch admittance $\underline{Y}$ can be computed from the sensitivity of the terminal impedance matrix either as

$$\frac{\partial\underline{Y}}{\partial p} = \frac{1}{\underline{Z}_c\sinh(\gamma l)\cosh(\gamma l)}\frac{\partial}{\partial p}\left(\frac{\underline{Z}_{ii}}{\underline{Z}_{ij}}\right), \tag{5.40}$$

or as

$$\frac{\partial \underline{Y}}{\partial p} = \frac{1}{\cosh^2(\gamma l)} \frac{\partial}{\partial p} \left(\frac{1}{\underline{Z}_{ij}} \right). \tag{5.41}$$

In this algorithm the frequency responses are obtained from EM field simulation, and therefore it is expected that there are some differences between the results obtained with (5.38) and (5.39) and with (5.40) and (5.41). These differences are a measure of the quality of the extracted TL-Y-TL scheme.

The extraction algorithm we propose is based on three RF simulations: the lines alone, switch in the down position and switch in the up position. For the last two cases, not only the frequency responses are computed, but also their sensitivities with respect to the parameter that varies.

From the simulations of the line alone, the frequency dependence of the line parameters are obtained (from equations (5.36) and (5.37), with $\underline{Y} = 0$, derive γ and $\underline{Z}_c$ and from here the line parameters). Next, we take an average value of the line parameters for the frequency range of interest, since the relative error in the reconstruction of the frequency response is less than 1 %.

Alternatively, the line parameters can be derived by solving two complementary field problems: one 2D, electroquasistatic, to derive the transversal line parameters (line conductance and capacitance) and one 2D full wave transversal magnetic, to derive the longitudinal line parameters (line resistance and inductance), as explained in [235].

From the simulation in the UP position, we extract $\underline{Y}_{\mathrm{UP}}$ both from (5.36) and (5.37) and take their average value. The imaginary part of the admittance is always positive and much greater than the real part, which implies that a pure capacitive component $\underline{C}_{\mathrm{up}}$ can be used to model the admittance. Since

$$\Im(\underline{Y}_{\mathrm{UP}}) = \omega \underline{C}_{\mathrm{UP}}, \tag{5.42}$$

a first order least square is carried out for the values of the imaginary part of the extracted admittance, with respect to the frequency, and find $\underline{C}_{\mathrm{UP}}$.

Using the sensitivities extracted during the RF simulation, we extract the sensitivity $\partial(\underline{Y}_{\mathrm{UP}})/\partial p$ both from (5.40) and (5.41) and take their average value. Finally, since

$$\frac{\partial \Im(\underline{Y}_{\mathrm{UP}})}{\partial p} = \omega \frac{\partial \underline{C}_{\mathrm{UP}}}{\partial p}, \tag{5.43}$$

a first order least square is carried out for the values of the extracted sensitivity of the admittance, with respect to the frequency and find $\partial \underline{C}_{\mathrm{UP}}/\partial p$.

From the simulation in the DOWN position, we extract $\underline{Y}_{\mathrm{DOWN}}$ both from (5.36) and (5.37) and take their average value.

Resistive switch: IMT2.5

In the case of a resistive switch, the imaginary part of the inverse of the admittance is always positive, which implies that a R-L series connection can be used to model the

admittance. Since

$$\Im\left(1/\underline{Y}_{\mathrm{UP}}\right) = \omega \underline{L}_{\mathrm{DOWN}}, \tag{5.44}$$

$$\Re\left(1/\underline{Y}_{\mathrm{UP}}\right) = \underline{R}_{\mathrm{DOWN}}, \tag{5.45}$$

a first order least square is carried out for the imaginary values of the extracted impedance, with respect to the frequency, and find $\underline{L}_{\mathrm{DOWN}}$ and an average of the real part of the extracted impedance is computed to find $\underline{R}_{\mathrm{DOWN}}$.

Using the sensitivities extracted during the RF simulation, we extract the sensitivity $\partial(\underline{Y}_{\mathrm{DOWN}})/\partial p$ both from (5.40) and (5.41) and take their average value. Finally, since

$$\frac{\partial}{\partial p}\left(\Im\left(1/\underline{Y}_{\mathrm{UP}}\right)\right) = \omega \frac{\partial \underline{L}_{\mathrm{DOWN}}}{\partial p}, \tag{5.46}$$

$$\frac{\partial}{\partial p}\left(\Re\left(1/\underline{Y}_{\mathrm{UP}}\right)\right) = \frac{\partial \underline{R}_{\mathrm{DOWN}}}{\partial p}, \tag{5.47}$$

a first order least square is carried out for the values of the extracted sensitivity of the switch impedance, with respect to the frequency and find $\partial \underline{L}_{\mathrm{DOWN}}/\partial p$ and an average is computed to find $\partial \underline{R}_{\mathrm{DOWN}}/\partial p$

Capacitive switch: QIAN

In the case of a capacitive switch, a resonance can be noticed, which implies that a R-L-C series connection can be used to model the admittance. The previous method used an algorithm based on the identification of the resonance frequency, but this algorithm is not suitable for parametrization. That is why, we have tested other two possibilities to extract the lumped values and their sensitivities.

- *Rational approximation based on Vector Fitting*

One possibility tested is to use a rational approximation obtained by using the Vector Fitting (VF) method [236, 237, 238, 239]. Since we are looking for a R-L-C series connection, the approximation $\underline{Y} \approx \underline{Y}_{\mathrm{VF}}$ searched for is of order two, strictly proper

$$\underline{Y}_{\mathrm{VF}} = \underline{Y}_{\infty} + \frac{k_1}{j\omega - p_1} + \frac{k_2}{j\omega - p_2}, \tag{5.48}$$

where the poles and residues are complex conjugate, and ideally, we would like to have $\underline{Y}_{\infty}$ negligible with respect to $\underline{Y}$. By mapping this expression with the admittance of a R-L-C series connection, it follows that

$$\begin{aligned} C_{\mathrm{DOWN}} &= \frac{k_1 + k_2}{p_1 p_2} = \frac{2\Re(k_1)}{|p_1|^2}, \\ L_{\mathrm{DOWN}} &= \frac{1}{k_1 + k_2} = \frac{1}{2\Re(k_1)}, \\ R_{\mathrm{DOWN}} &= -\frac{p_1 + p_2}{k_1 + k_2} = -\frac{\Re(p_1)}{\Re(k_1)}. \end{aligned} \tag{5.49}$$

The sensitivities of the lumped parameters thus extracted can be computed if we take the derivative with respect to the parameter that varies of (5.48), we write this relationship for all frequencies and solve an overdetermined system in the least square sense, and thus obtain the sensitivities of the poles and residue. These sensitivities are needed to compute the sensitivities of the lumped parameters given by (5.49).

- *Solving a least square problem*

The second possibility tested is based on the expression of the admittance of an R-L-C series connection, which leads to

$$(j\omega)^2 LC\underline{Y} + (j\omega)RC\underline{Y} - j\omega C = -\underline{Y} \tag{5.50}$$

If we denote the unknowns $a = LC$, $b = RC$, $c = C$, it follows that

$$\begin{aligned} (\omega^2\Re(\underline{Y}))a + (\omega\Im(\underline{Y}))b &= \Re(\underline{Y}), & (5.51)\\ (\omega^2\Im(\underline{Y}))a + (-\omega\Re(\underline{Y}))b + \omega c &= \Im(\underline{Y}) & (5.52) \end{aligned}$$

Equations (5.51) and (5.52) are written for all the solved frequencies, and the system is solved in the least square sense to find a, b, c. The lumped parameters in the down position are

$$C_{\text{DOWN}} = c, \quad L_{\text{DOWN}} = b/c, \quad R_{\text{DOWN}} = a/c. \tag{5.53}$$

The sensitivities $a' = \partial a/\partial p$, $b' = \partial b/\partial p$, $c' = \partial c/\partial p$ can be computed if we take the derivatives of (5.51) and (5.52):

$$\begin{aligned} (\omega^2\Re(\underline{Y}))a' + (\omega\Im(\underline{Y}))b' &= \Re(\underline{Y}') - \omega^2\Re(\underline{Y}')a - \omega\Im(\underline{Y}')b,\\ (\omega^2\Im(\underline{Y}))a' - (\omega\Re(\underline{Y}))b' + \omega c' &= \Im(\underline{Y}') - \omega^2\Im(\underline{Y}')a + \omega\Re(\underline{Y}')b, \end{aligned} \tag{5.54}$$

where $\Re(\underline{Y}')$ and $\Im(\underline{Y}')$ are the real and imaginary parts of the sensitivities of the switch admittance, computed as the average of (5.40) and (5.41).

5.3.4 Numerical Results - RF Compact Parametric Models

Capacitive switch: QIAN

The parameter that varies is the membrane width, having a nominal value of $w_0 = 120\,\mu$m. In order to validate the algorithm, four other EM simulation were carried out, for $w \in \{80, 100, 140, 160\}\mu$m.

Fig.5.27 illustrates the extraction of the up capacitance by least square approximation of the average imaginary part of the extracted admittance. The comparison between the macro-model S parameters and those of EM simulation is shown in Fig.5.28.The relative errors reported in this section are computed as the root mean square of the difference between the analyzed characteristic and the reference characteristic over the maximum value of the reference. For the UP position, the error with respect to the reference macro-model obtained by simulation of the TL-Y_{average}-TL model decreased from 4.7 % to 4.0 %, which means a slight improvement with respect to previous results.

Table 5.4: Relative errors in S obtained - UP position

Algorithm	Error wrt the initial UP file	Error w.r.t to the reconstructed TL-Ymed-TL
Old (average)	7.8 %	4.7 %
New (LS)	8.0 %	4.0 %

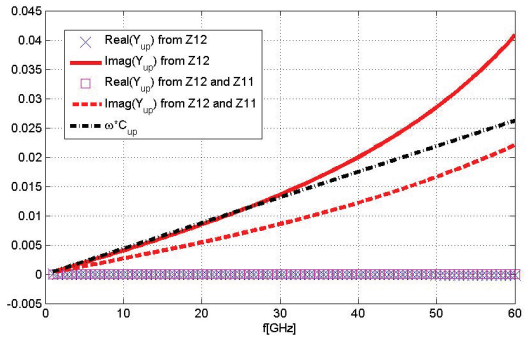

Figure 5.27: Extraction of C_{UP}.

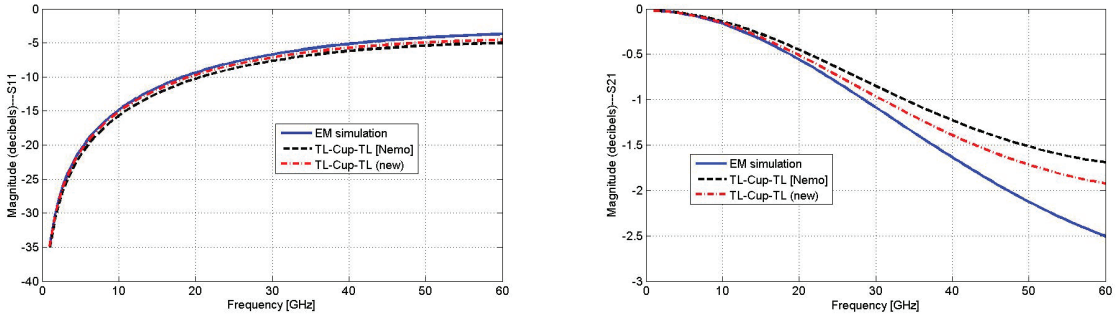

Figure 5.28: QIAN UP position, EM results vs. macro-model results: reflection loss S_{11} and insertion loss S_{21}

Results shown in Figs.5.29 and 5.30 validate the procedure that computes the sensitivities from the EM simulation. In Fig.5.29 the sensitivity is the slope of the straight line that is tangent to the curve obtained only with EM simulations. Fig.5.30 displays the parameter impact on S. It is interesting to note that quite large variation of the membrane width have a low impact on S.

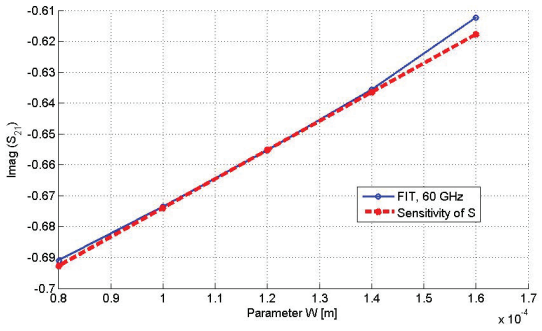

Figure 5.29: QIAN UP position: validation of the sensitivity computations from FIT.

Fig.5.31 shows the dependence of the extracted up capacitance with respect to the membrane width. It validates that a first order series Taylor expansion can be used for the up capacitance in the macro-model. The sensitivity computed by finite differences is $2.73 \cdot 10^{-4}$ pF/μm and matches well the sensitivity computed as explained before, which is $2.69 \cdot 10^{-4}$ pF/μm.

Table 5.5 holds the sensitivity results, computed either by simply taking numerical

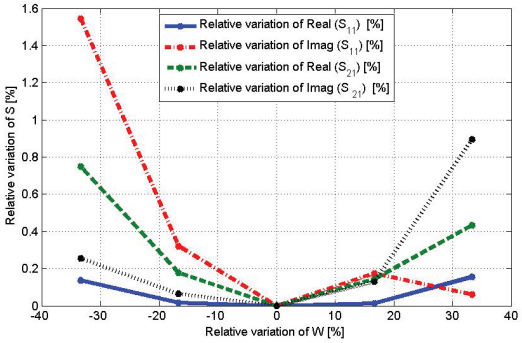

Figure 5.30: QIAN UP position: parameter impact on S.

derivatives or by applying the procedure described before.

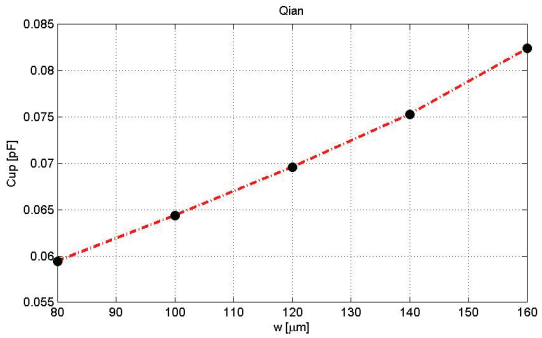

Figure 5.31: QIAN UP position: dependence of the extracted UP capacitance on the membrane width.

Table 5.5: Sensitivity of C_{UP}

	Finite differences	Computed
$\partial C_{\mathrm{UP}}/\partial w$ [pF/μm]	$2.73 \cdot 10^{-4}$	$2.69 \cdot 10^{-4}$

The validation of the parametric model is done by comparing the simulation of parametric macro-model for a value of the parameter which is not nominal with the macro-model extracted from the EM simulation for that non-nominal value. For instance, for $w = 100$ μm, the relative error between the macro-model having

$$C_{\mathrm{UP}}(w) = C_{\mathrm{UP}}(w_0) + \frac{\partial C_{\mathrm{UP}}}{\partial w}(w - w_0) \tag{5.55}$$

and the reference macro-model is 0.12 %.

Fig.5.32 shows the result of the down admittance extraction. The comparison between the macro-model results and the EM simulation is shown in Fig. 5.33 and the relative errors reported in Table 5.6 show that a certain improvement can be seen with respect to the previous algorithm.

Figs.5.34 and 5.35 show results that validate the procedure that computes the sensitivities from the EM simulation in the DOWN position. The RF characteristic in the DOWN position is much more dependent on the width variation, than in the UP position.

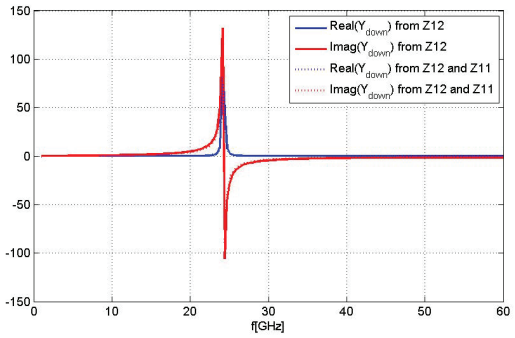

Figure 5.32: Extraction of DOWN position admittance $\underline{Y}_{\mathrm{DOWN}}$.

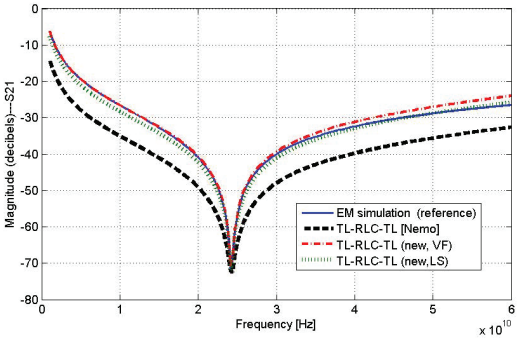

Figure 5.33: QIAN DOWN position: EM results vs. macro-model results: isolation S_{21}.

Table 5.6: Relative errors in S obtained - DOWN position

Algorithm	Error w.r.t. the initial DOWN file	Error w.r.t. to the reconstructed TL-Yaverage-TL
Ref.[240]	12.9 %	6.8 %
New (VF)	12.8 %	1.1 %
New (LS)	12.4%	2.3 %

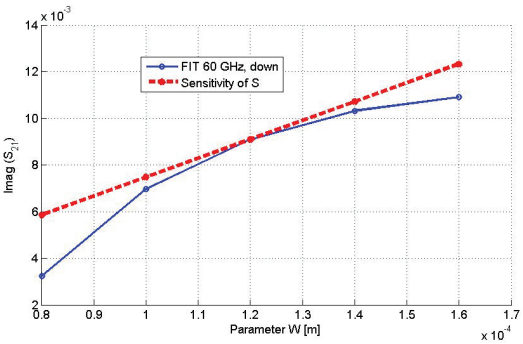

Figure 5.34: QIAN DOWN position: validation of the sensitivity computations from FIT.

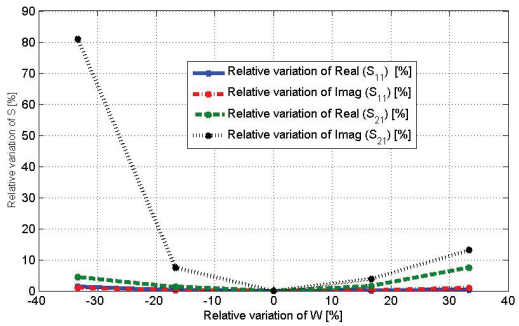

Figure 5.35: QIAN DOWN position: parameter impact on S.

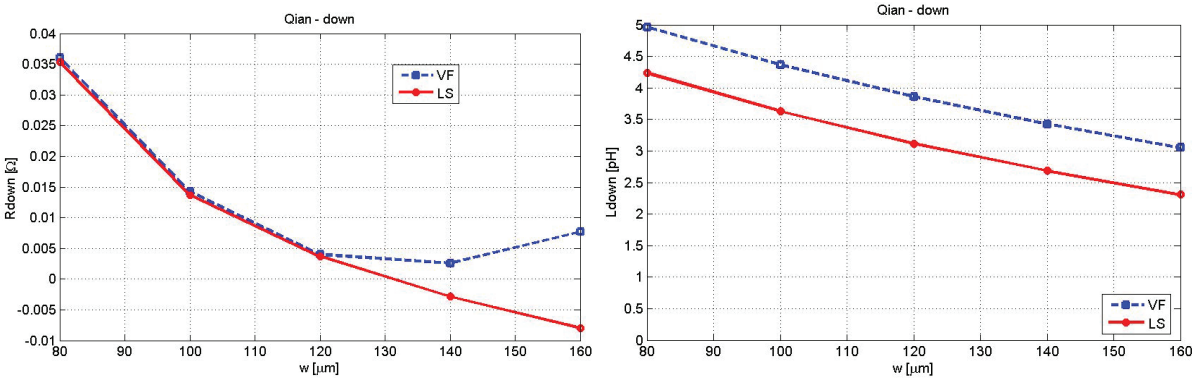

Figure 5.36: QIAN DOWN position: dependence of the extracted DOWN resistance on the membrane width – Left; dependence of the extracted DOWN inductance on the membrane width – Right.

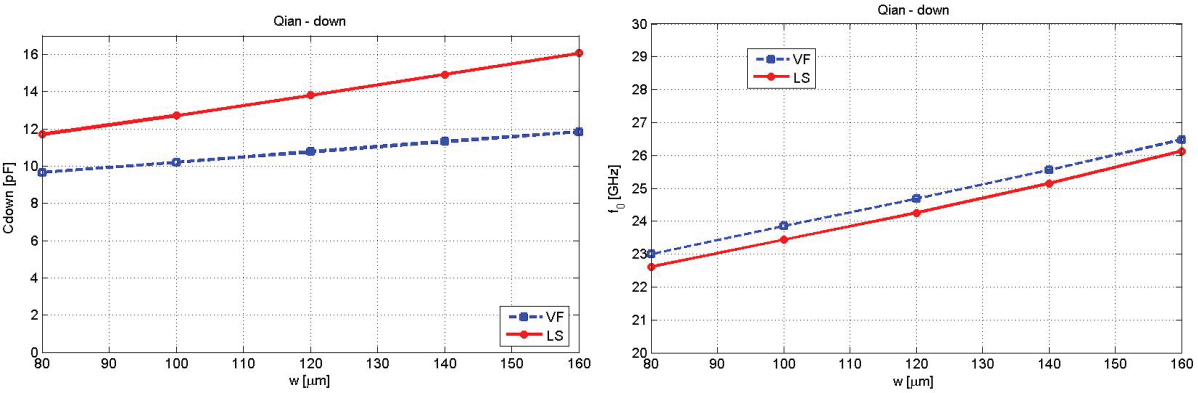

Figure 5.37: QIAN DOWN position: dependence of the extracted DOWN capacitance on the membrane width – Left; dependence of the resonance frequency on the membrane width – Right.

Figs. 5.36 and 5.37 show the dependence of the extracted DOWN resistance, inductance, capacitance and resonance frequency with respect to the membrane width. It validates that a first order series Taylor expansion can be used for the DOWN capacitance in the macro-model. For the resistance and the inductance, a first order series Taylor expansion for their reciprocal values can be a better option. It is interesting to note that the use of vector fitting might lead to an unexpected behavior. This is due to the fact that a passivity enforcement is carried out during the fitting, whereas the algorithm based on least square provides more reasonable dependence, but the extracted resistance is negative. The quality of the VF results is very much dependent on the number of frequency points used. In some cases, some results that may seem odd can be obtained, case in which the constant term $\underline{Y}_\infty$ in (5.48) has to be checked. If it is not negligible with respect to the switch admittance, it means that the R-L-C model is not enough, and a conductance has to be added in parallel.

Table 5.7 holds the sensitivity results which show a good agreement of the sensitivities computed by simply taking numerical derivatives with those obtained with the procedure described before.

Table 5.7: Sensitivities in the DOWN position

	Finite differences (c)=centered (b)=backward	Computed
$\partial C_{\mathrm{DOWN}}/\partial w$ [pF/μm] (VF)	$2.81 \cdot 10^{-2}$ (c)	$2.77 \cdot 10^{-2}$
(LS)	$5.53 \cdot 10^{-2}$ (c)	$5.11 \cdot 10^{-2}$
$\partial R_{\mathrm{DOWN}}/\partial w$ [mΩ/μm] (VF)	$-5.15 \cdot 10^{-1}$ (b)	$-3.90 \cdot 10^{-1}$
(LS)	$-4.14 \cdot 10^{-1}$ (c)	$-3.24 \cdot 10^{-1}$
$\partial L_{\mathrm{DOWN}}/\partial w$ [pF/μm] (VF)	$-2.73 \cdot 10^{-2}$ (c)	$-2.27 \cdot 10^{-2}$
(LS)	$-2.36 \cdot 10^{-2}$ (c)	$-2.31 \cdot 10^{-2}$
$\partial f_0/\partial w$ [GHz/μm] (VF)	$4.24 \cdot 10^{-2}$ (c)	$4.07 \cdot 10^{-2}$
(LS)	$4.28 \cdot 10^{-2}$ (c)	$4.49 \cdot 10^{-2}$

The validation of the parametric model is done by comparing the simulation of parametric macro-model for a value of the parameter which is not nominal with the macro-model extracted from the EM simulation for that non-nominal value. For instance, for $w = 100$ μm, the relative error between the LS macro-model having first order Taylor series expansions for $C_{\mathrm{down}}(w)$, $L_{\mathrm{down}}(w)$ and $R_{\mathrm{down}}(w)$:

$$C_{\mathrm{DOWN}}(w) = C_{\mathrm{DOWN}}(w_0) + \frac{\partial C_{\mathrm{DOWN}}}{\partial w}(w - w_0), \tag{5.56}$$

$$L_{\mathrm{DOWN}}(w) = L_{\mathrm{DOWN}}(w_0) + \frac{\partial L_{\mathrm{DOWN}}}{\partial w}(w - w_0), \tag{5.57}$$

$$R_{\mathrm{DOWN}}(w) = R_{\mathrm{DOWN}}(w_0) + \frac{\partial R_{\mathrm{DOWN}}}{\partial w}(w - w_0), \tag{5.58}$$

$$\tag{5.59}$$

and the reference macro-model is 1.12 % and the relative error between the macro-model

having first order Taylor series expansions for $C_{\mathrm{DOWN}}(w)$, $1/L_{\mathrm{DOWN}}(w)$ and $1/R_{\mathrm{DOWN}}(w)$:

$$C_{\mathrm{DOWN}}(w) = C_{\mathrm{DOWN}}(w_0) + \frac{\partial C_{\mathrm{DOWN}}}{\partial w}(w - w_0), \tag{5.60}$$

$$1/L_{\mathrm{DOWN}}(w) = 1/L_{\mathrm{DOWN}}(w_0) + \frac{\partial (1/L_{\mathrm{DOWN}})}{\partial w}(w - w_0), \tag{5.61}$$

$$1/R_{\mathrm{DOWN}}(w) = 1/R_{\mathrm{DOWN}}(w_0) + \frac{\partial (1/R_{\mathrm{DOWN}})}{\partial w}(w - w_0), \tag{5.62}$$

$$\tag{5.63}$$

and the reference macro-model is 1.05 %. The improvement is not obvious, but according to physical considerations it is more appropriate for a broader range of the parameter variations. This parametric affine model based on first order sensitivities can be described by a SPICE circuit.

Resistive switch (IMT2.5)

Fig. 5.38 show the results obtained for the resistive switch in the UP position, for which measurements are available. To validate the simulations obtained with our in-house code (called *chamy*), CST® (www.cst.com) models have been also created and simulated both with the time domain and with the frequency domain solver. The accuracy of the macro-model depends on the accuracy of the EM model. The relative error between the macro-model and the reference macro-model is 3 %. Fig. 5.39 shows the extracted admittance of the switch for the down position, and validates its RL behavior. Fig. 5.40 show the frequency characteristic, the relative error between the macro-model and the reference macro-model being 1 %.

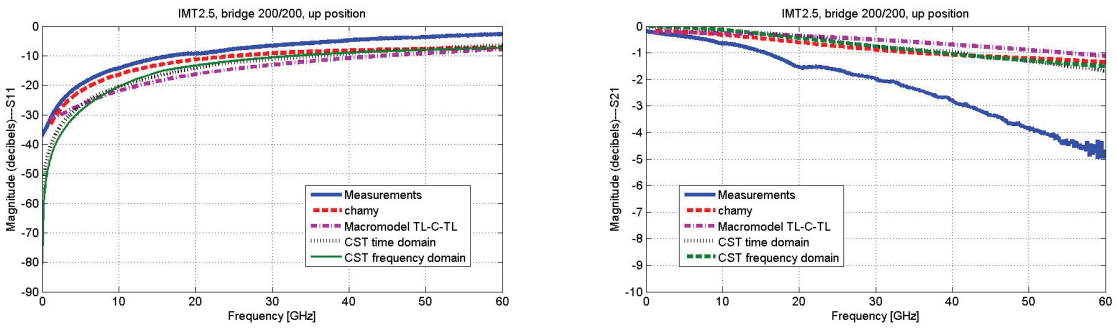

Figure 5.38: IMT2.5 switch: S_{11} and S_{21} results for the UP position.

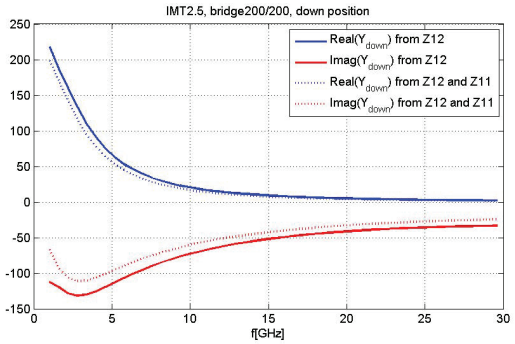

Figure 5.39: IMT2.5 switch: extraction of Y_{DOWN}.

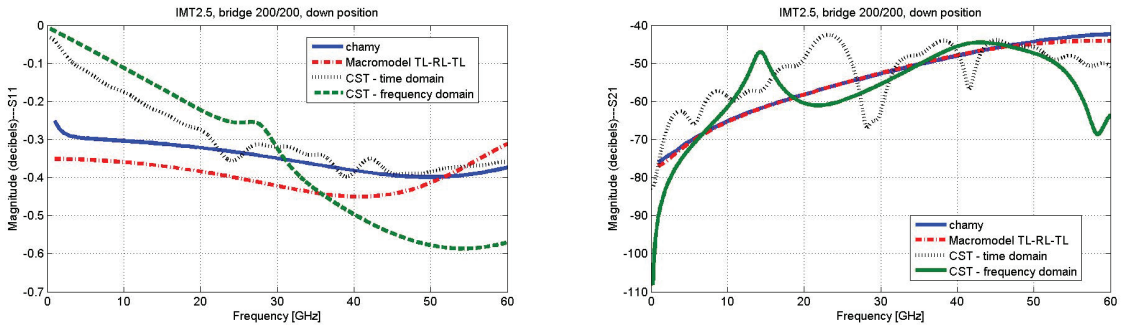

Figure 5.40: IMT2.5 switch: S_{11} and S_{21} results for the DOWN position.

In conclusion the parametric TL-lumped RF macro-models for MEMS switches can be extracted with a robust procedure from the solution of Maxwell equations with electromagnetic circuit element (ECE) boundary conditions in three cases: lines alone, UP and DOWN positions.

The main idea is based on the use of closed form relationships which allow a natural de-embedding of the RF results in order to compute the switch admittance, which is eventually fitted either with a capacitance in the UP position, or with a RL or RLC series connection in the DOWN position. Two fitting possibilities have been tested: one based on vector fitting and the other based on a simple least square approach. In some cases, the obtained values might not reflect physical phenomena, but for the capacitive switch tested, both methods predicted accurately the resonance frequency and its sensitivity.

If sensitivities of the port quantities are computed simultaneously with the EM solution, then they can be used to evaluate the sensitivities of the switch admittance and, consequently, the sensitivities of the lumped parameters. Thus, only RF computations for the nominal value of the design parameter are carried out, thus avoiding the need to re-mesh the problem for other values of the design parameters.

The proposed algorithm was illustrated for shunt switches but no conceptual difficulties are foreseen for series (inline) switches. The algorithm may easily incorporate the frequency dependence of line parameters if needed.

The parametric macro-models are very accurate (error less than 3 %) with respect to reference macro-models extracted from independent EM simulations.

5.4 Mixed Domain Coupled Macro-models

In order to describe the entire behavior of the switch, the complete compact model has to include both RF model and multiphysics- movement model (we will call it as a mixed macro-model). The RF signal lines are best described by transmission lines (TL) models with 1D distributed parameters, whereas for the switching part the components with RLC lumped parameters are used. The parameters extraction as it was presented before is based on the results obtained from three RF simulations carried at device-level model, with the finite integration technique, and use of a fitting procedure based on closed form relationships for the TL-lumped macro-model.

The SPICE equivalent circuit of mixed-coupled macro-model is obtained by simply replacing the switch capacitance in the RF schematic by a model that connects it with the multiphysics compact model, as in Fig.5.42. A fixed capacitance has been added in parallel with the parametric one. It corresponds to the electric field lines that close through the substrate, and it has been computed by a separate electrostatic problem for the substrate.The validation of the model built so far is done by comparing the RF results (S parameters) of the mixed schematic with the results from the EM simulation (Fig.5.41). A relative error of 2.5 % is obtained.

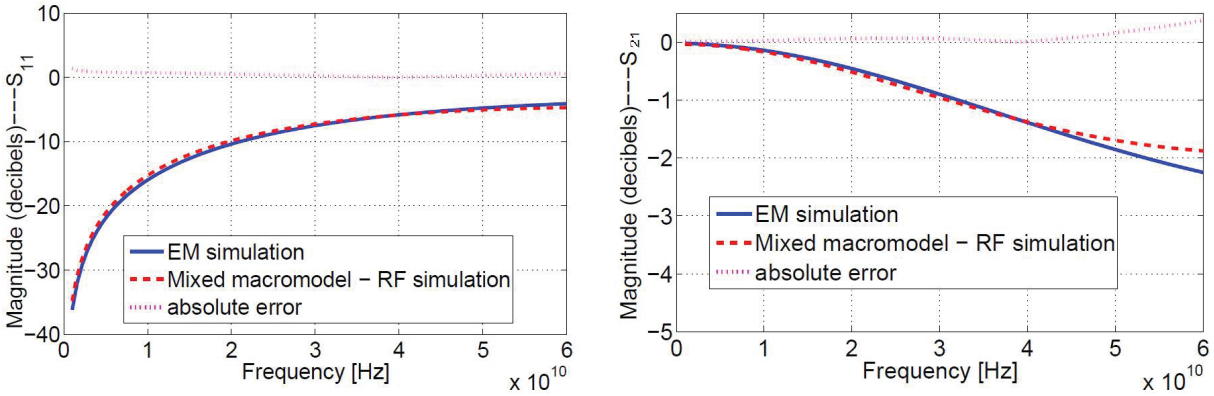

Figure 5.41: EM simulation vs. mixed macro-model RF simulation: left - return loss (S_{11} signal pass), right - insertion loss (S_{21}, signal pass).

The mixed macro-model of a RF-MEMS switch, with few degrees of freedom is extracted from several (FEM-FIT) numerical analysis of the device with distributed parameters (solving structural, fluid flow, electrostatic and full wave EM fields). All extracted parameters are combined into a single *netlist* model (circuit implemented in Spice , as in the annex A2), which is controlled by the MEMS actuation voltage and is excited with the RF signals. This model comprising two coupled circuits (one describing the movement is depicted in Fig.5.13 and other is the RF circuit from Fig.5.42) allows fast and accurate simulations of electro-mechanical and RF behavior of RF-MEMS switches under several excitations. These two circuits are mutually coupled by means of controlled sources. A relative error less than 3 % in the S parameters and less than 1 % in the pull-in voltage is obtained, which is very satisfactory given the low order imposed for the reduced model. This model is able to describe also the dynamics of mechanical movement, and if the a model for the contact is added, it is able to model the switching time also.

5.5 Conclusions

In this chapter a procedure with 14 steps for extraction of the effective m, b and k multiphysics coefficients and the RF compact model's parameters was developed and it is illustrated and validated for two study-case.

For the extraction of the effective elastic coefficient the averaging approaches behave worse than the analytical approach, and the cubic least square is able to recover not only a very accurate pull-in voltage (relative error less than 0.5 %), but the whole behavior of the displacement curve.

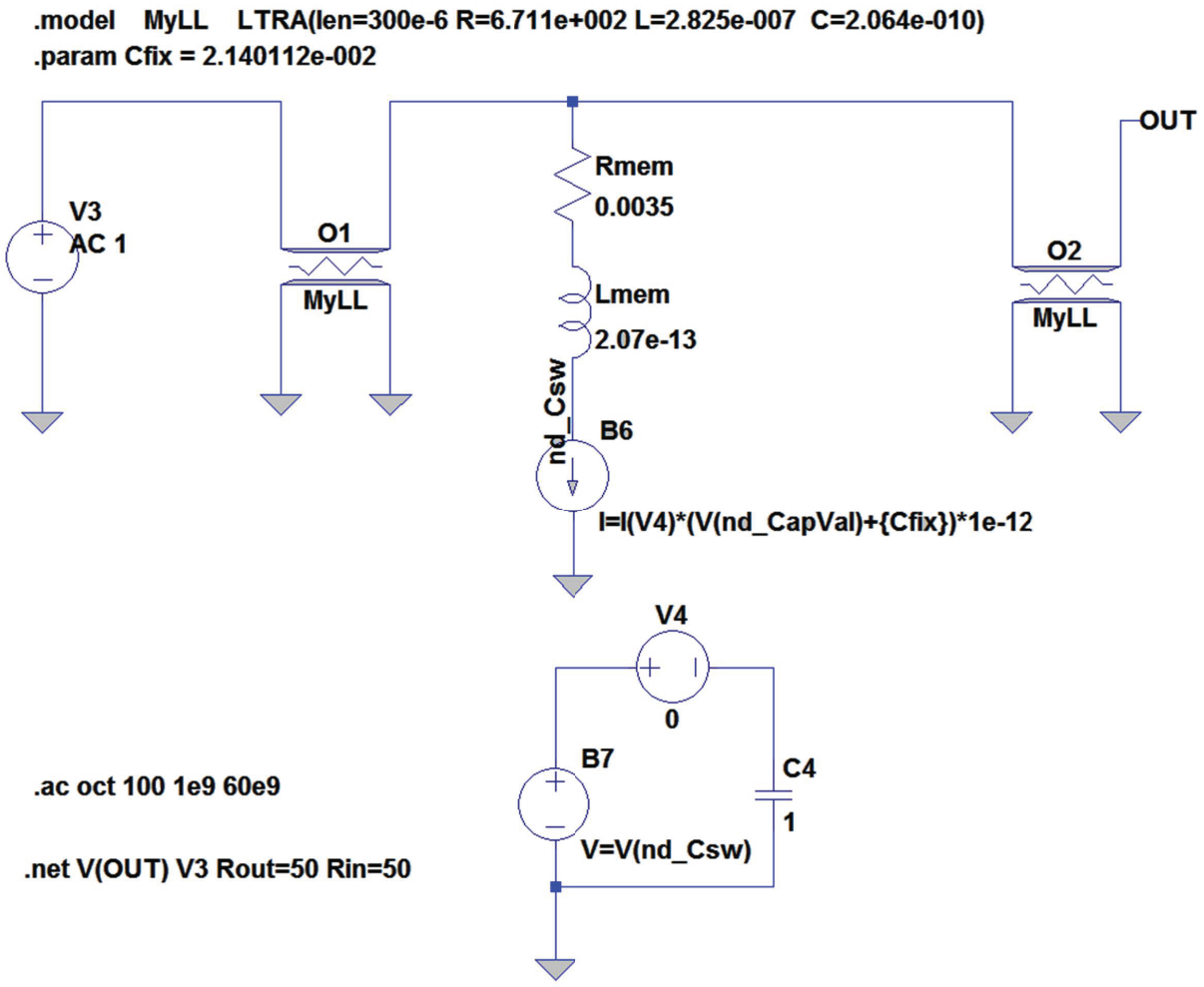

Figure 5.42: Mixed macro-model: the RF part, the switch model is a current source controlled by the capacitance value that is taken from the multiphysics part (voltage at node "n_CapVal" in the multiphysics part of the schematic).

By solving a three field coupled problem electrostatic-structural-fluid flow and by fitting of the relation the damping force - velocity is obtained the dumped coefficient is b = 2.710^6[Kg/s]. The dynamic answer of the macro-model as well as the reference answer obtained from the field simulation for the excitation of 5V step used do derive the lumped parameters (relative error is 0.19 %), as well as for an excitation of 6V step (error is 0.35%).

The frequency simulation of the RF compact model for the QIAN benchmark in the down position reveals an error of 8.1 % in the case of constant inductivity for the switch and 2.5 % when a frequency dependent inductivity is used. In the case of the IMT benchmark, there is no improvement if a frequency dependent inductivity is used, the relative error is 7.1 %.

A special attention is given to the parametric models of RF MEMS switches and their realization in SPICE. At the end of this chapter mixed macro-model of a RF-MEMS switch, with few degrees of freedom is extracted from several (FEM-FIT) numerical analysis of the device with distributed parameters (solving structural, fluid flow, electrostatic and full wave EM fields). All extracted parameters are combined into a single *netlist* model (circuit implemented in Spice), which is controlled by the MEMS actuation voltage and is excited with the RF signals. This model comprising two coupled circuits (one describing the movement is depicted in Fig.5.13 and other is the RF circuit from Fig.5.42) allows fast and accurate simulations of electro-mechanical and RF behavior of RF-MEMS switches under several excitations. A relative error less than 3 % in the S parameters and less than 1 % in the pull-in voltage is obtained, which is very satisfactory given the low order imposed for the reduced model.

The developed model was validated for the RF behavior point of view, by experimental means and by comparisons of SPICE simulation results with field simulations done by chamy/FIT, COMSOL/FEM, CST (in both frequency domain FIT-FD and time domain -FIT-TD) and HFSS/FEM.

Chapter 6

Final conclusions and original contributions

6.1 General Conclusions

RF-MEMS switches are very small mechanical devices built on semiconductor chips having the size less than one millimeter and therefore they are measured in micrometers that use mechanical movement to create a short circuit or an open circuit of the RF signal in the transmission lines. The growing demand for micro-fabricates having a superior energy performance, determined the reorientation of manufacturers to integrated circuits and hence the scientific community to the technology of micro-electro-mechanical systems, whose benefits, particularly in radio frequencies were highlighted in the last decade.

Modelling a device or a real system is an fundamental action of science and engineering, which consists in developing a series of abstract scientific and mathematical images and representations of the modelled object, or digital type-numeric representation of that object. Usually, precise models are more complicated and their extraction and simulation have a higher cost. Choosing the most appropriate model depends on the context and it reflects a compromise between the optimum accuracy and simplicity which are contradictory requirements. A parametric model describes the entire class of real, similar objects. The number of geometric parameter and/or material constants which allows the identification of the instance-object in the class defines the complexity of the parametric model.

Modelling of MEMS devices is an important issue, both theoretically and practically. This is because the modelling and simulation of these devices should take in consideration more physic phenomena, it is necessary, finally, a coupled modeling, more complicated, of multiphysics nature. Otherwise, the nowadays technology of integrated circuits production is unthinkable without a prior modelling, simulation and optimization of the new designed devices.

The design of this micro-electro-mechanical devices that operate at radio frequencies requires effective procedures for modelling and software capable of simulating coupled multiphysics models involving mechanical, electrical, thermic or fluid flow phenomena.

Research in the field of RF-MEMS is to develop at a cost as low as possible effective models with high accuracy, but to have a reduced complexity. Simulation and optimization of these models using computing machines, leads to the development of designs for MEMS devices with the best performance.

After the introduction were the main objectives of the thesis ware presented and the actuality and importance of the thesis subject was highlighted, in the first chapter the current state micro-electro-mechanical systems modelling was presented, the chapter contains a summary of the general concepts, then talks about the current state and the importance of the subjects also making a critical study of the publications from the recent years and prior research in this domain.

The second chapter is dedicated to a brief presentation of the theoretical concepts, knowledge and background on which the entire work is developed. In tihis chapter the open problems are formulated and the suitable research methodology is identified.

In the third chapter are presented the analytical and numerical modelling of the most simple 1D model which can be imagine for a RF-MEMS device, the similar of a parallel plane capacitor with one armature suspended from a spring. The fourth chapter focuses on the creation of numerical multiphysics and RF modelling. Static, dynamic and EM analysis were performed in order to compute the field-solution of the problems. The validation of the results was made using several software packages.

The fifth chapter presents the mixed macro-model of a RF-MEMS switch extracted from several (FEM-FIT) numerical analysis of the device with distributed parameters (solving structural, fluid flow, electrostatic and full wave EM fields) together with an effective 14 steps procedure of extraction of the effective m, b and k multiphysics coefficients and the RF compact model's parameters is presented. All extracted parameters are combined into a single *netlist* model (circuit implemented in Spice), which is controlled by the MEMS actuation voltage and is excited with the RF signals.

6.2 Original Contributions

1. Critical presentation a State of the Art in Modelling of RF-MEMS Devices;
2. The analysiss based on analytic-approximation of the simplest 1D model for RF MEMS switches. Development of 2D and 3D models for RF-MEMS device. The multiphysics models based on coupled Electrostatic, Structural and Fluid Flow phenomena were simulated and validated. Study of the influence of geometrical parameters on relevant characteristics of MEMS switches was carried out [241, 242, 243, 244, 245];
3. An efficient algorithm for extracting a compact model with multiphysics lumped parameters, validate by comparison with field solution [246, 247];
4. An efficient algorithm for extracting the lumped parameters for new compact reduced RF model for RF MEMS switches, validated with experimental and computational means [199, 248, 249, 250];

5. A hybrid Parametric Mixed Domain Macro-models of RF-MEMS switches that includes both a model for the RF signal lines and a multiphysics model for electromechanical behavior [251, 240].

These contributions were made by teamwork, especially in the ToMeMS research project coordinated by prof. Gabriela Ciuprina within LMN. As results from the list of 15 papers published by the author of the thesis, (first author on 4 of them) the original contributions are shared by the members of the research teams.

6.3 Future Research and Development

1. Development of new efficient modeling methodologies based on High Performance Computing Techniques.;
2. Problem formulation, modelling, simulation and analysis of coupled Electrostatic - Structural - Fluid Flow - Contact - RF phenomena for accurate MEMS 3D models;
3. Experimental characterization of RF MEMS for computational models validation;
4. Efficient extraction of parametrized MEMS macro-models and their including it into optimization loops;
5. Efficient optimization of RF-MEMS devices for their optimal design;
6. Development of new MEMS for bio-applications
7. Publication of the original results

6.4 Dissemination of the Results

1. Gabriela Ciuprina, **Aurel Sorin Lup** and Alina Tomescu, "Parametrii S în Aplicaţii de Înaltă Frecvenţă", Lucrările Simpozionului Naţional de Electrotehnică Teoretică, SNET2012, ISSN 2067-4147 (online), 6 pages.
2. Andreea Alexandru, **Sorin Lup** and Bogdan Dita, "GDS2M Preprocessing Tool for MEMS Devices" Proceedings of the 8th International Symposium on Advanced Topics in Electrical Engineering, ATEE2013, May 23-25, 2013, Bucharest, Romania, 4 pages, ISBN 978-1-4673-5978-8, Pages: 1 - 4, DOI: 10.1109 / ATEE.2013.656345, WOS: 000332928500105. This paper was awarder 3^{rd} place in the IEEE student paper competition.
3. **Aurel-Sorin Lup** and Gabriela Ciuprina, "Analysis of membrane perforations on the RF behavior of capacitive MEMS switches", Acta Electrotehnica, ISSN 1841-3323 vol. 54, no.5, pp. 252-255, 2013. - CNCSIS categoria B+ BDI VINITII (Russia), DOAJ (Sweden).
4. Gabriela Ciuprina, **Aurel-Sorin Lup**, Bogdan Dita, Daniel Ioan, Stefan Sorohan, Dragos Isvoranu and Sebastian Kula "Mixed Domain Macro-models for RF MEMS

Capacitive Switches", The 10th International Conference on Scientific Computing in Electrical Engineering, SCEE 2014, July 22 - July 25, 2014, Wuppertal, Germany, SCEE 2014 Proceedings, 8 pages (ISI-WOS).

5. **Aurel-Sorin Lup**, Gabriela Ciuprina and Stefan Sorohan, "Parametric Multiphysics Static Models for a Bridge Type MEMS Capacitive Switch", Conference Proceedings of 49th Universities' Power Engineering Conference - UPEC2014, 02-05/09/2014, Cluj-Napoca, Romania, Pages: 1-4, DOI:10.1109/UPEC.2014.6934635.

6. Sebastian Kula and **Aurel-Sorin Lup**, "Electrical schematics for 1d analysis of a bridge type MEMS capacitive switch", Computer Applications in Electrical Engineering, volume 12, pages 407-421, ISSN 1508-4248, ISBN 978-83-7775-352-1.

7. **Aurel-Sorin LUP** and Gabriela Ciuprina, "Extraction of effective elastic coefficient from a coupled structural electrostatic simulation of a MEMS switch", International Symposium on Fundamentals of Electrical Engineering 2014, ISFEE2014, NOVEMBER 28-29, 2014, Bucharest, Romania, Pages: 1 - 5, DOI: 10.1109/ISFEE.2014.7050539.

8. Ruxandra Barbulescu, **Aurel-Sorin Lup**, Gabriela Ciuprina, Daniel Ioan and A. Egemen Yilmaz, "Intelligent Particle Swarm Optimization of Superconducting Magnetic Energy Storage devices", International Symposium on Fundamentals of Electrical Engineering 2014, ISFEE2014, NOVEMBER 28-29, 2014, Bucharest, Romania, Pages: 1 - 4, DOI: 10.1109/ISFEE.2014.7050607.

9. Cosmin-Bogdan Dita, **Aurel-Sorin Lup** and Daniel Ioan, "Reduced order RF macromodel for a MEMS capacitive switch", The 9th International Symposium on Advanced Topics in Electrical Engineering, may 7-9, 2015, Bucharest, Romania, Pages: 436 - 441, IEEE Xplore, DOI: 10.1109/ATEE.2015.7133844, (ISI).

10. Mihai Popescu, **Aurel-Sorin Lup** and Daniel Ioan, "Data structures for coupled structural electrostatic modeling of MEMS Switch", The 9th International Symposium on Advanced Topics in Electrical Engineering, may 7-9, 2015 Bucharest, Romania, Pages: 448 - 451, IEEE Xplore, DOI: 10.1109/ATEE.2015.7133846, (ISI).

11. Gabriela Ciuprina, **Aurel-Sorin Lup**, Daniel Ioan, Dragos Isvoranu and Stefan Sorohan, "Combined Multiphysics and RF Macromodels for Electrostatic Actuated Micro-Electro-Mechanical Switches", Conf. on the Computation of Electromagnetic Fields in Montreal from 28 June - 2 July, COMPUMAG 2015.

12. Gabriela Ciuprina, Cosmin-Bogdan Dita, **Aurel-Sorin Lup**, Daniel Ioan and Alexandra Stefanescu, "Extraction of TL-lumped RF macromodels for MEMS switches"', IEEE MTTS International Conference on Numerical Electromagnetic and Multiphysics Modeling and Optimization for RF, Microwave and Terahertz Applications, Aug. 11-14, 2015, Ottawa, Canada, NEMO2015.

13. **Aurel-Sorin Lup**, Gabriela Ciuprina, Mihai Popescu and Daniel Ioan, "Parametric Multiphysics 3D Modelling of a Bridge Type Mems Capacitive Switch", The 17th International Symposium on Electromagnetic Fields in Mechatronics, Electrical and Electronic Engineering - ISEF'2015, 10-12 September, 2015, Conference Proceedings ISBN: 978-84-606-9102-0.

14. Mihai Popescu, **Aurel-Sorin Lup**, Ruxandra Barbulescu, Gabriela Ciuprina and Daniel Ioan, "Using Object Oriented Data Structures for Optimizing MEMS Devices on Parallel Computers", The 17th International Symposium on Electromagnetic Fields in Mechatronics, Electrical and Electronic Engineering - ISEF'2015, 10-12 September, 2015, Conference Proceedings ISBN: 978-84-606-9102-0.

15. Mihai Popescu, **Aurel-Sorin Lup** and Ruxandra Barbulescu, "Professional Package Software for Multiphysics Modelling. Application to MEMS devices", Scientific Bulletin, Series C Electrical Engineering and Computer Science, 2015.

Annexes

A1. Automatic procedure to extract reduced model's parameters

Extraction of k with analytic method.

```
function k1_a = k_analitic(modelinfo)
% compute stifness constant with analytical formulas
%
Lm = modelinfo.geom.Lm; % length of the membrane [m]
Hm = modelinfo.geom.Hm; % thickness of the membrane [m]
Wm = modelinfo.geom.Wm; % width of the membrane [m]
E_Au = modelinfo.mat.E;
%
switch modelinfo.type
    case 'bridge'
        Wpad = modelinfo.geom.Wpad;
        l1 = modelinfo.geom.l1;
        %determinarea constantei de elasticitate k1[N/m] analitic, fara
        %tensiuni reziduale
        k1_a = (4*E_Au*Wm*Hm^3)/(Lm*((l1 + Wpad)^2 + l1* (l1 + Wpad) + l1^2)-...
(2*l1 + Wpad)* ((l1 + Wpad)^2 + l1^2));  %Liu book page 72 - ...
%                                       punte dublu incastrata
    case 'cantilever'
        k1_a = 2*E_Au*Wm/3*(Hm/Lm)^3;
    otherwise
        error('analytical formula for this type of switch is not available');
end
end
```

Extraction of k with numerical methods.

```
function [keff,capacitance,F] = param_statici_v2(datastatic,coef_for_energy)
% extract keff, capacitance dependence on z and force dependence on z
% from numerical data input
%       datastatic = matrix with 3 columns having the following meaning
%       datastatic(:,1) = the vectors of static potential applied [V]
%       datastatic(:,2) = vectors of displacement z in microns
%       datastatic(:,3) = vector of electric energy [J]
%       coef_for_energy = integer, it will multiply the read energy to
%                         obtain the energy of the full model
% ouput
%       keff = structure with three fields
%           keff.k = value of keff when f(z) is approximated with a first...
```

```
%order k*z dependence
%           keff.k3 = values of keff when f(z) is approximated with
%        k1*z + k3*z^3 = vector with two components, the first is k1,...
%                                              the second is k3
%           keff.k_Fesm = value of Keff when the force is averaged over z
%           keff.k_km = value of Keff when K is averaged
%       capacitance = structure with the fiels
%           capacitance.values = vector of capacitances computed...
%                                    from the numerical data
%           capacitance.coefs = vector with two components [a b]...
%                                       (capacitance values are...
%approximated
%           with 1/(a*z + b))
%       F - computed from C, vector with the same size as the displacement
%       vector
%
[n,nocol] = size(datastatic);
if nocol ~= 3
    error('Wrong input static data. It should be a matrix with 3 columns...
 meaning: voltage [V], displacement [um], energy [J]');
else
    disp('-------->Extract parameters from static data:');
    disp('         voltage [V], displacement [um], energy [J]');
end
%
V = datastatic(:,1);
z = datastatic(:,2); % z in micrometers
W = datastatic(:,3);
V = V{1};
z = z{1};
W = W{1};
W = W*coef_for_energy;
zm = z*1e-6;          % z in meters
%
% capacitance
C = 2*W./V.^2;
Cp = C*1e12; % C in pF
invC = 1./Cp;
%
% linear approx of 1/Cp
%a = ((invC(n)-invC(2))/(z(n) - z(2)));  % 1/(pF*um)
%b = (-(z(2))*(invC(n)-invC(2))/(z(n) - z(2)))+invC(2); %1/pF
%
r = pinv([z(2:end) ones(size(z(2:end)))])*invC(2:end);
a = r(1);
b = r(2);
%
capacitance.values = C;
capacitance.coefs = [a b];
%
% computation of force from capacitance
F = -V.^2/2*a*1e18./((a*1e12*z + b*1e12).^2);
%
%%% Fes mediation
keff.k_Fesm = trapz(zm,F)/zm(end)^2;
```

```
%
%%% k = F/z mediation
k_z = F./zm;
keff.k_km = trapz(zm(2:end),k_z(2:end))/zm(end);
%
%%% least square approximation with k*z
keff.k = pinv(zm)*F;
%
%%% least square approximation with k1*z + k3*z^3
keff.k3 = pinv([zm zm.^3])*F;
end
```

Extraction of the dynamic parameters.

```
function [meff,beff,capacitance,F] = param_dinamici_v2compumag (datadinamic,f0,k,k3)

% extract meff, beff, capacitance dependence on z and force dependence on z
% from numerical data input
%       datadinamic = matrix with 4 columns having the following meaning
%       datadinamic(:,1) = vector of time, in second
%       datadinamic(:,2) = vectors of displacement z in microns
%       datadinamic(:,3) = vector of electric energy [J]
%       datadinamic(1,4) = value of step voltage applied
%       f0 = resonance frequency in Hertz
%       k = stifness coefficient in N/m
%
% ouput
%       meff = effective mass in mg
%       beff = effective damping coefficient N*ms/m
%       capacitance = structure with the fiels
%           capacitance.values = vector of capacitances computed from the ...
%                                numerical data
%           capacitance.coefs = vector with two components [a b] (capacitance ...
% values are approximated
%           with 1/(a*z + b))
%       F - computed from C, in uN

[n,nocol] = size(datadinamic);
if nocol ~= 4
    error('Wrong input dynamic data. It should be a matrix with 4 columns meaning:...
time [s], displacement [um], energy [J], voltage [V]');
else
    disp('-------->Extract parameters from dynamic data:');
    disp('         time [s], displacement [um], energy [J], voltage [V]');
end
%
meff = k/(2*pi*f0)^2; %meff in Kg
meff= meff*1e6; %meff in mg
fprintf('meff = %e mg\n',meff');
%meff = (k)/((2*pi*f0*1e-3)^2); % f0 in kHz, meff in mg
%meff = 1/2*3.628800e-005;

t = datadinamic(:,1); % t in seconds
t = t*1e3; %t in ms
z = datadinamic(:,2); % z in micrometers
W = datadinamic(:,3); % energy in Joule
```

```
V = datadinamic(1,4); % value of step voltage applied
%
% capacitance
C = 2*W./V.^2;
Cp = C*1e12; % C in pF
invC = 1./Cp;
%
% linear approx of 1/Cp
disp('a si b din dinamic, unde 1/C aprox az + b');
a = ((invC(n)-invC(2))/(z(n) - z(2)));  % 1/(pF*um)
fprintf('a = %e 1/(pF*um)',a);
%a = -6.0252 din valoarea statica
b = (-(z(2))*(invC(n)-invC(2))/(z(n) - z(2)))+invC(2); %1/pF
fprintf('b = %e 1/pF',b);
%
% disp('folosesc valorile din static');
% a=  -6.0252
% b = 30.1216
%
capacitance.values = C;
capacitance.coefs = [a b];
%
% computation of force from capacitance
F = -V.^2/2*a*1e18./((a*1e12*z + b*1e12).^2); % in N
F = F*1e6; % force in uN
%
% compute the velocity v(t)
v = derivare_ordin_doi(t,z);    % um / ms
%
% comute the acceleration a(t)
a = derivare_ordin_doi(t,v);    % um / (ms)^2
%a2 = derivare2_ordin_doi(t,z);    % um / (ms)^2
%
% extracting the damping coeficient
Fdamping = (F - meff.*a - k.*z - k3.*(z.^3));
%
figure(51); clf
disp('===din LS liniar');
plot(v,Fdamping,'*b');
beff = pinv(v)*Fdamping;  % ms/um*uN
fprintf('Extracted value of beff (to be used in Spice) = %e [(ms/um)*uN] sau [g/sec] ...
% sau \n',beff);
fprintf('                         = %e [kg/sec]\n',beff*1e-3);
%
% %%%% alternativa
% disp('===din LS afin');
% vext_2 = [v ones(length(v),1)];
% bext_2 = pinv(vext_2)*Fdamping
% beff_2 = bext_2(1)
%
hold on;
plot(v,beff*v,'-r','Linewidth',2);
%plot(v,beff*v+bext(2),'-r','Linewidth',2);
xlabel('v [um/ms]');
ylabel('Fdamping [uN]');
```

```
grid on;
legend('damping force','approximation b*v');
%
% figure(510)
% vpatrat = v.^2;
% plot(vpatrat,Fdamping,'*b');
% xlabel('v^2 [um/ms]^2');
% ylabel('Fdamping [uN]');
% grid on;
%
figure(52); clf;
plot(z,F,'*b','Linewidth',2);
hold on;
plot(z,k*z+k3*z.^3,'or','Linewidth',2);
plot(z,meff*a,'sm','Linewidth',2);
plot(z,beff*v,'pk','Linewidth',2);
xlabel('z [um]');
ylabel('Forces [uN]');
grid on;
legend('electrostatic','elastic','inertial','damping');
%
figure(53); clf;
plot(t,z,'-b','Linewidth',2);
xlabel('t [ms]');
ylabel('z [{\mu}m]');
grid on;
%
figure(54); clf
plot(t,v,'-r','Linewidth',2);
xlabel('t [ms]');
ylabel('v [{\mu}m/ms]');
grid on;
hold on;
%plot(t,Fdamping*1000,':b','Linewidth',2); % doar ca idee
%
figure(55); clf
plot(t,a,'-k','Linewidth',2);
% hold on;
% plot(t,a2,':r','Linewidth',2);
grid on;
xlabel('t [ms]');
ylabel('a [{\mu}m/(ms)^2]');
%
datasave.info = 'extragere b';
datasave.k = k;
datasave.kunit = 'N/m';
datasave.f0 = f0;
datasave.f0unit = 'Hz';
datasave.meff = meff;
datasave.meffUnit = 'mg';
datasave.t = t;
datasave.tunit = 'ms';
datasave.z = z;
datasave.zunit = 'um';
datasave.v = v;
```

```
datasave.vunit = 'um/ms';
datasave.a = a;
datasave.aunit = 'um/(ms)^2';
datasave.Fdamping = Fdamping;
datasave.FdampingUnit = 'uN';
datasave.beff = beff;
datasave.beffUnit = 'milisec N/m = mili Kg/sec = g/sec';
save('DataFromDynamicExtraction.mat','datasave');
end
```

Extraction of TL's parameters.

```
function [] = extract_TL_from_Yup(snp_up_file,Cup,len,problempath)
% compute the line parameters from the RF data (switch in the up pozition)
% obtained with a chamy simulation and the value of Cup
% len is the length of half a line
%
%snp_up_file = 'liniar_100pc_Up_40x28x26_inS.s2p';
%Cup = 37.2863e-15; %F din simularea multifizica pentru z=0
%Cup = 5.844653358098474e-014 ; % din simularea RF
%Cup = 5.8551e-014;
%
%len = 600e-6/2;
%
[ptype,pformatfile,frecv,value,Z0,units,nports] = loadsnp(snp_up_file);
switch upper(ptype)
case 'S'
    %disp('S');
    valueZ = mys2z(value,Z0);
    valueY = myz2y(valueZ);
case 'Z'
    %disp('Z');
    valueZ = value;
    valueY = myz2y(value);
case 'Y'
    %disp('Y');
    valueY = value;
    valueZ = myy2z(value);
otherwise
    fprintf('not implemented for type %s',ptype);
    return
end
units = upper(units);
if strcmp(units,'HZ')
    frecvrad = 2*pi*frecv;
elseif strcmp(units,'KHZ')
    frecvrad = 2*pi*frecv*1e3;
elseif strcmp(units,'MHZ')
    frecvrad = 2*pi*frecv*1e6;
elseif strcmp(units,'GHZ')
    frecvrad = 2*pi*frecv*1e9;
elseif strcmp(units,'RAD/S')
    frecvrad = frecv;
end;
[n,m,ll] = size(valueZ);
Zc = zeros(1,ll);
```

```
gammaL = zeros(1,ll);
%
for i=1:ll
    Z = valueZ(:,:,i);
    Yup = 1j*frecvrad(i)*Cup;
    Z11 = (Z(1,1) + Z(2,2))/2;
    Z12 = (Z(1,2) + Z(2,1))/2;
    rap = Z11/Z12;
    lhs = 2/Z12 - Yup + rap*Yup;
    rhs = (rap+1)/Z12;
    chpatrat = rhs/lhs;
    shpatrat = chpatrat - 1;
    ch = sqrt(chpatrat);
    sh = sqrt(shpatrat);
    expGamma = ch + sh;
    gammaL(i) = log(expGamma);
    Zc(i) = 1/(Yup*sh*ch)*(Z11/Z12 - shpatrat - chpatrat);
end
%
% check first point
a1 = real(gammaL(1))/len;
b1 = imag(gammaL(1))/len;
lam1 = 2*pi/b1;
if and(and(a1 >=0, b1>=0),lam1/len > 4)
    disp('First point is OK');
else
    disp('**************************WARNING*************');
    disp('WARNING: computation is not accurate');
    disp('First frequency point is too large');
end
%
g1 = gammaL;
figure(21);
ff = frecv/(2*pi*1e9);
h1 = plot(ff,real(g1/len),'-xr');
hold on;
h2 = plot(ff,imag(g1/len),'-.sb');
title('\alpha and \beta before corection');
leg{1} = '\alpha';
leg{2} = '\beta';
legend(leg,0);
set(h1,'LineWidth',2);
set(h2,'LineWidth',2);
xlabel('Frequency [GHz]');
%
for j = 1:ll
    if real(gammaL(j)) < -eps
        gammaL(j) = -real(gammaL(j)) - 1j*imag(gammaL(j));
    end
end
g2 = gammaL;
figure(22);
h1 = plot(ff,real(g2/len),'-xr');
hold on;
h2 = plot(ff,imag(g2/len),'-.sb');
```

```
title('\alpha and \beta after first correction step');
leg{1} = '\alpha';
leg{2} = '\beta';
legend(leg,0);
set(h1,'LineWidth',2);
set(h2,'LineWidth',2);
xlabel('Frequency [GHz]');
for j = 2:ll
    if  imag(gammaL(j-1)) > imag(gammaL(j))
        for k = j:ll
            gammaL(k) = real(gammaL(k)) + 1j*(imag(gammaL(k))) + 2*pi*1j;
        end
    end
end
g3 = gammaL;
figure(23);
h1 = plot(ff,real(g3/len),'-xr');
hold on;
h2 = plot(ff,imag(g3/len),'-.sb');
title('\alpha and \beta after second correction step');
leg{1} = '\alpha';
leg{2} = '\beta';
legend(leg,0);
set(h1,'LineWidth',2);
set(h2,'LineWidth',2);
xlabel('Frequency [GHz]');
%
gamma = zeros(1,ll);
for i = 1:ll
    gamma(i) = gammaL(i)/len;
    ZZ = gamma(i)*Zc(i);
    YY = gamma(i)/Zc(i);
    R(:,:,i) = real(ZZ);
    L(:,:,i) = imag(ZZ)/frecvrad(i);
    G(:,:,i) = real(YY);
    C(:,:,i) = imag(YY)/frecvrad(i);
    dataZ(:,:,i) = ZZ;
    dataY(:,:,i) = YY;
end
%
dataZ = squeeze(dataZ); dataY = squeeze(dataY);
filenameZ = 'Zl_fromYtr.s1p';
filenameRlLl = 'RlLl_fromYtr.s1p';
filenameY = 'Yl_fromYtr.s1p';
filenameGlCl = 'GlCl_fromYtr.s1p';
writesnp_v2(strcat(problempath,filenameZ), frecv, dataZ, 'Z', units,Z0,'RI');
snp_imag_over_omega(problempath,filenameZ,filenameRlLl);
writesnp_v2(strcat(problempath,filenameY), frecv, dataY, 'Y', units,Z0,'RI');
snp_imag_over_omega(problempath,filenameY,filenameGlCl);
Rlmediu = trapz(frecv,squeeze(R))/(frecv(end)-frecv(1))
Llmediu = trapz(frecv,squeeze(L))/(frecv(end)-frecv(1))
%Glmediu = trapz(frecv,squeeze(G))/(frecv(end)-frecv(1))
Clmediu = trapz(frecv,squeeze(C))/(frecv(end)-frecv(1))
%
R0 = R(1,1,1);
```

```
L0 = L(1,1,1);
C0 = C(1,1,1);
```

Computing S and Z parameters.

```
function [paramZ,paramS,responseZ,responseS] = ...
    ZsiS_pe_doua_linii_Ytransversal(paramTL1,paramTL2,paramSwitch,frecv)
%
Rl1 = paramTL1.Rl;
Ll1 = paramTL1.Ll;
Cl1 = paramTL1.Cl;
Gl1 = paramTL1.Gl;
l1 = paramTL1.l;
%
Rl2 = paramTL2.Rl;
Ll2 = paramTL2.Ll;
Cl2 = paramTL2.Cl;
Gl2 = paramTL2.Gl;
l2 = paramTL2.l;
%
omega = 2*pi*frecv;
Zswitch = paramSwitch.R + 1i*omega*paramSwitch.L + 1./(1i*omega*paramSwitch.C);
Y = 1./Zswitch; % admitanta elementului plasat transveral
%
%%%%%%
z1 = Rl1 + 1i*omega*Ll1;
y1 = Gl1 + 1i*omega*Cl1;
z2 = Rl2+ 1i*omega*Ll2;
y2 = Gl2 + 1i*omega*Cl2;
%
nof = length(frecv);
Z = zeros(2,2);
Z0 = 50;
Z11 = zeros(nof,1);
Z21 = zeros(nof,1);
Z22 = zeros(nof,1);
S11 = zeros(nof,1);
S21 = zeros(nof,1);
S22 = zeros(nof,1);
%
for k = 1:nof
    gammal1 = sqrt(z1(k)*y1(k))*l1;
    zc1 = sqrt(z1(k)/y1(k));
    ch1 = cosh(gammal1);
    sh1 = sinh(gammal1);
    gammal2 = sqrt(z2(k)*y2(k))*l2;
    zc2 = sqrt(z2(k)/y2(k));
    ch2 = cosh(gammal2);
    sh2 = sinh(gammal2);
 %
    delta = ch1*sh2/zc2 + Y(k)*ch1*ch2 + ch2*sh1/zc1;
    Z(1,1) = (zc1/zc2*sh1*sh2 + zc1*Y(k)*sh1*ch2 + ch1*ch2)/delta;
    Z(1,2) = 1/delta;
    Z(2,1) = Z(1,2);
    Z(2,2) = (zc2/zc1*sh1*sh2 + zc2*Y(k)*sh2*ch1 + ch1*ch2)/delta;
    Z11(k) = Z(1,1);
```

```
    Z21(k) = Z(2,1);
    Z22(k) = Z(2,2);
    S = (Z - Z0*eye(2,2))/(Z + Z0*eye(2,2));
    S11(k) = S(1,1);
    S21(k) = S(2,1);
    S22(k) = S(2,2);
end
%
% formulele de mai sus sunt generale
paramZ.Z11.real = real(Z11);
paramZ.Z11.imag = imag(Z11);
paramZ.Z11.abs = abs(Z11);
paramZ.Z11.angle = angle(Z11);
paramZ.Z11.absdb = 20*log10(abs(Z11));
%
paramZ.Z21.real = real(Z21);
paramZ.Z21.imag = imag(Z21);
paramZ.Z21.abs = abs(Z21);
paramZ.Z21.angle = angle(Z21);
paramZ.Z21.absdb = 20*log10(abs(Z21));
%
paramS.S11.real = real(S11);
paramS.S11.imag = imag(S11);
paramS.S11.abs = abs(S11);
paramS.S11.angle = angle(S11);
paramS.S11.absdb = 20*log10(abs(S11));
%
paramS.S21.real = real(S21);
paramS.S21.imag = imag(S21);
paramS.S21.abs = abs(S21);
paramS.S21.angle = angle(S21);
paramS.S21.absdb = 20*log10(abs(S21));
%
responseZ(1,1,:) = paramZ.Z11.real + 1i*paramZ.Z11.imag;
responseZ(2,1,:) = paramZ.Z21.real + 1i*paramZ.Z21.imag;
responseZ(2,2,:) = responseZ(1,1,:);
responseZ(1,2,:) = responseZ(2,1,:);
%
responseS(1,1,:) = paramS.S11.real + 1i*paramS.S11.imag;
responseS(2,1,:) = paramS.S21.real + 1i*paramS.S21.imag;
responseS(2,2,:) = responseS(1,1,:);
responseS(1,2,:) = responseS(2,1,:);
%
end
```

FFT computing procedure.

```
function [f,Y,fzero] = my_fft_function(vec_t,vec_y)
%
tmax = vec_t(end);
nop = 2^12;
%
t = linspace(0,tmax,nop); %genereaza vectori de timp spatiati echidistant
y = interp1(vec_t,vec_y,t,'linear','extrap');
fprintf('nr de puncte in vectorul de timp = %d\n',nop);
%
```

```
% f0 = 100; % Hz
% omega = 2*pi*f0;
% T = 1/f0;
% alpha = 0; %100;
%
% nop = 500;  % eu stiam ca tb sa fie putere a lui 2 pt un alg eficient
% t = linspace(0,4*T,nop);
% %y = exp(-alpha*t).*sin(omega*t);
% %y = exp(-alpha*t).*sin(3*omega*t);
% %y = exp(-alpha*t).*(sin(omega*t) + sin(3*omega*t));
% %y = exp(-alpha*t).*sin(omega*t) + exp(-2*alpha*t).*sin(3*omega*t);
% y = exp(-alpha*t).*2.*sin(omega*t) + 1.5;
% %y = exp(-alpha*t).*(sin(omega*t) + sin(3*omega*t)) + 0.5;
%
% figure(100);
% %subplot(2,2,1);
% plot(t,y)
% xlabel('t');
% ylabel('y');
% grid on;
% title('Data passed to fft');
%
fft_data = fft(y);
%Y = 2*abs(fft_data)/nop;
Y = abs(fft_data)/nop;
Y(2:end) = Y(2:end)*2;
Y = Y(1:nop/2);
deltat = t(2)-t(1);
Fs = 1/deltat;
f_nyq = Fs/2;
f = linspace(0,f_nyq,length(Y));
fprintf('nr de puncte in vectorul de frecventa = %d\n',length(Y));
%
fprintf('d.c. component = %e\n',Y(1));
[valmax,idx] = max(Y(2:end));
fzero = f(idx+1);
fprintf('First resonant frequency = %f  Hz\n',fzero);
%
% %subplot(2,2,2)
% figure(2);
% plot(f,Y,'r*-');
% xlabel('f');
% ylabel('Y');
% grid on;
%
%
% %subplot(2,2,3)  % ca sa vad bine
% figure(3)
% plot(f/1e3,Y,'r*-');
% xlim([0,50]);
% grid on;
% xlabel('f [kHz]');
% ylabel('Y [{\mu}m]');
end
```

Main program that computes the lumped parameters and writes the circuit netlist.

```
clear all;
clc;
close all hidden;
%
%% prepare path to use mems functions - change this according to your path
restoredefaultpath;
if isunix
    sourcespath1 = genpath('/home/Sorin/matlab/MEMS/switch2spice/sourcesS');
    sourcespath2 = genpath('/home/Sorin/matlab/MEMS/switch2spice/sourcesS');
else
    sourcespath1 = genpath('E:\switch2spice\switch2spice_2iulie2014\sources');
    sourcespath2 = genpath('E:\switch2spice\switch2spice_2iulie2014\sources');
end
addpath(sourcespath1,sourcespath2)
%% problem path - change it according to the problem path
problempath = 'E:\[4] PhD Study\switch2spice_2iulie2014\problems\';
%% data files - static analysis - change them accordingly
datafile.static.deplasare = 'static_displacement.txt';% contine o...
% coloana de V si o coloana de micrometri
datafile.static.headerlinesdeplasare = 8; % cate linii de inceput...
% trebuie sarite la citirea fisiereului
datafile.static.energie = 'static_electric_energy.txt'; %contine o...
% coloana de V si una de J
datafile.static.headerlinesenergie = 8;
coef_for_energy = 2; %  energia modelului e pe jumatate,...
% in algoritm tb inmultita cu 2
%% data files - dynamic - without damping
% de introdus si prelucrat
datafile.dinamic.nodamping.deplasare = 'dinamic_emi_displacement.txt';
% contine o coloana de us si o coloana de um
datafile.dinamic.nodamping.headerlinesdeplasare = 8;
%
%% Alege una din urmatoarele doua
analizeaza_fluid = 1;  % 1 pentru da
analizeaza_rayleigh = 0;% 1 pentru da
%%
%% data files - dynamic - with air damping
czdin = 1;
switch czdin
    case 1  %excitatie step 5 v
        datafile.dinamic.deplasare =...
'deplasare_es_mec_fsi_open_boundary_box_mic_extra_coarse.txt';
% contine o coloana microsecunde si una micrometri
        datafile.dinamic.headerlinesdeplasare = 8;
% cate linii de inceput trebuie sarite la citirea fisiereului
        datafile.dinamic.energie = ...
'energieElectrica_es_mec_fsi_open_boundary_box_mic_extra_coarse.txt';
% contine o coloana microsecunde si una J
        datafile.dinamic.headerlinesenergie = 8;
        voltageStep = 5; % valoarea tensiunii treapta aplicate
    case 2 % excitatie step 6V
        datafile.dinamic.deplasare =...
'comsol_rez_step6V\deplasare_COMSOL_exc6V.txt';
```

```
% contine o coloana microsecunde si una micrometri
        datafile.dinamic.headerlinesdeplasare = 8;
% cate linii de inceput trebuie sarite la citirea fisiereului
        datafile.dinamic.energie =...
'comsol_rez_step6V\energieElectrica_exc6V.txt';
% contine o coloana microsecunde si una J
        datafile.dinamic.headerlinesenergie = 8;
        voltageStep = 6; % valoarea tensiunii treapta aplicate
%     case 3 %excitateie impuls 10 V
%         datafile.dinamic.deplasare = 'comsol_rez_impuls\deplasare_...
%                                 exc_impuls10V.txt';
%         datafile.dinamic.headerlinesdeplasare = 8;
% cate linii de inceput trebuie sarite la citirea fisiereului
%         datafile.dinamic.energie = 'comsol_rez_impuls\energie...
%                               Electrica_exc_impuls10V.txt';
%         datafile.dinamic.headerlinesenergie = 8;
%         voltageImpuls = 10;
%         voltageStep = 0;
%         % asta nu merge pentru ca imi calculez capacitatea...
%                         ca C din energia = C*U^2 pe 2,
%         % unde U a fost presupusa constanta
    otherwise
        error('caz neexistent');
end
%
%% data files - dynamic with Rayleigh damping
caz = 3;
switch caz
    case 1
        beta = 6e-5; %impose value in FEM [1/sec]
        datafile.dinamic.deplasareRayleigh = 'rayleigh\deplasare_emi_beta6e-5.txt';
        datafile.dinamic.energieRayleigh = 'rayleigh\energieElectrica_emi_beta6e-5.txt';
        datafile.spicek.deplasareRayleigh = 'rayleigh\spice\cantilever_emi_beta6e-5.txt';
        datafile.spicek1k3.deplasareRayleigh = 'rayleigh\spice\...
cantilever_emi_beta6e-5_k1_k3.txt';
        titlestring = 'beta = 6e-5 [s]';
    case 2
        beta = 6e-6; %impose value in FEM [1/sec]
        datafile.dinamic.deplasareRayleigh = 'rayleigh\deplasare_emi_beta6e-6.txt';
        datafile.dinamic.energieRayleigh = 'rayleigh\energieElectrica_emi_beta6e-6.txt';
        datafile.spicek.deplasareRayleigh = 'rayleigh\spice\cantilever_emi_beta6e-6.txt';
        datafile.spicek1k3.deplasareRayleigh = 'rayleigh\spice\...
cantilever_emi_beta6e-6_k1_k3.txt';
        titlestring = 'beta = 6e-6 [s]';
    case 3
        beta = 1.5e-6; %impose value in FEM [1/sec]
        datafile.dinamic.deplasareRayleigh = 'rayleigh\deplasare_emi_beta1.5e-6.txt';
        datafile.dinamic.energieRayleigh='rayleigh\energieElectrica_emi_beta1.5e-6.txt';
        datafile.spicek.deplasareRayleigh='rayleigh\spice\cantilever_emi_beta1.5e-6.txt';
        datafile.spicek1k3.deplasareRayleigh = 'rayleigh\spice\...
cantilever_emi_beta1.5e-6_k1_k3.txt';
        titlestring = 'beta = 1.5e-6 [s]';
    case 4
        beta = 6e-7; %impose value in FEM [1/sec]
        datafile.dinamic.deplasareRayleigh = 'rayleigh\deplasare_emi_beta6e-7.txt';
```

```
        datafile.dinamic.energieRayleigh = 'rayleigh\energieElectrica_emi_beta6e-7.txt';
        datafile.spicek.deplasareRayleigh = 'rayleigh\spice\cantilever_emi_beta6e-7.txt';
        datafile.spicek1k3.deplasareRayleigh = 'rayleigh\spice\...
cantilever_emi_beta6e-7_k1_k3.txt';
        titlestring = 'beta = 6e-7 [s]';
 %
end
%
%% spice flag
spiceflag = 1; % trebuie mai jos introduse numele de ...
%                fisiere txt salvate din ltspice
% acest flag pus pe 1 inseamna ca va citi si fisiere spice.
% Are rost numai dupa ce rulat o data programul si extrasi
% parametrii concentrati
datafile.spice.static.k ='spice_asc_manual/cantilever_...
multifizic_static_simulations_onlyk.txt';
datafile.spice.static.k1k3 = 'spice_asc_manual/cantilever...
_multifizic_static_simulations_onlyk1sik3.txt';
datafile.spice.dinamic.nodamping.k ='spice_asc_manual/...
cantilever_multifizic_no_damping_onlyk.txt';
datafile.spice.dinamic.nodamping.k1k3 = 'spice_asc_manual/...
cantilever_multifizic_no_damping_onlyk1sik3.txt';
%
%% info about the model - useful for analytic computations
modelinfo.type = 'cantilever'; % bridge or cantilever
modelinfo.comment = 'Electrostatic actuated cantilever';
modelinfo.geom.Hm = 2e-6;     % thickness of the membrane [m]
modelinfo.geom.Lm = 300e-6;   % length of the membrane [m]
modelinfo.geom.Wm = 20e-6;   % width of the membrane [m] (toata latimea)
%
modelinfo.mat.name = 'nec';
modelinfo.mat.E = 153e9; %[Pa]
modelinfo.mat.nu = 0.23;
modelinfo.mat.rho = 2330;%[Kg/m3]
%
%% BEGIN COMPUTATIONS - display info on console
chdir(problempath);
disp(modelinfo.comment);
%% STEP0 - analitical computations
kanalitic = k_analitic(modelinfo);
manalitic = m_analitic(modelinfo);
fprintf('m_analitic = %e mg \n',manalitic*1e6);
%% STEP 1 - process static data
fid = fopen(datafile.static.deplasare);
data.st.deplasare = textscan(fid, '%f %f','HeaderLines',...
%                               datafile.static.headerlinesdeplasare);
fclose(fid);
%data.st.deplasare{1} - reprezinta tensiuni - in V
%data.st.deplasare{2} - reprezinta deplasari - in micrometri
fid = fopen(datafile.static.energie);
data.st.energie = textscan(fid, '%f %f','HeaderLines',...
%                                 datafile.static.headerlinesenergie);
fclose(fid);
%data.st.energie{1} - reprezinta tensiuni - in V
%data.st.energie{2} - reprezinta energii - in J
```

```
nop = length(data.st.deplasare{1});
datastatic = zeros(nop,3);
datastatic(:,1) = data.st.deplasare{1};
datastatic(:,2) = -data.st.deplasare{2};
datastatic(:,3) = data.st.energie{2};
[keff,capacitance,F] = param_statici_v3compumag(datastatic,coef_for_energy);
% extract parameters
% --------- display results on console
fprintf('Analytical value for k [N/m]: \n \t \t \t k = %e\n',kanalitic);
fprintf('B1. Numerical extracted value for k - k = ...
F/z average over z for F = k*z [N] \n \t \t \t k = %e [N/m]\n',keff.k_km);
fprintf('B2. Numerical extracted value for k - ...
force average over z for F = k*z [N] \n \t \t \t k = %e [N/m]\n',keff.k_Fesm);
fprintf('B3. Numerical extracted value for k - ...
least square for F = k*z [N] \n \t \t \t k = %e [N/m]\n',keff.k);
fprintf('B4. Numerical extracted value for k - ...
least square for F = k1*z + k3*z^3  \n \t \t \t k1 =
%e [N/m] \n \t \t \t k3 = %e [N/(m*um*um)] \n',keff.k3(1),keff.k3(2)*1e-12);
fprintf('Expression of C(z) = 1/(az + b) [F], z [m] ...
\n \t \t \t a = %e [1/(pF*um)] \n \t \t \t b =
%e [1/pF]\n',capacitance.coefs(1), capacitance.coefs(2));

% --------- plot results - Force vs z
%z = data.static(:,2); z = z{1};
%V = data.static(:,1); V = V{1};
z = datastatic(:,2);
V = datastatic(:,1);
%z(end) = [];  % daca ultimul punct este instabil, el trebuie scos
%F(end) = [];
zm = z*1e-6;  % in meters
FwithKanalitic = kanalitic*zm;
FwithKnumeric = keff.k*zm;
FwithKnumeric3 = keff.k3(1)*zm + keff.k3(2)*zm.^3;
FwithKnumeric3b = keff.k3(1)*zm;
FwithKnumericFesm = keff.k_Fesm*zm;
FwithKnumerickm = keff.k_km*zm;
%
figure (1); clf;
plot(z,F*1e6,'b*',z,FwithKnumeric*1e6,'--k','LineWidth',2,'MarkerSize',6);
hold on;
plot(z,FwithKnumeric3*1e6,'-r',z,FwithKanalitic*1e6,'om','LineWidth',2,'MarkerSize',3);
grid on;
xlabel('z [um]');
ylabel('Felastic [{\mu}N]');
legend('2D FEM, MEC+ES, static','k_{eff} z','k_1 z + k_3 z^3','k_{eff,analytic} z');
title(modelinfo.comment);
% -------- plot results - Capacitance vs z
C = capacitance.values;
%C(end) = []; %daca ultimul punct e instabil, atunci trebuie scos
Capprox = 1./(capacitance.coefs(1)*1e12*z + capacitance.coefs(2)*1e12);
figure (2)
plot(z,C*1e12,'-b*',z,Capprox*1e12,'--r','LineWidth',2,'MarkerSize',6);
grid on;
xlabel('z [{\mu}m]');
ylabel('C [pF]');
```

```
legend('From the FEM model','Approximation 1/(az+b)');
title(modelinfo.comment);
if spiceflag == 1
    % ploturi dupa ce au fost salvate fisierele din spice
    figure(3); clf; % comparatie deplasari
    file_A = datafile.spice.static.k;
    file_B1 = datafile.spice.static.k1k3;
    fid = fopen(file_A);
    dataA = textscan(fid, '%f %f','HeaderLines',1);
    fclose(fid);
    zA = dataA{2};
    VA = dataA{1};
    fid = fopen(file_B1);
    dataB1 = textscan(fid, '%f %f','HeaderLines',1);
    fclose(fid);
    zB1 = dataB1{2};
    VB1 = dataB1{1};
    plot(V,z,'*b','Linewidth',2);
    hold on;
    plot(VA,zA,'-.m','Linewidth',2);
    plot(VB1,zB1,'--g','Linewidth',2);
    legend('FEM','Spice (LSord1): F = kz','Spice (LSord3)): F = k1 z  + k3 z^3');
    xlabel('Actuation voltage [V]');
    ylabel('Displacement [{\mu}m]');
    grid on;
end
%
%% STEP 1 - process dinamic data - case without damping
fid = fopen(datafile.dinamic.nodamping.deplasare);
data.din.deplasare = textscan(fid, '%f %f','HeaderLines'...
%,datafile.dinamic.nodamping.headerlinesdeplasare);
fclose(fid);
t = data.din.deplasare{1}; % timp in microsecunde
y = data.din.deplasare{2}; % deplasari in micrometri
t = t*1e-6;
y = y*1e-6;
figure(11)
plot(t,y)
xlabel('t [{\mu}s]');
ylabel('z [{\mu}m]');
%
[f,Y,fzero] = my_fft_function(t,y);
fprintf('First resonant frequency = %f  kHz\n',fzero/1e3);
figure(12); clf; % plot cu domenii implicite, dictate de valori
plot(f,Y*1e6,'r*-');
xlabel('f [Hz]');
ylabel('Magnitude [{\mu}m]');
grid on;
%
figure(13);clf;
plot(f/1e3,Y*1e6,'r*-');
xlim([0,50]);
grid on;
xlabel('f [kHz]');
ylabel('Magnitude [{\mu}m]');
```

```
%
meff = keff.k/(2*pi*fzero)^2; %meff in Kg
meff= meff*1e6; %meff in mg
fprintf('- calcul din k - meff = %e mg\n',meff');
if spiceflag == 1
    % ploturi dupa ce au fost salvate fisierele din spice
    figure(14); clf; % comparatie deplasari
    file_A = datafile.spice.dinamic.nodamping.k; % timpii ...
%sunt in ms, deplasarile in um
    file_B1 = datafile.spice.dinamic.nodamping.k1k3;
    fid = fopen(file_A);
    dataA = textscan(fid, '%f %f','HeaderLines',1);
    fclose(fid);
    zA = dataA{2};
    tA = dataA{1}*1e3; % timpi in us
    fid = fopen(file_B1);
    dataB1 = textscan(fid, '%f %f','HeaderLines',1);
    fclose(fid);
    zB1 = dataB1{2};
    tB1 = dataB1{1}*1e3; % timpi in us
    plot(t*1e6,y*1e6,'*b','Linewidth',2);
    hold on;
    plot(tA,zA,'-.m','Linewidth',2);
    plot(tB1,zB1,'--g','Linewidth',2);
    legend('FEM','Spice: F_{elastic} = kz','Spice (LSord3)):...
F_{elastic} = k1 z  + k3 z^3');
    xlabel('Time [{\mu}s]');
    ylabel('Displacement [{\mu}m]');
    grid on;
end
%
if analizeaza_fluid == 1
    %% process dinamic data - aer cu amortizare fluidica
    fid = fopen(datafile.dinamic.deplasare);
    data.din.deplasare = textscan(fid, '%f %f',...
%'HeaderLines',datafile.dinamic.headerlinesdeplasare);
    fclose(fid);
    %data.din.deplasare{1} - reprezinta timpi - in secunde
    %data.din.deplasare{2} - reprezinta deplasari - in metri
    fid = fopen(datafile.dinamic.energie);
    data.din.energie = textscan(fid, '%f %f','HeaderLines',...
%datafile.dinamic.headerlinesenergie);
    fclose(fid);
    %data.din.energie{1} - reprezinta timpi - in secunde
    %data.din.energie{2} - reprezinta J
    nop = length(data.din.deplasare{1});
    datadinamic = zeros(nop,4);
    datadinamic(:,1) = data.din.deplasare{1}*1e-6; % vector de timp in secunde
    datadinamic(:,2) = data.din.deplasare{2}; % deplasarea in microni
    datadinamic(:,3) = data.din.energie{2}*2; % energia totala in Joule
    datadinamic(1,4) = voltageStep; %V step-ul aplicat
    f0 = 25000; %frecventa naturala de oscilatie
    tFEM  = data.din.deplasare{1}; %timp in microsecunde
    zFEM = data.din.deplasare{2}; %deplasare in microni
   %
```

```
    if 1 == 1
        disp('beta extras cu forta elastica kx');
        k = keff.k;
        k3 = 0;
        [meff,beff,capacitance,F] = param_dinamici_v2compumag(datadinamic,f0,k,k3);
        beta_extras = beff*1e-3/k;
        fprintf('beta extras = beff/keff = %e [sec]\n',beta_extras );
    else
        disp('beta extras cu forta elastica k1 x + k3 x^3 [1/sec]');
% varianta asta nu pare ca merge OK
        k = keff.k3(1);
        k3 = keff.k3(2);
        [meff,beff,capacitance,F] = param_dinamici_v2compumag(datadinamic,f0,k,k3);
        beta_extras = beff*1e-3/k;
        fprintf('beta extras = beff/keff = %e [sec]\n',beta_extras );
    end
%
    if spiceflag == 1
        % ploturi dupa ce au fost salvate fisierele din spice
        figure(21); clf % comparatie deplasari
        file_A = 'spice_asc_manual/cantilever_multifizic_fluid_damping.txt';
        file_B1 = 'spice_asc_manual/cantilever_multifizic_fluid_damping_k1_k3.txt';
        %
        fid = fopen(file_A);
        dataA = textscan(fid, '%f %f','HeaderLines',1);
        fclose(fid);
        tA = dataA{1}; %timp in milisecunde
        tA = tA*1e3; %timp in microsecunde
        zA = dataA{2}; %deplasare in microni
        %
        fid = fopen(file_B1);
        dataB1 = textscan(fid, '%f %f','HeaderLines',1);
        fclose(fid);
        tB1 = dataB1{1};  %timp in milisecunde
        tB1 = tB1*1e3; %timp in microsecunde
        zB1 = dataB1{2};%deplasare in microni
        %
        plot(tFEM,zFEM,':k','Linewidth',4);
        hold on;
        plot(tA,zA,'-.b','Linewidth',2);
        plot(tB1,zB1,'--r','Linewidth',2);
        %
        legend('FEM - ES+MEC+Fluid','Spice, kz elastic force','Spice, k1 z  + k3 z^3');
        xlabel('Time [{\mu}s]');
        ylabel('Displacement [{\mu}m]');
        %
        disp('================amortizare cu fluid=================');
        disp('comparatie FEM - spice cu Fel = kz');
        calculeza_erori_dintre_curbe(tFEM,zFEM,tA,zA);
        disp('comparatie FEM - spice cu Fel = k1 z k3 z^3');
        calculeza_erori_dintre_curbe(tFEM,zFEM,tB1,zB1);
        %grid on;
    end
end
%
```

```
if analizeaza_rayleigh == 1
    %% process dinamic data - amortizare Rayleigh
    fid = fopen(datafile.dinamic.deplasareRayleigh);
    data.din.deplasare = textscan(fid, '%f %f','HeaderLines'
%,datafile.dinamic.headerlinesdeplasare);
    fclose(fid);
    %data.din.deplasare{1} - reprezinta timpi - in secunde
    %data.din.deplasare{2} - reprezinta deplasari - in metri
    fid = fopen(datafile.dinamic.energieRayleigh);
    data.din.energie = textscan(fid, '%f %f','HeaderLines',
%datafile.dinamic.headerlinesenergie);
    fclose(fid);
    %data.din.energie{1} - reprezinta timpi - in secunde
    %data.din.energie{2} - reprezinta J
    nop = length(data.din.deplasare{1});
    datadinamic = zeros(nop,4);
    datadinamic(:,1) = data.din.deplasare{1}*1e-6; % vector de timp in secunde
    datadinamic(:,2) = data.din.deplasare{2}; % deplasarea in microni
    datadinamic(:,3) = data.din.energie{2}*2; % energia totala in Joule
    datadinamic(1,4) = voltageStep; %V step-ul aplicat
    f0 = 25000; %frecventa naturala de oscilatie
    tFEM  = data.din.deplasare{1}; %timp in microsecunde
    zFEM = data.din.deplasare{2}; %deplasare in microni
   %
    if 1 == 1
        disp('beta extras cu forta elastica kx');
        k = keff.k;
        k3 = 0;
        [meff,beff,capacitance,F] = param_dinamici_v2compumag(datadinamic,f0,k,k3);
        beta_extras = beff*1e-3/k;
        fprintf('beta extras = beff/keff = %e [sec]\n',beta_extras );
    else
        disp('beta extras cu forta elastica k1 x + k3 x^3 [1/sec]');
% varianta asta nu pare ca merge OK
        k = keff.k3(1);
        k3 = keff.k3(2);
        [meff,beff,capacitance,F] = param_dinamici_v2compumag(datadinamic,f0,k,k3);
        beta_extras = beff*1e-3/k;
        fprintf('beta extras = beff/keff = %e [sec]\n',beta_extras );
    end
    %
    if spiceflag == 1
        % ploturi dupa ce au fost salvate fisierele din spice
        figure(21); clf % comparatie deplasari
        file_A = datafile.spicek.deplasareRayleigh;
        file_B1 = datafile.spicek1k3.deplasareRayleigh;
        %
        fid = fopen(file_A);
        dataA = textscan(fid, '%f %f','HeaderLines',1);
        fclose(fid);
        tA = dataA{1}; %timp in milisecunde
        tA = tA*1e3; %timp in microsecunde
        zA = dataA{2}; %deplasare in microni
        %
        fid = fopen(file_B1);
```

```
        dataB1 = textscan(fid, '%f %f','HeaderLines',1);
        fclose(fid);
        tB1 = dataB1{1};  %timp in milisecunde
        tB1 = tB1*1e3; %timp in microsecunde
        zB1 = dataB1{2};%deplasare in micron
        %
        plot(tFEM,zFEM,':k','Linewidth',4);
        hold on;
        plot(tA,zA,'-.b','Linewidth',2);
        plot(tB1,zB1,'--r','Linewidth',2);
        %
        legend('FEM - ES+MEC (Rayleigh)','Spice, kz elastic force',...
'Spice, k1 z  + k3 z^3');
        xlabel('Time [{\mu}s]');
        ylabel('Displacement [{\mu}m]');
        title(titlestring);
        %grid on;
        disp('====================amortizare Rayleigh==================');
        disp('comparatie FEM - spice cu Fel = kz');
        calculeza_erori_dintre_curbe(tFEM,zFEM,tA,zA);
        disp('comparatie FEM - spice cu Fel = k1 z k3 z^3');
        calculeza_erori_dintre_curbe(tFEM,zFEM,tB1,zB1);
   end
end
```

A2. ROM's SPICE Circuit Netlist

```
V1 nd_Vact 0 0
C1 nd_zVal 0 1
G1 0 nd_zVal nd_vVal 0 1
B1 0 nd_vVal I = -V(nd_Vact)*V(nd_Vact)/2*V(nd_derC)
B2 0 nd_vVal I= -K1*V(nd_zVal) - K3*V(nd_zVal)*V(nd_zVal)*V(nd_zVal)
C2 nd_vVal 0 {M}
F1 nd_Vact 0 V2 1
B3 N003 0 V=V(nd_Vact)*V(nd_CapVal)
C3 N004 0 1
V2 N004 N003 0
R1 nd_CapVal 0 1
B4 nd_CapVal 0 V=1/( c1*V(nd_zVal)+c2)
R3 nd_derC 0 1
B5 nd_derC 0 V= c1*1/(c1*V(nd_zVal)+c2)/(c1*V(nd_zVal)+c2)
V3 N001 0 AC 1
O1 N001 0 N002 0 MyLL
O2 N002 0 OUT 0 MyLL
B6 nd_Csw 0 I=I(V4)*(V(nd_CapVal)+{Cfix})*1e-12
B7 N006 0 V=V(nd_Csw)
C4 N007 0 1
V4 N006 N007 0
Lmem N005 nd_Csw 2.07e-13
Rmem N002 N005 0.0035
.param M = 2.620274e-005
.param K1 =8.493218e-001
* V(nd_CapVal) = C(z) [pF]
* V(nd_zVal) = z(t) [um]
* V(nd_Vact) = actuation voltage (t)  [V]
* V(nd_vVal) = v(t) = dz(t)/dt  [um/ms]
* V(nd_derC) = dC/d(g0-z) [pF/um]
.param c1 =-6.628623e+000
.param c2 = 2.691799e+001
* [1/(pF*um]
* [1/pF]
* [mg]
* [N/m]
.param K3 = 1.660979e+000
* [N/(m*um*um)]
.model    MyLL    LTRA(len=300e-6 R=6.711e+002 L=2.825e-007  C=2.064e-010)
.ac oct 100 1e9 60e9
.net V(OUT) V3 Rout=50 Rin=50
.param Cfix = 2.140112e-002
.backanno
.end
```

A3. COMSOL Model Code Representation

```
function out = model
%
% Anexa3.m
%
% Model exported by COMSOL 4.4.0.248.

import com.comsol.model.*
import com.comsol.model.util.*

model = ModelUtil.create('Model');

model.modelPath('E:\PhD');

model.name('Qian3D_Contact_FSI_withPerforation.mph');

model.param.set('Lm', '280[um]', 'L mem');
model.param.set('Wm', '120[um]', 'W mem');
model.param.set('Hm', '0.4[um]', 'H mem');
model.param.set('h_cpw', '4[um]', 'H CPW');
model.param.set('h_electrod', '0.4[um]', 'H electrod');
model.param.set('Td', '0.1[um]', 'H dielectric');
model.param.set('l_cpw', '120[um]', 'W CPW');
model.param.set('Vstep', '25[V]', 'Actuation Voltage');
model.param.set('V0', '0.1[V]');
model.param.set('en', '1e15[Pa/m]');
model.param.set('tn', '5e4[Pa]');
model.param.set('hole', '20[um]', 'L perforation');

model.modelNode.create('comp1');

model.func.create('step1', 'Step');
model.func.create('step2', 'Step');
model.func('step1').model('comp1');
model.func('step1').active(false);
model.func('step1').set('smooth', '0.05*Td');
model.func('step1').set('location', '1.05*Td');
model.func('step2').model('comp1');
model.func('step2').set('smooth', '0.5e-5');
model.func('step2').set('location', '1e-5');

model.geom.create('geom1', 3);
model.geom('geom1').lengthUnit([native2unicode(hex2dec({'00' 'b5'}), 'unicode') 'm']);
model.geom('geom1').feature.create('blk1', 'Block');
model.geom('geom1').feature.create('blk2', 'Block');
model.geom('geom1').feature.create('blk3', 'Block');
model.geom('geom1').feature.create('blk4', 'Block');
model.geom('geom1').feature.create('blk5', 'Block');
model.geom('geom1').feature.create('blk6', 'Block');
model.geom('geom1').feature.create('blk7', 'Block');
model.geom('geom1').feature.create('blk8', 'Block');
model.geom('geom1').feature.create('blk9', 'Block');
model.geom('geom1').feature.create('blk10', 'Block');
model.geom('geom1').feature.create('blk11', 'Block');
```

```
model.geom('geom1').feature('blk1').name('membrana');
model.geom('geom1').feature('blk1').set('size', {'Lm/2' 'Wm/2' 'Hm'});
model.geom('geom1').feature('blk1').set('pos', {'0' '0' 'h_cpw'});
model.geom('geom1').feature('blk2').name('Spatiu Aer');
model.geom('geom1').feature('blk2').set('size', {'Lm/2' 'Wm/2+20' '2*h_cpw'});
model.geom('geom1').feature('blk2').set('pos', {'0' '0' 'h_electrod'});
model.geom('geom1').feature('blk3').name('Dielectric');
model.geom('geom1').feature('blk3').set('size', {'l_cpw/2' 'Wm/2' 'Td'});
model.geom('geom1').feature('blk3').set('pos', {'Lm/2-l_cpw/2' '0' 'h_electrod'});
model.geom('geom1').feature('blk4').active(false);
model.geom('geom1').feature('blk4').name('Aer_jos');
model.geom('geom1').feature('blk4').set('size', {'Lm/2' 'Wm/2' 'Td'});
model.geom('geom1').feature('blk4').set('pos', {'0' '0' 'h_electrod'});
model.geom('geom1').feature('blk5').active(false);
model.geom('geom1').feature('blk5').name('Aer_jos 1');
model.geom('geom1').feature('blk5').set('size', {'Lm/2' 'Wm/2+20' 'Td'});
model.geom('geom1').feature('blk5').set('pos', {'0' '0' 'h_electrod'});
model.geom('geom1').feature('blk6').active(false);
model.geom('geom1').feature('blk6').name('Aer_intre');
model.geom('geom1').feature('blk6').set('size', {'Lm/2' 'Wm/2+20' 'h_cpw'});
model.geom('geom1').feature('blk6').set('pos', {'0' '0' 'h_electrod'});
model.geom('geom1').feature('blk7').active(false);
model.geom('geom1').feature('blk7').name('Aer_intre 1');
model.geom('geom1').feature('blk7').set('size', {'Lm/2' 'Wm/2' '2*h_cpw'});
model.geom('geom1').feature('blk7').set('pos', {'0' '0' 'h_electrod'});
model.geom('geom1').feature('blk8').active(false);
model.geom('geom1').feature('blk8').name('Aer_intre 2');
model.geom('geom1').feature('blk8').set('size', {'Lm/2' 'Wm/2+20' 'h_cpw-Hm'});
model.geom('geom1').feature('blk8').set('pos', {'0' '0' 'h_electrod'});
model.geom('geom1').feature('blk9').name('hole1.1');
model.geom('geom1').feature('blk9').set('size', {'hole' 'hole' 'Hm'});
model.geom('geom1').feature('blk9').set('pos', {'hole+hole/2' 'hole' 'h_cpw'});
model.geom('geom1').feature('blk10').name('hole1.2');
model.geom('geom1').feature('blk10').set('size', {'hole' 'hole' 'Hm'});
model.geom('geom1').feature('blk10').set('pos', {'3*hole+hole/2' 'hole' 'h_cpw'});
model.geom('geom1').feature('blk11').name('hole1.3');
model.geom('geom1').feature('blk11').set('size', {'hole' 'hole' 'Hm'});
model.geom('geom1').feature('blk11').set('pos', {'5*hole+hole/2' 'hole' 'h_cpw'});
model.geom('geom1').run;

model.selection.create('sel1', 'Explicit');
model.selection('sel1').geom('geom1', 3, 2, {'exterior'});
model.selection('sel1').set([2]);
model.selection.create('sel2', 'Explicit');
model.selection('sel2').geom('geom1', 3, 2, {'exterior'});
model.selection('sel2').set([5]);
model.selection('sel1').name('Membrana');
model.selection('sel1').name('Explicit 1');
model.selection('sel2').name('Aer_jos');
model.selection('sel2').name('Explicit 2');

model.variable.create('var1');
model.variable('var1').model('comp1');
model.variable('var1').set('gap', 'h_cpw-Td+h_electrod+w_solid');
model.variable('var1').set('contactpresure', '...
```

```
(gap<=0)*(tn-en*gap)+(gap>0)*tn*exp(-gap*en/tn)');
model.variable('var1').set('Va', 'V0+Vstep*step2(t/1[s])');

model.view('view1').hideEntities.create('hide1');
model.view('view1').hideEntities('hide1').geom('geom1', 2);
model.view('view1').hideEntities('hide1').set([9]);
model.view.create('view2', 3);
model.view.create('view3', 2);

model.material.create('mat1');
model.material.create('mat2');
model.material('mat2').selection.set([2]);
model.material.create('mat3');
model.material('mat3').selection.set([5]);

model.physics.create('es', 'Electrostatics', 'geom1');
model.physics('es').feature.create('gnd1', 'Ground', 2);
model.physics('es').feature('gnd1').selection.set(...
[1 3 4 5 6 8 10 12 13 16 17 18 19 22 28 29 30 33 34 37]);
model.physics('es').feature.create('term1', 'Terminal', 2);
model.physics('es').feature('term1').selection.set([25]);
model.physics('es').feature.create('term2', 'Terminal', 2);
model.physics('es').feature('term2').selection.set([25]);
model.physics.create('fsi', 'FluidStructureInteraction', 'geom1');
model.physics('fsi').selection.set([1 2 3 4 6]);
model.physics('fsi').feature('dlemm1').selection.set([2]);
model.physics('fsi').feature.create('sym1', 'SymmetrySolid', 2);
model.physics('fsi').feature('sym1').selection.set([5 37]);
model.physics('fsi').feature.create('fix1', 'Fixed', 2);
model.physics('fsi').feature('fix1').selection.set([4]);
model.physics('fsi').feature.create('bndl1', 'BoundaryLoad', 2);
model.physics('fsi').feature('bndl1').selection.set([6]);
model.physics('fsi').feature.create('open1', 'OpenBoundary', 2);
model.physics('fsi').feature('open1').selection.set([9 11 27]);
model.physics('fsi').feature.create('sym2', 'SymmetryFluid', 2);
model.physics('fsi').feature('sym2').selection.set([2 7 24 35 36]);
model.physics('fsi').feature.create('disp2', 'PrescribedMeshDisplacement', 2);
model.physics('fsi').feature('disp2').selection.set([2 7]);
model.physics('fsi').feature.create('disp3', 'PrescribedMeshDisplacement', 2);
model.physics('fsi').feature('disp3').selection.set([36]);
model.physics('fsi').feature.create('bndl2', 'BoundaryLoad', 2);
model.physics('fsi').feature('bndl2').selection.set([6]);

model.mesh.create('mesh1', 'geom1');
model.mesh('mesh1').feature.create('ftet1', 'FreeTet');
model.mesh('mesh1').feature('ftet1').feature.create('size1', 'Size');
model.mesh('mesh1').feature('ftet1').feature.create('size2', 'Size');
model.mesh('mesh1').feature('ftet1').feature.create('size3', 'Size');
model.mesh('mesh1').feature('ftet1').feature.create('size4', 'Size');
model.mesh('mesh1').feature('ftet1').feature.create('size5', 'Size');
model.mesh('mesh1').feature('ftet1').feature('size2').selection.geom('geom1', 2);
model.mesh('mesh1').feature('ftet1').feature('size2').selection.set([...
4 5 10 12 13 16 17 18 19 22 23 24 27 28 29 30 33 34 35 37]);
model.mesh('mesh1').feature('ftet1').feature('size3').selection.geom('geom1', 1);
model.mesh('mesh1').feature('ftet1').feature('size3').selection.set([...
```

```
4 12 18 23 26 29 30 35 38 43 46 49 50 55 58 61 62 66 71 73 74]);
model.mesh('mesh1').feature('ftet1').feature('size4').selection.geom('geom1', 2);
model.mesh('mesh1').feature('ftet1').feature('size4').selection.set([23 24 27 35]);
model.mesh('mesh1').feature('ftet1').feature('size5').selection.geom('geom1', 1);
model.mesh('mesh1').feature('ftet1').feature('size5').selection.set([38 43 62 71 74]);

model.result.table.create('mm1', 'Table');

model.view('view1').set('renderwireframe', true);
model.view('view1').set('scenelight', 'off');
model.view('view2').set('scenelight', 'off');
model.view('view2').set('transparency', 'on');
model.view('view3').axis.set('xmin', '-0.3853249251842499');
model.view('view3').axis.set('ymin', '-0.02500000037252903');
model.view('view3').axis.set('xmax', '0.8853248357772827');
model.view('view3').axis.set('ymax', '0.5249999761581421');

model.material('mat1').name('Air');
model.material('mat1').propertyGroup('def').set('relpermittivity', {...
'1' '0' '0' '0' '1' '0' '0' '0' '1'});
model.material('mat1').propertyGroup('def').set('density', '1.22');
model.material('mat1').propertyGroup('def').set('dynamicviscosity', '18.6e-6');
model.material('mat1').materialType('nonSolid');
model.material('mat2').name('Alum');
model.material('mat2').propertyGroup('def').set('density', '2700');
model.material('mat2').propertyGroup('def').set('poissonsratio', '0.35');
model.material('mat2').propertyGroup('def').set('youngsmodulus', '70e9');
model.material('mat2').propertyGroup('def').set('relpermittivity', {...
'1' '0' '0' '0' '1' '0' '0' '0' '1'});
model.material('mat3').name('Isolator');
model.material('mat3').propertyGroup('def').set('relpermittivity', {...
'7' '0' '0' '0' '7' '0' '0' '0' '7'});
model.material('mat3').materialType('nonSolid');

model.physics('es').feature('term1').set('V0', 'Va');
model.physics('es').feature('term1').set('TerminalType', 'Voltage');
model.physics('es').feature('term2').set('V0', 'V0');
model.physics('es').feature('term2').set('TerminalType', 'Voltage');
model.physics('fsi').prop('FreeDeformationSettings').set(...
'smoothingType', 'hyperelastic');
model.physics('fsi').feature('sym1').name('Symmetry MEC');
model.physics('fsi').feature('bndl1').set('LoadType', 'FollowerPressure');
model.physics('fsi').feature('bndl1').set('FollowerPressure', 'es.unTez');
model.physics('fsi').feature('disp2').set('useDx', {'0'; '1'; '0'});
model.physics('fsi').feature('disp3').set('useDx', {'1'; '1'; '0'});
model.physics('fsi').feature('bndl2').set('FperArea', {'0'; '0'; 'contactpresure'});
model.physics('fsi').feature('bndl2').set('FollowerPressure', 'contactpresure');

model.mesh('mesh1').feature('size').set('hauto', 9);
model.mesh('mesh1').feature('ftet1').feature('size1').set('hauto', 7);
model.mesh('mesh1').feature('ftet1').feature('size4').set('hauto', 3);
model.mesh('mesh1').feature('ftet1').feature('size5').set('hauto', 3);
model.mesh('mesh1').run;

model.frame('material1').sorder(1);
```

```
model.result.table('mm1').name('pg2/mmv1');
model.result.table('mm1').comments('Max/min volume');

model.study.create('std1');
model.study('std1').feature.create('stat', 'Stationary');
model.study('std1').feature.create('time', 'Transient');

model.sol.create('sol1');
model.sol('sol1').study('std1');
model.sol('sol1').attach('std1');
model.sol('sol1').feature.create('st1', 'StudyStep');
model.sol('sol1').feature.create('v1', 'Variables');
model.sol('sol1').feature.create('s1', 'Stationary');
model.sol('sol1').feature.create('su1', 'StoreSolution');
model.sol('sol1').feature.create('st2', 'StudyStep');
model.sol('sol1').feature.create('v2', 'Variables');
model.sol('sol1').feature.create('t1', 'Time');
model.sol('sol1').feature('s1').feature.create('se1', 'Segregated');
model.sol('sol1').feature('s1').feature.create('i1', 'Iterative');
model.sol('sol1').feature('s1').feature.create('d1', 'Direct');
model.sol('sol1').feature('s1').feature('se1').feature.create('ss1', 'SegregatedStep');
model.sol('sol1').feature('s1').feature('se1').feature.create('ss2', 'SegregatedStep');
model.sol('sol1').feature('s1').feature('se1').feature.create('ss3', 'SegregatedStep');
model.sol('sol1').feature('s1').feature('se1').feature.remove('ssDef');
model.sol('sol1').feature('s1').feature('i1').feature.create('mg1', 'Multigrid');
model.sol('sol1').feature('s1').feature.remove('fcDef');
model.sol('sol1').feature('t1').feature.create('se1', 'Segregated');
model.sol('sol1').feature('t1').feature.create('i1', 'Iterative');
model.sol('sol1').feature('t1').feature.create('d1', 'Direct');
model.sol('sol1').feature('t1').feature.create('fc1', 'FullyCoupled');
model.sol('sol1').feature('t1').feature.create('tpDef', 'TimeParametric');
model.sol('sol1').feature('t1').feature('se1').feature.create('ss1', 'SegregatedStep');
model.sol('sol1').feature('t1').feature('se1').feature.create('ss2', 'SegregatedStep');
model.sol('sol1').feature('t1').feature('se1').feature.create('ss3', 'SegregatedStep');
model.sol('sol1').feature('t1').feature('se1').feature.remove('ssDef');
model.sol('sol1').feature('t1').feature('i1').feature.create('mg1', 'Multigrid');
model.sol('sol1').feature('t1').feature.remove('fcDef');

model.study('std1').feature('stat').set('initstudyhide', 'on');
model.study('std1').feature('stat').set('initsolhide', 'on');
model.study('std1').feature('stat').set('notstudyhide', 'on');
model.study('std1').feature('stat').set('notsolhide', 'on');
model.study('std1').feature('time').set('initstudyhide', 'on');
model.study('std1').feature('time').set('initsolhide', 'on');
model.study('std1').feature('time').set('notstudyhide', 'on');
model.study('std1').feature('time').set('notsolhide', 'on');

model.result.dataset.create('surf1', 'Surface');
model.result.dataset.create('mir1', 'Mirror3D');
model.result.dataset.create('mir2', 'Mirror3D');
model.result.dataset('surf1').selection.set([3 6 8 10 14 15 20 21 23 26 31 32]);
model.result.dataset('mir2').set('data', 'mir1');
model.result.create('pg1', 'PlotGroup3D');
model.result.create('pg2', 'PlotGroup3D');
```

```
model.result.create('pg3', 'PlotGroup3D');
model.result.create('pg4', 'PlotGroup1D');
model.result.create('pg5', 'PlotGroup3D');
model.result.create('pg6', 'PlotGroup1D');
model.result.create('pg7', 'PlotGroup3D');
model.result.create('pg8', 'PlotGroup3D');
model.result('pg1').feature.create('mslc1', 'Multislice');
model.result('pg1').feature.create('surf1', 'Surface');
model.result('pg2').feature.create('surf1', 'Surface');
model.result('pg2').feature.create('arwv1', 'ArrowVolume');
model.result('pg2').feature.create('mmv1', 'MaxMinVolume');
model.result('pg2').feature('arwv1').feature.create('col', 'Color');
model.result('pg3').feature.create('surf1', 'Surface');
model.result('pg3').feature.create('con1', 'Contour');
model.result('pg4').feature.create('ptgr1', 'PointGraph');
model.result('pg4').feature('ptgr1').selection.set([39]);
model.result('pg5').feature.create('vol1', 'Volume');
model.result('pg6').feature.create('glob1', 'Global');
model.result('pg7').feature.create('vol1', 'Volume');
model.result('pg8').feature.create('surf1', 'Surface');

model.study('std1').feature('time').set('disabledphysics', {'es/term2'});
model.study('std1').feature('time').set('tunit', [native2unicode(hex2dec...
({'00' 'b5'}), 'unicode') 's']);
model.study('std1').feature('time').set('useadvanceddisable', true);
model.study('std1').feature('time').set('tlist', 'range(0,1,100)');

model.sol('sol1').attach('std1');
model.sol('sol1').feature('st1').name('Compile Equations: Stationary');
model.sol('sol1').feature('st1').set('studystep', 'stat');
model.sol('sol1').feature('v1').set('control', 'stat');
model.sol('sol1').feature('v1').feature('comp1_u_solid').set('scalemethod', 'manual');
model.sol('sol1').feature('v1').feature('comp1_u_solid').set(...
'scaleval', '1e-2*1.614434885648845E-4');
model.sol('sol1').feature('s1').set('control', 'stat');
model.sol('sol1').feature('s1').feature('se1').set('subusecflcmp', 'on');
model.sol('sol1').feature('s1').feature('se1').set('maxsegiter', '200');
model.sol('sol1').feature('s1').feature('se1').feature('ss1').set(...
'linsolver', 'i1');
model.sol('sol1').feature('s1').feature('se1').feature('ss1').set(...
'segvar', {'comp1_V'});
model.sol('sol1').feature('s1').feature('se1').feature('ss2').set(...
'subdamp', '0.5');
model.sol('sol1').feature('s1').feature('se1').feature('ss2').set(...
'segvar', {'comp1_xyz' 'comp1_u_solid'});
model.sol('sol1').feature('s1').feature('se1').feature('ss3').set(...
'linsolver', 'd1');
model.sol('sol1').feature('s1').feature('se1').feature('ss3').set(...
'subdamp', '0.5');
model.sol('sol1').feature('s1').feature('se1').feature('ss3').set(...
'segvar', {'comp1_u_fluid' 'comp1_p'});
model.sol('sol1').feature('s1').feature('i1').set('linsolver', 'cg');
model.sol('sol1').feature('s1').feature('i1').feature('mg1').set('prefun', 'amg');
model.sol('sol1').feature('s1').feature('d1').set('linsolver', 'pardiso');
model.sol('sol1').feature('st2').name('Compile Equations: Time Dependent (2)');
```

```
model.sol('sol1').feature('st2').set('studystep', 'time');
model.sol('sol1').feature('v2').set('initsol', 'sol1');
model.sol('sol1').feature('v2').set('notsolmethod', 'sol');
model.sol('sol1').feature('v2').set('control', 'time');
model.sol('sol1').feature('v2').set('initmethod', 'sol');
model.sol('sol1').feature('v2').set('initsoluse', 'sol2');
model.sol('sol1').feature('v2').set('solnum', 'auto');
model.sol('sol1').feature('v2').set('notsol', 'sol1');
model.sol('sol1').feature('v2').set('notsolnum', 'auto');
model.sol('sol1').feature('v2').set('notsoluse', 'sol2');
model.sol('sol1').feature('v2').feature('comp1_u_solid').set(...
'scalemethod', 'manual');
model.sol('sol1').feature('v2').feature('comp1_u_solid').set(...
'scaleval', '1e-2*1.614434885648845E-4');
model.sol('sol1').feature('t1').set('tlist', 'range(0,1,100)');
model.sol('sol1').feature('t1').set('timemethod', 'genalpha');
model.sol('sol1').feature('t1').set('control', 'time');
model.sol('sol1').feature('t1').set('tout', 'tsteps');
model.sol('sol1').feature('t1').set('atolglobal', '5.0E-4');
model.sol('sol1').feature('t1').set('tunit', [native2unicode(...
hex2dec({'00' 'b5'}), 'unicode') 's']);
model.sol('sol1').feature('t1').feature('se1').feature('ss1').active(false);
model.sol('sol1').feature('t1').feature('se1').feature('ss1').set('segvar', {'comp1_V'});
model.sol('sol1').feature('t1').feature('se1').feature('ss1').set('linsolver', 'i1');
model.sol('sol1').feature('t1').feature('se1').feature('ss2').active(false);
model.sol('sol1').feature('t1').feature('se1').feature('ss2').set(...
'segvar', {'comp1_xyz' 'comp1_u_solid'});
model.sol('sol1').feature('t1').feature('se1').feature('ss2').set('subdamp', '0.5');
model.sol('sol1').feature('t1').feature('se1').feature('ss2').set('subjtech', 'once');
model.sol('sol1').feature('t1').feature('se1').feature('ss3').active(false);
model.sol('sol1').feature('t1').feature('se1').feature('ss3').set(...
'segvar', {'comp1_u_fluid' 'comp1_p'});
model.sol('sol1').feature('t1').feature('se1').feature('ss3').set('subdamp', '0.5');
model.sol('sol1').feature('t1').feature('se1').feature('ss3').set('linsolver', 'd1');
model.sol('sol1').feature('t1').feature('se1').feature('ss3').set('subjtech', 'once');
model.sol('sol1').feature('t1').feature('i1').set('linsolver', 'cg');
model.sol('sol1').feature('t1').feature('i1').feature('mg1').set('prefun', 'amg');
model.sol('sol1').feature('t1').feature('d1').active(true);
model.sol('sol1').feature('t1').feature('d1').set('linsolver', 'pardiso');
model.sol('sol1').feature('t1').feature('fc1').active(true);
model.sol('sol1').feature('t1').feature('fc1').set('jtech', 'onevery');
model.sol('sol1').feature('t1').feature('fc1').set('maxiter', '8');
model.sol('sol1').feature('t1').feature('fc1').set('linsolver', 'd1');
model.sol('sol1').feature('t1').feature('fc1').set('plotgroup', 'pg4');
model.sol('sol1').feature('t1').feature('fc1').set('plot', 'on');
model.sol('sol1').feature('t1').feature('tpDef').active(false);
model.sol('sol1').feature('t1').feature('tpDef').set('control', 'time');
model.sol('sol1').feature('t1').feature('tpDef').set('pname', {'Vstep'});
model.sol('sol1').feature('t1').feature('tpDef').set('plistarr', {'range(20,2,26)'});
model.sol('sol1').runAll;

model.result.dataset('mir1').set('quickplane', 'xz');
model.result.dataset('mir2').set('quickx', '120');
model.result('pg1').name('Electric Potential (es)');
model.result('pg1').set('showhiddenobjects', true);
```

```
model.result('pg1').set('frametype', 'spatial');
model.result('pg1').feature('surf1').active(false);
model.result('pg2').name('Flow and Stress (fsi)');
model.result('pg2').set('frametype', 'spatial');
model.result('pg2').set('looplevel', {'48'});
model.result('pg2').feature('surf1').set('expr', 'fsi.mises');
model.result('pg2').feature('surf1').set('unit', 'N/m^2');
model.result('pg2').feature('surf1').set('descr', 'von Mises stress');
model.result('pg2').feature('surf1').set('colortable', 'Traffic');
model.result('pg2').feature('arwv1').set('arrowlength', 'normalized');
model.result('pg2').feature('arwv1').set('descr', 'Velocity field (Spatial)');
model.result('pg2').feature('arwv1').set('arrowbase', 'head');
model.result('pg2').feature('arwv1').set('arrowxmethod', 'coord');
model.result('pg2').feature('arwv1').set('xcoord', '120');
model.result('pg2').feature('arwv1').set('znumber', '5');
model.result('pg2').feature('arwv1').set('scaleactive', true);
model.result('pg2').feature('arwv1').set('scale', '2500');
model.result('pg2').feature('arwv1').set('expr', {'u_fluid' 'v_fluid' 'w_fluid'});
model.result('pg2').feature('arwv1').set('ynumber', '16');
model.result('pg2').feature('mmv1').active(false);
model.result('pg2').feature('mmv1').set('expr', 'fsi.disp');
model.result('pg2').feature('mmv1').set('unit', [native2unicode(...
hex2dec({'00' 'b5'}), 'unicode') 'm']);
model.result('pg2').feature('mmv1').set('descr', 'Total displacement');
model.result('pg3').name('Pressure (fsi)');
model.result('pg3').set('data', 'surf1');
model.result('pg3').set('frametype', 'spatial');
model.result('pg3').feature('surf1').set('color', 'gray');
model.result('pg3').feature('surf1').set('expr', '1');
model.result('pg3').feature('surf1').set('unit', '');
model.result('pg3').feature('surf1').set('descr', '1');
model.result('pg3').feature('surf1').set('coloring', 'uniform');
model.result('pg3').feature('con1').set('number', '10');
model.result('pg3').feature('con1').set('expr', 'p');
model.result('pg3').feature('con1').set('descr', 'Pressure');
model.result('pg3').feature('con1').set('unit', 'Pa');
model.result('pg4').name('Displacement Z');
model.result('pg4').set('ylabel', ['Displacement Z (...
' native2unicode(hex2dec({'00' 'b5'}), 'unicode') 'm)']);
model.result('pg4').set('xlabel', ['Time (...
' native2unicode(hex2dec({'00' 'b5'}), 'unicode') 's)']);
model.result('pg4').set('xlabelactive', false);
model.result('pg4').set('ylabelactive', false);
model.result('pg4').feature('ptgr1').set('expr', 'w_solid');
model.result('pg4').feature('ptgr1').set(...
'unit', [native2unicode(hex2dec({'00' 'b5'}), 'unicode') 'm']);
model.result('pg4').feature('ptgr1').set('descr', 'Displacement Z');
model.result('pg4').feature('ptgr1').set('linewidth', '3');
model.result('pg4').feature('ptgr1').set('descractive', true);
model.result('pg5').name('permittivity');
model.result('pg5').feature('vol1').set('unit', '1');
model.result('pg5').feature('vol1').set('expr', 'es.epsilonrxx');
model.result('pg5').feature('vol1').set(...
'descr', 'Relative permittivity, xx component');
model.result('pg6').name('V(t)');
```

```
model.result('pg6').set('xlabel', ['Time (...
' native2unicode(hex2dec({'00' 'b5'}), 'unicode') 's)']);
model.result('pg6').set('xlabelactive', false);
model.result('pg6').feature('glob1').set('expr', {'Va'});
model.result('pg6').feature('glob1').set('descr', {''});
model.result('pg6').feature('glob1').set('unit', {'V'});
model.result('pg7').name('Total Displacement');
model.result('pg7').feature('vol1').set('unit', [...
native2unicode(hex2dec({'00' 'b5'}), 'unicode') 'm']);
model.result('pg7').feature('vol1').set('expr', 'fsi.disp');
model.result('pg7').feature('vol1').set('descr', 'Total displacement');
model.result('pg8').name('ContactForce');
model.result('pg8').set('frametype', 'geometry');
model.result('pg8').feature('surf1').set('expr', 'es.unTez');
model.result('pg8').feature('surf1').set('unit', 'N/m^2');
model.result('pg8').feature('surf1').set(...
'descr', 'Maxwell upward electric surface stress tensor, z component');

out = model;
```

A4. Analysis Report by COMSOL

Component 1 (comp1)

1.1 Materials

1.1.1 Air

Selection

Geometric entity level	Domain
Selection	Domains 1, 3–4, 6

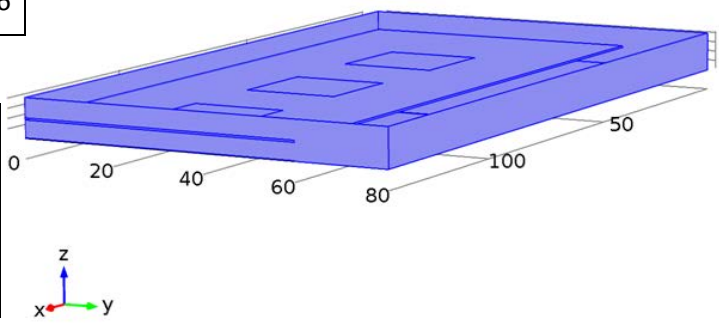

Material parameters

Name	Value	Unit
Relative permittivity	1	1
Density	1.22	kg/m^3
Dynamic viscosity	18.6e-6	Pa*s

Basic Settings

Description	Value
Relative permittivity	{{1, 0, 0}, {0, 1, 0}, {0, 0, 1}}
Density	1.22
Dynamic viscosity	18.6e-6

1.1.2 Alum

Selection

Geometric entity level	Domain
Selection	Domain 2

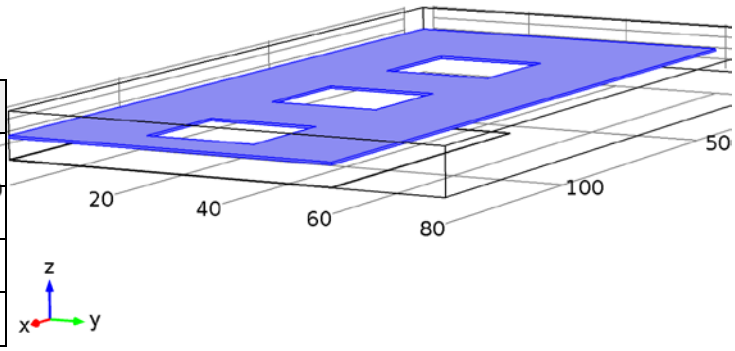

Material parameters

Name	Value	Unit
Density	2700	kg/m^3
Poisson's ratio	0.35	1
Young's modulus	70e9	Pa
Relative permittivity	1	1

Basic Settings

Description	Value
Density	2700
Poisson's ratio	0.35
Young's modulus	70e9
Relative permittivity	{{1, 0, 0}, {0, 1, 0}, {0, 0, 1}}

1.1.3 Isolator

Selection

Geometric entity level	Domain
Selection	Domain 5

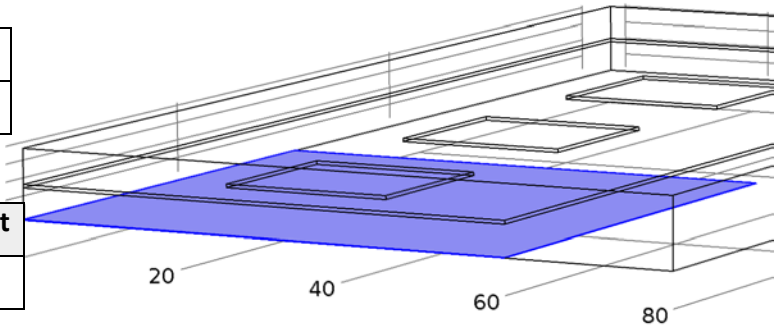

Material parameters

Name	Value	Unit
Relative permittivity	7	1

Basic Settings

Description	Value
Relative permittivity	{{7, 0, 0}, {0, 7, 0}, {0, 0, 7}}

1.2 Electrostatics (es)

Equations

$$\nabla \cdot \mathrm{D} = \rho_v$$

$$\mathrm{E} = -\nabla V$$

Settings

Description	Value
Electric potential	Quadratic
Value type when using splitting of complex variables	Complex
Frame	Spatial
Activate terminal sweep	Off
Reference impedance	50[ohm]
Parameter to export	Z

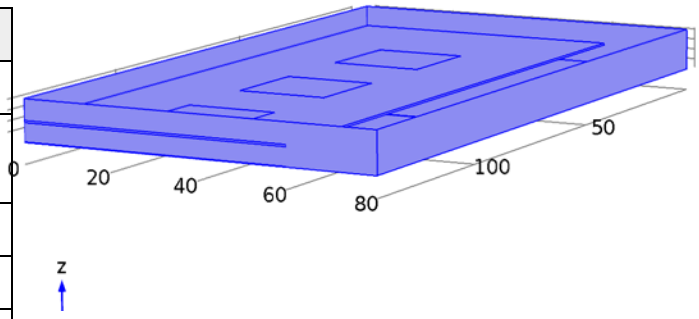

1.2.1 Charge Conservation 1

Equations

$$\mathrm{E} = -\nabla V$$

$$\nabla \cdot (\epsilon_0 \epsilon_r \mathrm{E}) = \rho_v$$

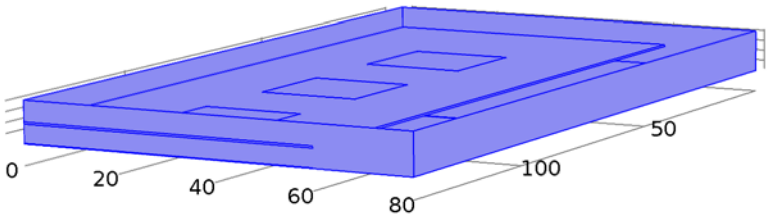

1.2.1.1 Settings

Settings

Description	Value
Constitutive relation	Relative permittivity
Relative permittivity	From material
Relative permittivity	{{1, 0, 0}, {0, 1, 0}, {0, 0, 1}}

Properties from material

Property	Material	Property group

Property	Material	Property group
Relative permittivity	Air	Basic
Relative permittivity	Alum	Basic
Relative permittivity	Isolator	Basic

1.2.1.2 Shape functions

Name	Shape function	Unit	Description	Shape frame	Selection
V	Lagrange (Quadratic)	V	Electric potential	Spatial	Domains 1–6
V	Lagrange (Quadratic)	V	Electric potential	Material	Domains 1–6

1.2.1.3 Weak expressions

Weak expression	Integration frame	Selection
-(es.Dx*test(Vx)+es.Dy*test(Vy)+es.Dz*test(Vz))*es.d	Spatial	Domains 1–6

1.2.2 Zero Charge 1

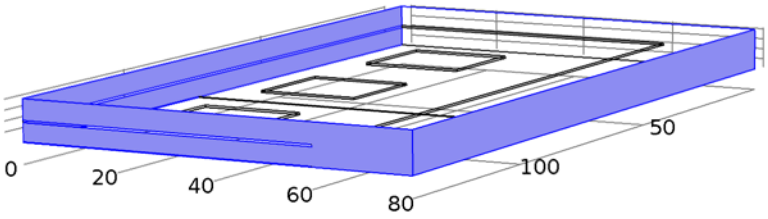

Equations

$$\mathbf{n} \cdot \mathbf{D} = 0$$

1.2.2.1 Shape functions

Name	Shape function	Unit	Description	Shape frame	Selection
V	Lagrange (Quadratic)	V	Electric potential	Spatial	No boundaries
V	Lagrange (Quadratic)	V	Electric potential	Material	No boundaries

1.2.3 Initial Values

1.2.3.1 Settings

Settings

Description	Value
Electric potential	0

1.2.4 Ground 1

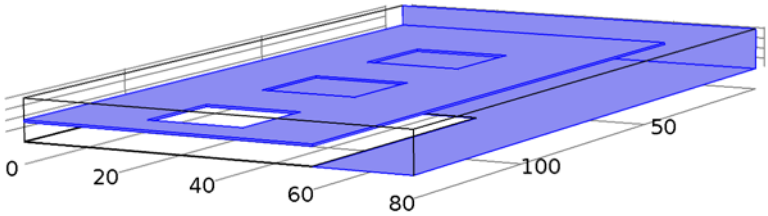

Equations

$$V = 0$$

1.2.4.1 Settings

Settings

Description	Value
Apply reaction terms on	All physics (symmetric)

Description	Value
Use weak constraints	Off

1.2.4.2 Shape functions

Constraint	Constraint force	Shape function	Selection
-V	test(-V)	Lagrange (Quadratic)	Boundaries 1, 3–6, 8, 10, 12–13, 16–19, 22, 28–30, 33–34, 37

1.2.5 Terminal 1

Equations

$V = V_0$

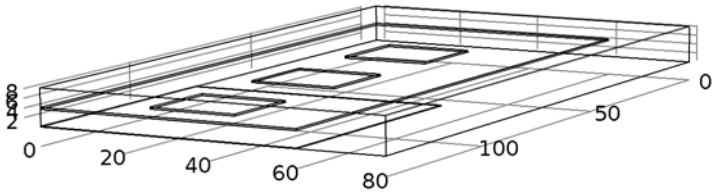

1.2.5.1 Settings

Settings

Description	Value
Terminal name	1
Terminal type	Voltage
Voltage	Va
Apply reaction terms on	All physics (symmetric)

1.2.6 Terminal 2

Equations

$V = V_0$

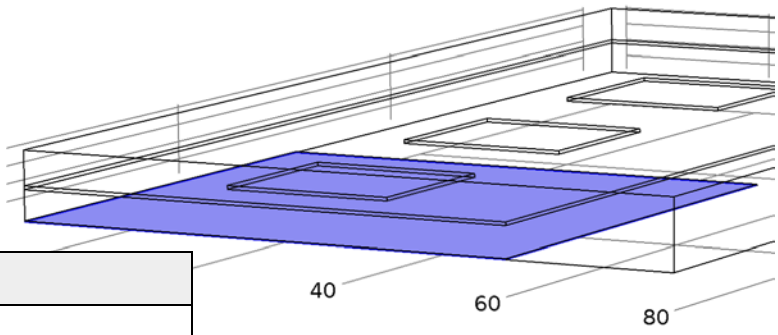

1.2.6.1 Settings

Settings

Description	Value
Terminal name	2
Terminal type	Voltage
Voltage	V0
Apply reaction terms on	All physics (symmetric)

1.2.6.2 Shape functions

Constraint	Constraint force	Shape function	Selection
es.Vterm-V	test(es.Vterm-V)	Lagrange (Quadratic)	Boundary 25

1.3 Fluid-Structure Interaction (fsi)

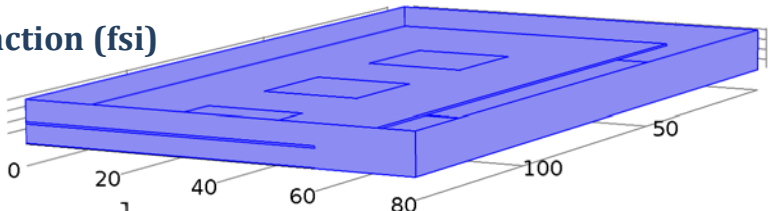

Equations

$$\rho\frac{\partial \mathbf{u}_{\text{fluid}}}{\partial t} + \rho(\mathbf{u}_{\text{fluid}} \cdot \nabla)\mathbf{u}_{\text{fluid}} =$$
$$\nabla \cdot \left[-p\mathbf{I} + \mu\left(\nabla \mathbf{u}_{\text{fluid}} + (\nabla \mathbf{u}_{\text{fluid}})^T\right) - \frac{2}{3}\mu(\nabla \cdot \mathbf{u}_{\text{fluid}})\mathbf{I}\right] + \mathbf{F}$$

$$\frac{\partial \rho}{\partial t} + \nabla \cdot (\rho \mathbf{u}_{fluid}) = 0$$
$$\rho \frac{\partial^2 \mathbf{u}_{solid}}{\partial t^2} - \nabla \cdot \sigma = F_V$$

Settings

Description	Value
Discretization of fluids	P1 + P1
Displacement field	Quadratic
Compute boundary fluxes	Off
Value type when using splitting of complex variables	{Complex, Real, Real, Real, Real, Real, Real, Real, Real, Complex}
Frame	Material
Neglect inertial term (Stokes flow)	Off
Displacements control spatial frame	On
Reference point for moment computation	{0, 0, 0}
Add mixed form pressure everywhere	Off
Structural transient behavior	Include inertial terms
Typical wave speed for perfectly matched layers	fsi.cp
SmeApplModeID	SolidMechanics
EquationType	smetffs

1.3.1 Fluid Properties 1

Equations

$$\rho \frac{\partial \mathbf{u}_{fluid}}{\partial t} + \rho(\mathbf{u}_{fluid} \cdot \nabla)\mathbf{u}_{fluid} =$$
$$\nabla \cdot \left[-p\mathbf{I} + \mu\left(\nabla \mathbf{u}_{fluid} + (\nabla \mathbf{u}_{fluid})^T\right) - \frac{2}{3}\mu(\nabla \cdot \mathbf{u}_{fluid})\mathbf{I}\right] + F$$
$$\frac{\partial \rho}{\partial t} + \nabla \cdot (\rho \mathbf{u}_{fluid}) = 0$$

1.3.1.1 Settings

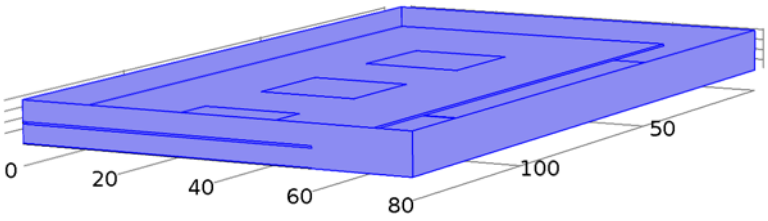

Settings

Description	Value
Density	From material
Dynamic viscosity	From material
Reference length	1
Reference length scale	Automatic
Mixing length limit	Automatic

Properties from material

Property	Material	Property group
Density	Air	Basic

Property	Material	Property group
Dynamic viscosity	Air	Basic

1.3.1.2 Shape functions

Name	Shape function	Unit	Description	Shape frame	Selection
u_fluid	Lagrange (Linear)	m/s	Velocity field, x component	Spatial	Domains 1, 3–4, 6
v_fluid	Lagrange (Linear)	m/s	Velocity field, y component	Spatial	Domains 1, 3–4, 6
w_fluid	Lagrange (Linear)	m/s	Velocity field, z component	Spatial	Domains 1, 3–4, 6
p	Lagrange (Linear)	Pa	Pressure	Spatial	Domains 1, 3–4, 6

1.3.1.3 Weak expressions

Weak expression	Integration frame	Selection
(p-fsi.K_stress_tensorxx)*test(u_fluidx)-fsi.K_stress_tensorxy*test(u_fluidy)-fsi.K_stress_tensorxz*test(u_fluidz)-fsi.K_stress_tensoryx*test(v_fluidx)+(p-fsi.K_stress_tensoryy)*test(v_fluidy)-fsi.K_stress_tensoryz*test(v_fluidz)-fsi.K_stress_tensorzx*test(w_fluidx)-fsi.K_stress_tensorzy*test(w_fluidy)+(p-fsi.K_stress_tensorzz)*test(w_fluidz)	Spatial	Domains 1, 3–4, 6
fsi.Fx*test(u_fluid)+fsi.Fy*test(v_fluid)+fsi.Fz*test(w_fluid)-fsi.rho*(u_fluidx*u_fluid+u_fluidy*v_fluid+u_fluidz*w_fluid)*test(u_fluid)-fsi.rho*(v_fluidx*u_fluid+v_fluidy*v_fluid+v_fluidz*w_fluid)*test(v_fluid)-fsi.rho*(w_fluidx*u_fluid+w_fluidy*v_fluid+w_fluidz*w_fluid)*test(w_fluid)	Spatial	Domains 1, 3–4, 6
test(p)*(-fsi.rho*fsi.divu-u_fluid*d(fsi.rho,x)-v_fluid*d(fsi.rho,y)-w_fluid*d(fsi.rho,z))	Spatial	Domains 1, 3–4, 6
fsi.crosswindns	Spatial	Domains 1, 3–4, 6
fsi.streamlinens	Spatial	Domains 1, 3–4, 6
-fsi.rho*nojac(fsi.time_step_inv/fsi.locCFL)*((u_fluid-nojac(u_fluid))*test(u_fluid)+(v_fluid-nojac(v_fluid))*test(v_fluid)+(w_fluid-nojac(w_fluid))*test(w_fluid))	Spatial	Domains 1, 3–4, 6

1.3.2 Free Deformation 1

1.3.2.1 Settings

Settings

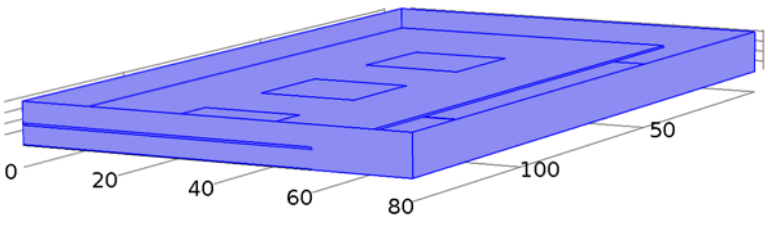

Description	Value
Initial mesh displacement	{0, 0, 0}

1.3.2.2 Shape functions

Name	Shape function	Unit	Description	Shape frame	Selection
x	Lagrange (Linear)	m	Spatial coordinate x	Material	Domains 1, 3–4, 6
y	Lagrange (Linear)	m	Spatial coordinate y	Material	Domains 1, 3–4, 6
z	Lagrange (Linear)	m	Spatial coordinate z	Material	Domains 1, 3–4, 6
x	Lagrange (Linear)	m	Spatial coordinate x	Material	Boundaries 6, 8, 10, 12–13, 16–19, 22, 28–30, 33–34
y	Lagrange (Linear)	m	Spatial coordinate y	Material	Boundaries 6, 8, 10, 12–13, 16–19, 22, 28–30, 33–34
z	Lagrange (Linear)	m	Spatial coordinate z	Material	Boundaries 6, 8, 10, 12–13, 16–19, 22, 28–30, 33–34

1.3.2.3 Weak expressions

Weak expression	Integration frame	Selection
-test(fsi.W_mesh)	Material	Domains 1, 3–4, 6

1.3.3 Wall 1

Equations

$$\mathbf{u}_{\text{fluid}} = 0$$

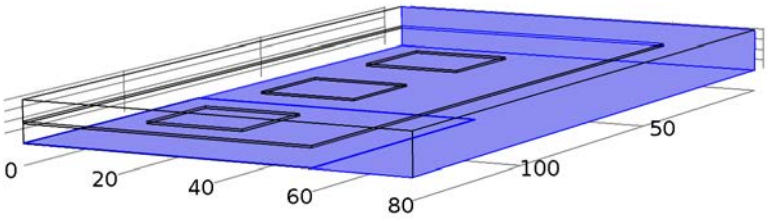

1.3.3.1 Settings

Settings

Description	Value
Temperature	User defined
Temperature	293.15[K]
Electric field	User defined
Electric field	{0, 0, 0}
Boundary condition	No slip
Apply reaction terms on	Individual dependent variables
Use weak constraints	Off

1.3.3.2 Shape functions

Constraint	Constraint force	Shape function	Selection
-u_fluid+fsi.ubndx	test(-u_fluid)	Lagrange (Linear)	Boundaries 1, 3, 23, 26
-v_fluid+fsi.ubndy	test(-v_fluid)	Lagrange (Linear)	Boundaries 1, 3, 23, 26
-w_fluid+fsi.ubndz	test(-w_fluid)	Lagrange (Linear)	Boundaries 1, 3, 23, 26

1.3.4 Prescribed Mesh Displacement 1

Settings

Description	Value
Prescribed # displacement	{On, On, On}
Prescribed mesh displacement	{0, 0, 0}
Use weak constraints	Off

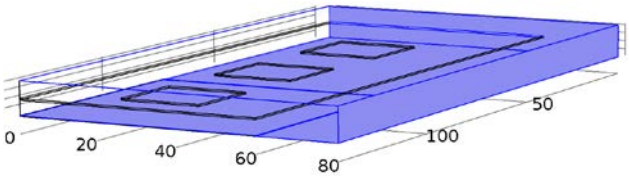

1.3.4.1 Shape functions

Constraint	Constraint force	Shape function	Selection
X-fsi.x_free	test(-fsi.x_free)	Lagrange (Linear)	Boundaries 1, 3, 9, 11, 23, 26–27
Y-fsi.y_free	test(-fsi.y_free)	Lagrange (Linear)	Boundaries 1, 3, 9, 11, 23, 26–27
Z-fsi.z_free	test(-fsi.z_free)	Lagrange (Linear)	Boundaries 1, 3, 9, 11, 23, 26–27

1.3.5 Fluid-Solid Interface Boundary 1

Equations

$$\mathbf{u}_{fluid} = \mathbf{u}_w$$

$$\mathbf{u}_w = \frac{\partial \mathbf{u}_{solid}}{\partial t}, \quad \mathbf{u}_w = \text{fsi.vWall}$$

$$\sigma \cdot \mathbf{n} = \Gamma \cdot \mathbf{n}, \quad \Gamma = \left[-p\mathbf{I} + \mu\left(\nabla \mathbf{u}_{fluid} + (\nabla \mathbf{u}_{fluid})^T\right) - \frac{2}{3}\mu(\nabla \cdot \mathbf{u}_{fluid})\mathbf{I}\right]$$

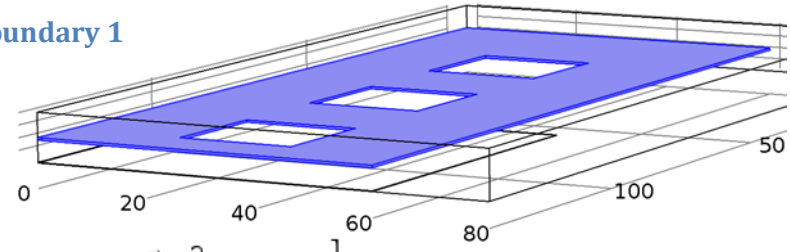

1.3.5.1 Weak expressions

Weak expression	Integration frame	Selection
fsi.KStressn_avx*test(u_fluid)+fsi.KStressn_avy*test(v_fluid)+fsi.KStressn_avz*test(w_fluid)+fsi.KStressTestn_avx*fsi.ujumpx+fsi.KStressTestn_avy*fsi.ujumpy+fsi.KStressTestn_avz*fsi.ujumpz-fsi.sigma_dg_ns*fsi.ujumpx*test(u_fluid)-fsi.sigma_dg_ns*fsi.ujumpy*test(v_fluid)-fsi.sigma_dg_ns*fsi.ujumpz*test(w_fluid)+fsi.upwind_ns+fsi.upwindCont+fsi.consFlux	Spatial	Boundaries 6, 8, 10, 12–13, 16–19, 22, 28–30, 33–34
-fsi.T_stressx*test(u_solid)-fsi.T_stressy*test(v_solid)-fsi.T_stressz*test(w_solid)	Material	Boundaries 6, 8, 10, 12–13, 16–19, 22, 28–30, 33–34

1.3.5.2 Shape functions

Constraint	Constraint force	Shape function	Selection
X+u_solid-fsi.x_free	test(-fsi.x_free)	Lagrange (Linear)	Boundaries 6, 8, 10, 12–13, 16–19, 22, 28–30, 33–34
Y+v_solid-fsi.y_free	test(-fsi.y_free)	Lagrange (Linear)	Boundaries 6, 8, 10, 12–13, 16–19, 22, 28–30, 33–34
Z+w_solid-fsi.z_free	test(-fsi.z_free)	Lagrange (Linear)	Boundaries 6, 8, 10, 12–13, 16–19, 22, 28–30, 33–34

1.3.6 Linear Elastic Material 1

Equations

$$\rho\frac{\partial^2 \mathbf{u}_{solid}}{\partial t^2} - \nabla\cdot\sigma = \mathbf{F}_V, \quad \sigma = J^{-1}\mathbf{F}S\mathbf{F}^T, \quad \mathbf{F} = (\mathbf{I} + \nabla\mathbf{u}_{solid}), \quad J = \det(\mathbf{F})$$

$$S - S_0 = \underline{\underline{C}} : (\epsilon - \epsilon_0 - \epsilon_{inel})$$

$$\epsilon = \frac{1}{2}\left[(\nabla\mathbf{u}_{solid})^T + \nabla\mathbf{u}_{solid} + (\nabla\mathbf{u}_{solid})^T\nabla\mathbf{u}_{solid}\right]$$

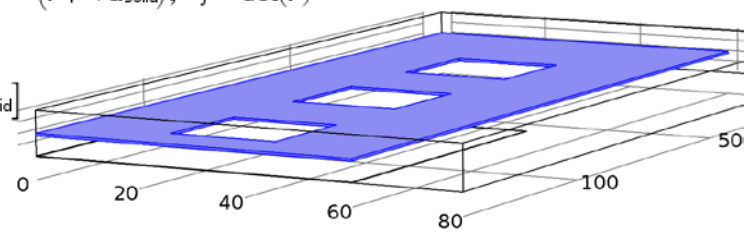

1.3.6.1 Settings

Settings

Description	Value
Young's modulus	From material
Poisson's ratio	From material
Elasticity matrix	{{0, 0, 0, 0, 0, 0}, {0, 0, 0, 0, 0, 0}, {0, 0, 0, 0, 0, 0}, {0, 0, 0, 0, 0, 0}, {0, 0, 0, 0, 0, 0}, {0, 0, 0, 0, 0, 0}}
Elasticity matrix, Voigt notation	{{0, 0, 0, 0, 0, 0}, {0, 0, 0, 0, 0, 0}, {0, 0, 0, 0, 0, 0}, {0, 0, 0, 0, 0, 0}, {0, 0, 0, 0, 0, 0}, {0, 0, 0, 0, 0, 0}}
Density	From material
Solid model	Isotropic
Specify	Young's modulus and Poisson's ratio
	Standard (XX, YY, ZZ, XY, YZ, XZ)
Nearly incompressible material	Off
Energy dissipation	0
Calculate dissipated energy	0

Properties from material

Property	Material	Property group
Young's modulus	Alum	Basic
Poisson's ratio	Alum	Basic
Density	Alum	Basic

1.3.6.2 Shape functions

Name	Shape function	Unit	Description	Shape frame	Selection
u_solid	Lagrange (Quadratic)	m	Displacement field, X component	Material	Domain 2
v_solid	Lagrange (Quadratic)	m	Displacement field, Y component	Material	Domain 2
w_solid	Lagrange (Quadratic)	m	Displacement field, Z component	Material	Domain 2

1.3.6.3 Weak expressions

Weak expression	Integration frame	Selection
-fsi.Sl11*test(fsi.el11)-2*fsi.Sl12*test(fsi.el12)-2*fsi.Sl13*test(fsi.el13)-fsi.Sl22*test(fsi.el22)-2*fsi.Sl23*test(fsi.el23)-fsi.Sl33*test(fsi.el33)	Material	Domain 2

1.3.7 Initial Values 1

1.3.7.1 Settings

Settings

Description	Value
Velocity field	{0, 0, 0}
Pressure	0
Displacement field	{0, 0, 0}
Structural velocity field	{0, 0, 0}

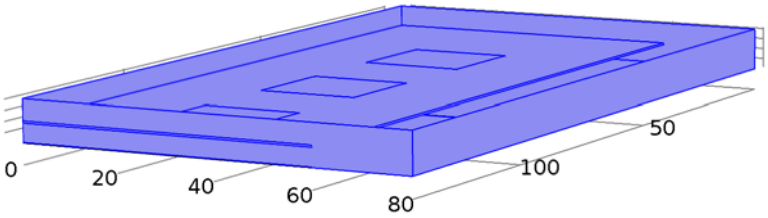

1.3.8 Symmetry MEC

Equations

$$\mathbf{n} \cdot \mathbf{u}_{solid} = 0$$

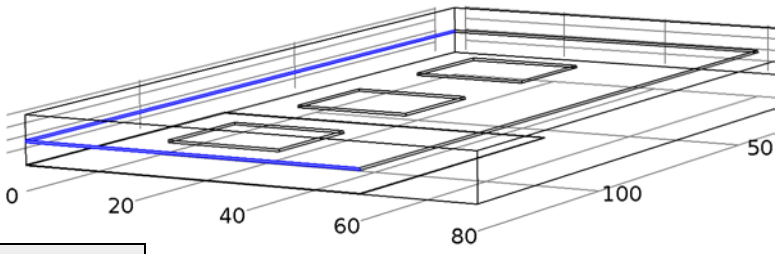

1.3.8.1 Settings

Settings

Description	Value
Apply reaction terms on	All physics (symmetric)
Use weak constraints	Off

1.3.8.2 Shape functions

Constraint	Constraint force	Shape function	Selection
-fsi.nX*u_solid-fsi.nY*v_solid-fsi.nZ*w_solid	test(-fsi.nX*u_solid-fsi.nY*v_solid-fsi.nZ*w_solid)	Lagrange (Quadratic)	Boundaries 5, 37

1.3.9 Fixed Constraint 1

Equations

$$u_{solid} = 0$$

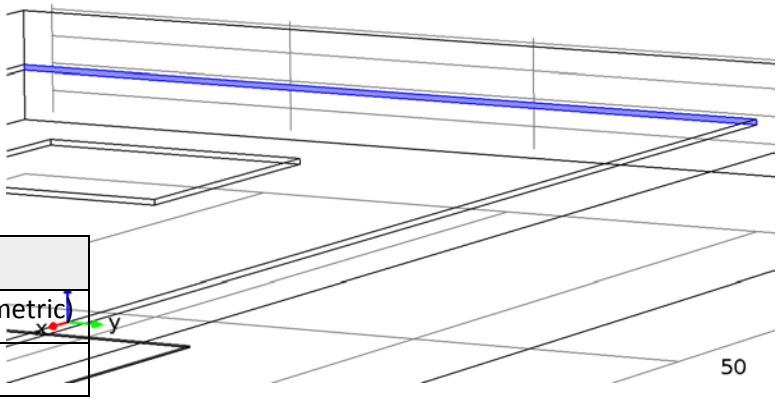

1.3.9.1 Settings

Settings

Description	Value
Apply reaction terms on	All physics (symmetric)
Use weak constraints	Off

1.3.9.2 Shape functions

Constraint	Constraint force	Shape function	Selection
-u_solid	test(-u_solid)	Lagrange (Quadratic)	Boundary 4
-v_solid	test(-v_solid)	Lagrange (Quadratic)	Boundary 4
-w_solid	test(-w_solid)	Lagrange (Quadratic)	Boundary 4

1.3.10 Boundary Load 1

Equations

$$\sigma \cdot \mathbf{n} = F_A$$
$$F_A = -p\mathbf{n}$$

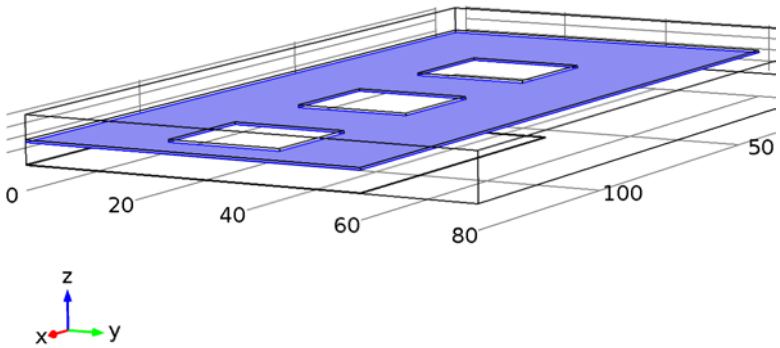

1.3.10.1 Settings

Settings

Description	Value
Load type	Pressure
Pressure	es.unTez

1.3.10.2 Weak expressions

Weak expression	Integration frame	Selection
es.unTez*dvol_spatial*(-fsi.nx*test(u_solid)-fsi.ny*test(v_solid)-fsi.nz*test(w_solid))/dvol	Material	Boundary 6

1.3.11 Open Boundary 1

Equations

$$\left[-p\mathbf{I} + \mu\left(\nabla \mathbf{u}_{fluid} + (\nabla \mathbf{u}_{fluid})^T\right) - \frac{2}{3}\mu(\nabla \cdot \mathbf{u}_{fluid})\mathbf{I}\right]\mathbf{n} = -f_0\mathbf{n}$$

1.3.11.1 Settings

Settings

Description	Value
Boundary condition	Normal stress

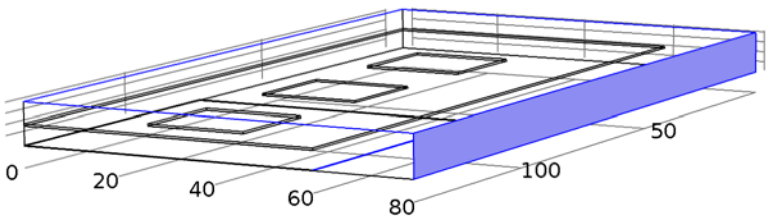

Description	Value
Normal stress	0

1.3.11.2 Weak expressions

Weak expression	Integration frame	Selection
-fsi.f0*(test(u_fluid)*fsi.nxmesh+test(v_fluid)*fsi.nymesh+test(w_fluid)*fsi.nzmesh)	Spatial	Boundaries 9, 11, 27

1.3.12 Symmetry 2

Equations

$$\mathbf{u}_{fluid} \cdot \mathbf{n} = 0$$

$$\mathbf{K} - (\mathbf{K} \cdot \mathbf{n})\mathbf{n} = 0, \quad \mathbf{K} = \left[\mu\left(\nabla \mathbf{u}_{fluid} + (\nabla \mathbf{u}_{fluid})^T\right)\right]\mathbf{n}$$

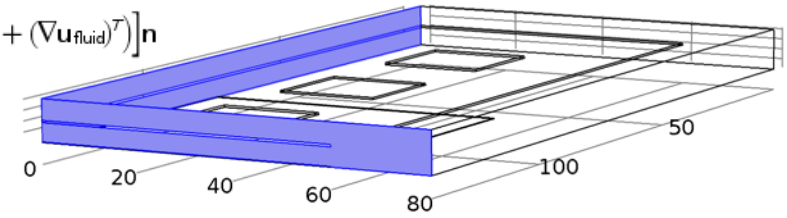

1.3.12.1 Settings

Settings

Description	Value
Use weak constraints	Off

1.3.12.2 Shape functions

Constraint	Constraint force	Shape function	Selection
u_fluid*fsi.nx+v_fluid*fsi.ny+w_fluid*fsi.nz	test(u_fluid)*fsi.nx+test(v_fluid)*fsi.ny+test(w_fluid)*fsi.nz	Lagrange (Linear)	Boundaries 2, 7, 36

1.3.13 Boundary Load 2

Equations

$$\sigma \cdot \mathbf{n} = \underline{F_A}$$

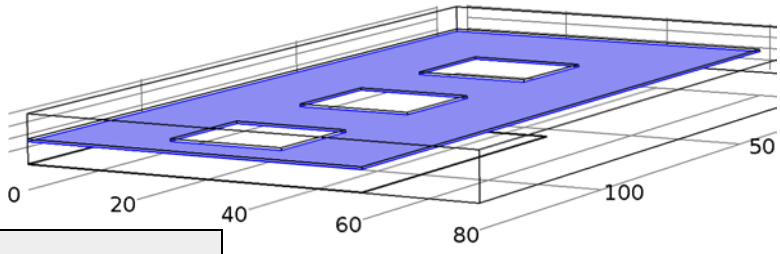

Settings

Description	Value
Load	User defined
Load	{0, 0, contactpresure}
Load type	Load defined as force per unit area
Pressure	contactpresure

1.3.13.1 Weak expressions

Weak expression	Integration frame	Selection
contactpresure*test(w_solid)	Material	Boundary 6

1.4 Mesh 1

Mesh statistics

Property	Value
Minimum element quality	1.931E-6
Average element quality	0.3722
Tetrahedral elements	41179
Triangular elements	15682
Edge elements	1651
Vertex elements	47

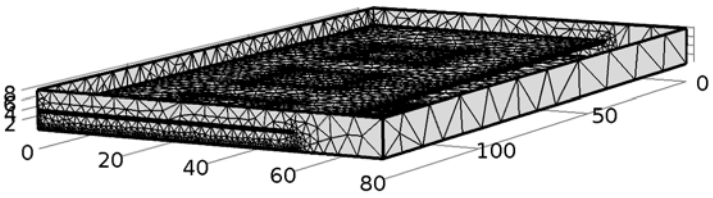

2 Study 1

2.1 Stationary

Study settings

Property	Value
Include geometric nonlinearity	On

Mesh selection

Geometry	Mesh
Geometry 1 (geom1)	mesh1

Physics selection

Physics	Discretization
Electrostatics (es)	physics
Fluid-Structure Interaction (fsi)	physics

2.2 Time Dependent

Study settings

Property	Value
Include geometric nonlinearity	On

Times: range(0,1,100)

Mesh selection

Geometry	Mesh
Geometry 1 (geom1)	mesh1

Physics selection

Physics	Discretization
Electrostatics (es)	physics
Fluid-Structure Interaction (fsi)	physics

2.3 Solver Configurations

2.3.1 Solver 1

2.3.1.1 Compile Equations: Stationary (st1)

Study and step

Name	Value
Use study	Study 1
Use study step	Stationary

2.3.1.2 Dependent Variables 1 (v1)

General

Name	Value
Defined by study step	Stationary

Initial values of variables solved for

Name	Value
Solution	Zero

Values of variables not solved for

Name	Value
Solution	Zero

Pressure (comp1.p) (comp1_p)

General

Name	Value
Field components	comp1.p

Displacement field (Material) (comp1.u_solid) (comp1_u_solid)

General

Name	Value
Field components	{comp1.u_solid, comp1.v_solid, comp1.w_solid}

Scaling

Name	Value
Method	Manual
Scale	1e-2*1.614434885648845E-4

Velocity field (Spatial) (comp1.u_fluid) (comp1_u_fluid)

General

Name	Value
Field components	{comp1.u_fluid, comp1.v_fluid, comp1.w_fluid}

Spatial coordinates (Material) (comp1.xyz) (comp1_xyz)

General

Name	Value
Field components	{x, y, z}

Electric potential (comp1.V) (comp1_V)

General

Name	Value
Field components	comp1.V

2.3.1.3 Stationary Solver 1 (s1)

General

Name	Value
Defined by study step	Stationary

Log

```
Stationary Solver 1 in Solver 1 started at 10-Dec-2015 16:43:02.
Segregated solver
Number of degrees of freedom solved for: 150751.
Segregated solver iteration 1.
Substep 1, for group 1.
Symmetric matrices found.
Scales for dependent variables:
Electric potential (comp1.V): 1
Iter     Damping    Stepsize #Res #Jac #Sol LinIt   LinErr   LinRes
   1   1.0000000        0.78    2    1    1     7   0.0003   4e-008
Substep 2, for group 2.
Nonsymmetric matrix found.
Scales for dependent variables:
Displacement field (Material) (comp1.u_solid): 1.6e-006
Spatial coordinates (Material) (comp1.xyz): 1.4e+002
Iter     Damping    Stepsize #Res #Jac #Sol   LinErr   LinRes
   1   0.5000000     0.00016    2    1    1  0.00015 8.4e-006
Substep 3, for group 3.
Nonsymmetric matrix found.
Scales for dependent variables:
Pressure (comp1.p): 1
Velocity field (Spatial) (comp1.u_fluid): 0.0048
Iter     Damping    Stepsize #Res #Jac #Sol   LinErr   LinRes
   1   0.5000000           0    2    1    1        0        0
Error estimates for segregated groups:
0.78, 8.2e-005, 0
Segregated solver iteration 2.
Substep 1, for group 1.
Iter     Damping    Stepsize #Res #Jac #Sol LinIt   LinErr   LinRes
   1   1.0000000    3.9e-006    4    2    2    14  0.00093 1.7e-006
Substep 2, for group 2.
Scales for dependent variables:
Spatial coordinates (Material) (comp1.xyz): 4.2e-005
Inconsistent pointwise unidirectional constraints found.
54 constraints are merged/removed.
Iter     Damping    Stepsize #Res #Jac #Sol   LinErr   LinRes
   1   0.5000000    8.2e-005    4    2    2   8e-005 3.7e-007
Substep 3, for group 3.
Scales for dependent variables:
Pressure (comp1.p): 1
Velocity field (Spatial) (comp1.u_fluid): 1
Iter     Damping    Stepsize #Res #Jac #Sol   LinErr   LinRes
   1   0.5000000           0    4    2    2        0        0
Error estimates for segregated groups:
3.9e-006, 4.1e-005, 0
Segregated solver iteration 3.
Substep 1, for group 1.
```

```
Iter     Damping    Stepsize #Res #Jac #Sol LinIt   LinErr   LinRes
   1   1.0000000    1.8e-006    6    3    3    21  0.00034 5.3e-007
Substep 2, for group 2.
Inconsistent pointwise unidirectional constraints found.
54 constraints are merged/removed.
Iter     Damping    Stepsize #Res #Jac #Sol   LinErr   LinRes
   1   0.5000000    4.1e-005    6    3    3  0.00011 2.4e-007
Substep 3, for group 3.
Iter     Damping    Stepsize #Res #Jac #Sol   LinErr   LinRes
   1   0.5000000           0    6    3    3        0        0
Error estimates for segregated groups:
1.8e-006, 2.1e-005, 0
Segregated solver iteration 4.
Substep 1, for group 1.
Iter     Damping    Stepsize #Res #Jac #Sol LinIt   LinErr   LinRes
   1   1.0000000      9e-007    8    4    4    28  0.00034 5.3e-007
Substep 2, for group 2.
More inconsistent pointwise unidirectional constraints found...
Iter     Damping    Stepsize #Res #Jac #Sol   LinErr   LinRes
   1   0.5000000    2.1e-005    8    4    4  0.00025 2.2e-007
Substep 3, for group 3.
Iter     Damping    Stepsize #Res #Jac #Sol   LinErr   LinRes
   1   0.5000000           0    8    4    4        0        0
Error estimates for segregated groups:
9e-007, 1e-005, 0
Stationary Solver 1 in Solver 1: Solution time: 36 s
                                 Physical memory: 1.62 GB
                                 Virtual memory: 1.75 GB
```

Segregated 1 (se1)

General

Name	Value
Pseudo time-stepping	On

Segregated Step 1 (ss1)

General

Name	Value
Variables	Electric potential (comp1.V)
Linear solver	Iterative 1

Segregated Step 2 (ss2)

General

Name	Value
Variables	{Spatial coordinates (Material) (comp1.xyz), Displacement field (Material) (comp1.u_solid)}
Linear solver	Direct

Segregated Step 3 (ss3)

General

Name	Value
Variables	{Velocity field (Spatial) (comp1.u_fluid), Pressure (comp1.p)}

Name	Value
Linear solver	Direct 1

Iterative 1 (i1)

General

Name	Value
Solver	Conjugate gradients

Multigrid 1 (mg1)

General

Name	Value
Solver	Algebraic multigrid

Direct 1 (d1)

General

Name	Value
Solver	PARDISO

2.3.1.4 Store Solution 2 (su1)

General

Name	Value
Solution	Store Solution 2

2.3.1.5 Compile Equations: Time Dependent (2) (st2)

Study and step

Name	Value
Use study	Study 1
Use study step	Time Dependent

2.3.1.6 Dependent Variables 2 (v2)

General

Name	Value
Defined by study step	Time Dependent

Initial values of variables solved for

Name	Value
Method	Solution
Solution	Solver 1

Values of variables not solved for

Name	Value

Name	Value
Method	Solution
Solution	Solver 1

Pressure (comp1.p) (comp1_p)

General

Name	Value
Field components	comp1.p

Displacement field (Material) (comp1.u_solid) (comp1_u_solid)

General

Name	Value
Field components	{comp1.u_solid, comp1.v_solid, comp1.w_solid}

Scaling

Name	Value
Method	Manual
Scale	1e-2*1.614434885648845E-4

Velocity field (Spatial) (comp1.u_fluid) (comp1_u_fluid)

General

Name	Value
Field components	{comp1.u_fluid, comp1.v_fluid, comp1.w_fluid}

Spatial coordinates (Material) (comp1.xyz) (comp1_xyz)

General

Name	Value
Field components	{x, y, z}

Electric potential (comp1.V) (comp1_V)

General

Name	Value
Field components	comp1.V

2.3.1.7 Time-Dependent Solver 1 (t1)

General

Name	Value
Defined by study step	Time Dependent
Time	{0, 1, 2, 3, 4, 5, 6, 7, 8, 9, 10, 11, 12, 13, 14, 15, 16, 17, 18, 19, 20, 21, 22, 23, 24, 25, 26, 27, 28, 29, 30, 31, 32, 33, 34, 35, 36, 37, 38, 39, 40, 41, 42, 43, 44, 45, 46, 47, 48, 49, 50, 51, 52, 53, 54, 55, 56, 57, 58, 59, 60, 61, 62, 63, 64, 65, 66, 67, 68, 69, 70, 71, 72, 73, 74, 75, 76, 77, 78,

Name	Value
	79, 80, 81, 82, 83, 84, 85, 86, 87, 88, 89, 90, 91, 92, 93, 94, 95, 96, 97, 98, 99, 100}

Absolute tolerance

Name	Value
Tolerance	5.0E-4

Time stepping

Name	Value
Method	Generalized alpha

Output

Name	Value
Times to store	Steps taken by solver

Log

```
Time-Dependent Solver 1 in Solver 1 started at 10-Dec-2015 16:43:42.
Time-dependent solver (Generalized-alpha)
Number of degrees of freedom solved for: 150751.
Nonsymmetric matrix found.
Scales for dependent variables:
Pressure (comp1.p): 3.1e+005
Displacement field (Material) (comp1.u_solid): 1.6e-006
Velocity field (Spatial) (comp1.u_fluid): 1.6e+003
Spatial coordinates (Material) (comp1.xyz): 80
Electric potential (comp1.V): 4.8e+006
Step        Time    Stepsize      Res  Jac  Sol Order Tfail NLfail   LinErr   LinRes
   0           0             out    2    3    2                 0   1e-011 1.5e-013
   1       1e-007      1e-007 out    3    4    3     2     0     0 7.9e-011 5.2e-015
   2       3e-007      2e-007 out    4    5    4     2     0     0 1.1e-007 1.9e-015
   3       7e-007      4e-007 out    5    6    5     2     0     0 7.9e-007 2.2e-015
   4     1.5e-006      8e-007 out    6    7    6     2     0     0 1.2e-006 2.2e-015
   5     3.1e-006    1.6e-006 out    7    8    7     2     0     0 4.5e-006 1.3e-015
   6     6.3e-006    3.2e-006 out    8    9    8     2     0     0 7.5e-006 1.9e-015
   7   8.176e-006  1.876e-006 out   13   14   13     2     1     0 6.6e-006 9.9e-016
   8 9.3021e-006 1.1261e-006 out   18   19   18     2     2     0 2.1e-006 1.2e-014
   9 9.4825e-006  1.804e-007 out   25   26   25     2     4     0 1.5e-007   3e-010
  10 9.6629e-006  1.804e-007 out   27   28   27     2     4     0 9.7e-008 4.5e-011
  11 1.0024e-005 3.6081e-007 out   29   30   29     2     4     0 4.6e-007 1.2e-010
  12 1.0385e-005 3.6081e-007 out   31   32   31     2     4     0 2.4e-007 5.2e-012
  13 1.0745e-005 3.6081e-007 out   33   34   33     2     4     0 1.6e-007 8.7e-013
  14 1.1106e-005 3.6081e-007 out   35   36   35     2     4     0 2.3e-007 7.8e-013
  15 1.1467e-005 3.6081e-007 out   37   38   37     2     4     0 2.2e-007 1.1e-013
  16 1.2189e-005 7.2161e-007 out   39   40   39     2     4     0   8e-007 1.5e-012
  17  1.291e-005 7.2161e-007 out   41   42   41     2     4     0 1.3e-006 1.6e-012
  18  1.356e-005 6.4945e-007 out   43   44   43     2     4     0 1.1e-006 1.1e-012
  19 1.4209e-005 6.4945e-007 out   45   46   45     2     4     0   9e-007 2.8e-012
  20 1.4859e-005 6.4945e-007 out   47   48   47     2     4     0 8.2e-007 4.7e-013
  21 1.5508e-005 6.4945e-007 out   49   50   49     2     4     0 5.2e-007 6.2e-013
  22 1.6157e-005 6.4945e-007 out   51   52   51     2     4     0 5.8e-007 3.8e-013
  23 1.6807e-005 6.4945e-007 out   53   54   53     2     4     0   5e-007 4.7e-013
  24 1.7456e-005 6.4945e-007 out   55   56   55     2     4     0 8.5e-007 4.5e-013
  25 1.8755e-005 1.2989e-006 out   57   58   57     2     4     0 2.1e-006 1.4e-012
  26 2.0054e-005 1.2989e-006 out   59   60   59     2     4     0 2.7e-006 1.2e-012
  27 2.2652e-005 2.5978e-006 out   61   62   61     2     4     0 4.9e-006   4e-012
  28  2.525e-005 2.5978e-006 out   63   64   63     2     4     0 1.6e-006 2.7e-012
  29 2.7848e-005 2.5978e-006 out   65   66   65     2     4     0 2.5e-006 7.1e-012
  30 3.0445e-005 2.5978e-006 out   67   68   67     2     4     0 1.5e-006 4.2e-012
  31 3.3043e-005 2.5978e-006 out   69   70   69     2     4     0 2.3e-006 7.9e-012
  32 3.5641e-005 2.5978e-006 out   71   72   71     2     4     0 3.3e-006   6e-012
  33 3.8239e-005 2.5978e-006 out   73   74   73     2     4     0 3.2e-006 1.4e-011
  34 4.0837e-005 2.5978e-006 out   75   76   75     2     4     0 2.7e-006 6.6e-012
  35 4.3434e-005 2.5978e-006 out   77   78   77     2     4     0 1.8e-006 1.9e-011
```

```
  36 4.6032e-005 2.5978e-006 out   79   80   79     2     4      0 1.4e-006 9.9e-012
  37  4.863e-005 2.5978e-006 out   81   82   81     2     4      0 1.9e-006 1.6e-011
  38 5.1228e-005 2.5978e-006 out   83   84   83     2     4      0   4e-006 1.4e-011
  39 5.3826e-005 2.5978e-006 out   85   86   85     2     4      0 2.4e-006 1.4e-011
  40 5.6423e-005 2.5978e-006 out   87   88   87     2     4      0 1.1e-006   2e-011
  41 5.9021e-005 2.5978e-006 out   89   90   89     2     4      0 1.8e-006 1.4e-011
  42 6.1619e-005 2.5978e-006 out   91   92   91     2     4      0 3.8e-006 1.9e-011
  43 6.4217e-005 2.5978e-006 out   93   94   93     2     4      0 2.4e-006 1.1e-011
  44 6.6815e-005 2.5978e-006 out   95   96   95     2     4      0 4.6e-006 1.1e-011
  45  7.201e-005 5.1956e-006 out   97   98   97     2     4      0 3.5e-006 7.2e-011
  46 7.7206e-005 5.1956e-006 out   99  100   99     2     4      0 2.9e-006 2.4e-011
  47 8.2401e-005 5.1956e-006 out  101  102  101     2     4      0 3.8e-006 4.5e-011
  48 8.7597e-005 5.1956e-006 out  103  104  103     2     4      0   2e-006 1.1e-011
  49 9.7597e-005      1e-005 out  105  106  105     2     4      0 3.8e-006 3.4e-011
         0.0001           - out
  50   0.0001076      1e-005      107  108  107     2     4      0 9.5e-006 3.6e-012
Time-Dependent Solver 1 in Solver 1: Solution time: 1443 s (24 minutes, 3 seconds)
                                     Physical memory: 2.68 GB
                                     Virtual memory: 2.8 GB
```

Direct 1 (d1)

General

Name	Value
Solver	PARDISO

Fully Coupled 1 (fc1)

General

Name	Value
Linear solver	Direct 1

Results while solving

Name	Value
Plot	On
Plot group	Displacement Z

3 Results

3.1 Data Sets

3.1.1 Solution 1

Solution

Name	Value
Solution	Solver 1
Component	Save Point Geometry 1

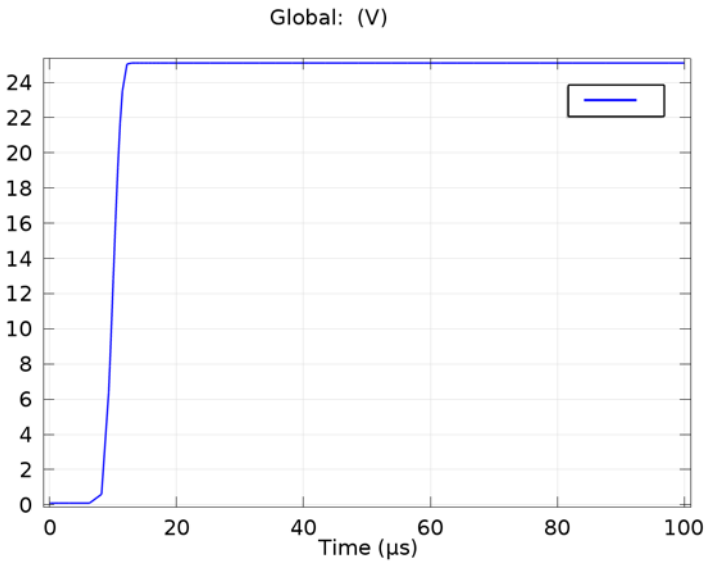

3.1.2 Solution 2

Solution

Name	Value

Name	Value
Solution	Store Solution 2
Component	Save Point Geometry 1

Surface 1

Data

Name	Value
Data set	Solution 1

Parameterization

Name	Value
x- and y-axes	Surface parameters

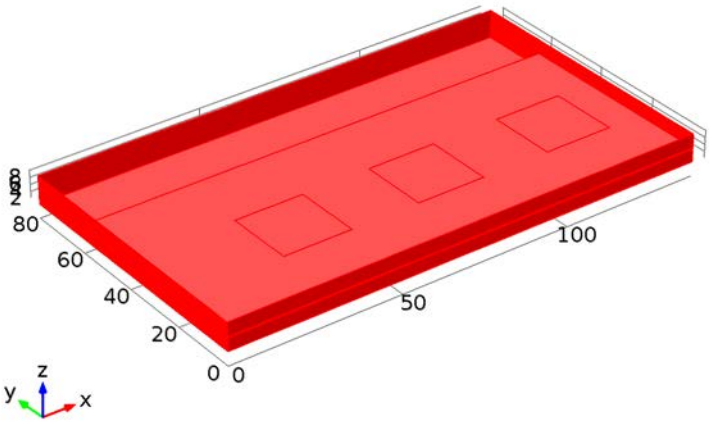

3.1.3 Mirror 3D 1

Data

Name	Value
Data set	Solution 1

Plane data

Name	Value
Plane type	Quick
Plane	xz - planes
y-coordinate	0

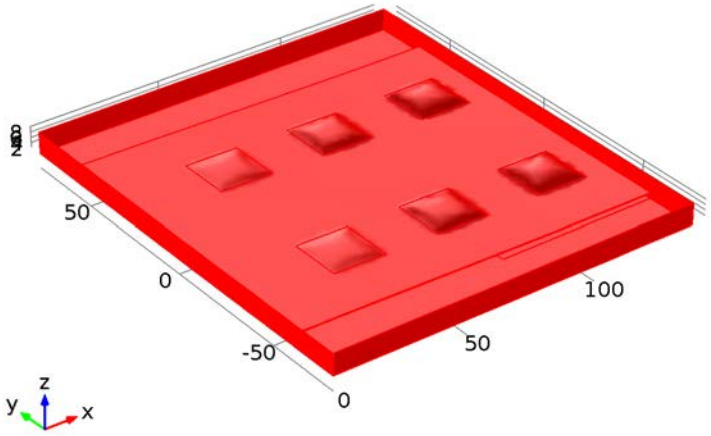

3.1.4 Mirror 3D 2

Data

Name	Value
Data set	Mirror 3D 1

Plane data

Name	Value
Plane type	Quick

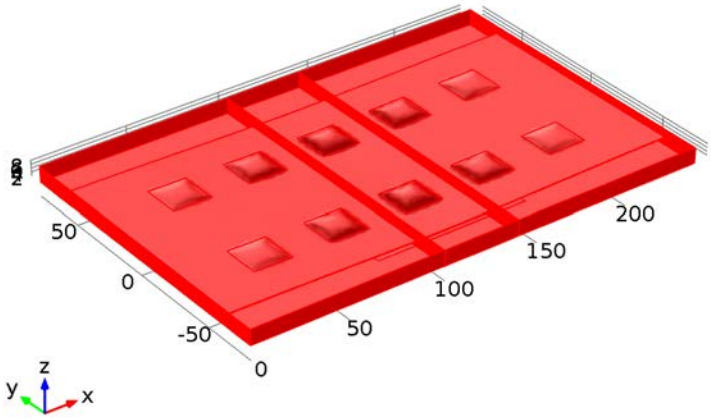

3.2 Plot Groups

3.2.1 Electric Potential (es)

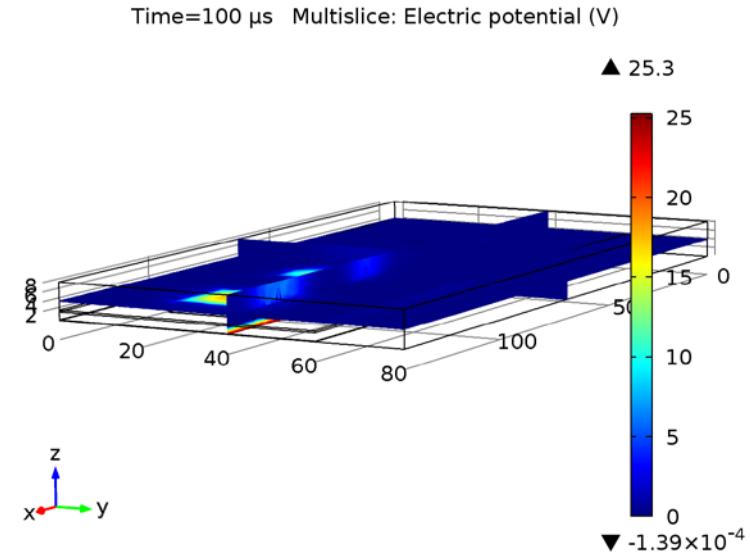

3.2.2 Flow and Stress (fsi)

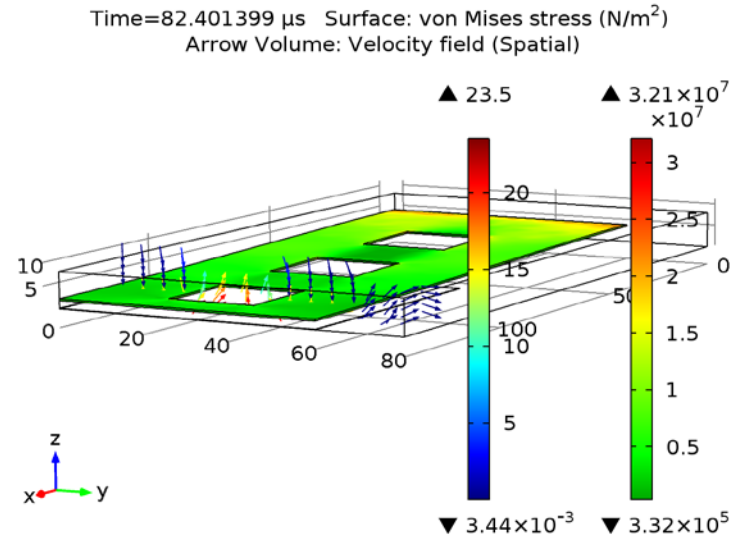

3.2.3 Displacement Z

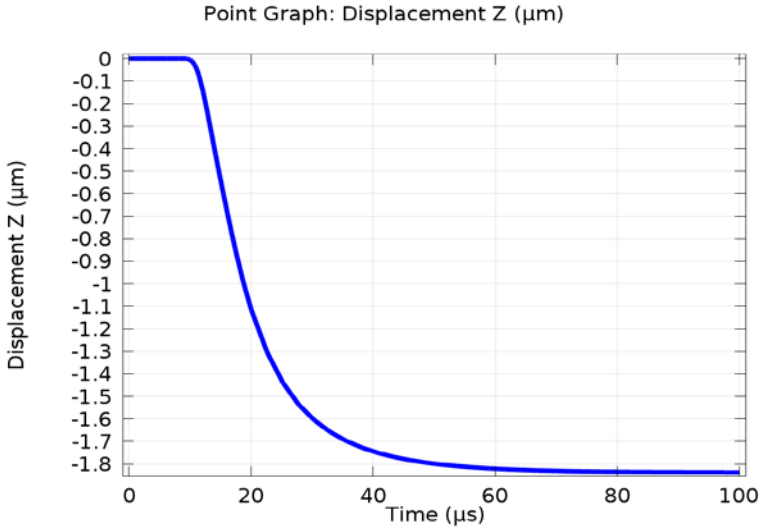

Total Displacement

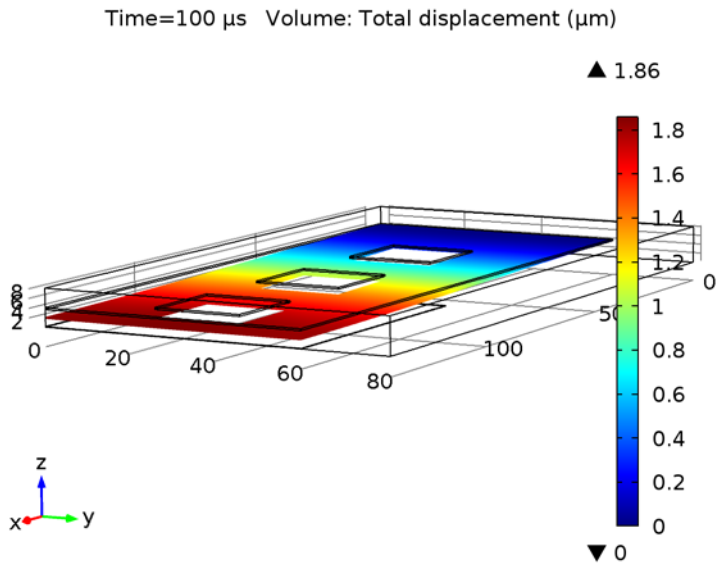

References

[1] J.J. Yao. Topical review RF-MEMS from a device perspective. *Journal of Micromechanics and Microengineering*, 10(4):R9 – R38, 2000. DOI:S0960-1317(00)06704-8.

[2] S.K. Lahiri, H. Saha, and A. Kundu. RF MEMS SWITCH: An overview at- a-glance. In *Computers and Devices for Communication, 2009. CODEC 2009. 4th International Conference on*, pages 1–5, Dec 2009.

[3] G.M. Rebeiz. Phase-noise analysis of mems-based circuits and phase shifters. *Microwave Theory and Techniques, IEEE Transactions on*, 50(5):1316–1323, May 2002. ISSN:0018-9480, DOI:10.1109/22.999145.

[4] A. Vorobyov, R. Sauleau, E. Fourn, J. Oberhammer, and Z. Baghchehsaraei. MEMS based waveguide phase shifters for phased arrays in automotive radar applications. *Proceedings of the 5th European Conference on Antennas and Propagation (EUCAP)*, pages 2087 – 2090, 2011. ISBN:978-1-4577-0250-1.

[5] A. Malczewski, B. Pillans, F. Morris, and R. Newstrom. A family of MEMS tunable filters for advanced RF applications. *IEEE MTT-S InternationalMicrowave Symposium Digest (MTT)*, pages 1–4, 2011. ISSN0149-645X, ISBN:978-1-61284-754-2.

[6] A. Abbaspour-Tamijani, L. Dussopt, and G.M. Rebeiz. Miniature and tunable filters using MEMS capacitors. *IEEE Transactions on Microwave Theory and Techniques*, 51(7):1878–1885, 2003. ISSN:0018-9480.

[7] G.H. Huff and J.T. Bernhard. Integration of packaged RF MEMS switches with radiation pattern reconfigurable square spiral microstrip antennas. *IEEE Transactions on Antennas and Propagation*, 54(2):464–469, Feb 2006. ISSN:0018-926X, DOI:10.1109/TAP.2005.863409.

[8] M.A. Campo, O. Litschke, T. Vaha-Heikkila, L. Markku, and R. Baggen. MEMS-4-MMIC: Design of antenna array front end at 24 GHz. *Proceedings of the 5th European Conference on Antennas and Propagation (EUCAP)*, pages 1907–1911, 2011.

[9] G.M. Rebeiz. RF MEMS switches: status of the technology. In *TRANSDUCERS, Solid-State Sensors, Actuators and Microsystems, 12th International Conference on, 2003*, volume 2, pages 1726–1729 vol.2, June 2003. DOI:10.1109/SENSOR.2003.1217118.

[10] A.Q. Liu. *RF-MEMS Switches, and Integrated Switching, Circuits, Design, Fabri-*

cation, and Test. Springer, New York Dordrecht Heidelberg London, 2011. ISBN: 978-0-387-46261-5.

[11] K.B. Lee. *Principles of Microelectromechanical Systems*. John Wiley and Sons, Inc, Hoboken, New Jersey, USA, 2011. ISBN:978-0-470-46634-6.

[12] H. Fu and R. Pfahl. Mems roadmap and inemi initiatives. In *14th International Conference on Electronic Packaging Technology (ICEPT)*, pages 1222–1226, 2013. DOI:10.1109/ICEPT.2013.6756678.

[13] C. Maleville. Engineered substrates for moore and more than moore's law: Device scaling: Entering the substrate era. In *SOI-3D-Subthreshold Microelectronics Technology Unified Conference (S3S), 2015 IEEE*, pages 1–5, 2015. DOI:10.1109/S3S.2015.7333494.

[14] G.Q. Zhang. More than moore, 2005. European Nanoelectronics Initiative Advisory Council (ENIAC).

[15] W. Arden, M. Brillout, P. Cogez, M. Graef, B Huizing, and R. Mahnkopf. More-than-moore white paper, 2010. More-than-moore-white-paper.

[16] S. Lampo. National mems technology roadmap markets, applications and devices. Master's thesis, Aalto University, 2012. `http://lib.tkk.fi/Dipl/2012/urn100673.pdf`.

[17] E. Mounier. Future of mems: a market & technologies perspective, 2014. Yole Developpement - MEMS Tech Seminar 2014.

[18] J. Bouchaud, R. Sorrentino, B. Knoblich, H.A.C. Tilmans, and F. Coccetti. Industry roadmap for rf mems. In Stepan Lucyszyn, editor, *Advanced RF MEMS*, pages 359–403. Cambridge University Press, 2010. ISBN: 9780511781995,Cambridge Books Online.

[19] W.M. van Spengen. Capacitive RF MEMS switch dielectric charging and reliability: a critical review with recommendations. *Journal of Micromechanics and Microengineering*, 22(7), 2012. DOI:10.1088/0960-1317/22/7/074001, `http://stacks.iop.org/0960-1317/22/i=7/a=074001`.

[20] F. Martin and J. Bonache. Application of RF-MEMS-based split ring resonators (SRRs) to the implementation of reconfigurable stopband filters: A review. *Sensors*, 14, 2014. DOI: 10.3390/s141222848.

[21] G.M. Rebeiz. *MEMS: Theory, Design and Technology*. John Wiley and Sons, Inc, Hoboken, New Jersey, USA, 2003. ISBN:0-471-20169-3.

[22] D.R. Pryputniewicz. ACES approach to the development of microcomponent. Master's thesis, Worcester Polytechnic Institute, Worcester, MA., 1997.

[23] A. Alexandru, G. Ciuprina, B. Diţă, D. Ioan, D. Isvoranu, M. Rebican, A.S. Lup, S. Sorohan, and A. Tomescu. Stadiul actual al cercetărilor în domeniul RF-MEMS. ToMeMS - internal report - D1.1a "Modelarea cuplata electrostatica si mecanica a microcomutatoarelor de RF - Formularea problemei", 2012.

[24] Q. Meng, M. Mehregany, and R.L. Mullen. Theoretical modeling of microfabricated beams with elastically restrained supports. *Journal of microelectromechanical systems*, 2(3):128–137, 1993. ISSN:1057-7157.

[25] E.R. Brown. RF-MEMS switches for reconfigurable integrated circuits. *Microwave Theory and Techniques, IEEE Transactions on*, 46(11):1868–1880, 1998. ISSN:0018-9480.

[26] J.B. Muldavin and G.M. Rebeiz. X-band tunable MEMS resonators. *Digest of Papers: Silicon Monolithic Integrated Circuits in RF Systems*, pages 116 – 118, 2000. DOI:10.1109/SMIC.2000.844312.

[27] G.M. Rebeiz and J.B. Muldavin. RF-MEMS switches and switch circuits. *IEEE Microwave Magazine*, 2(4):59–71, 2001. ISSN:1527-3342.

[28] Z.D. Milosavljevic. RF-MEMS switches. *Microwave Review*, 10(1):1–8, 2004. www.mtt-serbia.org.rs/microwave_review/pdf.

[29] S. Lucyszyn. Review of radio frequency microelectromechanical systems technology. *Science, Measurement and Technology, IEE Proceedings* -, 151(2):93–103, March 2004. ISSN:1350-2344, DOI:10.1049/ip-smt:20040405.

[30] J. Bouchaud and H. Wicht. RF-MEMS: status of the industry and roadmaps. *Digest of Papers, Radio Frequency integrated Circuits (RFIC) Symposium. IEEE*, pages 379–384, 2005. DOI:10.1109/RFIC.2005.1489818.

[31] J. Bouchaud, B. Knoblich, H. Tilmans, F. Coccetti, and A. El Fatatry. RF-MEMS roadmap. *European Microwave Integrated Circuit Conference, EuMIC 2007*, pages 343–346, 2007. ISBN:978-2-87487-002-6.

[32] M.B. Henry and L. Nazhandali. From transistors to MEMS: Throughput-aware power gating in CMOS circuits. *Design, Automation and Test Europe Conference and Exhibition (DATE)*, pages 130–135, 2010. ISBN:978-3-9810801-6-2.

[33] B. Pillans. RF-MEMS: Revolutionary technology for microwave frequencies, 2011. MTT presentation.

[34] I. Puchades. Development of RF-MEMS systems, 2012. 30th RIT's MicroE Conference RF-MEMS, Conference presentation.

[35] T.W. Jau. RF MEMS switches: High-frequency performance and hot-switching reliability. *High Frequency Design*, pages 32–38, 2013. www.highfrequencyelectronics.com.

[36] H. Zareie and G.M. Rebeiz. Compact High-Power SPST and SP4T RF MEMS Metal-Contact Switches. *Microwave Theory and Techniques, IEEE Transactions on*, 62(2):297–305, 2014. ISSN:0018-9480, DOI:10.1109/TMTT.2013.2296749.

[37] D. Dhal and M.K. Demde. Compact High-Power SPST and SP4T RF MEMS Metal-Contact Switches. *International Journal on Recent and Innovation Trends in Computing and Communication*, 3:297–305, 2015. ISSN:273-276.

[38] C.L. Goldsmith, A. Malczewski, Z.J. Yao, S. Chen, and D.H. Hinzel

J. Ehmke. RF-MEMS variable capacitors for tunable filters. *International Journal of RF and Microwave Computer-Aided Engineering*, 9(4):362–374, 1999. www.memtronics.com/files.

[39] A. Mohamed, H. Elsimary, and M. Ismail. Design of MEMS tunable capacitor all metal microstructure for RF wireless applications. *Technical Proceedings of the 2000 International Conference on Modeling and Simulation of Microsystems*, pages 174 – 177, 2000. ISBN:0-9666135-7-0, `http://nsti.org/publications/MSM/2000/pdf/T56.07.pdf`.

[40] R.L. Borwick, P.A. Stupara, J. DeNatalea, R. Andersona, C. Tsaia, K. Garretta, and R. Erlandsonb. A high Q, large tuning range MEMS capacitor for RF filter systems. *Sensors and Actuators A: Physical*, 103(1-2):33–41, 2003.

[41] H.D. Nguyen, D. Hah, P.R. Patterson, R. Chao, W. Piyawattanametha, E.K. Lau, and M.C. Wu. Angular vertical comb-driven tunable capacitor with high-tuning capabilities. *Journal of Microelectromechanical Systems*, 13(3):406–413, 2004. ISSN:1057-7157.

[42] K. Entesari and G.M. Rebeiz. A differential 4-bit 6.5-10-GHz RF MEMS tunable filter. *IEEE Transactions on Microwave Theory and Techniques*, 53(3):1103–1110, March 2005. ISSN:0018-9480, DOI:10.1109/TMTT.2005.843501.

[43] K. Entesari and G.M. Rebeiz. A 12-18-GHz three-pole RF MEMS tunable filter. *IEEE Transactions on Microwave Theory and Techniques*, 53(8):2566–2571, Aug 2005. ISSN:0018-9480, DOI:10.1109/TMTT.2005.852761.

[44] L. Liu. High performance RF MEMS series contact switch - design and simulations. In *57th Electronic Components and Technology Conference*, pages 158–164, May 2007. ISSN:0569-5503, DOI:10.1109/ECTC.2007.373791.

[45] J.X. Chen, J. Shi, and Z.H. Bao. Tunable and switchable bandpass filters using slot-line resonators. *PIER, Progress In Electromagnetics Research*, 111:25 – 41, 2010. `http://jpier.org/PIER/pier.php?paper=10100808`.

[46] J Perruisseau-Carrier, E. Girard, and H. Legay. Analysis of a reconfigurable reflectarray cell comprising a multitude of MEMS control elements. *Proceedings of the Fourth European Conference on Antennas and Propagation (EuCAP)*, pages 1–4, 2011. ISBN:978-1-4244-6431-9.

[47] Y. Shim, J. Ruan, Z. Wu, and M. Rais-Zadeh. An integrated RF-MEMS tunable filter. *IEEE 25th International Conference on Micro Electro Mechanical Systems (MEMS)*, pages 15 – 18, 2012. ISBN:978-1-4673-0324-8, wims2.org/publications/papers/.

[48] E.S. Hung, Y.J. Yang, and S.D. Senturia. Low-order models for fast dynamical simulation of MEMS microstructures. *International Conference on Solid State Sensors and Actuators, TRANSDUCERS'97 Chicago*, 2:1101–1104, 1997. ISBN:0-7803-3829-4.

[49] S.D. Senturia, N. Azuru, and J. White. Simulating the behavior of MEMS devices:

computational methods and needs. *Computational Science and Engineering, IEEE*, 4(1):30–43, 1997. ISSN:1070-9924.

[50] J.R. Phillips and J.K. White. A precorrected-FFT method for electrostatic analysis of complicated 3-d structures. *IEEE Transactions on Computer-Aided Design of Integrated Circuits and Systems*, 16(10):1059–1072, 1997. ISSN:0278-0070.

[51] N.R. Aluru and J. White. A multilevel newton method for mixed-energy domain simulation of MEMS. *Journal of Microelectromechanical Systems*, 8(3):299–308, 1999. ISSN:1057-7157.

[52] J.B. Muldavin and G.M. Rebeiz. High-isolation CPW MEMS shunt switches. 1. modeling. *Microwave Theory and Techniques, IEEE Transactions on*, 48(6):1045–1052, Jun 2000. ISSN:0018-9480, DOI:10.1109/22.904743.

[53] J.B. Muldavin and G.M. Rebeiz. High-isolation CPW MEMS shunt switches. 2. Design. *Microwave Theory and Techniques, IEEE Transactions on*, 48(6):1053–1056, Jun 2000. ISSN:0018-9480, DOI:10.1109/22.904744.

[54] S.P. Pacheco, L.P.B. Katehi, and C.T.-C. Nguyen. Design of low actuation voltage RF MEMS switch. In *Microwave Symposium Digest. 2000 IEEE MTT-S International*, volume 1, pages 165–168 vol.1, June 2000. ISSN:0149-645X, DOI:10.1109/MWSYM.2000.860921.

[55] J.Y. Qian, G.P. Li, and F. de Flavis. A parametric model of MEMS capacitive switch operating at microwave frequencies. *IEEE MTT-S International Microwave Symposium Digest*, 2:1229 – 1232, 2000. ISBN:0-7803-5687-X.

[56] J.Y. Qian, G.P. Li, and F. De Flaviis. A parametric model of low-loss RF-MEMS capacitive switches. *Asia-Pacific Microwave Conference APMC 2001*, 3:1020 – 1023, 2001. ISBN:0-7803-7138-0.

[57] J.B. Muldavin and G.M. Rebeiz. Nonlinear electro-mechanical modeling of MEMS switches. In *Microwave Symposium Digest, 2001 IEEE MTT-S International*, volume 3, pages 2119–2122 vol.3, May 2001. ISSN:0149-645X, DOI:10.1109/MWSYM.2001.967332.

[58] D. Mercier, P. Blondy, D. Cros, and P. Guillon. An electromechanical model for MEMS switches. In *Microwave Symposium Digest, 2001 IEEE MTT-S International*, volume 3, pages 2123–2126 vol.3, May 2001. ISSN:0149-645X, DOI:10.1109/MWSYM.2001.967333.

[59] L. Pierantoni, M. Farina, T. Rozzi, F. Coccetti, W. Dressel, and P. Russer. Comparison of the efficiency of electromagnetic solvers in the time- and frequency-domain for the accurate modeling of planar circuits and MEMS. In *Microwave Symposium Digest, 2002 IEEE MTT-S International*, volume 2, pages 891–894 vol.2, June 2002. ISSN:0149-645X, DOI:10.1109/MWSYM.2002.1011773.

[60] D. Dubuc, L. Rabbia, M. Saadaoui, E. Flourens, B. Ducarouge, M. Aissi, F. Boughriha, K. Grenier, P. Pons, J. Graffeuil, and R. Plana. Modelling and design of MEMS for RF and millimeter wave applications. *Proceedings Semiconductor Conference*, 1:13 – 18, 2002. DOI:10.1109/SMICND.2002.1105791.

[61] L.X. Zhang and Y.P. Zhao. Electromechanical model of RF-MEMS switches. *Microsystem Technologies, Springer*, 9(6-7):420 – 426, 2003. ISSN:0946-7076.

[62] M. Kurodi, N. Miura, K. Kawano, and M.M. Tentzeris. Numerical modeling of the transient behavior of MEMS structures involving motion in arbitrary directions. *IEEE Antennas and Propagation Society International Symposium*, 1:359 – 362, 2003. ISBN:0-7803-7846-6.

[63] S. Simion. Modeling and design aspects of the MEMS switch. *Proceedings Semiconductor Conference*, 1:125 – 128, 2003. DOI:10.1109/SMICND.2003.1251360.

[64] J.H. Lee, N. Bushyager, and M.M. Tentzeris. Comparative evaluation of DSP techniques coupled with electromagnetic time-domain simulators for the efficient modeling and design of highly resonant RF-MEMS structures. *Microwave and Wireless Components Letters, IEEE*, 14(7):361 – 363, 2004. DOI:10.1109/LMWC.2004.828012.

[65] K. Kawano, S. Shahrani, T. Mori, M. Kuroda, and M.M. Tentzeris. Dynamic and electrical analysis of MEMS capacitor with accelerated motion effects. In *Wireless Communications and Applied Computational Electromagnetics, 2005. IEEE/ACES International Conference on*, pages 759–762, April 2005. DOI:10.1109/WCACEM.2005.1469696.

[66] S.K. De and N.R. Aluru. Full-lagrangian schemes for dynamic analysis of electrostatic MEMS. *Microelectromechanical Systems, Journal of*, 13(5):737–758, Oct 2004. ISSN:1057-7157, DOI:10.1109/JMEMS.2004.835773.

[67] B.P. Johnson, S. Kim, S.D. Senturia, and J. White. MEMCAD capacitance calculations for mechanically deformed square diaphragm and beam microstructures. In *Solid-State Sensors and Actuators, 1991. Digest of Technical Papers, TRANSDUCERS'91., 1991 International Conference on*, pages 494–497, 1991. DOI:10.1109/SENSOR.1991.148920.

[68] M. Schlegel, F. Bennini, J.E. Mehner, G. Herrmann, D. Muller, and W. Dotzel. Analyzing and simulation of MEMS in VHDL-AMS based on reduced-order FE models. *IEEE Sensors Journal*, 5(5):1019 – 1026, 2005. ISSN:1530-437X, DOI:10.1109/JSEN.2004.841445.

[69] Y. Lee and D.S. Filipovic. ANN based electromagnetic models for the design of RF-MEMS switches. *IEEE Microwave and Wireless Components Letters*, 15(11):823 – 825, 2005. ISSN:1531-1309.

[70] S. Simion. Design of distributed MEMS switch based on full- 3d electromagnetic simulator. *The International Conference on Computer as a Tool, EUROCON 2005*, 1:531 – 534, 2005. ISBN:1-4244-0049-X.

[71] D.A. Czaplewski, C.W. Dyck, H. Sumali, J.E. Massad, J.D. Kuppers, I. Reines, W.D. Cowan, and C.P. Tigges. A soft-landing waveform for actuation of a single-pole single-throw ohmic RF-MEMS switch. *Journal of Microelectromechanical Systems*, 15(6):1586 – 1594, 2006. ISSN:1057-7157.

[72] D. Peyrou, P. Pons, H. Granier, D. Leray, A. Ferrand, K. Yacine, M. Saadaoui, A. Nicolas, J.W. Tao, and R. Plana. Multiphysics softwares benchmark on Ansys/Comsol applied for RF MEMS switches packaging simulations. In *7th International Conference on Thermal, Mechanical and Multiphysics Simulation and Experiments in Micro-Electronics and Micro-Systems*, pages 1–8, April 2006. DOI:10.1109/ESIME.2006.1644011.

[73] X. Yuan, Z. Peng, J. Hwang, D. Forehand, and C.L. Goldsmith. A transient SPICE model for dielectric-charging effects in RF-MEMS capacitive switches. *IEEE Transactions on Electron Devices*, 53(10):2640–2648, 2006. ISSN:0018-9383.

[74] X.L. Yuan, Q.A. Huang, and X.P. Liao. Electromagnetic interference induced during the switching of a capacitive RF MEMS switch. In *8th International Conference on Solid-State and Integrated Circuit Technology*, pages 578–580, Oct 2006. DOI:10.1109/ICSICT.2006.306380.

[75] L. Del Tin, J. Iannacci, R. Gaddi, A. Gnudi, E.B. Rudnyi, A. Greiner, and J.G. Korvink. Non linear compact modeling of RF-MEMS switches by means of model order reduction. In *Solid-State Sensors, Actuators and Microsystems Conference*, pages 635–638, June 2007. DOI:10.1109/SENSOR.2007.4300210.

[76] D. Peyrou, H. Achkar, F. Pennec, P. Pons, and R. Plana. A macro model based on finite element method to investigate temperature and residual stress effects on RF MEMS switch actuation. In *International Conference on Thermal, Mechanical and Multi-Physics Simulation Experiments in Microelectronics and Micro-Systems*, pages 1–4, 2007. DOI:10.1109/ESIME.2007.360055.

[77] G. De Pasquale and A. Soma. Design and finite element simulation of MEMS for fatigue test. In *Semiconductor Conference, 2007. CAS 2007. International*, volume 1, pages 159–162, 2007. ISSN:1545-827X, DOI:10.1109/SMICND.2007.4519671.

[78] D. Peyrou, F. Coccetti, F. Pennec, H. Achkar, P. Pons, and R. Plana. A new methodology for RF MEMS contact simulation. In *International Conference on Thermal, Mechanical and Multi-Physics Simulation and Experiments in Microelectronics and Micro-Systems*, pages 1–4, 2008. DOI:10.1109/ESIME.2008.4525016.

[79] P.S. Sumant, N.R. Aluru, and A.C. Cangellaris. A methodology for fast finite element modeling of electrostatically actuated MEMS. *International Journal for Numerical Methods in Engineering*, 77(13):1789 – 1808, 2009. DOI:10.1002/nme.2469.

[80] S. Halder, P. Zhen, J. Hwang, D.I. Forehand, and C.L. Goldsmith. Compact RF model for transient characteristics of MEMS capacitive switches. *IEEE Transactions on Microwave Theory and Techniques*, 57(1):237 – 242, 2009. ISSN:0018-9480.

[81] M.A. Llamas, D. Girbau, E. Pausas, L. Pradell, S. Aouba, C. Villeneuve, V. Puyal, P. Pons, R. Plana, S. Colpo, and F. Giacomozzi. Capacitive and resistive RF-MEMS switches 2.5D & 3D electromagnetic and circuit modelling. In *Spanish Conference on Electron Devices*, pages 451–454, 2009. DOI:10.1109/SCED.2009.4800531.

[82] H. Achkar, P. Pons, M. Sartor, and R. Plana. Simulating the real geometry of an electrostatic switch to study the effect of uncertainties on the pull-in voltage. In *10th*

International Conference on Thermal, Mechanical and Multi-Physics simulation and Experiments in Microelectronics and Microsystems EuroSimE 2009, pages 1–4, 2009. DOI:10.1109/ESIME.2009.4938451.

[83] S. Halder, C. Palego, J. Hwang, and C.L. Goldsmith. Compact RF large-signal model for MEMS capacitive switches. In *IEEE MTT-S International Microwave Symposium Digest (MTT)*, pages 421–424, 2010. ISSN:0149-645X, DOI:10.1109/MWSYM.2010.5515520.

[84] J. Iannacci. Mixed-domain fast simulation of RF and Microwave MEMS-based complex networks within standard IC development frameworks. *Advanced Microwave Circuits and Systems*, pages 313–338, 2010. ISBN:978-953-307-087-2, DOI:10.5772/8438.

[85] M. Niessner, G. Schrag, G. Wachutka, and J. Iannacci. Modeling and fast simulation of RF-MEMS switches within standard IC design frameworks. In *International Conference on Simulation of Semiconductor Processes and Devices (SISPAD)*, pages 317–320, 2010. ISSN:1946-1569, DOI:10.1109/SISPAD.2010.5604496.

[86] S. Chaterjee and G. Pohit. Squeeze-film damping characteristics of cantilever microresonators for higher modes of flexural vibration. *International Journal of Engineering Science and Technology*, 2(4):187–199, 2011. ISSN:2141-2839.

[87] A. Jain, S. Palit, and M.A. Alam. A physics-based predictive modeling framework for dielectric charging and creep in RF-MEMS capacitive switches and varactors. *Journal of Microelectromechanical Systems*, 21(2):420–430, 2012. ISSN:1057-7157.

[88] A. Jain, D. Chechi, and P. Chawla. Performance study of RF-MEMS ohmic series switch. *International Journal of Advanced Research in Computer Science and Software Engineering*, 2(8):485–488, 2012. ISSN:2277 128X.

[89] C. Do, M. Lishchynska, and M.Hill. Impact force modelling for MEMS ohmic switch. *Proceedings MME 2012*, 2012. www.tu-ilmenau.de/fileadmin.

[90] S. Kurth, S. Leidich, and T. Gessner. Ohmic RF-MEMS switches, 2012. www.rmcip.ru/files/.

[91] M.A. Bazaz, Mashuq un Nabi, and S. Janardhanan. A review of parametric model order reduction techniques. In *Signal Processing, Computing and Control (ISPCC), 2012 IEEE International Conference on*, pages 1–6, 2012.

[92] B. Salimbahrami and B. Lohmann. Order reduction of large scale second-order systems using Krylov subspace methods. *Linear Algebra and its Applications*, 415(23):385–405, 2006. Special Issue on Order Reduction of Large-Scale Systems.

[93] T.-J. Su and R.R. Raig. Model reduction and control of flexible structures using Krylov vectors. *Journal of guidance, control, and dynamics*, 14(2):260–267, 1991.

[94] C.A. Beattie and S. Gugercin. Krylov-based model reduction of second-order systems with proportional damping. In *Decision and Control, 2005 and 2005 European Control Conference. CDC-ECC '05. 44th IEEE Conference on*, pages 2278–2283, 2005.

[95] D. Vasilyev, M. Rewienski, and J. White. A tbr-based trajectory piecewise-linear algorithm for generating accurate low-order models for nonlinear analog circuits and mems. In *Design Automation Conference, 2003. Proceedings*, pages 490–495, 2003. DOI:10.1109/DAC.2003.1219055.

[96] M. Rewienski and J. White. A trajectory piecewise-linear approach to model order reduction and fast simulation of nonlinear circuits and micromachined devices. In *Computer Aided Design, 2001. ICCAD 2001. IEEE/ACM International Conference on*, pages 252–257, 2001. DOI:10.1109/ICCAD.2001.968627, ISSN: 1092-3152.

[97] M. Rewienski and J. White. A trajectory piecewise-linear approach to model order reduction and fast simulation of nonlinear circuits and micromachined devices. *Computer-Aided Design of Integrated Circuits and Systems, IEEE Transactions on*, 22(2):155–170, 2003. DOI:10.1109/TCAD.2002.806601, ISSN: 0278-0070.

[98] E.B. Rudnyi and J.G. Korvink. Review: Automatic model reduction for transient simulation of MEMS-based devices. *Sensors Update*, 11(1):3–33, 2002.

[99] E.B. Rudnyi, J. Lienemann, A. Greiner, and J.G. Korvink. mor4ansys: Generating compact models directly from ANSYS models. In *Technical Proceedings of the 2004 Nanotechnology Conference and Trade Show, Nanotech 2004, March 7-11, 2004*, pages 279–282, 2004.

[100] J.S. Han, E.B. Rudnyi, and J.G. Korvink. Efficient optimization of transient dynamic problems in mems devices using model order reduction. *Journal of Micromechanics and Microengineering*, 15(4):822, 2005. DOI:10.1088/0960-1317/15/4/021.

[101] A. Kohler, S. Reitz, and P. Schneider. Sensitivity analysis and adaptive multi-point multi-moment model order reduction in MEMS design. In *Design, Test, Integration and Packaging of MEMS/MOEMS (DTIP), 2011 Symposium on*, pages 64–71, 2011.

[102] J. Santorelli, F. Nabki, and R. Khazaka. Practical considerations for parameterized model order reduction of MEMS devices. In *New Circuits and Systems Conference (NEWCAS), 2014 IEEE 12th International*, pages 129–132, 2014.

[103] A. Parent, A. Krust, G. Lorenz, and T. Piirainen. A novel model order reduction approach for generating efficient nonlinear verilog-a models of MEMS gyroscopes. In *Inertial Sensors and Systems (ISISS), 2015 IEEE International Symposium on*, pages 1–4, 2015.

[104] V.A. Kolchuzhin, J.E. Mehner, T. Gessner, and W. Doetzel. Parametric finite element analysis for reduced order modeling of MEMS. *EuroSime 2006. 7th International Conference on Thermal, Mechanical and Multiphysics Simulation and Experiments in Micro-Electronics and Micro-Systems*, pages 1–6, 2006. DOI:10.1109/ESIME.2006.1644004.

[105] V.A. Kolchuzhin, J.E. Mehner, T. Gessner, and W. Doetzel. Application of higher order derivatives method to parametric simulation of MEMS. *EuroSime 2007. 9th International Conference on Thermal, Mechanical and Multiphysics Simulation and Experiments in Micro-Electronics and Micro-Systems*, pages 1–6, 2007. ISBN:1-4244-1105-X.

[106] K. Suhas and K. Sripadaraja. Mechanical modeling issues in optimization of dynamic behavior of RF-MEMS switches. *International Journal of Computer and Information Engineering*, 2(2):261–265, 2008. ISSN:1307-6892, `https://www.waset.org/journals/ijcie/v2/v2-4-32.pdf`.

[107] M.S. Allen, J.E. Massad, R.V. Field, and C.W. Dyck. Input and design optimization under uncertainty to minimize the impact velocity of an electrostatically actuated MEMS switch. *Journal of Vibration and Acoustics*, 2, 2008. DOI:10.1115/1.2827981.

[108] V.A. Kolchuzhin, W. Doetzel, and J.E. Mehner. Challenges in MEMS parametric macro-modeling based on mode superposition technique. *EuroSimE 2009. 10th International Conference on Thermal, Mechanical and Multi-Physics simulation and Experiments in Microelectronics and Microsystems*, pages 1–4, 2009. DOI:10.1109/ESIME.2009.4938481.

[109] M.M. Shalaby, Z. Wang, L.L.W. Chow, B.D. Jensen, J.L. Volakis, K. Kurabayashi, and K. Saitou. Robust design of RF-MEMS cantilever switches using contact physics modeling. *IEEE Transactions on Industrial Electronics*, 56(4):1012 – 1021, 2009. ISSN:0278-0046.

[110] A.M. Pasha and M.A. Saqib. Design optimization for low voltage DC contact RF-MEMS shunt switch. *ICEE'09. Third International Conference on Electrical Engineering*, pages 1–6, 2009. ISBN:978-1-4244-4360-4.

[111] V.A. Kolchuzhin and J.E. Mehner. A parametric multilevel MEMS simulation methodology using finite element method and mesh morphing. In *Thermal, Mechanical and Multi-Physics Simulation and Experiments in Microelectronics and Microsystems (EuroSimE), 2012 13th International Conference on*, pages 1–5, April 2012. DOI:10.1109/ESimE.2012.6191776.

[112] M. Angira, G.M. Sundram, and K. Rangra. Design and pull-in voltage optimization of series metal-to-metal contact RF MEMS switch. In *Computing, Communication and Applications (ICCCA), 2012 International Conference on*, pages 1–4, Feb 2012. DOI:10.1109/ICCCA.2012.6179150.

[113] G. Ding, W. Wang, S. Halder, C. Palego, D. Molinero, J.C.M. Hwang, and C.L. Goldsmith. Intelligent CMOS control of RF MEMS capacitive switches. In *Microwave Symposium Digest (MTT), 2012 IEEE MTT-S International*, pages 1–3, June 2012. ISSN:0149-645X, DOI:10.1109/MWSYM.2012.6257781.

[114] M.A. Philippine, O. Sigmund, G.M. Rebeiz, and T.W. Kenny. Topology optimization of stressed capacitive RF-MEMS switches. *Journal of Microelectromechanical Systems*, 22(1):206 – 215, 2012. ISSN:1057-7157.

[115] D. Girbau, A. Lazaro, and L. Pradell. Characterization of dynamics and power handling of RF MEMS using vector measurement techniques. *Microwave Theory and Techniques, IEEE Transactions on*, 52(11):2627–2633, 2004. ISSN:0018-9480, DOI:10.1109/TMTT.2004.837198, upcommons.upc.edu.

[116] Jin Woo Lee, A.K. Mahapatro, D. Peroulis, and Arvind Raman. Vibration-based monitoring and diagnosis of dielectric charging in RF-MEMS switches. *Micro-*

electromechanical Systems, Journal of, 19(6):1490–1502, 2010. ISSN:1057-7157, www.purdue.edu/discoverypark.

[117] J.J. Ruan, N. Monnereau, D. Tremouilles, N. Mauran, F. Coccetti, N. Nolhier, and R. Plana. An accelerated stress test method for electrostatically driven MEMS devices. *Instrumentation and Measurement, IEEE Transactions on*, 61(2):456–461, 2012. ISSN:0018-9456, DOI:10.1109/TIM.2011.2161937, http://hal.archives-ouvertes.fr/docs/00/66/88/27/PDF.

[118] C. Kosla, C. Do, and M. Hill. Monitoring MEMS switch closure time as a measure of reliability, 2012. www.tu-ilmenau.de/fileadmin.

[119] K. Makasheva, B. Despax, L. Boudou, and G. Teyssedre. Dielectric layers for RF-MEMS switches: Design and study of appropriate structures preventing electrostatic charging. *Dielectrics and Electrical Insulation, IEEE Transactions on*, 19(4):1195–1202, 2012. ISSN:1070-9878, DOI:10.1109/TDEI.2012.6259990.

[120] S. Palit, A. Jain, and M.A. Alam. A non-obtrusive technique to characterize dielectric charging in RF-MEMS capacitive switches. In *Reliability Physics Symposium (IRPS), 2012 IEEE International*, pages 3F.3.1–3F.3.6, 2012. ISSN:1541-7026, DOI:10.1109/IRPS.2012.6241824.

[121] M. Koutsoureli, L. Michalas, and G. Papaioannou. Advanced dielectric charging characterization in capacitive MEMS. In *Industrial Technology (ICIT), 2012 IEEE International Conference on*, pages 545–550, 2012. DOI:10.1109/ICIT.2012.6209995.

[122] C. Kosla, P. Fitzgerald, and M. Hill. Continuous dynamic timing measurements to monitor spring and surface forces in MEMS switch reliability. In *Micro Electro Mechanical Systems (MEMS), 2014 IEEE 27th International Conference on*, pages 596–599, 2014. DOI:10.1109/MEMSYS.2014.6765711.

[123] B.N. Bond. Parameterized model order reduction for nonlinear dynamical systems. Master's thesis, Massachusetts Institute of Technology, Boston, US, 2006. `http://www.bnbond.com/pubs/bond_sm.pdf`.

[124] G.K. Fedder. *Simulation of Microelectromechanical Systems*. PhD thesis, University of California at Berkeley, Berkeley, US, 1994. www.ece.cmu.edu/ mems.

[125] J. Phillips. *Rapid Solution of Potential Integral Equations in Complicated 3-dimesional Geometries*. PhD thesis, Massachusetts Institute of Technology, Boston, US, 1997. `http://www.rle.mit.edu/cpg/publications/phillips.pdf`.

[126] D. Ramaswamy. *Simulation Tools for Microelectromechanical Systems*. PhD thesis, Massachusetts Institute of Technology, Boston, US, 2001. `http://www.rle.mit.edu/cpg/publications/ramaswamy.pdf`.

[127] X. Wang. *FastStokes: A Fast 3-D Fluid Simulation Program for Micro-Electro-Mechanical Systems*. PhD thesis, Massachusetts Institute of Technology, Boston, US, 2002.

[128] D. Peroulis. *RF MEMS Devices for Multifunctional Integrated Circuits and An-*

tennas. PhD thesis, University of Michigan, Ann Arbor, US, 2003. http://www.eecs.umich.edu/RADLAB/html/NEWDISS/Peroulis.pdf.

[129] I.V. Avdeev. *New Formulation for Finite Element Modeling Electrostatically Driven Microelectromechanical Systems*. PhD thesis, University of Pittsburgh, Pittsburgh, US, 2003. http://d-scholarship.pitt.edu/9783/1/avdeev_ilya_phd.pdf.

[130] Q. Jing. *Modeling and Simulation for Design of Suspended MEMS*. PhD thesis, University of Carnegie Mellon, Pittsburgh, US, 2003. http://www.dtic.mil/dtic/tr/fulltext/u2/a500969.pdf.

[131] C. Pinto Coelho. *Efficient tools for the design and simulation of microelectromechanical and microfluidic systems*. PhD thesis, Massachusetts Institute of Technology, Boston, US, 2007. http://www.rle.mit.edu/cpg/documents/cfspc_phd_thesis.pdf.

[132] F. Solazzi. *Novel Design Solutions for High Reliability RF MEMS Switches*. PhD thesis, University of Trento, Trento, Italy, 2010. static.digns.com/uploads/doctoral.

[133] S. Hannot. *Modeling Strategies for Electro-Mechanical Microsystems with Uncertainty Quantification*. PhD thesis, Delft University of Technology, Delft, Netherlands, 2010.

[134] V.A. Kolchuzhin. *Methods and Tools for Parametric Modeling and Simulation of Microsystems based on Finite Element Methods and Order Reduction Technologies*. PhD thesis, Chemnitz University of Technology, Chemnitz, Saxony, Germany, 2010. www.qucosa.de/fileadmin.

[135] C. B. Diţă. *Multiprocessor Electromagnetic Modelling of Integrated Microsystems*. PhD thesis, University Politehnica of Bucharest, Bucharest, Romania, 2013. http://www.lmn.pub.ro/~bogdan/documents/Teza_Cosmin_Bogdan_Dita_v4.pdf.

[136] P. Esposito, N. Ghoussoub, and Y. Guo. *Mathematical Analysis of Partial Differential Equations Modeling Electrostatic MEMS*. AMS and the Courant Institute of Mathematical Sciences at New York University, 2007. ISBN: 978-0-8218-4957-6, www.birs.ca/ nassif/papers-download.

[137] COMSOL multiphysics® modeling software. http://www.comsol.com/.

[138] ANSYS simulation software. http://www.ansys.com/.

[139] ANSYS MEMS modelling diagram, available at. www.ansys.com/Industries/.

[140] ANSYS MEMS modelling presentation, available at. www.ozeninc.com/downloads/.

[141] M. Popescu, A.-S. Lup, and R. Bărbulescu. Professional software packages for multiphysics modelling. *University Politecnica of Bucharest, Scientific Bulletin, Series C*, 2015. ISSN:1223-7027, submitted for review.

[142] D. Ioan. *Metoda elementului finit pentru modelarea electromagnetică*. UPB, Bucureşti, 2013.

[143] D. Ioan. Modelarea multifizică. ToMeMS - internal report - D1.1a "Modelarea cuplata electrostatica si mecanica a microcomutatoarelor de RF - Formularea problemei", 2012.

[144] D. Ioan. *Modelarea dispozitivelor electromagntice*. UPB, Bucureşti, 2000. `http://www.lmn.pub.ro/~daniel/cursmde.pdf`.

[145] D. Ioan. Modeling multiphysics systems and their complexity reduction, 2015. Short PhD course held at Institute of Mathematical Modelling, Analysis and Computational Mathematics (IMACM) Bergische Universitt Wuppertal (BUW).

[146] J.G. Michopoulos, C. Farhat, and J. Fish. Survey on modeling and simulation of multiphysics systems. *Journal of Computing and Information Science in Engineering*, 3(5):198–213, 2005. DOI:10.1115/1.2031269, http://citeseerx.ist.psu.edu/viewdoc/download?

[147] A. Timotin. Passive em element of circuit. *Rev. Roum. Sci Techn. Electrotech et Energ.*, 21(2):347–342, 1971.

[148] H.G Matthies, R. Niekamp, and J. Steindorf. Algorithms for strong coupling procedures. *Computer methods in applied mechanics and engineering*, 195(17):2028–2049, 2006.

[149] O.C. Zienkiewicz and R.L. Taylor. *The finite element method*, volume 3. McGraw-hill London, 1977.

[150] B. Markert. Weak or strong : on coupled problems in continuum mechanics, 2010. www.mechbau.uni-stuttgart.de.

[151] Wikipedia the free encyclopedia. `http://en.wikipedia.org/wiki/Weak_formulation`.

[152] Wikipedia the free encyclopedia. `http://en.wikipedia.org/wiki/Solid_modeling`.

[153] Wikipedia the free encyclopedia. `http://en.wikipedia.org/wiki/Computational_geometry`.

[154] Wikipedia the free encyclopedia. `http://en.wikipedia.org/wiki/Computer-aided_engineering`.

[155] H.A. Haus and J.R. Melcher. *Electromagnetic fields and energy*. Prentice Hall, 1989. ocw.mit.edu/resources.

[156] Shui-Lin Weng and Donald T. Greenwood. General dynamical equations of motion for elastic body systems. *Journal of Guidance, Control and Dynamics*, 15(6):1434–1442, 1992. deepblue.lib.umich.edu.

[157] D.J. Acheson. *Elementary Fluid Dynamics*. Oxford Applied Mathematics and Computing Science Series. Clarendon Press, 1990. `https://books.google.ro/books?id=GgC69-WUTs0C`.

[158] J. Holman. *Heat Transfer*. McGraw-Hill Education, 2009. `https://books.google.ro/books?id=7TGGPwAACAAJ`.

[159] A.H.D. Cheng and D.T. Cheng. Heritage and early history of the boundary element method. *Engineering Analysis with Boundary Elements*, 29(3):268–302, 2005. ISSN:0955-7997, DOI:http://dx.DOI.org/10.1016/j.enganabound.2004.12.001, http://www.sciencedirect.com/science/article/pii/S0955799705000020.

[160] B. Seibold. Numerical methods for partial differential equations, 2009. Massachusetts Institute of Technology: MIT OpenCourseWare http://ocw.mit.edu.

[161] Wikipedia the free encyclopedia. http://en.wikipedia.org/wiki/Well-posed_problem.

[162] Wikipedia the free encyclopedia. http://en.wikipedia.org/wiki/Condition_number.

[163] M.I. Younis. *Modeling and simulation of microelectromechanical systems in multiphysics fields*. PhD thesis, Citeseer, 2004.

[164] Y. Bazilevs and T.Jr. Hughes. Weak imposition of dirichlet boundary conditions in fluid mechanics. *Computers & Fluids*, 36(1):12–26, 2007.

[165] C. Li and S. Li. Multiple solutions and sign-changing solutions of a class of nonlinear elliptic equations with Neumann boundary condition. *Journal of Mathematical Analysis and Applications*, 298(1):14–32, 2004.

[166] V.A. Marchenko. Sturm-Liouville operators and their applications. *Kiev Izdatel Naukova Dumka*, 1, 1977.

[167] D. Xiu and G.E. Karniadakis. The Wiener–Askey polynomial chaos for stochastic differential equations. *SIAM journal on scientific computing*, 24(2):619–644, 2002.

[168] D. Ioan. *Metode pentru calculul campului electromagnetic. Separarea variabileleor*. Institutul Politehnic Bucuresti, Editura IPB, Bucureşti, 1988.

[169] K.J. Binns, P.J. Lawrenson, and C.W. Trowbridge. *The Analytical and Numerical Solution of Electric and Magnetic Fields*. Wiley, 1993. https://books.google.ro/books?id=nY1-QgAACAAJ.

[170] M.M Zand, M.T. Ahmadian, and B. Rashidian. Semi-analytic solutions to nonlinear vibrations of microbeams under suddenly applied voltages. *Journal of Sound and Vibration*, 325(12):382 – 396, 2009.

[171] A. Bossavit and I.D. Mayergoyz. *Computational Electromagnetism: Variational Formulations, Complementarity, Edge Elements*. Electromagnetism. Elsevier Science, 1998. https://books.google.ro/books?id=RQ_9hc8U7MsC.

[172] G. Strang and G. Fix. *An Analysis of the Finite Element Method*. Wellesley-Cambridge Press, 2008. ISBN:9780980232707, https://books.google.ro/books?id=K5MAOwAACAAJ.

[173] M.N.O. Sadiku. *Numerical Techniques in Electromagnetics, Second Edition*. Taylor & Francis, 2000. https://books.google.ro/books?id=zjepkDILFp8C.

[174] M.N.O. Sadiku, J. Sagliocca, and O. Soriyan. *Solutions Manual Accompanying Elements of Electromagnetics, Third Edition*. The Oxford Series in Electrical and

Computer Engineering. Oxford University Press, 2000. https://books.google.ro/books?id=mwtpAJrhB5kC.

[175] P. Monk. *Finite Element Methods for Maxwell's Equations*. Numerical Mathematics and Scientific Computation. Clarendon Press, 2003. https://books.google.ro/books?id=zI7Y1jT9pCwC.

[176] A. Tsakanian, E. Gjonaj, H. De Gersem, T. Weiland, and M. Dohlus. SIBC formulation for a low-dispersion finite volume method in the time domain, 2015. www.compumag2015.com/FVM.

[177] W.R. Stone. *Review of Radio Science: 1999-2002 URSI*. URSI monographs. Wiley, 2002. https://books.google.ro/books?id=5EdCJ2EYJ4EC.

[178] R.F. Harrington. *Field Computation by Moment Methods*. Wiley-IEEE Press, 1993. ISBN:978-0-7803-1014-8, http://read.pudn.com/downloads108.

[179] J.T. Katsikadelis. *Boundary Elements: Theory and Applications: Theory and Applications*. Elsevier Science, 2002. ISBN:9780080528243, http://home.kku.ac.th/wattou/research/resources/e-book/bem02.pdf.

[180] E.T. Ong, K.M. Lim, and H.P. Lee. Techniques in electrostatics analysis of MEMS and their applications. In C.T. Leondes, editor, *MEMS/NEMS*, pages 235–291. Springer US, 2006. ISBN:978-0-387-24520-1, DOI:10.1007/0-387-25786-1_8.

[181] G. Schrag, O. Brand, G.K. Fedder, C. Hierold, and J.G. Korvink. *System-level Modeling of MEMS*. Number vol. 10 in Advanced Micro and Nanosystems. Wiley, 2012.

[182] A. Preumont. *Vibration Control of Active Structures: An Introduction*. Solid Mechanics and Its Applications. Springer Netherlands, 2012.

[183] M.F. Rubinstein. *Structural systems–statics, dynamics and stability*. Prentice-Hall civil engineering and engineering mechanics series. Prentice-Hall, 1970.

[184] A. Vandendorpe and P. Van Dooren. Krylov techniques for model reduction of second-order systems. *Unpublished Note, March*, 2, 2004. http://perso.uclouvain.be/paul.vandooren/publications/VandendorpeV04.pdf.

[185] Y. Chahlaoui, K.A. Gallivan, A. Vandendorpe, and P. Van Dooren. Model reduction of second-order systems. In P. Benner, D.C. Sorensen, and V. Mehrmann, editors, *Dimension Reduction of Large-Scale Systems*, volume 45 of *Lecture Notes in Computational Science and Engineering*, pages 149–172. Springer Berlin Heidelberg, 2005.

[186] A.C. Antoulas and D.C. Sorensen. Approximation of large-scale dynamical systems: An overview. *Applied Mathematics and Computer Science*, 11(5):1093–1122, 2001.

[187] E.J. Yoo. *Parametric Model Order Reduction for Structural Analysis and Control*. PhD thesis, Munchen University of Technology, Munchen, Germany, 2010. .

[188] A. Timotin, V. Hortopan, A. Ifrim, and M. Preda. *Lecţii de Bazele Electrotehnicii*. Editura Didactică şi Pedagogică, Bucureşti, 1970.

[189] M. Preda and P. Cristea. *Bazele electrotehnicii, Circuite electrice*, volume 1. Editura Didactică şi Pedagogică, Bucureşti, 1980.

[190] M. Preda and P. Cristea. *Bazele electrotehnicii, Circuite electrice*, volume 2. Editura Didactică şi Pedagogică, Bucureşti, 1980.

[191] D. Dugdale and D.E. Dugdale. *Essentials of Electromagnetism*. Macmillan physical science. American Inst. of Physics, 1993. https://books.google.ro/books?id=LIwBcIwrwv4C.

[192] Wikipedia the free encyclopedia. http://en.wikipedia.org/wiki/Lax-Milgram_theorem.

[193] E. Suli. *Finite Element Methods for Partial Differential Equations*. University of Oxford, 2012. ElectromagneticModelingDoctoral/Books/FEM/SuliFEM.pdf.

[194] C.I. Mocanu. *Teoria campului electromagnetic*. Editura Didactică şi Pedagogică, Bucureşti, 1981.

[195] R. Radulet. *Bazele Electrotehnicii - Probleme I*. Editura Didactică şi Pedagogică, Bucureşti, 1975.

[196] D.J. Griffiths. *Introduction to Electrodynamics*. Pearson Education, 2014. https://books.google.ro/books?id=J9ygBwAAQBAJ.

[197] D. Ioan and G. Ciuprina. Reduced order models of on-chip passive components and interconnects, workbench and test structures. In Wilhelmus H.A. Schilders, Henk A. van der Vorst, and Joost Rommes, editors, *Model Order Reduction: Theory, Research Aspects and Applications*, volume 13 of *Mathematics in Industry*, pages 447–467. Springer Berlin Heidelberg, 2008. ISBN:978-3-540-78840-9, DOI:10.1007/978-3-540-78841-6_20, http://dx.DOI.org/10.1007/978-3-540-78841-6_20.

[198] A. Tomescu and F.M.G. Tomescu. *Sisteme cu Microunde*. MatrixROM, 2001.

[199] G. Ciuprina, A.S. Lup, and A. Tomescu. Parametrii s în aplicaţii de înaltă frecvenţă. In *Lucrarile Simpozionului National de Electrotehnică Teoretică*. SNET2012, Bucharest, Romania, 2012. ISSN:V, (online), 6 pages.

[200] R.B. Marks and D.F. Williams. A general waveguide circuit theory. *Journal of Research of the National Institute of Standards and Technology*, 97(5):533562, 1992. http://www.eeel.nist.gov/dylan_papers/GeneralWaveguideCricuitTheory.pdf.

[201] S.J. Orfanidis. *Electromagnetic Waves and Antennas*. Sophocles J. Orfanidis, Rutgers University, 2008. http://www.ece.rutgers.edu/~orfanidi/ewa/orfanidis-ewa-book.pdf.

[202] D. Youla. On the factorization of rational matrices. *IRE Transactions on Information Theory*, 7(3):172–189, 1961. DOI:10.1109/TIT.1961.1057636.

[203] D.A. Frickey. Conversions between s, z, y, h, abcd, and t parameters which are valid for complex source and load impedances. *IEEE Transactions on Microwave Theory and Techniques*, 42(2):205–211, 1994. Doi:10.1109/22.275248.

[204] R.B. Marks, D.F. Williams, and D.A. Frickey. Comments on "conversions between s, z, y, h, abcd, and t parameters which are valid for complex source and load impedances" [with reply]. *IEEE Transactions on Microwave Theory and Techniques*, 43(4):914–915, 1995. DOI:10.1109/22.375247.

[205] G. Lojewski. *Dispozitive şi Circuite de Microunde*. Editura Tehnica, 2005.

[206] Joel Voidman. course materials for 6. 777j 1 2.372j design and fabrication of microelectromechanical devices, 2007. MIT OpenCourseWare (http://ocw.mit.edu/), Massachusetts Institute of Technology, JV: 6.777J/2.372J Spring 2007, Lecture 8-24.

[207] COMSOL multiphysics® v 5.2 documentation. `http://www.comsol.com/`.

[208] O.C. Zienkiewicz and R.L. Taylor. *The Finite Element Method for Solid and Structural Mechanics*. Elsevier Science, 2005. ISBN:9780080455587.

[209] W. Weaver, S.P. Timoshenko, and D.H. Young. *Vibration Problems in Engineering*. A Wiley-Interscience publication. John Wiley & Sons, 1990. `https://books.google.ro/books?id=YZ7t8LgRqi0C`.

[210] W. Beneson and S Horst. *Handbook of Physics*. Springer Verlag New York, Inc, 1 edition, 2001. ISBN:0-387-95269-1, books.google.ro/handbook+of+physics.

[211] R.J. Roark, W.C. Young, and R.G. Budynas. *Roark's Formulas for Stress and Strain*. McGraw-Hill, Two Penn Plaza, New York, NY 10121-2298, US, 7 edition, 1989. ISBN:0-07-072542-X, materiales.azc.uam.mx/gjl.

[212] J.B. Starr. Squeeze-film damping in solid-state accelerometers. In *Solid-State Sensor and Actuator Workshop, 1990. 4th Technical Digest., IEEE*, pages 44–47, 1990. DOI:10.1109/SOLSEN.1990.109817.

[213] K. J. Rangra. *Electrostatic Low Actuation Voltage RF MEMS Switches for Telecommunications*. PhD thesis, University of Trento, Trento, Italy, 2005. assets.disi.unitn.it/rangra_kamal.pdf.

[214] Wikipedia the free encyclopedia. `https://en.wikipedia.org/wiki/Impedance_analogy`.

[215] N. Maluf and K. Williams. *An Introduction to Micromechanical Systems Engineering*. Artec House, 685 Canton Street, Norwood,, MA, US, 2 edition, 2004. ISBN:1-58053-590-9, ebooks.cawok.pro/Artech.House.Publishers.An.Introduction.

[216] J. Anderson. *Fundamentals of Aerodynamics*. McGraw-Hill Education, 2010. ISBN:9780073398105, http://aaun.ir/wp-content/uploads/2015/07/John-D.

[217] Wikipedia the free encyclopedia. `https://en.wikipedia.org/wiki/Computational_fluid_dynamics`.

[218] G.Z. Tomasz. Fundamentals of fluid dynamics: Elementary viscous flow, 2013. Introductory Course on Multiphysics Modelling, Institute of Fundamental Technological Research Warsaw, Poland,.

[219] R. Pratap, S. Mohite, and A.K. Pandey. Squeeze film effects in mems devices. *Journal of the Indian Institute of Science*, 87(1):75–94, 2007.

[220] P. Gravesen, J. Branebjerg, and O.S. Jensen. Microfluidics-a review. *Journal of Micromechanics and Microengineering*, 3(4):168–182, 1993. `http://stacks.iop.org/0960-1317/3/i=4/a=002`.

[221] National instruments APLAC. APLAC documentation, v8.

[222] A.-S. Lup, G. Ciuprina, D. Ioan, and S. Kula. Parallel plate suspended capacitor: modelled in dynamic, static and RF regimes. ToMeMS - internal report, 2014.

[223] T. Veijola. *Equivalent circuit model for micromechanical inertial sensors*. Circuit Theory Laboratory Report Series CT-39, Helsinky University of Technology, 1999.

[224] D Kuhl and M.A. Crisfield. Energy-conserving and decaying algorithms in non-linear structural dynamics. *International journal for numerical methods in engineering*, 45(5):569–599, 1999.

[225] M.A. Crisfield. *Non-linear finite element analysis of solids and structures*. Number vol. 2 in Non-linear Finite Element Analysis of Solids and Structures. Wiley, 1997. ISBN:9780471956495.

[226] T. Imura, H. Okabe, and Y. Hori. Basic experimental study on helical antennas of wireless power transfer for electric vehicles by using magnetic resonant couplings. In *Vehicle Power and Propulsion Conference, VPPC '09. IEEE*, pages 936–940, 2009. DOI:10.1109/VPPC.2009.5289747.

[227] FP6/STREP-027378 Research project, "Comprehensive High-Accuracy Modelling of Electromagnetic Effects in Complete Nanoscale RF Blocks (Chameleon-RF)", 2005-2008, coordinated by Philips/NXP http://www.hitech-projects.com/euprojects/chameleon%20RF/.

[228] D. et al. Ioan. Compact parametric models for passive integrated components EM coupled with environment. CHAMELEON-RF D1.2c - internal report, 2006.

[229] B. Gustavsen and A. Semlyen. Rational approximation of frequency domain responses by vector fitting. *IEEE Transactions on Power Delivery*, 14(3):1052–1061, 1999. ISSN:0885-8977, DOI:10.1109/61.772353.

[230] D. Ioan, G. Ciuprina, M. Radulescu, and E. Seebacher. Compact modeling and fast simulation of on-chip interconnect lines. *IEEE Transactions on Magnetics*, 42(4):547–550, 2006. ISSN:0018-9464, DOI:10.1109/TMAG.2006.871466.

[231] I.A. Lazar, G. Ciuprina, and D. Ioan. Effective extraction of accurate reduced models for HF-IC using multi-CPU architectures. *Inverse Problems in Science and Engineering*, 20(1):15–27, 2010. DOI:10.1080/17415977.2011.624622, www.researchgate.net/publication/233058322.

[232] G. Ciuprina, D. Ioan, I.A. Lazar, and C.B. Dita. Vector fitting based adaptive frequency sampling for compact model extraction on HPC systems. *IEEE Transactions on Magnetics*, 48(2):431–434, 2012. ISSN:0018-9464, DOI:10.1109/TMAG.2011.2174344.

[233] M. Clemens and T. Weiland. Discrete electromagnetism with the finite integration technique. In *32th Progress In Electromagnet-*

ics Research Symposium (PIERS), pages 65–87, 2001. available at http://www.jpier.org/PIER/pier32/03.00080103.clemens.pdf.

[234] G. Ciuprina, D. Ioan, D. Niculae, J.F. Villena, and L.M. Silveira. Parametric models based on sensitivity analysis for passive components. *Book chapter in the book Intelligent Computer Techniques in Applied Electromagnetics, in the book series Studies in Computational Intelligence, Springer Berlin*, 119:231–239, 2008.

[235] G. Ciuprina, A. Stefanescu, S. Kula, and D. Ioan. Parameterized model order reduction. robust procedures for parametric model order reduction of high speed interconnects. *Book chapter in the book Coupled Multiscale Simulation and Optimization in Nanoelectronics (M. Gunther Editor), in the book series Mathematics in Industry, Springer-Verlag*, 21:287–319, 2015.

[236] B. Gustavsen and A. Semlyen. Rational approximation of frequency domain responses by vector fitting. *IEEE Trans. Power Deliv.*, 14(3):2109–2121, 1999.

[237] D. Deschrijver, M. Mrozowski, T. Dhaene, and D. De Zutter. Macromodeling of multiport systems using a fast implementation of the vector fitting method. *IEEE Microw. Wirel.Compon. Lett.*, 18(8):383385, 2008.

[238] B. Gustavsen. Improving the pole relocating properties of vector fitting. *IEEE Trans. Power Deliv.*, 21(3):15871592, 2006.

[239] The Vector Fitting Web Site. https://www.sintef.no/projectweb/vectfit/.

[240] G. Ciuprina, C.-B. Diţă, A.-S. Lup, D. Ioan, and A. Ştefanescu. Extraction of TL-lumped RF macromodels for MEMS switches. In *Numerical Electromagnetic and Multiphysics Modeling and Optimization, NEMO 2015,*. NEMO2015, Ottawa, Canada, 2015.

[241] S. Kula and A.-S. Lup. Electrical schematics for 1D analysis of a bridge type MEMS capacitive switch. *Computer Applications in Electrical Engineering*, 12:407–421, 2014. ISSN:1508-4248.

[242] M. Popescu, A.-S. Lup, G. Ciuprina, and D. Ioan. An object oriented data structure designed for multiphysics simulations on parallel computers. In *Advanced Topics in Electrical Engineering (ATEE), 2015 9th International Symposium on*, pages 448–451, May 2015. DOI:10.1109/ATEE.2015.7133846.

[243] A.-S. Lup, G. Ciuprina, and Ş. Sorohan. Parametric multiphysics static models for a bridge type MEMS capacitive switch. In *Power Engineering Conference (UPEC), 2014 49th International Universities*, pages 1–5, Sept 2014. DOI:10.1109/UPEC.2014.6934635.

[244] A.-S. Lup, D. Ioan, M. Popescu, and G. Ciuprina. Parametric multiphysics 3D modelling of a bridge type MEMS capacitive switch. In *International Symposium on Electromagnetic Fields in Mechatronics, Electrical and Electronic Engineering*, 2015.

[245] M. Popescu, A.-S. Lup, G. Ciuprina, and D. Ioan. Using object oriented data structures for optimizing MEMS devices on parallel computers. In *International*

Symposium on Electromagnetic Fields in Mechatronics, Electrical and Electronic Engineering, 2015. ISBN:978-84-606-9102-0.

[246] A.-S. Lup, G. Ciuprina, and A. Ştefanescu. Extraction of effective elastic coefficients from a coupled structural electrostatic simulation of a MEMS switch. In *Fundamentals of Electrical Engineering (ISFEE), 2014 International Symposium on*, pages 1–5, Nov 2014. DOI:10.1109/ISFEE.2014.7050539.

[247] G. Ciuprina, A.-S. Lup, B. Dita, D. Ioan, S. Sorohan, D. Isvoranu, and S. Kula. Mixed domain macromodels for RF MEMS capacitive switches. *The 10th International Conference on Scientific Computing in Electrical Engineering SCEE 2014*, 2014. accepted to be published in Springer journal "Mathematics in Industry" (ISI-WOS).

[248] A.-S Lup and G. Ciuprina. Analysis of membrane perforations on the RF behavior of capacitive MEMS switches. *Acta Electrotehnica*, 54(5):252–255, 2013. ISSN:1841-332.

[249] A. Alexandru, S. Lup, and B. Dita. GDS2M: Preprocessing tool for MEMS devices. In *Advanced Topics in Electrical Engineering (ATEE), 2013 8th International Symposium on*, pages 1–4, May 2013. DOI:10.1109/ATEE.2013.6563451, WOS:000332928500105.

[250] C.-B. Diţă, A.-S. Lup, G. Ciuprina, and D. Ioan. Compact TL-RLC-TL model extraction from FW field solution for RF MEMS capacitive switch. In *Advanced Topics in Electrical Engineering (ATEE), 2015 9th International Symposium on*, pages 436–441, May 2015. DOI:10.1109/ATEE.2015.7133844.

[251] G. Ciuprina, A.-S. Lup, D. Ioan, D. Isvoranu, and Ş. Sorohan. Combined multiphysics and RF macromodels for electrostatic actuated micro-electro-mechanical switches. In *Conference on the Computation of Electromagnetic Fields*. COMPUMAG2015, Montreal, Canada, 2015.